Long/Continuous Bio-derived Fibre Reinforced PLA Composites for FDM 3D Printing

A thesis

submitted for partial fulfilment

of the requirements for the degree

of

Doctor of Philosophy in Materials and Processing

at

The University of Waikato

by

LAKSHMI PRIYA MUTHE

THE UNIVERSITY OF
WAIKATO
Te Whare Wānanga o Waikato

January 2024

Abstract

High mechanical performance applications often rely on fibre-reinforced composites using continuous synthetic fibres and petrochemical-based polymers. A shift towards bio-derived fibres and bio-derived polymers can reduce the reliance on non-sustainable materials. Long/continuous high-strength bio-derived fibres, such as flax and viscose, offer the potential to achieve mechanical properties similar to synthetic fibre composites. Polylactic acid (PLA), a sustainable bio-derived thermoplastic polymer known for its relatively high strength and stiffness compared to other polymers, is a promising alternative to petrochemical-derived counterparts. This study used long flax fibres and continuous viscose fibres in yarn form to reinforce PLA matrices, resulting in high-performance composite filaments. These filaments are designed for a recently developed and evolving manufacturing method, Fused Deposition Modelling (FDM) 3D printing, for which product performance has been limited by the commercially available filaments. Achieving high-performance FDM filaments requires addressing challenges related to fibre wetting and uniform fibre/polymer distribution, which this study addresses through impregnation and consolidation techniques. The research covers comprehensive experimental investigations into the physical, mechanical, and thermal properties of viscose, flax fibres, and PLA matrices. Successful outcomes include the development of long/continuous bio-derived fibre-reinforced composite filaments by employing two impregnation methods: solution and emulsion impregnation. Analysis covers the morphology, porosity, fibre weight fraction, and mechanical and thermal properties of the composite filaments and 3D printed composites.

Composite filaments were produced using three reinforcement yarns in their as-received form: viscose, two types of flax – standard flax and bleached flax. Viscose fibres were purchased in the form of fully continuous bio-derived fibres, while flax fibres were long and discontinuous, twisted into continuous yarns. Two PLA grades, PLA 2003D (in the form of granules) and PL 1005 (in the form of a PLA/water emulsion), were employed for solution and emulsion impregnation, respectively. Tensile testing of single fibres and matrices yielded results consistent with literature values. Bleached flax fibres exhibited the highest tensile strength (921.6 MPa), standard flax fibres displayed the highest Young's modulus (31.8 GPa), and viscose fibres demonstrated the highest elongation at break (13.2%). PLA 2003D exhibited the highest tensile properties of the two PLA grades. Thermal stability, as assessed by TGA, demonstrated stability of both bio-derived reinforcements and matrices up to 250 ^{o}C. DSC analysis confirmed the semi-crystalline nature of PLA 2003D and the amorphous nature of PL 1005.

An impregnation and consolidation methodology was developed to produce composite filaments using both PLA solution and emulsion. Initially employing a single impregnation bath, it was later upgraded to dual baths in tandem for enhanced efficiency. A yarn spooler directed the fibre into the impregnation bath with squeezing rollers, followed by excess resin removal through a nozzle. The impregnated filament was collected on a winding mandrel and passed through a heated consolidation die. Various

formulations with different impregnation cycles were tested for solution and emulsion impregnation methods. Polymer uptake depended on the affinity between the fibre and impregnating liquid, while yarn twist influenced polymer distribution. Emulsion impregnated composites exhibited higher polymer uptake due to better affinity between water and bio-derived fibres. However, solution impregnated composites showed better polymer distribution, particularly for twisted flax-reinforced filaments, relating to the efficient impregnation of PLA/DCM solution. For both impregnation methods, standard flax and bleached flax reinforced composites exhibited improved interfacial adhesion compared to viscose, attributed to mechanical interlocking between the rough surface of flax fibres and PLA in contrast to smooth viscose fibres. For PLA/viscose composites, emulsion impregnation resulted in higher tensile strength (254.7 MPa) and Young's modulus (9.1 GPa), surpassing reported values in the literature. On the other hand, for PLA/standard flax and PLA/bleached flax, solution impregnation yielded superior tensile properties. Solution impregnated PLA/bleached flax, for the 7wt% x 3 formulation, had the highest tensile strength (356.1 MPa), while the 7wt% x2 tandem formulation showed the highest Young's modulus (17.6 GPa) of all composites. The achieved tensile strength for PLA/bleached flax in this study also exceeded values reported in existing literature for PLA/flax composites.

The highest-performing formulations for each reinforcement, employing both solution and emulsion impregnation, were chosen to produce 3D printing filaments. A Makergear® FDM 3D printer, compatible with filament diameters of 1.4 to 2 mm, was utilized. Three filaments were pultruded together into one using a consolidation die to achieve the required filament diameter. PLA/viscose and PLA/bleached flax were selected for 3D printing in both solution and emulsion impregnation formulations, following an analysis of morphology, porosity, fibre weight fraction, and tensile properties of the multiple consolidated filaments. To further optimize diameter and enhance printability, the multiple consolidated filaments underwent melt-impregnation with additional polymer, resulting in 1.45±0.5 mm diameter filaments. Characterization of the 3D printing filaments revealed a reduction in tensile strength and Young's modulus due to increased polymer content.

Optical microscopy and porosity analysis of the 3D printed composites revealed increased porosity in the printed specimens compared to the filaments due to voids between the printed layers and pulling of the fibres onto the surface of the printed part because of the nozzle's drag force exerted during the printing process. Emulsion impregnated PLA/viscose exhibited lower porosity and printing defects compared to other composites relating to better affinity between PLA emulsion and viscose as mentioned earlier. Tensile strength and Young's modulus values of the 3D printed composites decreased compared to the filaments due to printing induced defects mentioned previously. The highest tensile and flexural properties were obtained for emulsion impregnated PLA/viscose composites, demonstrating the significance of efficient impregnation. The 3D printed emulsion impregnated

PLA/viscose composites displayed an impact strength greater than 127KJ/m^2, which is higher than what has been reported in the literature for any PLA biocomposite.

Publications

A Review of 3D/4D Printing of Poly-Lactic Acid Composites with Bio-derived Reinforcements

Lakshmi Priya Muthe, Kim Pickering, Christian Gauss

Composites Part C: Open Access, Volume 8, Pages 2666-6820, 2022.

Acknowledgements

I would like to express my sincere gratitude to my supervisor, **Professor Kim Pickering**, for her unwavering guidance, invaluable support, and mentorship throughout my PhD journey. I am also deeply thankful to my co-supervisor, **Dr. Christian Gauss**, for constant encouragement, patience, guidance, and constructive feedback. I extend my appreciation to **Dr. Mohammad Beg**, a fellow researcher whose insightful contributions and assistance helped me, even though not formally part of my supervisory panel.

I am very fortunate to have worked with the dedicated lab technicians **Jonathan Van Harselar, Sophia Rodrigues, Brett Nichol, and Helen Turner,** and would like to extend my heartfelt gratitude towards them. I would also like to thank **Mary Dalbeth, Natalie Shaw, Carol Robinson, and Nadine Viljoen** for the administrative support throughout my studies. Special thanks to my amazing teammates **John Akindoyo, Jing Xu, and William Allouche,** for their collaborative spirit and assistance in the university and the laboratory, making this research a truly enriching experience. Thank you to my fellow students and friends **Balakrishnan Manogar, Darshi Egodage, and Phil Bachman** for the wonderful conversations, support, and positive energy throughout this academic journey. A big thanks to **Dr. Chanelle Gavin** for inspiring and encouraging me.

My heartfelt appreciation goes to my husband, **Siddharth Bajpai**, whose unwavering support, understanding, and encouragement sustained me during challenging times. I am also grateful to my parents, in-laws, uncle, and his wife for their love, encouragement, and belief in my capabilities. This accomplishment would not have been possible without the collective support of these remarkable individuals.

I would also like to acknowledge Science for Technological Innovation (SfTI) and the University of Waikato for the financial support during my PhD.

Table of Contents

List of Figures

List of tables

Symbols and Abbreviations

Symbols

ρ_{ct}	Density of the composite
M_a	Mass of the composite in air
M_w	Mass of the printed sample in water
ρ_w	Density of water
ρ_f	Density of fibre
ρ_m	Density of matrix
V_f	Volume fraction of fibre
V_m	Volume fraction of matrix
σ_l	Tensile strength in the longitudinal direction
σ_m	Tensile stress in the matrix at fibre failure
σ_f	Ultimate tensile strength of the fibre
E_l	Young's modulus in the longitudinal direction
E_m	Young's modulus of the matrix
E_f	Young's modulus of the fibre

Abbreviations

PLA	Polylactic acid
DCM	Dichloromethane
FDM	Fused Deposition Modelling
IM	Injection Moulding
CM	Compression Moulding
NMMO	N-methyl morpholine-oxide
PHA	Polyhydroxyalkanoates
Bio PE	Bio-derived polyethylene
PEF	Poly(ethylene-2,5-furandicarboxylate)
Bio PC	Bio-derived polycarbonate
PA	Polyamide

IFSS Interfacial shear strength

AM Additive manufacturing.

ISO international organization for standardisation

ASTM American Society for testing and materials

UV Ultraviolet

SSF Single fibre fragmentation

UD Unidirectional

SEM Scanning electron microscopy

TEMPO 2,2,6,6-Tetramethylpiperidin-1-yloxy

PP Polypropylene

ROP Ring opening polymerisation

PLLA Poly (L-lactide)

PDLA Poly (D-lactide)

LA Lactic acid

FFF Fused filament fabrication.

CAD Computer-aided design

SCBF Sugarcane bagasse fibre

MA Maleic anhydride

BP Bamboo powder

MCC Microcrystalline cellulose

MFC Micro fibrillated cellulose

CNF Cellulose nano fibres

CNC Cellulose nanocrystals

BC Bacterial nano cellulose

PEG Polyethylene glycol

DSC Differential scanning calorimetry

TGA Thermogravimetric analysis

LMW Low molecular weight

TMTA Trimethylolpropane triacrylate

TAIC Trially isocyanurate

LF Lemongrass fibre

GSM Grams per square metre

UTM Universal testing machine

NA Not available

DTG Derivative thermogravimetric

Glossary

This thesis frequently uses the terms additive manufacturing, bioderived materials, reinforcement, fibre, yarn, composites, and filaments. A list of terms and definitions has been given below to enable readers to understand the components of the research in the way they have been presented throughout this document.

Additive manufacturing (or) 3D printing

Additive manufacturing refers to the manufacturing method in which material is added in the form of layers to create three-dimensional objects based on a computer design – thereby also known as 3D printing. Additive manufacturing processes have different approaches to layering materials to create objects, including, but not limited to, the deposition of layers of material in a bottom-up approach [1].

Biodegradable materials

Biodegradability is the ability to undergo physical and chemical changes and decompose by the action of biological organisms [2]. Biodegradable materials can be derived from natural or synthetic sources [3].

Bio-derived materials

Bio-derived materials are defined as materials that are obtained from living matter or biomass. These materials can be naturally occurring or can be synthesised from biological starting materials (e.g., sugar, starch, plant oil, etc.). Bio-derived only refers to what involves the production of a material. Bio-derived materials can be biodegradable or non-biodegradable [4].

Reinforcement

Reinforcement is considered the principal component in a composite system, with the primary function of improving the mechanical properties of the composite [5]. In this thesis, reinforcement has been defined as the component that at least improves Young's modulus of the resulting composite when added to the polymer.

Fibre

Fibre is an individual element with characteristic longitudinal and cross-sectional shapes and characteristic chemical composition. For example, human-made glass fibre is a silica fibre with silicic acid and metal oxides as its amorphous contents. On the other hand, a flax fibre consists of cellulose, a linear polysaccharide consisting of β(1-4) linked D-glucose units [6]. In the case of plant fibres, the term fibre strictly refers to the smallest intact element in a plant [7].

Tow/Yarn

A tow/yarn is an assembly of fibres laid or twisted together to form a continuous strand [8]. Yarn can be made of staple fibres such as cotton and wool or continuous human-made fibres such as regenerated cellulose and polyester. Yarn can be made of a single type of fibre or blended fibres [9]. Yarns are usually classified using "yarn count", which refers to the linear density or thickness of the yarn. The unit "tex" is used to measure the yarn count in terms of mass per unit length [10].

Filament

The filament is the feedstock used for the fused deposition modelling (FDM) 3D printing technique. FDM filaments are made of thermoplastics and their composites. The efficiency of FDM printing and the properties of the printed parts largely depend on the properties of the filament [11].

Chapter 1: Introduction

1.1 Research Background

Growing awareness of the need for increased sustainability is driving interest in bio-derived fibre-reinforced composites as eco-friendly, cost-effective alternatives to synthetic fibre-reinforced composites. In addition to their environmental benefits, bio-derived fibre-reinforced composites are also favoured for their affordability, low density, high specific strength, and low-hazard manufacturability [12]. However, compared to synthetic fibre-reinforced composites, some main disadvantages of these composites are lower tensile and impact strength, high property variability, and poor chemical compatibility with matrices.

A significant amount of research in the past decade focused on overcoming these disadvantages and achieving high mechanical properties. A combination of manufacturing process, matrix, and fibre define the end properties of a fibre-reinforced composite, and it is essential to select suitable materials and processes to achieve desired properties. Moulding and extrusion are the two manufacturing methods used to produce fibre-reinforced composites. Moulding involves shaping a composite using a mould, while extrusion forms the composite by pushing it through a die. While moulding requires significant upfront costs related to mould design and tool fabrication and is generally preferred for high-precision, large-scale manufacturing of complex parts, extrusion is cost-effective to setup and preferred for high-speed production [13–15].

Fused deposition modelling (FDM), an extrusion-based 3D printing method, has gained popularity as a manufacturing method for polymers and polymer composites because of its ease of setup, ability to 3D print complex geometries, and potential for reduced material waste compared to traditional manufacturing methods like injection moulding (IM) and compression moulding (CM) [16–18]. FDM 3D printing is primarily compatible with thermoplastic polymer filaments as the working principle of FDM is based on material melting and solidification. Thermosetting polymers undergo irreversible curing and are not conventionally used in FDM. However, a recent study explored a modified FDM process for printing with thermoset polymer composites [19]. Bio-derived thermoplastics and their composites have been extensively studied for FDM applications to combine the advantages of bio-derived materials and FDM technology. However, a research gap exists in achieving mechanical properties comparable to or higher than traditional manufacturing methods like IM and CM [20–22].

The factors influencing the properties of FDM 3D printed bio-derived composites are fibre and matrix selection, fibre-matrix interfacial strength, fibre orientation, and fibre distribution. In a composite, generally, the fibres provide stiffness and strength to carry the applied loads, while the matrix binds the fibres together, transmits the loads through the interface to the fibres, and shields the fibres from mechanical damage and environmental factors [23].

A wide range of bio-derived fibres are available to be used as reinforcements. Bio-derived fibres can be broadly classified into natural and synthetic. Natural fibres can be classified into plant, animal, and mineral [24]. Plant fibres are further classified into six types of fibres, including bast, wood, leaf, straw, grass, and seed fibres. Animal fibres constitute protein and are classified into hair and silk. Mineral fibres are in the asbestos group of minerals and are not preferred due to their carcinogenic nature. Bast fibres such as flax, hemp, and ramie have the highest tensile strength and modulus amongst all the bio-derived fibres. Animal fibres have low mechanical properties compared to other bio-derived fibres except for silk. However, silk is expensive and has a lower stiffness than other fibres [23]. Man-made or regenerated cellulose fibres are classified into lyocell, viscose, and modal [25].

Similar to bio-derived fibres, a wide range of bio-derived matrices are also available. Poly (lactic acid) (PLA) is a bio-derived and biodegradable thermoplastic polymer that is the most used for FDM 3D printing because it has the highest tensile and flexural strengths compared to other bio-derived thermoplastics and is more readily available [12,26]. PLA composites with bio-derived reinforcements such as flax, hemp, jute, bamboo, and other natural fibres have been widely researched for FDM 3D printing to enhance mechanical properties, reduce material and production costs, and improve the sustainability of manufactured products [27,28].

Interfacial bonding between fibre and matrix is crucial for achieving optimal stress transfer and high mechanical properties in bio-derived fibre-reinforced composites. The fibre/matrix interface is influenced by factors such as the compatibility of reinforcement and matrix materials, fibre surface, and fibre wettability by the matrix [6]. Successful interfacial bonding occurs when the matrix adequately wets the fibre. This bonding can occur through mechanical interlocking, chemical bonding, or inter-diffusion bonding in bio-derived fibre-reinforced composites. Mechanical interlocking happens when the fibre surface is rough, allowing the matrix to penetrate and flow around the fibres, creating interlocking sites. Chemical bonding requires a reaction between chemical groups on the fibre surface and the matrix, often facilitated by surface treatments, compatibilisers, or coupling agents. Interdiffusion bonding occurs through the mutual exchange or diffusion of polymer chains across the fibre-matrix interface. Different bonding mechanisms may be observed at the interface in bio-derived fibre-reinforced composites [23].

High-performance bio-derived fibre-reinforced composites are associated with the alignment of fibres parallel to the load direction, longer fibres, and a homogeneous distribution of fibres in the matrix. Aligned fibres enhance load-bearing capacity and impact resistance by creating an effective load transfer path from the matrix to the fibres compared to randomly oriented fibres. The length of reinforcing fibres influences interfacial shear strength (IFSS), with longer fibres generally improving IFSS due to increased surface area for interaction with the matrix. Homogeneous fibre dispersion helps reduce voids and ensures the fibres are surrounded by the matrix [23]. However, achieving proper fibre

alignment and distribution poses challenges during manufacturing. Long fibres are easier to align than short fibres due to reduced entanglement chances and less influence of polymer flow. Natural fibres spun into yarns or continuous human-made bio-derived fibres offer high fibre alignment, but achieving homogeneous distribution becomes challenging due to yarn twist. Manufacturing processes also impact fibre alignment; for instance, incorporating long/continuous fibres in injection moulding (IM) is challenging. Compression moulding allows fibre alignment using prepregs or layup processes. Some alignment is possible for short fibre-reinforced composites during FDM 3D printing, where shear forces in the nozzle align fibres along the flow direction. Integrating long/continuous bio-derived fibres in FDM 3D printing as yarns presents challenges in achieving good fibre wetting and homogeneous distribution due to the twisted nature of yarns [29].

1.2 Research Rationale

Incorporating long/continuous fibres has proven efficient in significantly improving the mechanical properties of bio-derived composites. Therefore, developing long/continuous fibre-reinforced materials represents a critical step forward in achieving high-performance 3D printed composites. Literature shows that fibres such as flax, ramie, and jute have already been used to develop high-performance FDM 3D printed composites [30–33]. However, the mechanical properties of these composites are still not comparable to traditional long/continuous fibre composites produced by compression moulding techniques [34]. A weak fibre matrix interface between the hydrophilic bio-derived fibres and the hydrophobic thermoplastic matrix and poor interlayer adhesion from the FDM method are the main contributors to the low mechanical properties of these composites [23].

The present research focuses on developing high-performance composite materials reinforced with long/continuous bio-derived fibres while improving fibre wettability. Flax (standard and bleached variants) and viscose yarns were selected as reinforcements, and PLA was selected as the matrix based on mechanical properties and commercial availability. Most of the literature on FDM 3D printing with long/continuous reinforcements focuses on improving the FDM process to achieve better performance [30,32,35,36]. Some studies have been conducted to modify the fibre surface to improve interfacial bonding. However, existing studies on fibre modification of long/continuous fibres have not shown much improvement in composite properties [37]. A gap in the existing literature can be observed where there has been no reported literature on improving the FDM filament production process to enhance interfacial bonding using impregnation methods, which have been proven successful for techniques like compression moulding [38,39].

This study employed two impregnation methodologies – solution impregnation and emulsion impregnation- for fibre wetting by PLA. The impregnation bath was designed to facilitate thorough wetting of fibres and uniform matrix distribution. The impregnation processes were compared, and efforts were made to optimise the production. The filaments produced from the impregnation process

were further consolidated and used to produce 3D printing filament with optimised fibre content suitable for available FDM machines. FDM printing parameters were adjusted to enable printing with high fibre content and fewer voids.

1.3 Research Objectives

This study aims to improve the mechanical properties of FDM 3D printed bio-derived composites by incorporating flax and viscose yarns as reinforcements in the PLA matrix. The specific objectives of this research are specified as follows:

1. To study the properties of flax and viscose fibres as suitable reinforcements for PLA-based composite filaments.
2. To develop impregnation processes and methodology to achieve optimum impregnation of PLA into long/continuous bio-derived fibres.
3. To assess the effect of impregnation processes on the mechanical properties of composites produced and to compare the obtained properties with theoretical composite mechanical properties.
4. To produce composite filaments suitable for FDM 3D printing using the impregnated composites and assess the mechanical properties of the 3D printing filaments.
5. To produce 3D printed composites from the filaments, assess the mechanical properties of 3D printed composites, and evaluate the effects of the printing process and parameters.

1.4 Thesis Structure

This thesis is organised in 7 chapters. The purpose of each chapter is as follows.

Chapter 1: Introduction to the research topic with research background, research rationale, and an outline of the thesis.

Chapter 2: A literature review of the research topic. A complete review of bio-derived fibres and matrices, factors influencing the performance of bio-derived fibre-reinforced composites, FDM 3D printing, and current state of the art of FDM 3D printing of bio-derived composites.

Chapter 3: Characterisation of viscose, standard flax, bleached flax reinforcements and PLA matrix.

Chapter 4: Solution impregnation methodology and characterisation of consolidated filaments.

Chapter 5: Emulsion impregnation methodology and characterisation of consolidated filaments. Comparison of solution and emulsion impregnated filaments.

Chapter 6: Production and characterisation of 3D printing filaments, 3D printing methodology, and characterisation of 3D printed composites.

Chapter 7: Recommendations and future work based on the current findings.

Chapter 2: Literature Review

2.1 Introduction

The review starts with an introduction to 3D printing and the significance of bio-derived fibre reinforced composites for 3D printing. A detailed literature review of the reinforcements and matrices used in this study is presented. Following that, a current state of the art of FDM 3D printed biocomposites is given. The review ends with a literature survey of existing methods to develop and enhance the properties of 3D printed bio-derived fibre reinforced composites.

2.1.1 3D Printing

Additive manufacturing (AM), also known as 3D printing, enables the fabrication of complex geometries, consolidation of sophisticated assemblies, customisation of products, and reduction of material waste [40]. These advantages have supported massive growth in the 3D printing market in the past few years. There has also been a significant increase in the number of publications related to 3D printing in the two decades (Figure 1), with a total of 109,711 documents.

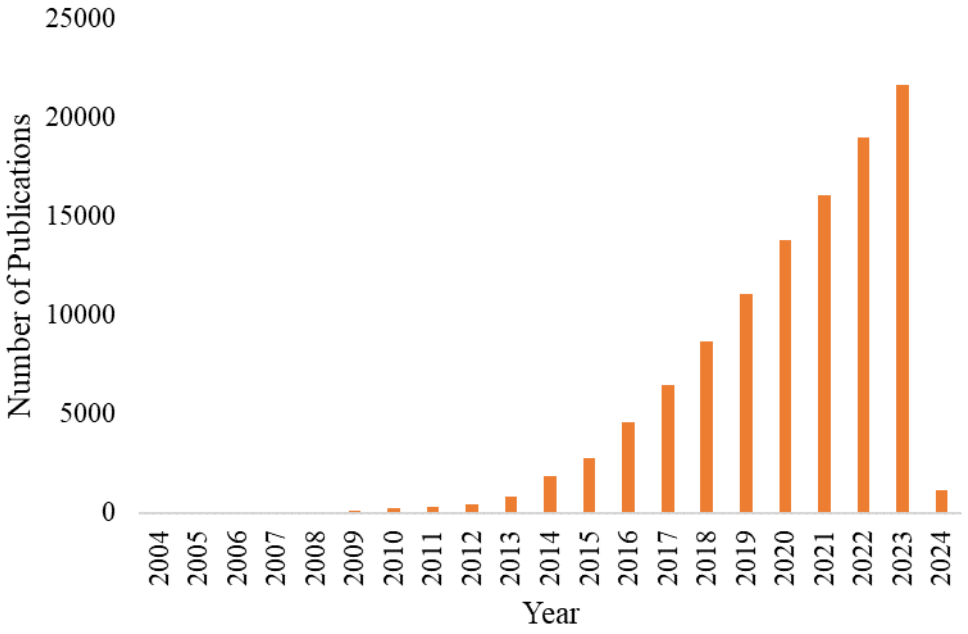

Figure 1 Number of publications in the Scopus database between 2005 and 2024 with the keywords: "3D printing" OR "additive manufacturing".

3D printing is an additive process in which a three-dimensional object is created from a digital model by adding material, typically in successive layers. 3D printing can be contrasted with traditional manufacturing processes that use subtractive approaches such as machining, grinding, and casting, where molten material is filled in a mould to create a product [41]. Some of the most commonly used 3D printing methods, classified according to ISO/ASTM 52900:2015, are material extrusion, vat photopolymerisation, powder bed fusion, and binder jetting [42–44]. Although most 3D printing

methods use a layer-by-layer manufacturing method, an innovative method named 3D freeform printing has been used to build complex geometries in open space with a robotic arm that houses an extrusion chamber. The robotic arm extrudes and places the material where required in a three-dimensional place to produce the final object [45,46].

A comparison of the number of publications in the last two decades for these 3D printing methods is shown in Figure 2, where fused deposition modelling (FDM), a material extrusion process, has the highest number of publications with a total of 5,183 documents. A variety of materials, including metals, polymers, resins, and powders, are used for 3D printing [47]. Polymers are the most commonly used materials, including thermoplastics, thermosets, hydrogels, functional polymers, and polymer-based composites [48,49].

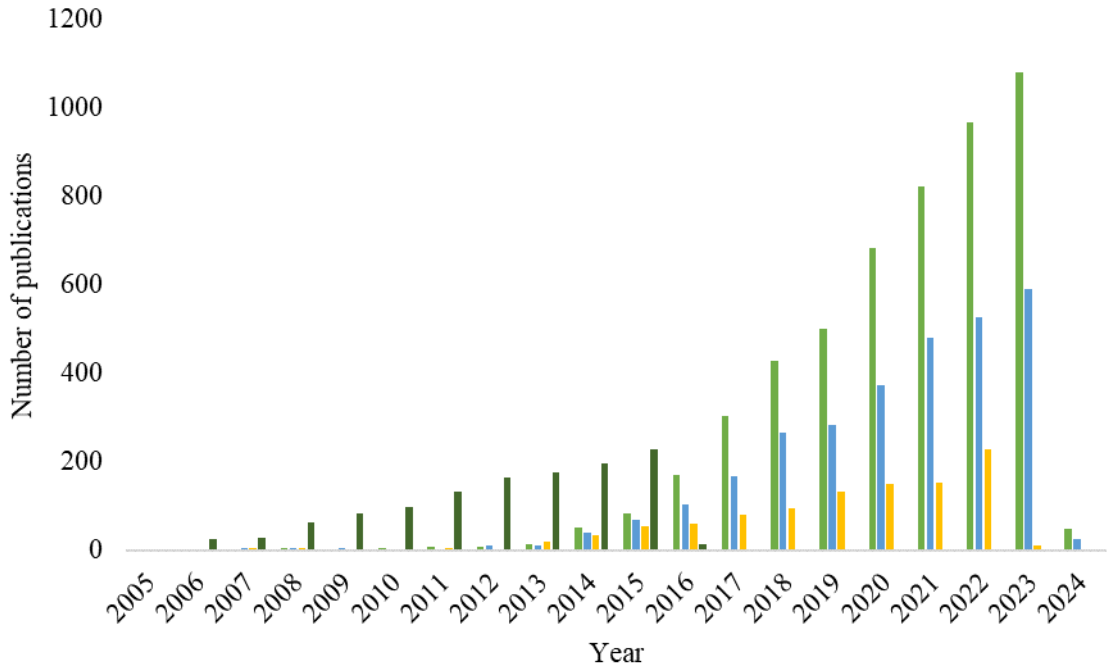

Figure 2 Number of publications in the Scopus database between 2005 and 2024 with the keywords: "3D printing" AND "fused deposition modelling"; "3D printing" AND "stereolithography", "3D printing" AND "selective laser sintering", and "3D printing" AND "selective laser melting".

Applications of 3D printing technologies include architecture, medicine, food, automotive, and various other industries [11,15]. A novel application of 3D printing technology is 4D printing, which involves manufacturing objects engineered to react to an external stimulus in a useful way [40]. 4D printing utilises smart materials programmed to exhibit changes in one or more properties in a controlled manner on the application of an external stimulus [50], such as heat, light, water, or UV light [51].

2.1.2 Bio-derived materials in 3D Printing

There is increasing awareness in the 3D printing industry regarding sustainable alternatives to current materials [12]. According to statistics [52], thermoplastics are the most commonly used materials for 3D printing [53], and FDM is the most used technology [52][54]. However, extensive use of petrochemical-based thermoplastics does not align well with achieving a circular economy. Consequently, there has been a significant interest in incorporating bio-derived polymers and their composites as alternatives for conventional oil-based polymers to make the additive manufacturing industry more sustainable [55].

As mentioned earlier, the use of bio-derived fibre reinforced composites as a replacement for synthetic materials comes with many advantages, including low environmental impact, favourable strength-to-weight ratio, and cost-efficiency. The main disadvantages include lower mechanical properties, moisture sensitivity, and low durability. Improving these properties can help broaden the application of 3D printed bio-derived composites to more structural applications that have high load-bearing requirements. Some of the current applications for 3D printed bio-derived composites include non-structural automotive elements, interior aerospace components, architectural models, medical devices, and shape memory applications [56].

2.2 Bio-Derived Fibre Reinforcements

Reinforcement is considered the principal component in a composite system, with the primary function of improving the mechanical properties of the composite [5]. In this work, reinforcement is defined as the component that at least improves Young's modulus of the resulting composite when added to the polymer. Bio-derived reinforcements used in composite production can be classified into micro (100 μm to 100 nm diameter) and nano (100 nm to 1 nm) reinforcements, which are further classified into fibre and particle reinforcements based on their shape and size, as shown in Figure 3. Fibres are elongated structures with a diameter of nm and high aspect ratios, whereas particles are often spherical rod-shaped with smaller aspect ratios. This classification is based on the forms of reinforcement used from a material processing perspective. Bio-derived micro fibre reinforcement forms are further classified into discontinuous and continuous, where single fibres and chopped fibre bundles are discontinuous reinforcement forms and yarns are continuous reinforcement forms [57]. It is worth noting that plant fibres such as flax are not continuous in nature. A continuous fibre is characterised by an unbroken, single strand extending long lengths without interruption. In contrast, natural fibres like flax are naturally limited to a few centimetres in length. So, these fibres are fabricated into yarns typically composed of individual fibres twisted or spun together to be used as continuous reinforcements. Within the bio-derived fibres, human-made regenerated cellulose fibres such as viscose

and lyocell are available in a continuous fibre form. Nano reinforcements are classified into nano fibre and nanoparticle reinforcements [58].

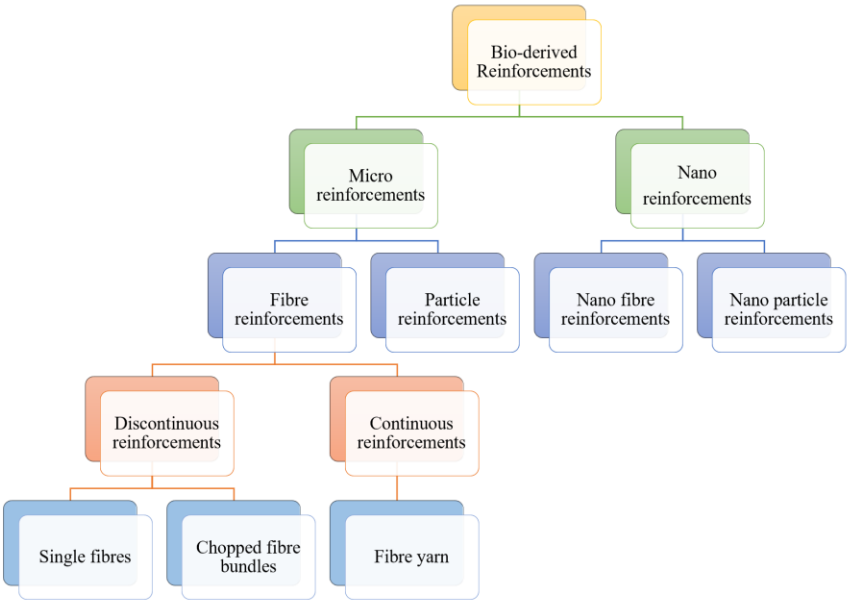

Figure 3 Types of bio-derived reinforcements used in FDM composites.

Bio-derived micro fibres are the most commonly used reinforcements, and their sources can be natural and human-made, as shown in Figure 4. A list of properties of bio-derived fibres is given in Table 1. Production of regenerated cellulose fibres typically involves pre-treatment of cellulose with a solvent to swell the cellulose molecules and induce chain relaxation, followed by a spinning process. The viscose process is the oldest method to produce regenerated cellulose fibres, where derivatizing is used to modify cellulose, followed by dissolution and spinning. The traditional viscose process results in a fibre with a skin and core-layer structure where the skin layer has a higher crystallinity than the core [59]. The process for obtaining modal fibres is similar to viscose, except the fibres undergo treatment after the spinning process to improve the molecular alignment thereby increasing the strength of the fibres [60]. Recently, commercial viscose fibres such as Cordenka® with all skin have been developed to have higher tensile properties than the modal fibres [61]. Lyocell fibres, on the other hand, are produced by a direct dissolution of cellulose using ionic liquids or N-methylmorpholine-oxide (NMMO). The Lyocell process is relatively new and is considered environmentally friendly compared to viscose and modal processes due to the ability to recover more than 90% of the solvents used [62]. Various natural fibre reinforcements, including flax, hemp, jute, and harakeke, have been widely used for FDM 3D printing [63–67]. Human-made fibres such as lyocell and viscose have only been recently explored for FDM applications [68] [69,70,70–73].

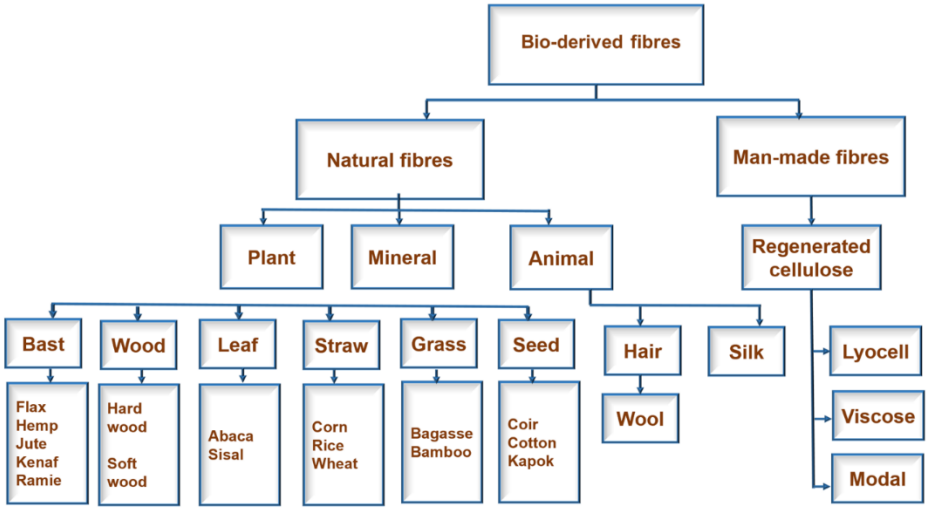

Figure 4 Classification of bio-derived fibres

Table 1 Properties of bio-derived fibres [23,74–77].

Fibre	**Density (g/cm^3)**	**Length (mm)**	**Tensile strength (MPa)**	**Young's modulus (GPa)**	**Failure strain (%)**
Ramie	1.5	900–1200	400-938	44-128	2-3.8
Flax	1.5	5-900	345-1830	27-80	1.2-3.2
Hemp	1.5	5-55	550-1110	58-70	1.6
Jute	1.3-1.5	1.5-120	392-800	10-55	1.5-1.8
Harakeke	1.3	4-5	440-990	14-33	4.2-5.8
Sisal	1.3-1.5	900	507-855	9.4-28	2.0-2.5
Alfa	1.4	350	188-308	18-25	1.5-2.4
Cotton	1.5-1.6	10-60	287-800	5.5-13	3.0-1.0
Coir	1.2	20-150	131-200	4-6	15-30
Curaua	1.1-1.4	1000-1500	700-1100	30-40	3.3-3.9
Silk	1.3	Continuous	100-1500	5-25	15-60
Feather	0.9	10-30	100-203	03-10	6.9

Wool	1.3	38-152	50-315	2.3-5	13.2-35
Viscose	1.32	Continuous	308-833	11-20	17-25
Modal	1.5	Continuous	515 - 570	14-16	11-13.2
Lyocell	1.5	Continuous	552-1019	4.7-13.36	8-9.4

As mentioned in section 1.2, flax and viscose fibre yarns were selected as reinforcements in the present work. The following sections provide a detailed overview of the structure, composition, and properties of these fibres.

2.2.2 Flax Fibre

Flax (*Linum usitatissimum*) is one of the most used bast fibres across various industries, including textile, packaging, construction, consumer goods, and composites [78]. Production and utilisation of flax have increased significantly in the last few decades as the focus towards sustainable materials increased. Most of the world's flax is produced in Canada, France, Belgium, and the Netherlands [79]. Flax fibre production begins by planting flax plants, which are later harvested when the leaves turn yellow. After harvest, the flax goes through retting, a biological process that separates the fibres from the straw using water, possibly as dew. After retting, the fibres are beaten to remove impurities such as residual straw, scutched, and hackled to straighten them. Finally, the processed flax fibres can be spun into yarns and used for textiles, composites, or other applications, as shown in Figure 5 [80]. Processed flax fibres can be used as reinforcements in different forms, such as short chopped fibres, twisted yarns, rovings, woven and non-woven fabrics, and unidirectional tapes, depending on the manufacturing method and desired properties [81].

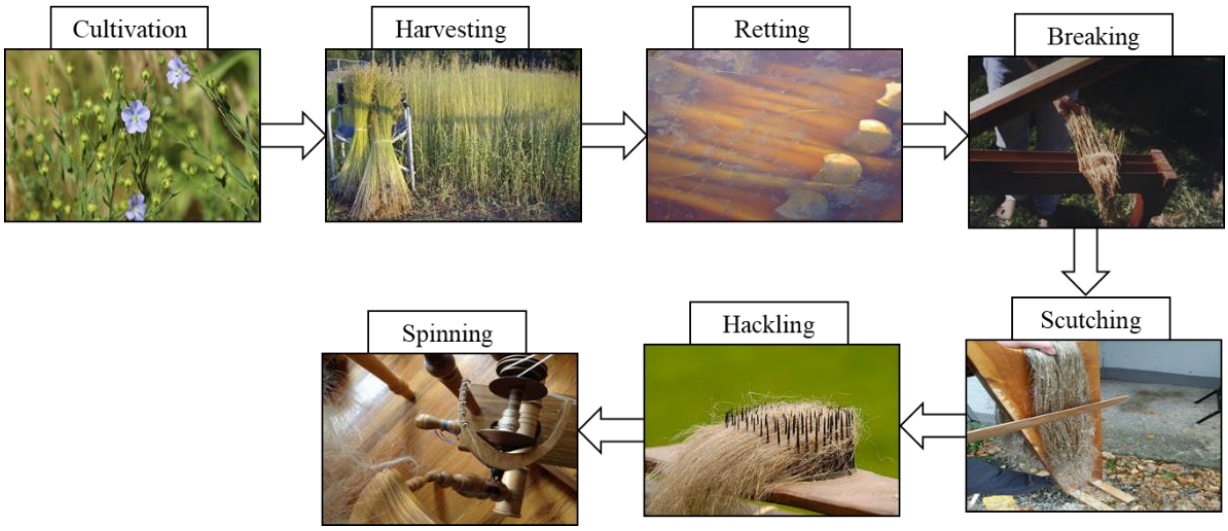

Figure 5 Flax fibre production process

Structure

Flax fibres, derived from the stem of the flax plant, exhibit a hierarchical structure characterised by intricate layers of cellulose microfibrils, hemicellulose, and lignin. Figure 6 shows the multi-scale schematic of flax fibres from the stem to the cellulosic fibril level. Flax fibre bundles have an average length of 90 mm, and a single fibre has an average diameter of 12 μm to 16 μm [82,83].

At a macroscopic level, a progression from the outermost to the inward structure of the flax stem typically comprises the bark, phloem, xylem, and, at its core, a central void. Several fibres linked with pectin and hemicellulose can be observed from the cross-sectional view. At the microscopic level, each elementary flax fibre comprises concentric cell walls of varying thickness and arrangement. The central lumen aids in water uptake, as shown in Figure 6. The primary cell wall, only 0.2 μm thick, coats the thicker secondary cell wall responsible for fibre strength. The bulk of the fibre comprises the S2 layer (Figure 7) in the secondary cell wall, containing crystalline cellulose micro-fibrils and amorphous hemicellulose oriented at 10° to the fibre axis, imparting high tensile strength [82].

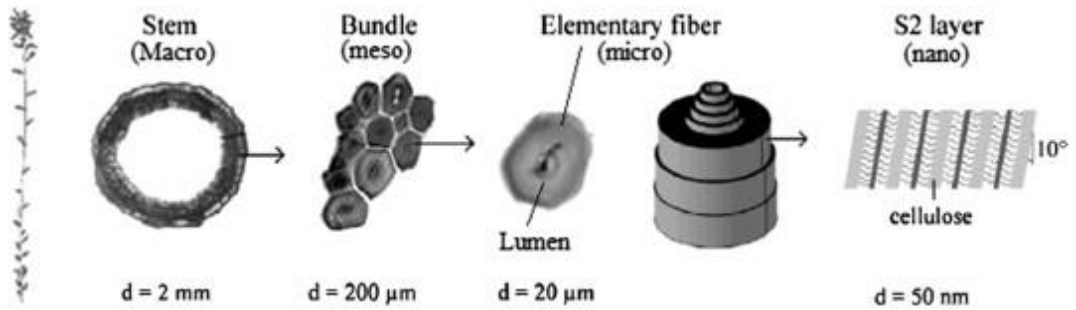

Figure 6 Structure of flax from stem to microscopic level [82]

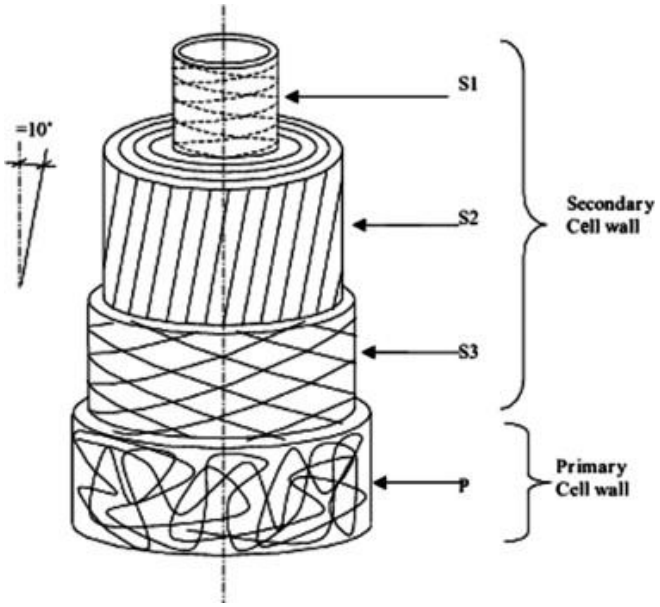

Figure 7 Microstructure of the flax fibre [82]

At the nanoscale, each microfibril can be considered a composite consisting of crystalline cellulose chains within an amorphous matrix of pectin and hemicellulose and amorphous cellulose. These microfibrils, forming approximately 70% of the fibre's weight, likely serve as its reinforcing material. The orientation angle of these micro-fibrils with respect to the fibre axis can impact the fibre's strength, with a spiral orientation contributing to greater ductility [82,83].

Chemical Composition

Constituents of flax include cellulose, hemicellulose, lignin, pectin, and wax in varying proportions. Cellulose, representing 65 to 75% of flax fibre weight, is the strongest and stiffest, characterized by its semi-crystalline structure with abundant hydroxyl groups, making the fibre hydrophilic. Cellulose exists in four polymorphs – cellulose I, II, III, and IV [84,85]. Plant fibres like flax have naturally occurring cellulose called cellulose I, which exists in parallel strands without intersheet hydrogen bonding. Repeating b-D-glucopyranosyl building blocks that are covalently linked by b-1,4-glycosidic bonds between the hydroxyl groups of C4 and the C1 carbons, as shown in Figure 8. Cellulose I is distinguished by its hydrophilic nature, crystalline structure, and its capacity for chemical modification owing to the abundant hydroxyl groups it contains. These hydroxyl groups serve as the foundation for an extensive network of hydrogen bonds, resulting in a highly rigid and well-ordered molecular structure of cellulose [86].

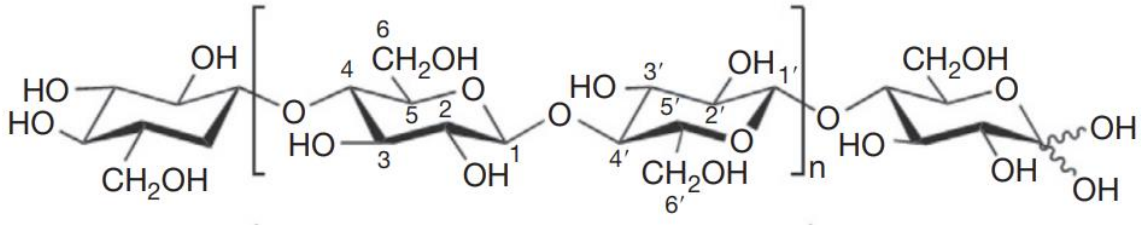

Figure 8 Chemical structure of Cellulose I present in flax fibres [86].

Hemicellulose makes up 20 to 30% of the fibre weight, plays a role in binding fibres, and contributes to flexibility. Lignin contributes 5 to 10% and adds rigidity and resistance to decay. Other minor components, such as pectin and wax, contribute 1 to 2% of the fibre weight. Lignin and pectin primarily serve as bonding agents, with lignin being an amorphous, complex, mainly aromatic polymer. Lignin exhibits the lowest water absorption among natural fibre components. Waxy substances in flax fibres negatively influence fibre wettability and adhesion characteristics. The variation in the proportions of flax fibre constituents depends on factors such as plant species, variety, soil quality, weather conditions, plant maturity, retting process, and measurement conditions [79,82,87,88].

Tensile Properties

Similar to the chemical composition, the tensile properties of flax fibres also vary highly. Data from various publications gives average values as tensile strength of 600 to 2000 MPa, stiffness of 12 to 85 GPa, and elongation at break 1 to 4% [87–89]. The tensile properties of single flax fibres are mostly recorded using the Single fibre fragmentation (SFF) test according to the ASTM D3379 standard [90].

The variation in the reported tensile properties is subject to loading conditions, environmental factors, and factors such as variety, growth conditions, and defects introduced during stages from retting to reinforcement preparation. One of the main challenges in using current methods to determine the mechanical properties of single fibres is calculating the fibre diameter. Flax fibres are non-circular and have a lumen running through their cross-section. However, without complete 3D characterization, the effective cross-sectional area is estimated using the apparent diameter, defined as the width observed under a microscope. Gauge length and diameter also influence the properties of flax fibres. Flax fibres are brittle and have been observed to follow Griffith's weakest link theory. This theory states that the presence of critical flaws limits strength, with longer or larger objects likely containing more defects and thus exhibiting lower strength, predictable by a Weibull distribution [83,91].

Tensile properties of flax fibres have also been observed to correlate with the fibre's chemical composition. Higher cellulose content relates to higher mechanical properties because of reduced interfibrillar distance with more cellulose. A negative correlation between the microfibril angle and Young's modulus was observed. Fibres with a smaller microfibril angle have microfibrils oriented more

closely to the fibre's longitudinal axis. This alignment contributes to higher stiffness because the microfibrils offer greater resistance to deformation [90].

The tensile behaviour of a single flax fibre can be understood from a typical stress-strain curve shown in Figure 9. The tensile stress-strain curve exhibits three distinct regions: an initial linear region (0% to 0.3%), representing global loading through cell wall deformation; a subsequent non-linear region (0.3–1.5%) attributed to elasto-visco-plastic deformation, particularly in the thickest cell wall (S2), due to micro-fibril alignment and re-arrangement of amorphous components; and a final linear region (1.5% to failure) corresponding to the elastic response of aligned micro-fibrils to applied tensile strain [82].

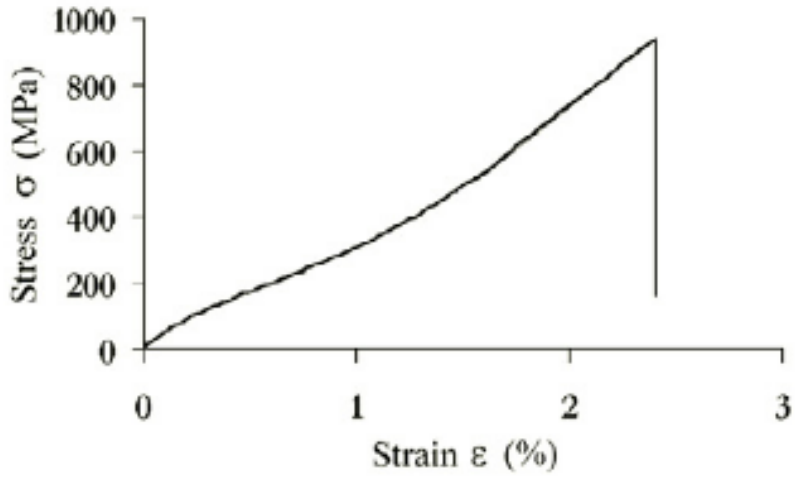

Figure 9 Example of a stress-strain curve of a single flax fibre [92]

Factors Influencing the Reinforced Composite Properties

Apart from the structure, composition, and mechanical properties of a reinforcing fibre, the choice of reinforcement architecture (yarn/short fibre/mat), manufacturing process, matrix material, and surface treatment also significantly influence the resulting composite properties. Flax fibre architecture usually depends on the application and properties desired. Table 2 lists commonly used forms of flax fibres as reinforcements and their applications. This table provides processes related to flax fibres reinforced with thermoplastic matrices only, and the data is in a generalised context without considering the factors of fibre weight percentage, fibre matrix adhesion, and processing conditions.

High mechanical properties were observed in composites reinforced with UD flax tapes compared to other forms due to the alignment of fibres in the direction of load. A high fibre content and less fibre/fibre and fibre/matrix friction are also the advantages of using UD tapes [38][93,94]. Rovings are similar to UD tapes but do not have a flat and highly aligned structure, making them more challenging to handle for composite production. Yarns also have the alignment of fibres, but a major disadvantage of using yarns is their twisted nature, which contributes to high fibre/fibre friction and complicates the

uniform matrix distribution around the fibres [95,96]. However, yarn-reinforced composites offer improved impact resistance due to their ability to absorb and distribute energy effectively [97]. Chopped fibres and non-woven mats have short-length fibres with random orientations, due to which the load-bearing capacity of the composite reduces and the possibility of fibre agglomeration increases [83,94,98,99].

Table 2 Commonly used types of flax reinforcements with different manufacturing processes.

Flax Architecture	**Manufacturing process**	**Tensile strength of the reinforced composite**	**Reference**
Unidirectional (UD) Flax Tapes	CM, Sheet lamination	High (>350 MPa)	[38][93,94]
Woven Flax Fabrics	CM, Sheet lamination	Moderate to high (250 to 350 MPa)	[99–102]
Non-Woven Flax Mats	CM	Low to moderate (<200 MPa)	[83,94,98,99]
Short Flax Fibres	IM, 3D Printing, CM	Low to moderate (<200 MPa)	[82,103,104]
Yarns	3D Printing, Tape laying	Moderate (200>TS<250 MPa)	[38][103]
Roving	CM, Tape laying	Moderate to high (250 to 350 MPa)	[94,99,101]

Flax fibre surface also plays a significant role in the resulting composite properties. Without any treatment, the interfacial bonding of the hydrophilic flax fibres with the hydrophobic matrices is limited. Fibre surface treatments can be physical, like plasma treatment, chemical, like alkaline treatment, or biological, like enzyme treatment. Table 3 summarises some commonly used surface treatments, their mechanisms, and their effects on composites.

Table 3 Flax fibre surface treatments and their effects on composites

Surface treatment	Mechanism	Effects on composite	References
Alkali Treatment (Chemical)	Removal of lignin and hemicellulose for increased surface roughness and hydroxyl group concentration using sodium hydroxide (NaOH)	Reduced water absorption, enhanced fibre-matrix adhesion	[105–107]
Silane Coupling Agents (Chemical)	Silanes (mostly trialkoxysilanes) form chemical bonds between the fibre surface and polymer matrix.	Enhanced fibre-matrix adhesion, improved mechanical properties	[97]
Acetylation (Chemical)	Introduction of acetyl functional group (CH_3COO^-) into an organic compound, reduction of fibre hydrophilicity	Reduced water absorption, improved compatibility with hydrophobic polymer matrices	[108]
Plasma Treatment (Physical)	Modifying surface polarity by exposing fibres to ionised gas, creating highly reactive species	Enhanced fibre-matrix adhesion, better fibre dispersion	[109,110]
Grafting (Chemical)	Addition of specific functional groups for enhanced interaction. Maleic anhydride grafting is most commonly used for flax.	Improved fibre-matrix adhesion and mechanical properties	[111,112]
Isocyanate Treatment (Chemical)	Introduction of isocyanate functional groups that form covalent bonds with the polymer matrix	Reduced stress concentrations, improved mechanical properties	[113,114]
Enzyme Treatment (Biological)	Enzymatic modification of fibre surfaces with enzymes such as cellulase to selectively remove the amorphous regions of the fibre surface	Enhanced fibre-matrix adhesion, improved mechanical properties	[115–117]

2.2.3 Viscose Fibre

Viscose fibre, a regenerated cellulose material with a long history in the textile industry, is gaining attention as a reinforcement for composite materials. Viscose fibre, which can be manufactured as continuous fibres, presents an attractive option as continuous bio-derived fibre reinforcement in composites compared to plant fibres, which are typically not readily available in continuous form.

Regenerated cellulose fibres like viscose and lyocell have high tensile strength and elongation at break, which can be beneficial for developing high-performance bio-derived composites. Lyocell fibres have slightly higher mechanical properties than viscose fibres, as seen in Table 1. However, unlike viscose fibres, they are not commercially available in the form of continuous fibre yarns to be used in composite production.

The production of viscose fibres started in 1891, and the process was patented in 1893 [118]. The viscose production cycle is shown in Figure 10. The process starts with a suspension of wood pulp in NaOH. Followed by shredding and ageing, where the viscosity of the pulp depends on ageing time. Treatment with carbon disulfide (CS_2) forms cellulose xanthate, which is dissolved in lower concentration NaOH, initiating viscose formation via xanthogenation. The obtained polymer is precipitated in acid, allowing for simultaneous neutralization and cellulose regeneration using wet-spinning equipment. Subsequent washing and drawing steps yield pure regenerated cellulose fibre. Carbon disulfide used in viscose production can be recycled up to 70%, with the remainder converted into recoverable sulfuric acid (H_2SO_4) [118].

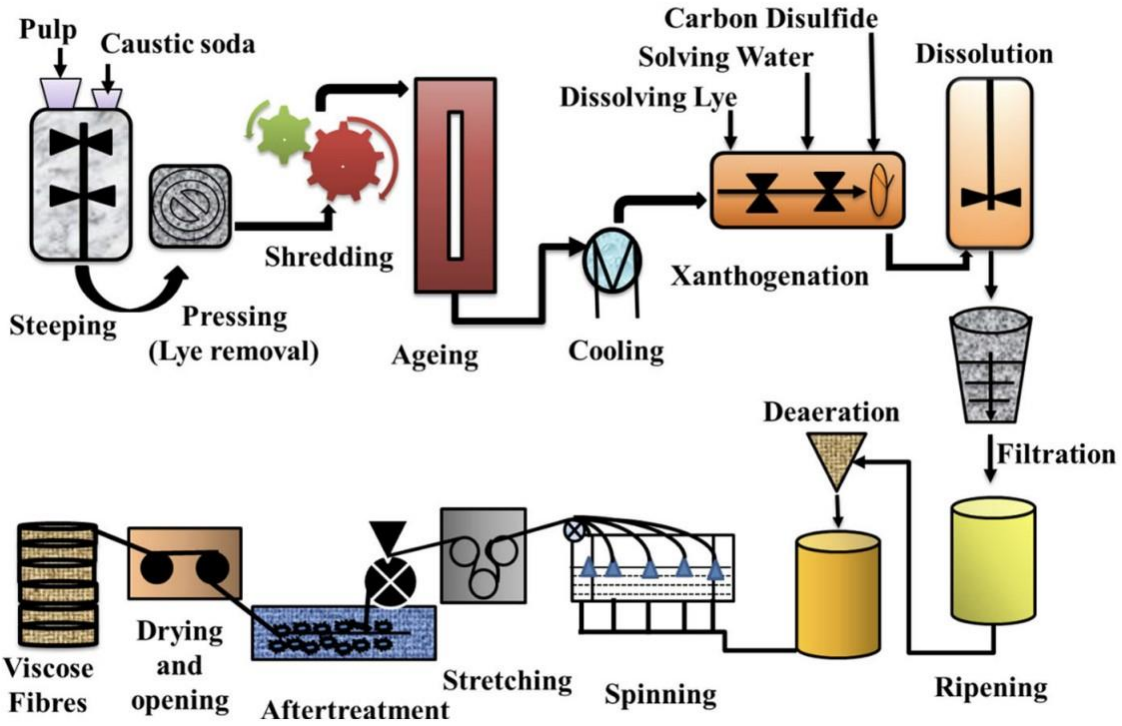

Figure 10 Viscose production process [119]

Structure

The structure of the viscose fibres develops during the manufacturing process. At the macro scale, viscose fibre appears as a long, flexible, slender strand with a smooth and cylindrical shape. At the

micro-scale, viscose fibres display an uneven surface structure and an irregular cross-sectional shape, as seen in Figure 11. This shape is a result of the production process. The stretching process can yield non-uniform cross-sectional shapes in the fibres as the viscose solution passes through spinnerets and encounters an acidic bath. Various factors, including spinneret design, coagulation conditions, and production parameters, can further influence the cross-sectional shape [62].

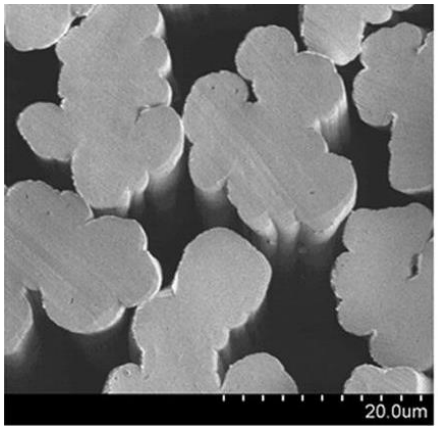

Figure 11 SEM image of the cross-section of viscose fibres [120]

Chemical Composition

The primary component of viscose fibres is cellulose. Some trace elements, such as cellulose xanthate and NaOH from the regeneration process, could also be found in viscose fibres. Cellulose in viscose is in the form of its polymorph cellulose II, composed of glucose units linked together by β-1,4-glycosidic bonds, as shown in Figure 12 (b) [121]. Cellulose II is formed from the chemical modification of cellulose I (Figure 12 (a)) during the introduction of xanthate groups in the viscose process and exists in anti-parallel cellulose chains to form a monoclinic unit cell with intersheet hydrogen bonding [120].

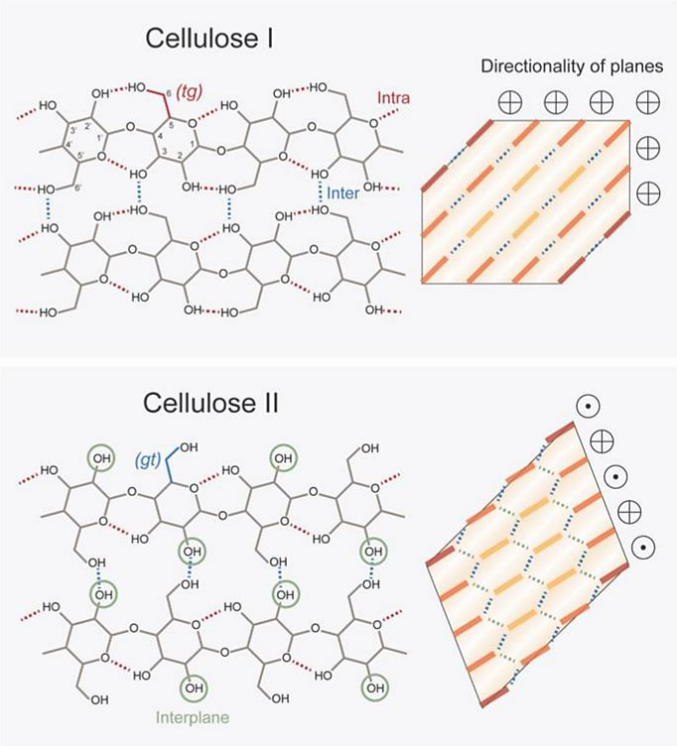

Figure 12 Chemical structure of (a) Cellulose I and (b) Cellulose II (The orientation of the hydroxymethyl groups is highlighted, denoted tg in cellulose I, and gt in cellulose II) [122]

Viscose fibres with cellulose II structure exhibit reduced tensile strength, reduced stiffness, and increased elongation at break as compared to natural fibres with cellulose I structure. The crystallinity of cellulose I (60% to 90%) [123] was measured to be higher than cellulose II (50% to 75%) [124], which could explain the high strength and stiffness in cellulose I fibres. The difference in mechanical properties could also be due to the differences in intramolecular and intermolecular hydrogen bonding, as seen in Figure 12. Cellulose I has two intra-molecular bonds ((O) 5-(OH) 3^{1} and (OH) 2-(O) 6^{1}) and one intermolecular bond ((O) 6- (O) 3^{11}), whereas cellulose II has one intra molecular bond ((OH)3-(O)5^{1}) and two intermolecular bonds ((OH)6-(O)211 for corner chains and (OH)6-(O)311 for centre chains). It has been reported that the intramolecular bonds contribute to the axial stiffness of cellulose. The number of intramolecular hydrogen bonds running parallel to the cellulose chains has been observed to influence the elastic moduli at the molecular level, where Cellulose I was observed to have higher moduli and higher resistance to stretching of crystalline regions in the fibre direction compared to Cellulose II [125,126]. The strength and stiffness of cellulose I and II also depend on different factors unique to each polymorph. The mechanical properties of Cellulose I improve with increasing cellulose content, increasing crystallinity, and decreasing microfibrillar angle, whereas the mechanical properties of cellulose II increase with smaller crystal size, increasing crystal alignment, and increasing crystallinity [119,120].

Tensile Properties

Viscose fibres are reported to have an average tensile strength of 308-833 MPa, Young's modulus of 11 to 20 GPa, and elongation at break of 17 to 25% [103]. Viscose fibres display an interesting stress-strain curve with significantly higher elongation capacity than natural fibres. A typical stress-strain curve of a viscose fibre can be seen in Figure 13 [127]. The stress-strain curve of viscose has two phases - initial linear elasticity up to the yield point, followed by a nearly linear phase leading to fracture [128].

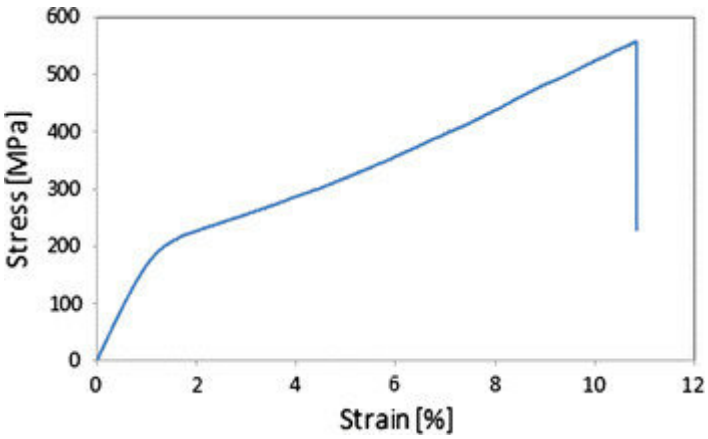

Figure 13 Stress-strain curve of viscose fibre [127].

Only a few researchers have studied the failure mechanism of viscose in the literature. Some researchers have mentioned that the failure mechanism of viscose fibre is not strictly brittle due to a large plastic deformation observed in the tensile behaviour [127,129]. However, it would be more accurate to distinguish that the viscose fibres display an increase in strength with an increase in elongation and a brittle or defect-driven failure. This is apparent from the fracture surface of the viscose fibre (Figure 14), which does not display any attributes of ductile failure, such as necking or striations from significant plastic deformation.

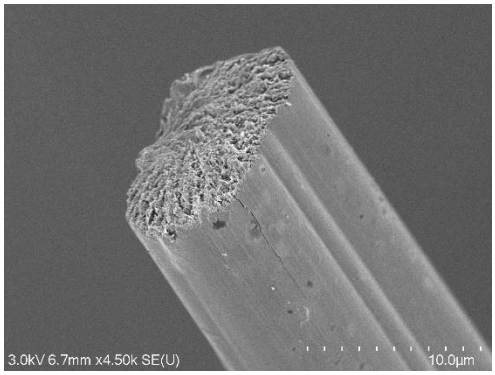

Figure 14 SEM of the fracture surface of viscose fibre

Attempts have been made to better understand the tensile behaviour of viscose fibres [94] [130] [127]. Weibull model was used to predict the distribution of tensile strengths of viscose fibres. Weibull model is a mathematical model usually used for brittle materials that follow Griffith's weakest link theory,

which states that the strength of the fibre is limited by the presence of critical flaws or defects, and the fibre will fail at the weakest point along its length. The Weibull distribution showed a good representation of experimental data for viscose fibres, and the results also agreed with the literature [127]. A study attributed the increase in strength in viscose fibres in the plastic deformation phase to the irreversible reorientation of cellulose crystallites in the longitudinal fibre direction [130].

Factors Influencing Reinforced Composite Properties

Similar to flax, the properties of viscose-reinforced composites also depend on fibre architecture, manufacturing process, selection of matrix, and fibre surface treatment. Viscose has a non-uniform cross-section, as mentioned before. This property of viscose was shown to be favourable for fibre/matrix adhesion as compared to a more uniform cross-section of lyocell, which is also a regenerated cellulose fibre. A comparative study of chopped viscose and lyocell as reinforcements for the PP matrix showed that viscose/PP composites exhibited improved strength and modulus compared to lyocell/PP composites. However, viscose/PP composites exhibited fibre/matrix adhesion issues, such as fibre pull-outs and clean fibre surfaces, which could be improved using MAPP as a coupling agent [131].

Only a few studies have explored the use of continuous viscose fibres as reinforcements so far. However, increased mechanical properties have established a clear potential for further research [132] [133] [134]. With the introduction of innovative high-strength fibres like Cordenka into the composites industry, the use of viscose as a reinforcement has increased. Composites produced with Cordenka fibre as reinforcement displayed higher impact strength than flax-reinforced composites. The impact strength of PLA/Cordenka (72 KJ/m^2) [135] was the highest compared to all other short bio-derived fibre-reinforced composites reported in the literature that used Charpy impact testing [136,137]. Continuous viscose (Cordenka) fibre reinforced composites have been recently explored for FDM 3D printing, and there was a significant increase in mechanical properties compared to neat polymer, proving the potential of these fibres [73].

2.3 Bio-Derived Polymer Matrices

Bio-derived polymers used for 3D printing include PLA, PHA (polyhydroxyalkanoates) [138] [139], Bio PE (bio-derived polyethylene)[140], PEF (poly(ethylene-2,5-furandicarboxylate))[141], Bio PC (bio-derived polycarbonate)[142], and Bio PA 11 (Polyamide 11) [143] as shown in Table 4. PLA is the most used and has the highest tensile and flexural strengths compared to other bio-derived thermoplastics used for 3D printing and is also preferred as it is more readily available [144].

Table 4 Mechanical properties of commonly used bio-derived thermoplastics.

Biopolymer	Tensile strength (MPa)	Young's modulus (GPa)	Elongation at break (%)	Flexural strength (MPa)	Flexural modulus (GPa)	Biodegradability	Reference
PLA	50 - 89.1	3 - 4	2 - 9	120-150	3.5 - 5	Biodegradable	[145]
PHA	15 - 40	1 - 2	1-15	17 - 61	1.4 - 3.2	Biodegradable	[138] [139]
Bio PE	18.4 – 17.9	1.4 – 1.9	5 - 7	18.7 - 19.8	0.8 - 1.01	Non-biodegradable	[146] [147]
PEF	67 - 77	2.7 - 2.9	2 - 4	-	-	Non-biodegradable	[148]
Bio PC	70.23 – 75.13	2.3 – 2.5	16.48 – 93.84	-	-	Non-biodegradable	[149][150]
Bio PA 11	52 – 54	1.7 – 1.8	28	-	-	Non-biodegradable	[143]

2.3.1 PLA

PLA is a bio-derived thermoplastic polymer synthesised from lactic acid obtained from corn, sugarcane, and other biomass. It is also a 100% biodegradable polymer with high tensile strength and modulus. PLA can be recycled up to 8 times and is compostable at the end of life [151]. The life cycle of PLA is shown in Figure 15.

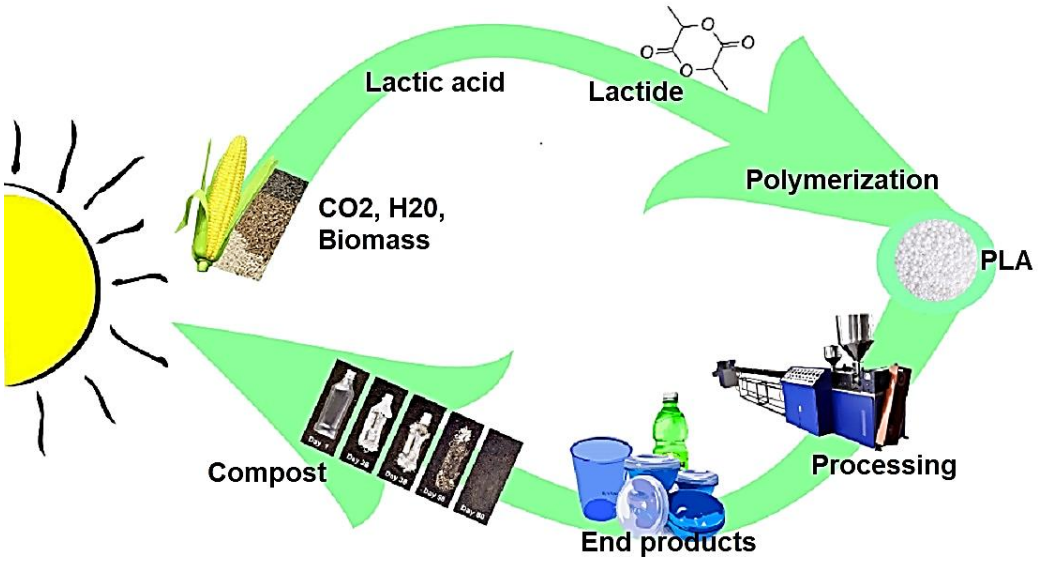

Figure 15 Life cycle of PLA.

PLA is synthesised from lactic acid in three ways – direct polycondensation of lactic acid (LA), azeotropic dehydrative condensation, and ring-opening polymerisation (ROP) of lactide (Figure 16). ROP is the most commonly used method as it yields high molecular weight PLA and requires low temperatures and short reaction times [152,153]. First, low molecular weight oligomers are produced by the continuous condensation reaction of aqueous lactic acid. Following this, the oligomer or prepolymer is catalytically converted into cyclic lactide. This cyclic lactide production results in three forms: D,D-lactide (D-lactide), L,L-lactide (L-lactide) and L,D- or D,L-lactide (meso lactide) as shown in Figure 17 [154]. The next step is distillation, where impurities are removed, and meso-lactide is separated. The final step involves the ROP of lactides to obtain different grades of PLA.

The stereochemical structure of PLA can be controlled by controlling the mixture of L- or D- isomers to obtain different proportions of crystalline and amorphous phases. The polymerisation of L-lactide produces poly (L-lactide) (PLLA), D-lactide produces poly (D-lactide) (PDLA), and racemic (50% L- and 50% D-) produces poly (DL-lactide) (PDLLA). PLLA and PDLA are optically pure polylactides and are crystalline, whereas PDLLA is amorphous. PLA can be degraded by simple hydrolysis without the use of enzymes to catalyse the hydrolysis [152].

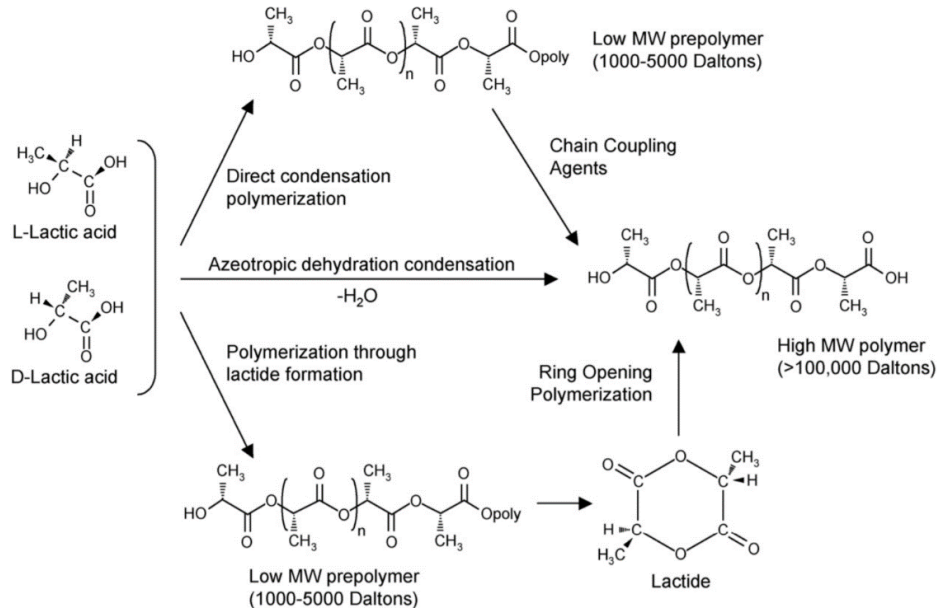

Figure 16 Methods of synthesising PLA from lactic acid [155] Reproduced with permission from Elsevier, license number 5124211449068.

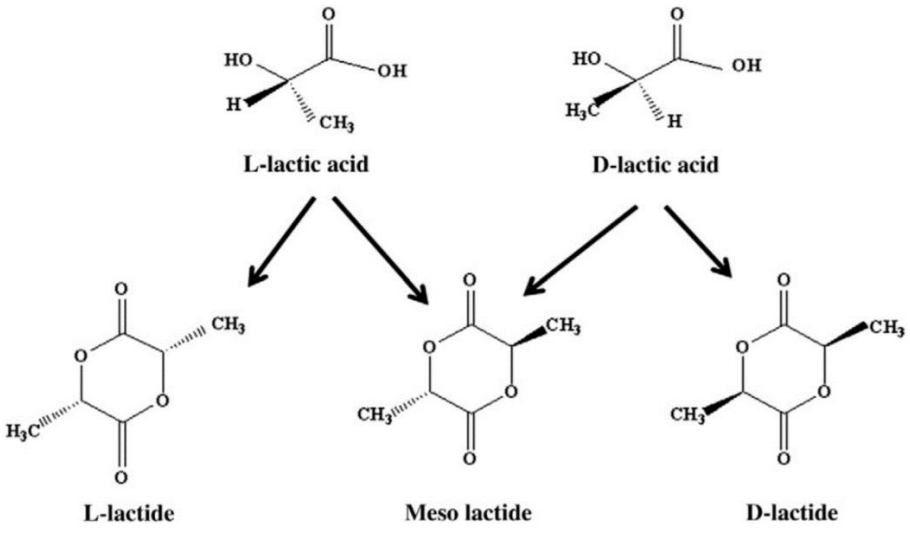

Figure 17 Stereoisomers of lactide [156]

The thermal, mechanical, and biodegradation properties of PLA depend on the distribution of the stereoisomers in the polymer chains. PLA with greater than 90% content of PLLA is highly crystalline, and a lower percentage of PLLA yields more amorphous PLA. The melting temperature (Tm) and glass transition temperature (Tg) of PLA increase with the increase of L-isomer content and decrease of D-isomer content [154].

Biodegradability of PLA

The degradation process of PLA begins with hydrolysis. In this process, water molecules break up the ester bonds along the chain of the polymer into smaller fragments of lower molecular weight; this is a process that depends both on temperature and pH, that is, at higher temperatures and acidic conditions, these reactions are faster [157]. After hydrolysis, fragments hydrolysed are broken down by microorganisms such as bacteria and fungi. These microorganisms secrete enzymes like proteases and lipases to break the polymer into lactic acid monomers. The microorganisms then break down the lactic acid monomers to form water, carbon dioxide, and biomass [158].

Degradation in Different Environments

Compost: PLA degrades efficiently in industrial composting installations. The temperatures of this process are about 58 °C – 60 °C and provide optimal hydrolysis conditions, with high microbial activity that leads to complete biodegradation within a few months. Home composting degrades PLA at a slower rate, ranging from several months up to years [159].

Soil: PLA degrades much more slowly in soil environments than in composting conditions since the temperatures are generally lower and microbial activity varies. Thus, even in optimal soil conditions, it may take some months, but it could also take several years for PLA to significantly degrade [158].

Marine Environment: PLA degrades very slowly in a marine environment compared to compost and soil. Low oxygen availability and, more importantly, the low concentration of microorganisms in seawater significantly lower the mechanism of hydrolysis and microbial activity. It is reported that PLA could remain intact for several years in the marine environment without any desirable type of degradation [160].

2.4 FDM 3D Printing

FDM, also referred to as fused filament fabrication (FFF) or material extrusion, is a 3D printing technique with various advantages, including low cost, moderate operating conditions, and large build volume capacity [16–18]. On the other hand, it has disadvantages such as limited accuracy, slow printing speeds, and shrinkage due to temperature changes [17].

The FDM process (Figure 18) begins by digitally slicing the 3D CAD model into layers, and the data, converted to a G-code (Geometric code for computer numerical control), is transferred to the 3D printing machine, which constructs the part layer by layer. Next, both the support material and the thermoplastic filaments, generally with diameters of 1.75 or 3 mm, are fed into the heated chamber and melted. The molten material is then extruded through nozzles in a layer-by-layer structure. Finally, the

finished part is removed from the build platform, and if necessary, the support material is removed [161].

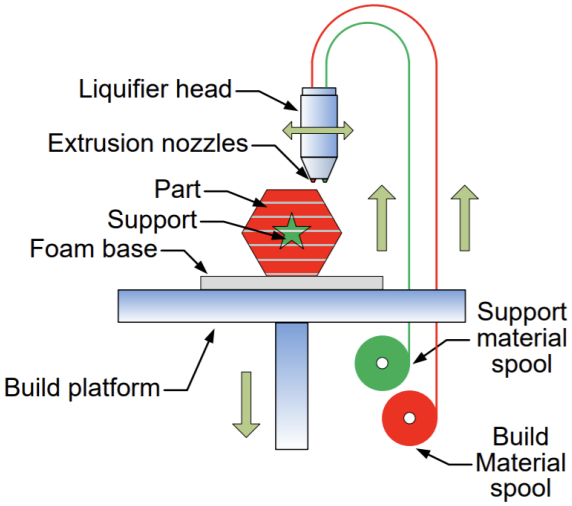

Figure 18 Schematic representation of fused deposition modelling method. Reproduced with permission from Elsevier, license number 5170280890406 [162].

Many studies have focused on the effects of FDM printing parameters on the performance of the 3D printed parts [16,163–166]. The parameters that affect an FDM printed part's quality include build orientation, raster angle, layer thickness, infill density, and extrusion temperature, as shown in Table 5 [167].

Table 5 Important printing parameters in FDM (adapted from [167–169]). Extrusion temperature: Reproduced with permission from Elsevier, license number 5166990649229; Infill density: Reproduced with permission from Elsevier, 5166991182219.

Parameters	Description	Graphical representation
Build orientation	Orientation of the component with respect to the build platform.	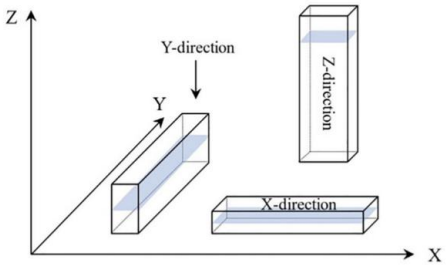

Raster angle	The angle between the path of material deposition and the x-axis of the build platform.	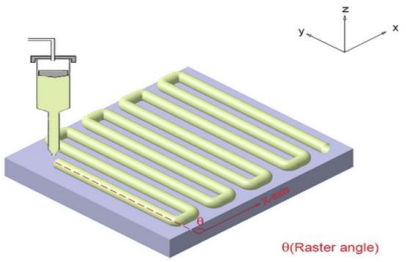
Layer thickness	A measure of the layer height deposited by the nozzle.	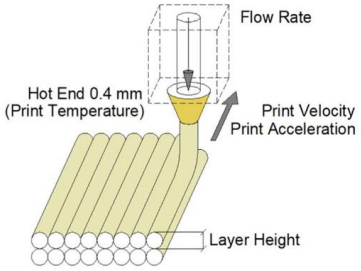
Infill density	Material percentage filling the internal structure of the printed component.	
Extrusion temperature	The temperature inside the nozzle before the material is extruded.	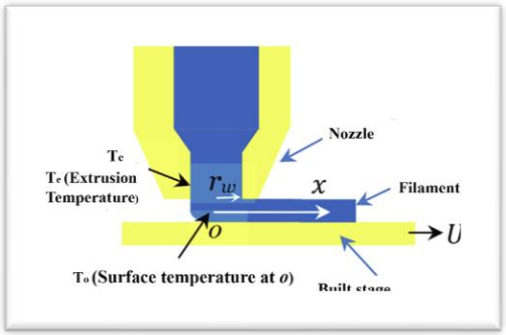

Build orientation is one of the most influential structural parameters in terms of the mechanical properties of FDM parts. Compared to parts printed in a perpendicular direction to the build platform, FDM parts printed in horizontal or vertical directions have a substantial decrease in mechanical properties [170–172]. Raster angle also influences the mechanical properties of FDM printed samples. Studies show that samples printed with a raster angle of 0° have the highest tensile properties, followed by 0°/90°, 45°/45°, and 90° [173–176]. Layer thickness and infill percentage are also important

parameters that influence the quality and mechanical properties of FDM printed objects. Increasing layer thickness improves print time but reduces surface finishing. A layer thickness between 0.1 to 0.4 is considered optimum for most FDM applications [174,177,178]. An increase in infill percentage improves the tensile properties in FDM printed parts. Hence, most studies on improving the mechanical performance of FDM parts select an infill percentage of 100% [16,163,179]. However, low infill percentages are preferred for reducing time and cost.

Besides the effect of geometry-related parameters, extrusion temperature and printing speed also influence the properties of FDM printed parts. Higher temperatures have been shown to improve bonding between the layers; at high temperatures, the melt flow of the polymer is higher, which increases the interfacial area between the layers, leading to a decrease in voids and an increase in mechanical performance. However, high temperatures also affect dimensional accuracy and cause shrinkage in some polymers [16]. The optimum printing speed in FDM is dependent on the material selected. In the studies related to the effects of printing speed on FDM parts, it has been observed that interlayer bonding between the filaments reduces with an increase in printing speed, which is attributed to lack of time for the polymer plasticisation [178,180–182]

2.5 FDM 3D Printing of PLA Composites with Bio-derived Fibre Reinforcements

2.5.1 Discontinuous bio-derived micro fibre reinforcements

Biocomposite filaments reinforced with discontinuous natural fibres for FDM are produced by mixing polymers, fibres, and, in some cases, additives through melt compounding followed by extrusion. Natural fibres, including hemp, harakeke, bamboo, flax, and others, have been researched for producing PLA biocomposite filaments [57].

Figure 19 compares tensile strength and Young's modulus of discontinuous bio-derived fibre reinforcement/PLA composites manufactured by FDM, injection moulding (IM), and compression moulding (CM). The mechanical properties of FDM printed biocomposites are comparatively lower than conventionally manufactured composites [167]. Numerous factors contribute to this, including weak interlayer adhesion, the low fibre content in FDM filaments, the low aspect ratio of bio-derived fibres, and the printed products' porosity [57]. Table 6 summarises the main findings of FDM 3D printed PLA composites with bio-derived discontinuous fibre reinforcements. Values presented in the table are selected based on the composition of reinforcement and PLA that showed the best results in each research work.

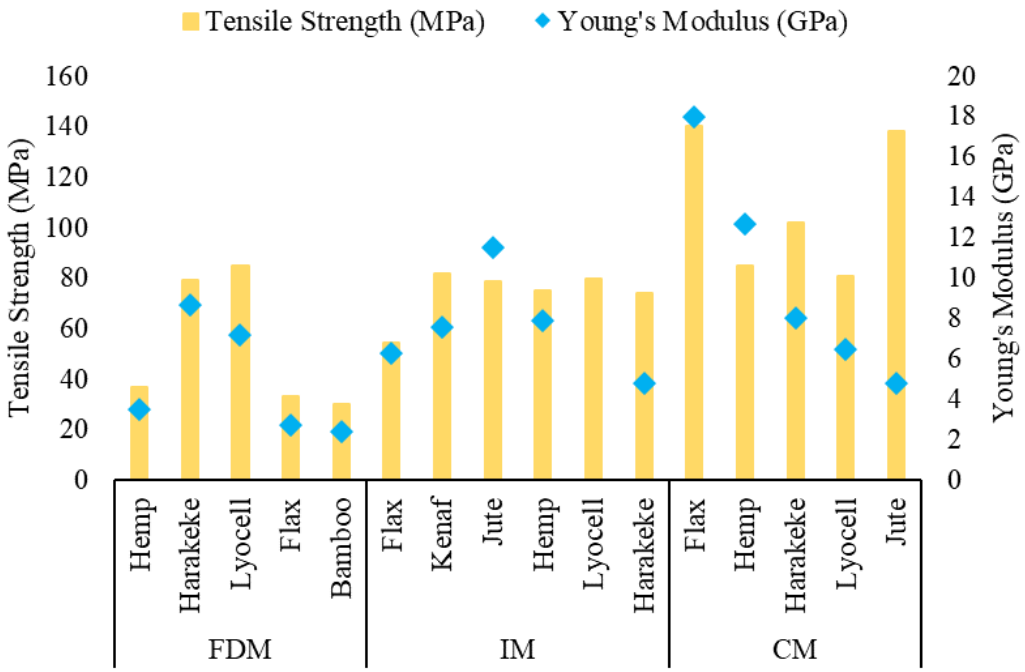

Figure 19 Tensile strength vs Young's modulus of discontinuous bio-derived fibre reinforcement/PLA composites [28] [72,8,73–77,78][63–67] [183] [188] [189] [190–193].

Where: FC – fibre content.

Table 6 Summary of main findings of FDM 3D printed PLA composites with bio-derived discontinuous fibre reinforcements.

Reinforcement	**Reinforcement (wt%)**	**Treatments**	**Specimen type**	**Tensile strength (MPa)**	**Young's modulus (GPa)**	**Observations**	**Ref.**
Hemp	10	Alkali fibre treatment with 5% NaOH	Printed sample	37	3.5	Improvement in tensile properties. The use of plasticiser was suggested to improve inter-layer adhesion and surface quality.	[183]

Harakeke	20	Alkali fibre treatment with 5% NaOH+ 2% sodium sulphite	Printed sample	36	4.2	42.3% and 5.4% increase in Young's modulus and tensile strength, respectively.	[183]
Flax	15	PLA was compounded with two types of plasticizers.	Filament	33	2.7	Filaments with only up to 4% voids were produced.	[188]
Bamboo fibre (BF)	13	PLA was compounded with two types of plasticizers.	Filament	30	2.4	BFs with a length of 2.14mm displayed an improvement of 215% in Young's modulus.	[188]
Sugar cane bagasse fibre (SCBF)	6	Raw sugarcane bagasse was treated with 7.5-wt% NaOH solution to obtain SCBF	Printed sample	57.1	-	The highest mechanical properties were observed for the samples printed in the parallel direction to the build plate.	[189]
Lyocell fibre	30	Lyocell fibres were subjected to fibrillation. PLA matrix was modified	Printed sample	85	7.2	This study reported the highest mechanical tensile strength for short fibre reinforced	[68]

		using Maleic anhydride (MA) through an in-situ modification. After 3D printing, the specimens were heat treated at 105 ± 2 °C				composites. A combination of fibre modification, the use of a coupling agent, and a post-printing heat treatment produced the best-performing composite.	
Lyocell fibre	30	None	Printed sample	55.8	5.1	Heat treatment improved PLA crystallinity, resulting in improved thermo-mechanical stability.	[71]
Harakeke fibre	30	Fibres were subjected to alkaline treatment using 10% NaOH and 2% Na_2SO_3 following which the fibres were bleached using hydrogen peroxide.	Printed sample	79.3	8.7	Fibre treatments resulted in well-dispersed fibres and improved interfacial bonding, and ultrasonication enhanced thermo-mechanical stability.	[191]

Fibre content has been shown to have the highest effect on the mechanical properties of discontinuous fibre reinforced composites. The tensile strength of FDM printed PLA biocomposites has been observed to increase with an increase in fibre content, but composites with fibre contents higher than 20 wt% are usually highly viscous, making extrusion non-uniform and causing clogging of the extruder die or printer nozzle [76,77]. For example, by using 20 wt% harakeke fibres as reinforcement for PLA, an increase of 42.5% and 5.4% in Young's modulus and tensile strength, respectively, were achieved compared to neat PLA. However, increasing fibre wt% above 20% caused uneven surface and poor interlayer adhesion. Fibre pull-out was observed in fractured samples showing weak fibre/matrix adhesion [183].

It has also been observed that porosity in a 3D printed sample increases with the increase in fibre content. Some of the proposed solutions to decrease porosity in 3D printed biocomposites include vacuum drying of the fibres, controlling humidity and temperature throughout the printing process, and using plasticisers [188,196]. Applying vacuum at the end of extrusion and adequate drying of the composite filaments has resulted in reduced porosity in FDM printed PLA composites reinforced with discontinuous flax and bamboo fibres [188]. For example, PLA was compounded with two types of plasticisers (provided by Proviron Industries NV) and then reinforced with bamboo and flax fibres individually. A vacuum pump was used at the end of the compounding line to reduce porosity, and 3D printing filaments with up to 4% voids were produced. It was observed that high extrusion speeds resulted in filaments with smoother surfaces. The highest improvement in Young's modulus was recorded for bamboo fibres, with a 230% improvement compared to PLA compounded with a plasticiser. Although the aspect ratio of flax fibres was higher than bamboo fibres, a higher increase in stiffness was not observed due to loss of orientation in the compounding process [188].

2.5.2 Long/Continuous bio-derived micro fibre reinforcements

Using long/continuous natural fibre reinforcements could provide an opportunity to achieve higher mechanical properties. Most commercially available FDM 3D printing filaments with continuous reinforcements use continuous carbon fibre and kevlar fibre. Recently, researchers have developed customised methods to produce composite filaments with long/continuous natural fibre yarns [197–200]. Studies show that composites with long/continuous reinforcements, such as jute and flax, have exceeded the mechanical properties of composites with discontinuous reinforcements [57]. FDM 3D printers used to fabricate composites with continuous reinforcements are modified to include two material supplies – the thermoplastic polymer and the continuous fibre. Examples of two different printers with single and dual nozzle systems are shown in Figure 20. In a single nozzle printer (see Figure 20 (a)), thermoplastic polymer and continuous reinforcement are passed through the heated nozzle. The temperature of the nozzle is set according to the melting temperature of the thermoplastic matrix. The matrix and fibre fuse together and are deposited layer by layer [201].

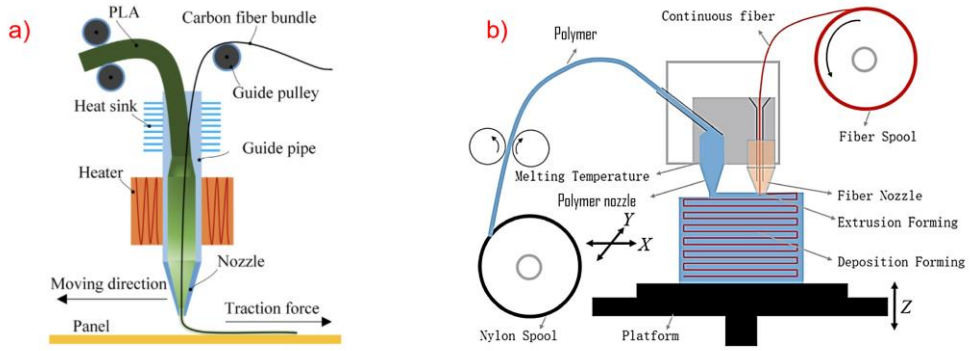

Figure 20 FDM 3D printing process for continuous fibre composites with a) single nozzle [202] Reproduced with permission from Elsevier, license number 5170290431014 b) dual nozzle Reproduced with permission from Elsevier, license number 5124221090291 [203].

Figure 20 (b) shows the working mechanism of the dual nozzle printer. This printer uses two different nozzles to deposit the matrix and continuous fibres separately. One nozzle stops while the other moves, and the continuous reinforcement is sized to the thermoplastic polymer to adhere to the previous layer. This dual nozzle printer allows customised fabrication and minimises cost [204]. So far, studies involving PLA/continuous natural fibre reinforcements have mostly used single nozzle type FDM printers [32,205]. Some studies also involved direct FDM 3D printing of PLA impregnated natural fibre yarns [198,206].

Results from current studies show the potential for achieving mechanical properties of 3D printed continuous natural fibre reinforcement/PLA composites comparable to that of continuous carbon fibre/PLA composites [207]. Reinforcement type, fibre content, production method, and tensile properties of 3D printed PLA composites reinforced with long/continuous bio-derived fibres are summarised in Table 7.

Table 7 Production and properties of FDM 3D printed PLA/long/continuous bio-derived fibre reinforced composites.

Reinforcement	Fibre Content	Production of composite filament and 3D printing	Tensile Strength (MPa)	Young's modulus (GPa)	Ref.
Flax fibre yarn	20.4 wt% for maximum tensile strength, 36.7 wt% for maximum Young's modulus	Molten PLA was squeezed through the crosshead extrusion die of a single-screw extruder. Flax yarn was introduced through the vertical opening of the die and coated by PLA. The filament was collected, and a five-axis FDM 3D printer was then used to print the composite filaments.	89	2.9	[198]
Flax fibre yarn	30.4 wt%	Flax yarn was coated with PLA using a single screw extruder. Flax yarn of 68 tex was used, and the extrusion temperature was set to 180°C. FDM printer modified to incorporate a custom 1.8mm nozzle was used for 3D printing.	254	23	[215]
Pineapple leaf fibre yarn	-	A single nozzle type 3D printer was used. The pineapple leaf fibre yarn and the PLA filament were blended in the extruder with a 1:4 volume fraction and were consolidated at the hot end to form a composite. The composite filament was extruded through the nozzle in a layer-by-layer fashion to form a 3D printed part.	96.8	-	[205]

Jute fibre yarn	6.1% volume fraction (V_f)	A single-nozzle 3D printer using PLA filament driven by gears and a stepping motor was developed. Jute yarn is automatically fed to the printer head, merging with molten PLA to create a composite filament extruded layer by layer onto a heated plate.	57.1	5.11	[32]
Ramie fibre yarn	-	A single nozzle type 3D printer, Combot-200, was used to fabric PLA/ramie composites using an in-situ impregnation method.	86.4	0.6	[30]
Flax fibre yarn	25 wt%	Flax yarns were pre-treated using silane coupling agents to enhance compatibility with PLA. Melt extrusion was used to combine flax and PLA directly during the 3D printing process.	170	9	[216]
Flax fibre yarn	44 wt%	Flax yarns were pre-treated using silane coupling agents to enhance compatibility with PLA. An impregnation block was used to infiltrate PLA into the flax yarns to produce filaments which were 3D printed.	293	24.7	[217]
Flax fibre yarn	33.4 wt%	Rotational vibration processing was used to facilitate the untwisting of the flax yarns, and a coaxial extrusion mould was used for melt impregnation.	244	20.7	[218]

It is essential to optimise processing parameters to produce continuously reinforced PLA 3D printed composites with maximum interfacial adhesion to avoid failure due to defects. Figure 21 shows SEM

images of longitudinal and transverse fracture surfaces of 3D printed flax yarn reinforced PLA composites. SEM images show that the failure involved pulling out of several flax fibres from the yarn. This shows that the flax yarn had weak cohesion because of the highly twisted structure and incomplete impregnation of PLA into the flax fibre [215]. Due to poor interfacial adhesion, a similar pull-out of fibres was observed in jute yarn/PLA FDM 3D printed composites. This was attributed to the incomplete wetting of jute yarn by PLA, and fibre surface treatment was suggested to improve the fibre/matrix adhesion [32].

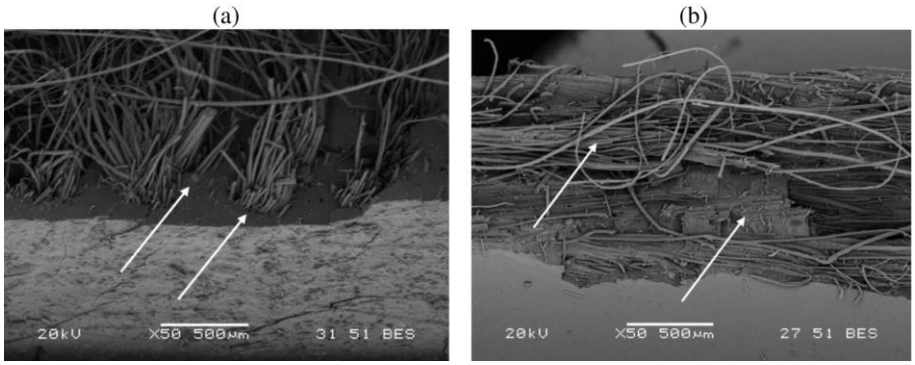

Figure 21 SEM images of fracture surfaces of FDM 3D printed flax yarn/PLA 3D printed composites a) longitudinal, transverse fracture b) transverse fracture [215].

The filament diameter also affects the interlayer adhesion and tensile properties of jute/PLA composites. For instance, flax yarn was coated with PLA to obtain continuously reinforced FDM filaments of different diameters. The filament with the lowest diameter (0.8mm) showed the worst tensile properties due to the non-uniform coating of PLA on the flax yarn, and as the diameter increased, a more uniform coating was achieved, as shown in Figure 22 [198].

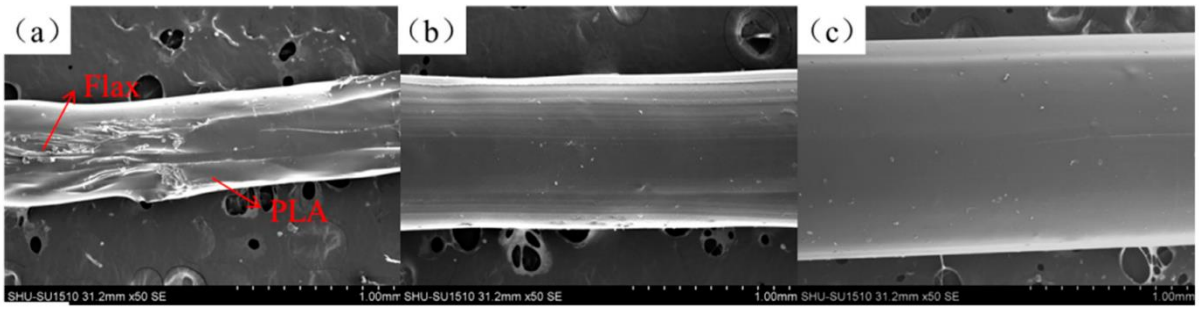

Figure 22 SEM images of the flax yarn/PLA composite filaments with diameters of (a) 0.8 mm, (b) 1.0 mm, and (c) 1.2 mm [198].

Future possibilities to improve the mechanical performance of long/continuous bio-derived reinforcements/PLA composites include developing customised filament production methods, optimising printing parameters, using low-twist yarns, and exploring more reinforcement options [57].

2.5.3 Particulate reinforcements

Bio-derived particle reinforcements in composites provide less effective reinforcement than fibres and are generally used in polymer matrices to improve Young's modulus [219]. Most commercially available PLA FDM filaments with bio-derived particles are based on wood powder [220,221]. Although many bio-derived particles have been extensively studied for 3D printability [219,222–231], only a few materials, including MCCs, hemp powder, and bamboo powder, have displayed a reinforcing effect when combined with PLA for FDM 3D printing, as shown in Table 8. Values presented in the table are selected based on the composition of reinforcement and PLA that showed the best results in each research work.

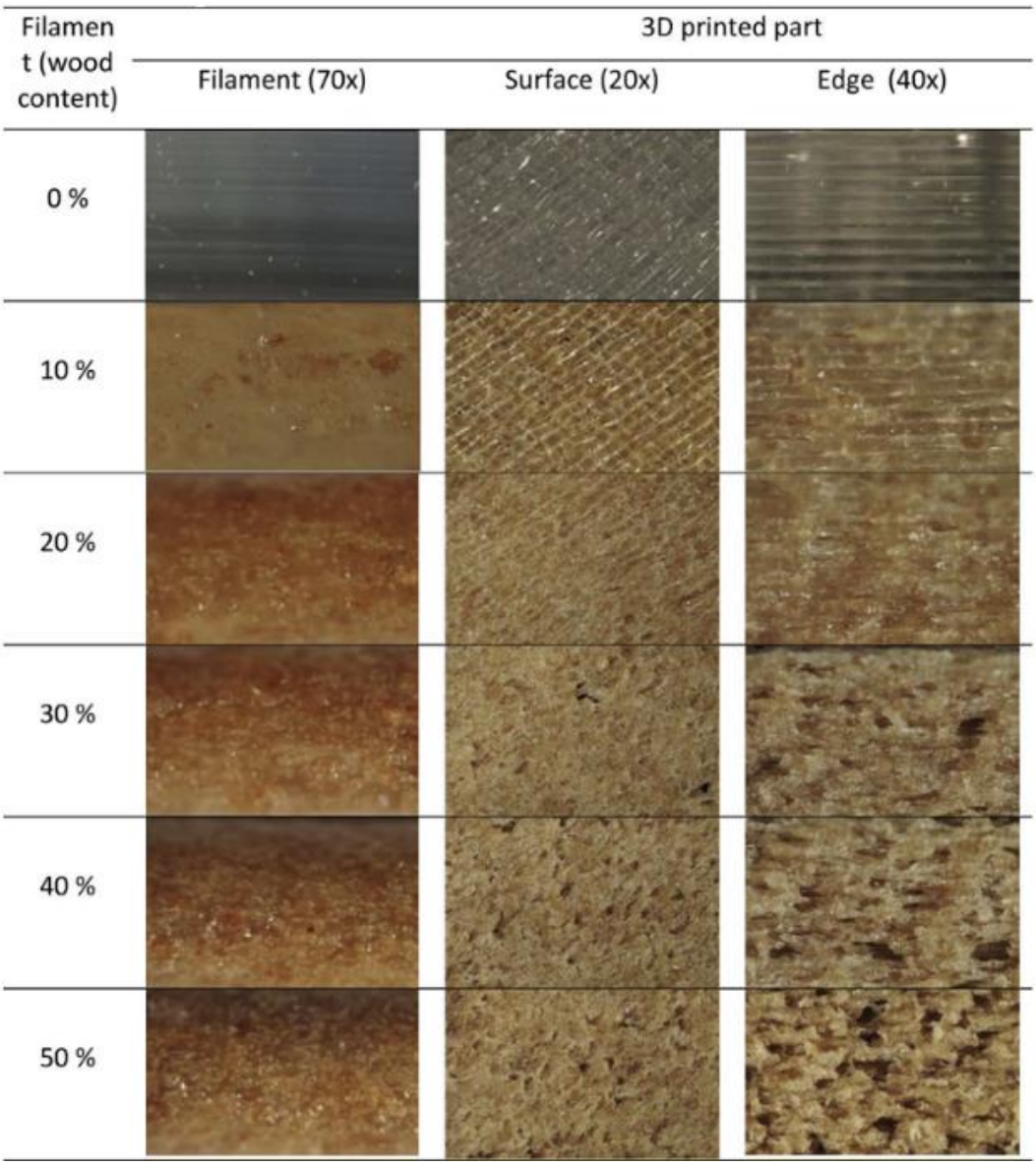

Figure 23 Optical micrographs of wood/PLA filament(left), surface (middle), and edge (right) [232]. Reproduced with permission from Elsevier, license number 5167000723403.

Table 8 Summary of main findings of FDM 3D printed PLA composites with bio-derived particle reinforcements.

Reinforcement	Reinforcement content	Modification/treatment	Tensile strength (MPa)	Young's moduli (GPa)	Elongation at break (%)	Observations	Ref.
Hemp powder	5wt% Hemp	Untreated	-	3.1	-	An increase in storage modulus with increased hemp volume fraction was observed. Only composites with 5 wt% Hemp displayed better storage modulus than neat PLA.	[233]
Bamboo powder (BP)	20wt% BP	The bamboo powder was treated with $CaCO_3$	51	-	-	$CaCO_3$ treated BP composites demonstrated the best results, with an increase of 40.33% in tensile strength.	[234]
MCC	5wt% MCC	Joncryl® ADR-4368C is used as an epoxy-based chain extender	45	3.2	-	Improvement in mechanical properties. Lower density samples due to the presence of voids.	[235]

Bio-derived particle reinforced 3D printing filaments are produced by compounding PLA with particle reinforcements by batch mixing with twin-screw extruders. For extrusion, filament diameter and dimensional tolerances play a significant role in determining the particle size [236,237]. Most benchtop FDM printers require mechanical refining or ball milling of reinforcements to avoid nozzle clogging during extrusion. The most commonly used particles are wood flour produced by ball milling and microcrystalline cellulose. PLA and bio-derived particles need to meet the requirement of less than 0.1% moisture content to avoid the reaction of PLA with water at high temperatures, which excises chains and reduces the properties of the 3D printed composite [230]. An increase in particle content leads to inconsistent flow and variation in diameter and reduces the mechanical properties of the filament. An example of the formation of voids and pores with increasing particle content can be seen in Figure 23 [232]. Various approaches to overcome these issues and improve the properties of PLA reinforced with bio-derived materials will be discussed in further sections.

2.5.4 Nano reinforcements

Bio-derived nano reinforcements used in FDM 3D printing PLA are all different types of nano celluloses and are categorised into cellulose nanocrystals (CNCs), nano fibrillated cellulose (NFC), and bacterial nanocellulose (BC) [238]. Nano celluloses have low density, ultra-fine structure, and high mechanical properties, making them potential candidates for reinforcement of thermoplastics. CNC is obtained from acid hydrolysis of cellulose and contains 100% cellulose, and its shape is rod-like with a diameter of 2-20nm and length of 100-500nm. NFC, also known as cellulose nanofibril (CNF), can be obtained by mechanically refining cellulose fibrils and has a composition of 100% cellulose with both amorphous and crystalline regions. NFC has a square cross-section with a 1-100nm diameter and a length of 500-2000nm [239]. Bacterial cellulose is obtained from microfibrils secreted from various bacteria separated from bacterial bodies and growth mediums. The morphology of BCs depends on their sources, and they usually have a square or rectangular cross-section. For example, Acetobacter microfibrils have a rectangular cross-section of 6–10 nm by 30–50 nm [25].

Table 9 summarises the main findings in FDM 3D printed PLA composites reinforced with CNCs, NFC, and BC. Values presented in the table are selected based on the composition of reinforcement and PLA that showed the best results in each research work.

Table 9 Summary of main findings of FDM 3D printed PLA composites with bio-derived nano reinforcements.

Materials	**Reinforcement content**	**Modifications/ treatments**	**Tensile strength (MPa)**	**Young's modulus (GPa)**	**Elongation at break (%)**	**Observations**	**Ref.**
CNF	2.5 wt.%	PEG600 was used as a plasticizer. To obtain CNF, enzymatic hydrolysis of MCC was performed.	57.5	-	8.5	CNF filled PLA biocomposite filament showed an increase of 33% in tensile strength and 19% in elongation at break.	[184]
CNF	3 wt%	PLA grafted CNFs (PLA-g-CNF) was obtained by grafting L-lactide monomers onto CNFs	45.2	3.5	-	Tensile testing of filaments showed a 66% increase in tensile strength and 28% in stiffness.	[240]
Nanocellulose	1 wt%	Nanocellulose was obtained by ultra-sonication of microcellulose	41.5	2.6	5.5	Tensile tests showed the highest improvement in stiffness and stress at the break with 1% nano cellulose in PLA.	[241]
PHB/	1wt%	Dicumyl peroxide	-	-	-	Improvement in interfacial adhesion	[242]

CNC		(DCP) is used as a cross-linking agent				and thermal stability.	
TEMPO-oxidized BC - (TOBC)	1.5wt %	BC was subjected to a TEMPO mediated oxidation	32	3.7	-	Improvement in crystallinity, mechanical strength, and toughness.	[243]
CNF	30wt%	Untreated	80	7.1	1.5	Improvement in tensile strength and Young's modulus by 45% and 130%, respectively. A decrease in elongation and toughness was observed. Significant improvement in storage modulus was achieved.	[244]
Sisal CNF	1 wt%	Untreated	52.14	3.7	2.39	Tensile strength and Young's modulus increased by 84% and 63%, respectively, with 1wt% CNF. Adding CNF also improved crystallisation and decreased voids.	[245]

CNF	10 wt%	The CNF fibres were grafted using L-Lactide. Post-printing heat treatment was also used	72.2	5.4	1.6	Heat treatment effectively increased tensile strength and Young's modulus by 10 % and 18 % higher, respectively, than the printed samples and 14 % and 66 % higher than neat PLA.	[246]

One of the main challenges in using nano cellulose as reinforcement in PLA is that the hydrophilic cellulose tends to aggregate in a hydrophobic PLA matrix, and thus, chemical/physical treatments have been used to improve dispersion [247]. Esterification/acetylation, silylation, TEMPO mediated oxidation, and grafting of molecules or macromolecular groups to nanocellulose are the widely used approaches for surface modification of nanocellulose [248].

CNFs have been grafted with L-lactide monomer to form PLA grafted CNFs (PLA-g-CNFs). A post extrusion annealing treatment was performed on the FDM filaments, which resulted in a 66% increase in tensile strength and 28% in stiffness with 3% of PLA- g-CNF [240]. The Pickering emulsion method was used to add TEMPO (2,2,6,6-Tetramethylpiperidin-1-yloxy) oxidised bacterial cellulose (BC) to PLA, resulting in an improvement in the dispersion of nanocellulose in the PLA matrix and enhanced mechanical properties [243].

In all the FDM 3D printing studies done so far, the best mechanical properties have been achieved for 30wt% CNF reinforced composites. To avoid agglomeration of CNFs at high loadings, chopped and freeze-dried CNF networks that act as microsponges were used that allowed PLA to flow into them during melt processing by creating mechanical interlocking. The high interfacial adhesion between CNFs and PLA was attributed to the low packing density of CNFs combined with the low viscosity of PLA in the molten state [244]. CNFs also tend to have better reinforcement than CNCs efficiency because of their higher aspect ratio. CNFs have an aspect ratio of 25-500 compared to 10-100 for CNCs. CNFs have a large surface area and length that is beneficial to bridge the gap between printed layers and improve interlayer adhesion, whereas CNCs have shorter lengths that are not sufficient to entangle

between two layers. Increased entanglement in CNFs leads to better stress distribution and stronger composites, as shown in Figure 24 [249].

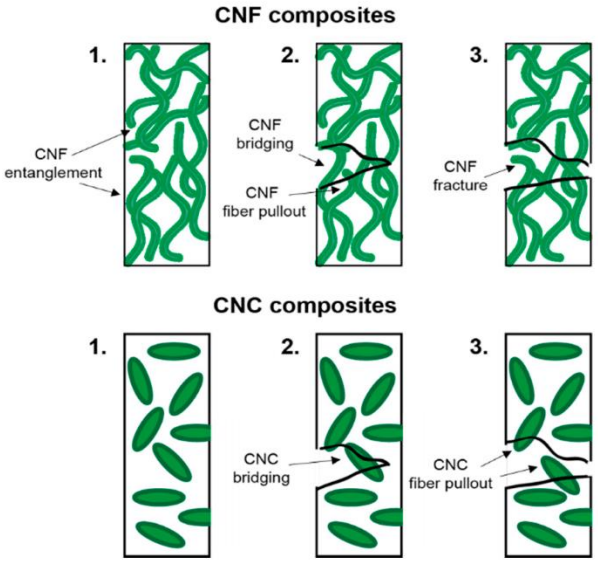

Figure 24 Fracture mechanisms in CNC and CNF composites 1) before mechanical stress 2) during mechanical stress 3) after mechanical stress [249].

2.5.5 Enhancing properties of FDM 3D printed PLA biocomposites.

Overall enhancement of properties of FDM 3D printed biocomposites can be achieved by introducing modifications at three different stages. The first stage is before 3D printing, where modifications can be introduced on a material level that helps improve interfacial bonding between PLA and bio-derived reinforcements. The second stage is 3D printing, where optimising printing parameters can help achieve efficient printing and improved properties. The third stage is post 3D printing, where enhancement of properties is achieved by reducing defects using post-processing methods. A detailed overview of processes followed for these three different stages to enhance FDM 3D printed PLA properties is presented here.

Pre-3D Printing Stage

PLA used for FDM is semi-crystalline, and molecular chains of PLA exhibit imperfect molecular symmetry, affecting the diffusion ability and crystallinity of PLA, mainly within the limited window of time in the FDM printing, leading to low mechanical properties and weak bonding between the printed layers [153–157]. Studies show that adding plasticisers such as polyethylene glycol (PEG) improved the crystallinity and tensile properties of PLA. On the other hand, more than 10 wt% of PEG was shown to depreciate PLA properties as a PEG crystallisation peak occurred in DSC, which shows the separate existence of PEG [250–252]. As mentioned earlier, the addition of plasticisers also helped in decreasing the porosity of FDM 3D printed PLA composites [188].

Cross-linking degree of molecular chains of PLA was improved by adding synthetic low molecular weight (LMW) PLA components to commercial PLA. It was observed that LMW PLA diffuses more quickly across the inter-filament interface during the deposition of layers, improving the interlayer bond [253]. However, filaments extruded through the nozzle during the FDM process stay in the molecular diffusion and crystallisation temperature for a short time. To overcome this issue, researchers have added radiation-sensitive materials to PLA filaments before 3D printing and then irradiated the printed parts by electron beam, γ-ray, or microwave. Upon irradiation, free radicals are generated in the primary or side chain of PLA, allowing further cross-linking [163]. Similarly, in another experiment, PLA was blended with γ-ray sensitive trimethylolpropane triacrylate (TMPTA) and trially isocyanurate (TAIC) and 3D printed by FDM. The 3D printed part was then radiated by γ-ray, and the temperature was set to near T_g. This experiment showed an improvement in the tensile properties of radiated PLA compared to the non-radiated one [254].

IFSS directly affects the efficiency of load transfer between fibre and matrix, thereby determining the mechanical performance of discontinuous fibre reinforced composites [25,167,255–258]. One of the main challenges to achieving good interfacial bonding is creating surface-chemical compatibility between the hydrophilic bio-derived reinforcements and the hydrophobic PLA matrix [259,260]. Several physical, chemical, and biological treatments have been proposed to reduce the hydrophilicity of the reinforcement surface and improve reinforcement/matrix adhesion [28]. Surface modification and compatibilisation of the matrix are the most used methods to improve interfacial adhesion [259]. Tables 10 and 11 summarise recent research on surface modification and PLA matrix compatibilisation, respectively.

Table 10 Recent works involving surface modification to improve interfacial adhesion in PLA composites with bio-derived reinforcements.

Composite	**Modifier**	**Effects on composite properties**	**Ref.**
PLA/Unidirectional Flax fibres	Lignin and Tannin	Tannin showed better results. A 17% and 29% increase in ultimate flexural strength and interlaminar shear strength, respectively, was observed.	[261]
PLA/Coir fibres/	Alkali treatment with 6% NaOH solution	Improvement of 128% and 112% was observed in tensile strength and Young's modulus, respectively.	[262]

Pineapple leaf fibres			
PLA/ Poplar Fibre	Maleic Anhydride and KH550	Tensile strength for 0.5% MA and 2% KH550 improved by 17% and 23%, respectively.	[263]
PLA/ Kenaf/ Montmorillonite (MMT) clay	Kenaf fibres were treated with 6% NaOH solution	Increase in impact, flexural and tensile strengths by 11%, 46% and 6%, respectively.	[264]
PLA/ Pineapple leaf fibre yarn **PLA/ sisal fibre yarn**	Alkali treatment with 5 wt% NaOH solution	Improvement in thermal stability and tensile properties.	[265]
PLA/Bacterial cellulose (BC)	BC was subjected to a TEMPO mediated oxidation	Improvement in crystallinity, mechanical strength, and toughness.	[243]
PLA/CNF	CNFs were grafted with L-lactide monomer to form PLA grafted CNFs (PLA-g-CNFs)	66% increase in tensile strength and 28% in stiffness with 3% of PLA- g-CNF	[240]
PLA/CNF	CNFs were grafted with L-lactide monomer to form PLA-g-CNFs	Increase in tensile strength, Young's modulus, elongation at break, and impact strength by 20%, 31.8%, 12%, and 27.9%, respectively, compared to PLA/CNF composite.	[266]
PLA/CNC	Immobilised Lipase was used to catalyse the formation of laurate ester groups on the CNC surface	66% increase in tensile strength, 61% increase in elongation at break, and improvement in crystallinity.	[267]

PLA/CNC	Acetic anhydride was used for surface modification of CNC. Dropwise acetylation was performed by using 3g CNC, 4.5g pyridine, and 114g acetic anhydride	Improvement in barrier properties, interfacial compatibility, and mechanical properties.	[268]

Table 11 Recent works involving matrix compatibilisation to improve interfacial adhesion in PLA composites with bio-derived reinforcements.

Composite	**Compatibilizer**	**Effects on composite properties**	**Ref.**
PLA/Lemongrass fibre (LF)	PLA grafted with maleic anhydride (PLA-g-MAH)	Improvement of tensile strength, impact strength, and flexural strength.	[269]
PLA/ Microcrystalline cellulose (MCC)	Maleic anhydride-grafted PLA (PLA-g-AMS/MAH)	The compatibilisation effect was seen to increase with an increase in D_g (grafting degree) of PLA-g-AMS/MAH.	[270]
PLA/ Tannin	Methylene diphenyl diisocyanate(p-MDI)	An increase in the tensile strength of the composite by 19.1% was recorded. Moreover, there was an improvement in melting temperature and thermal degradation onset temperature.	[271]
PLA/Sisal **PLA/Flax**	Maleic anhydride-modified PLA (MA-PLA)	Improvement in tensile strength was achieved. In comparison, the tensile properties of flax fibre composites were superior to sisal fibre composites.	[272]

PLA/ Wood fibres	Maleic anhydride-modified PLA	Good interfacial adhesion at higher wood fibre loadings (up to 80%).	[273]

3D Printing Stage

Various factors, including build orientation, printing temperature, and raster angle, affect the mechanical properties of a 3D printed polymer composite [164]. However, studies on the influence of printing parameters on the properties of FDM printed PLA biocomposites are limited and have only recently been reported [274]. Higher extrusion temperatures have been shown to improve adhesion between matrix and fibre and improve tensile properties. 3D printing PLA/PHA wood filaments and PLA/hemp filaments by increasing printing temperatures from 210°C to 230°C resulted in an improvement in tensile strength. However, increasing the printing temperature above 230°C led to a decline in tensile properties due to thermal degradation of bio-derived fibres [223,275]. Effects of printing orientation on PLA/sugarcane bagasse fibre (SCBF) composites were studied, and it was found that longitudinal orientation (0°) displayed the best tensile properties with a tensile strength of 57.1 MPa compared to 42.6 MPa in vertical (90°) direction [189]. However, in another research, PLA/agave fibre composites were studied to understand the effect of raster angle. It was found that tensile and flexural properties were not impacted significantly by the raster angle, but morphology was directly impacted, and absorption values and impact strength slightly increased at -45°/45° [276].

Along with printing parameters, interlayer adhesion of deposited filaments also significantly impacts the mechanical properties of FDM 3D printed PLA parts. The main reason for weak interlayer bonding is that PLA cannot maintain enough time at melting temperature. In the FDM process, the temperature of PLA drops quickly after the filament is extruded. As a result, molecular chains on the interface of PLA are not diffused completely, and these filaments cannot be fused with the newly extruded filaments effectively. This effect results in anisotropic material behaviour and reduced strength caused by voids formed during printing [277].

The cooling rate parameter plays a crucial role in improving interlayer bonding. If the cooling speed is too slow, PLA parts have poor surface quality and may also result in deformed shapes. If the cooling speed is too high, molecular diffusion on the surface decreases, and the interface bond between layers becomes weak [278]. Researchers have studied and implemented heating of the pre-deposition layer as a solution to resolve the anisotropy problem caused by interface bonding between layers in FDM printed PLA parts [279].

A synchronous and local laser heating system was proposed to heat the layered zone of PLA near the nozzle, as shown in Figure 25. The temperature at the interface was raised to exceed the T_g. Results showed that the interface diffusion of PLA molecules increased, improving the interface bond between layers. More than 60% improvement in strength and 100% improvement in elasticity was recorded [279,280]. A similar method was employed using an infrared lamp to increase the temperature at the interface of PLA layers. Three different experimental conditions were set, as shown in Figure 26 (a). A comparison of average mechanical properties is shown in Figure 26 (b). Conditions 1 and 2 show a significant improvement in fracture energy, whereas condition 3 shows a decline in properties. This was explained by the use of infrared radiation of 1 kW, which led to the degradation of the mechanical properties of PLA [281].

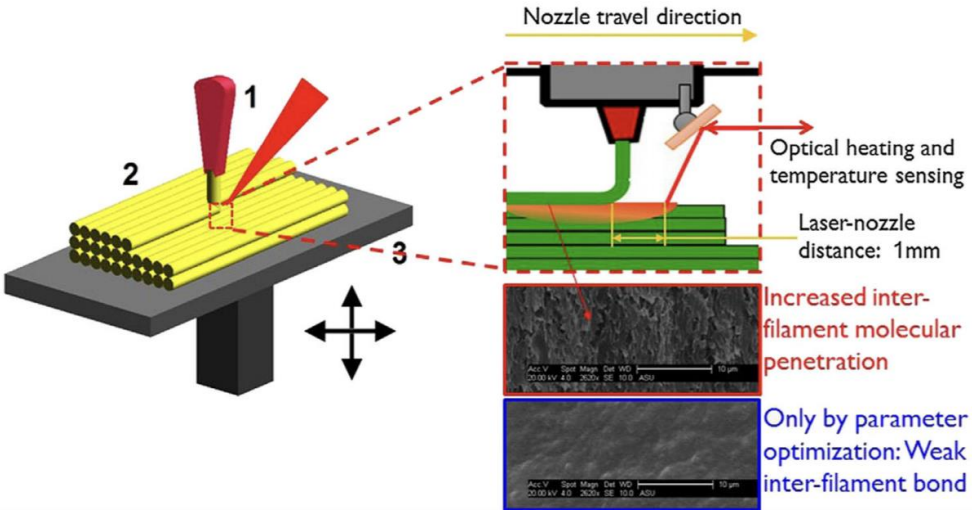

Figure 25 Concept diagram of laser local pre-deposition heating method to improve interface bond of PLA layers in FDM 3D printing [280]. Reproduced with permission from Elsevier, license number 5124230169886.

The local laser pre-deposition heating and infrared preheating use external heating sources to control the local printing temperature, which improves the interface bonding of printed layers. This results in improved mechanical properties of FDM 3D printed PLA as there are low residual stresses during controlled cooling. However, it is essential to consider cost and complexity factors while employing these technologies for FDM.

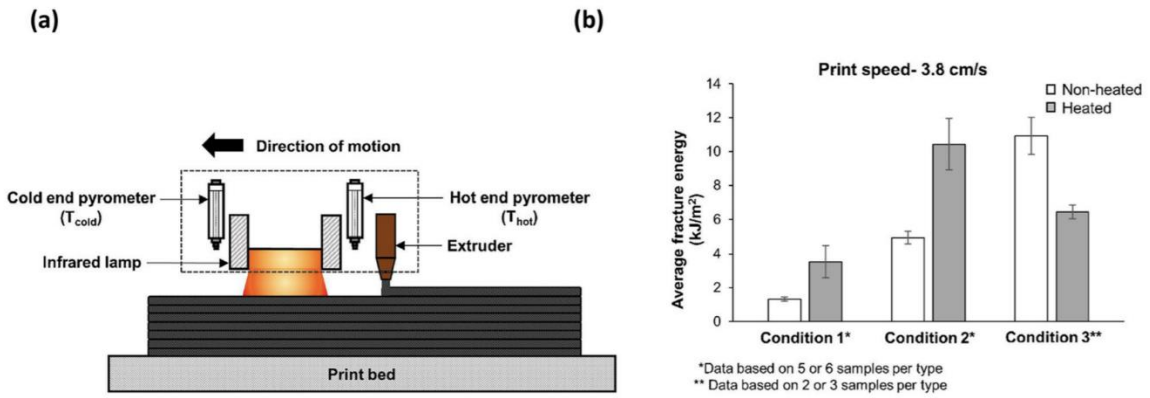

Figure 26 a) Infrared preheating experimental setup b) variation of fracture energy for various preheating conditions [281]. Reproduced with permission from Elsevier, license number 5124230347232.

Post 3D Printing Stage

Defects in 3D printed natural fibre-reinforced PLA composites that affect the mechanical strength are due to residual stresses, uneven fibre distribution, and poor bonding between fibre and matrix [57]. Annealing is used as a post-processing method to reduce residual stress and improve the crystallinity of FDM-printed PLA components. In FDM 3D printing, the polymer undergoes heating during extrusion from the nozzle, followed by rapid cooling, resulting in different tensile and compressive forces building up in the polymer structure. Annealing is a process where the material is reheated and held above or near its T_g and then allowed to cool slowly. This heating and prolonged cooling redistribute the stresses and increase the crystallinity, improving strength and stiffness [282,283]. A study showed that the best results in improved tensile strength were obtained when PLA was annealed at 80°C. However, annealing also causes deformation, leading to changes in the dimensions of the PLA parts depending on the grade of PLA used. To achieve accurate dimensions, deformation is a significant factor to be considered [284].

Chapter 3: Fibre and Matrix Characterisation

3.1 Introduction

This chapter focuses on the characterisation of fibres (viscose, standard flax, bleached flax) and the PLA matrix used in this research. Two different grades of PLA were selected for two impregnation methods – solution and emulsion impregnation implemented in this work. Solution impregnation involves dissolving PLA in an organic solvent, and PLA 2003D grade was selected for its high molecular weight (18,000g/mol) and mechanical properties (Tensile strength – 60 MPa, Young's modulus – 3.5 GPa). PL1005 grade was selected for emulsion impregnation as it was readily available as a water-based emulsion and could be an alternative to the toxic solvent-based impregnation method. Single fibre tensile testing was performed to evaluate the mechanical properties of viscose, standard flax, and bleached flax, to be later used to predict composite properties. Mechanical properties of PLA 2003D and PL 1005 were also evaluated using tensile testing of filaments produced from these grades. TGA and DSC of both fibres and matrices were performed to understand processing temperatures and thermal stability.

3.2 Materials and Methodology

3.2.1 Materials

Viscose (regenerated cellulose) yarns were kindly provided by Cordenka GmbH (Germany). These fibres have a nominal yarn count of 2440 dTex (linear density of 4.1 Nm), zero twist, and a density of 1.5 g cm^{-3}. Standard flax and bleached flax yarns were purchased from Jos Vanneste (Belgium) with a yarn count of 2083 dTex (linear density of 4.8 Nm) and a density of 1.3 g cm^{-3} to 1.4 g cm^{-3}. PLA 2003D with a specific gravity of 1.24 g cm^{-3} was purchased from NatureWorks®, Minnesota, USA. PL1005 grade emulsion, with 40 wt% PLA/water, with a nominal particle size of 5 μm, was provided by Miyoshi Oil & Fat Co., ltd, Japan.

3.2.2 Single fibre tensile testing

Viscose is a continuous bio-derived fibre, whereas flax is a plant fibre. The main difference between these fibres is that viscose is a solid fibre throughout its cross-section, and flax fibre comprises a solid region and the lumen, a hollow structure in the middle [285]. Flax fibres are assumed to be solid throughout the cross-section, and both flax and viscose fibres are assumed to have circular cross-sections for this experiment. These assumptions enable comparison with most existing literature for mechanical testing of single fibres [286,287].

Tensile properties of viscose, standard flax, and bleached flax fibres were obtained using the single fibre tensile test method according to ASTM D3379 standard [288]. Single fibres were separated from yarns and mounted on 350 GSM paper tabs using gauge lengths of 2mm, 5mm, 7mm, and 10mm,

respectively. 15 samples were tested for each gauge length. Epoxy was used to mount the fibres to the paper tabs, and the samples were subsequently cured for 4 hours at room temperature, followed by conditioning in a climatic chamber at 23°C and relative humidity of 50% for 48 hours. The diameters of the fibres were measured using an Olympus BX60F5 (Tokyo, Japan) optical microscope. The diameter of each fibre was measured at five different points, and the average value was used for testing and calculations. Instron® 5982 UTM (universal testing machine) (Massachusetts, USA) was used to perform the tensile test after cutting the supporting sides of the tabs, as shown in Figure 27. A crosshead displacement rate of 2mm/min and a load cell of 10N was used.

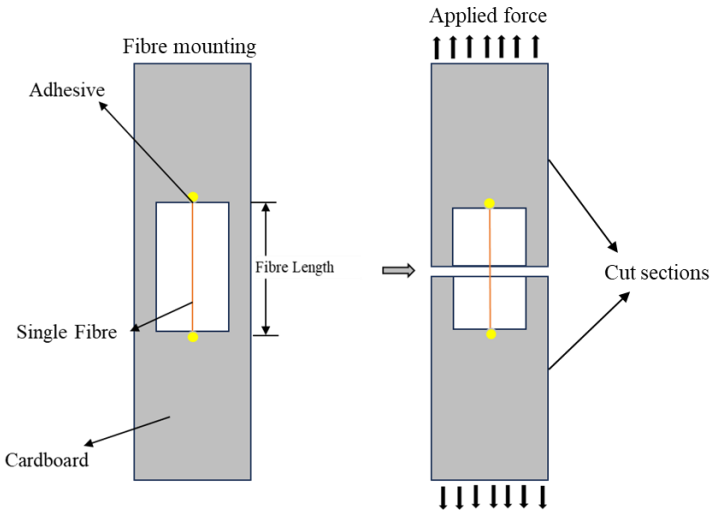

Figure 27 Schematic of single fibre tensile testing

Determination of Young's modulus

The determination of Young's modulus of a single fibre from tensile test data requires correction of displacement using the compliance correction method. The load cell of the tensile tester measures the load applied onto the specimen; most commonly, an extensometer or strain gauge is used to measure displacement. However, these tools cannot be applied to single fibres because their diameters are too small. Instead, displacement is read directly from the crosshead movement of the tensile testing machine, which includes fibre elongation and the deformations in the crosshead. The actual displacement of the fibres due to the compliance of the testing system can be calculated by using a correction factor.

The system compliance or the correction factor (Cs) was found by choosing the viscose fibre as the material with known Young's modulus (19 GPa). The apparent compliance Ca was calculated for each length of single fibres tested by inverting the gradient obtained from the force vs displacement curves. The value obtained for C_a was extrapolated to gauge the length of zero, as shown in Figure 28, to obtain system compliance C_s.

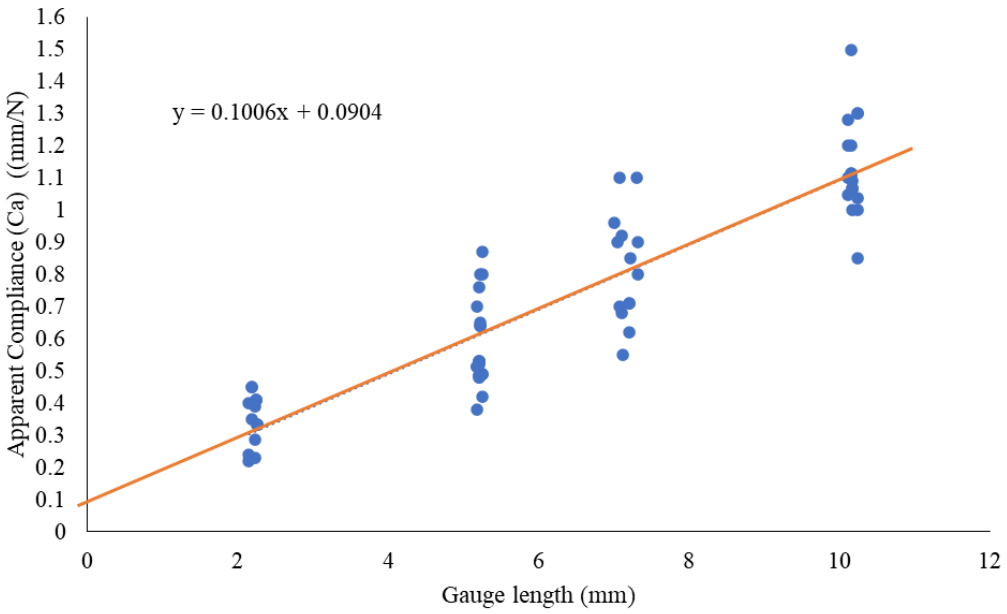

Figure 28 System compliance of the tensile testing

The true compliance C was then calculated as

$$C = C_a - C_s \quad (1)$$

The Young's modulus was calculated using the equation,

$$E_f = \frac{L}{CA} \quad (2)$$

where L is the specimen gauge length, C is the true compliance, and A is the average fibre cross-sectional area.

3.2.3 Tensile testing of matrix

Filaments were produced from PLA 2003D and PL1005 grades for tensile testing. PLA 2003D is available in the form of granules which were fed to the Filabot EX2 (Vermont, USA) single screw extruder, and a filament of diameter 1.75 ± 0.5 mm was extruded at a temperature of 180°C. PL 1005 is a commercial water-based emulsion which consists of PLA particles (diameter of 5µm) dispersed in water, as shown in Figure 29 (a). The emulsion was air-dried in the fume hood for 48 hours. The PLA powder obtained (Figure 29 (b)) was then dried in the vacuum oven for 24 hours at 30℃ and 3 hours at 50℃. A moisture analysis was done using KERN and Sohn GmbH moisture analyser (Balingen, Germany) to ensure the moisture was removed entirely from the PLA powder. The analysis protocol involved measuring the weight loss in the powder at a temperature of 102℃ with an accuracy of 0.01%. The Filabot single-screw extruder was then used to produce the filament with an extrusion temperature of 190℃ and a diameter of 1.75 ± 1 mm. The filaments were further granulated to produce pellets of

4mm length using a Moretto GR knife mill (Mercer County, PA, USA). The pellets were used to perform a second extrusion to improve the filament diameter tolerance, as shown in Figure 29. Filaments produced from the second extrusion had a diameter with a tolerance of 1.75 ± 0.5 mm. Tensile testing of the filaments was done using an Instron® 5982 tensile tester (Massachusetts, USA) with a 5 kN load cell using a 10 mm extensometer at a crosshead displacement of 5 mm/min. A gauge length of 30 mm was used for filament testing. Six repeats for each material were tested, and the samples were conditioned in a climatic chamber at 23°C and relative humidity of 50% for 48 hours before testing.

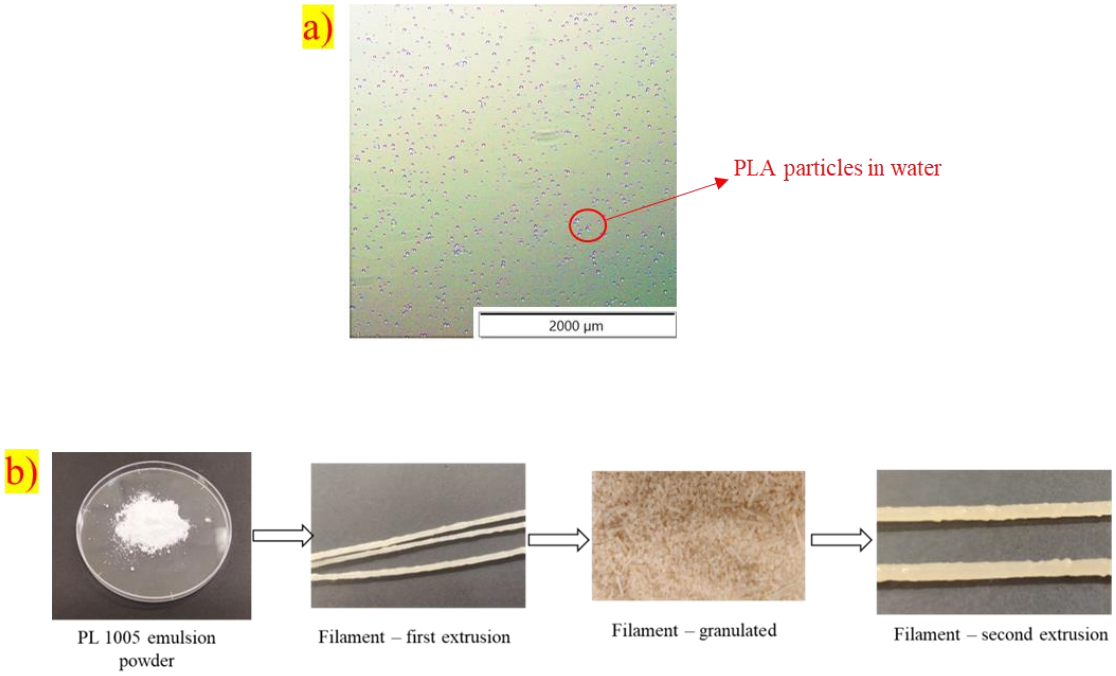

Figure 29 (a)Optical microscopy of PL 1005 emulsion (b) Production of PL 1005 filament

3.2.4 Scanning electron microscopy (SEM) and Stereomicroscopy

A Hitachi S-4000 field emission scanning electron microscope (Hibaraki, Japan), operated at 3 kV, was used to inspect the surface morphology and fracture behaviour of the fibres. The pre-dried samples were mounted on aluminium tabs with carbon tape and sputtered with platinum before the observation.

3.2.4 Thermogravimetric analysis (TGA)

Thermal properties of the reinforcements and matrix were analysed using a Perkin Elmer STA8000 (Connecticut, USA) thermogravimetric analyser from 30 ^{o}C to 600 ^{o}C at a heating rate of 10 ^{o}C/min under an argon flow of 40 mL/min.

3.2.5 Differential scanning calorimetry (DSC)

The calorimetric measurements of PLA were recorded using a Netzsch DSC3500 Sirius differential scanning calorimeter (Bavaria, Germany) using aluminium crucibles from 20-200 ^{o}C at 10 ^{o}C/min with

a Nitrogen flow of 60 mL/min. The glass transition (T_g), melting (T_m), and cold crystallisation (T_{cc}) temperatures were obtained from the DSC scans.

3.3 Results and Discussion

3.3.1 Fibre Morphology

Images of viscose, standard flax, and bleached flax are shown in Figure 30. The key distinction between viscose and flax yarns was that the viscose yarn had no twist, and the flax yarns were twisted. Viscose yarn also exhibited a characteristic smooth and uniform texture resulting from the viscose manufacturing process, which involves the dissolution and extrusion of cellulose [122]. Bleached flax was lighter in colour compared to the standard flax yarn because bleaching generally involves the use of chemical agents to break down and remove natural colourants, such as lignin and hemicellulose, present in unbleached flax fibres [289,290].

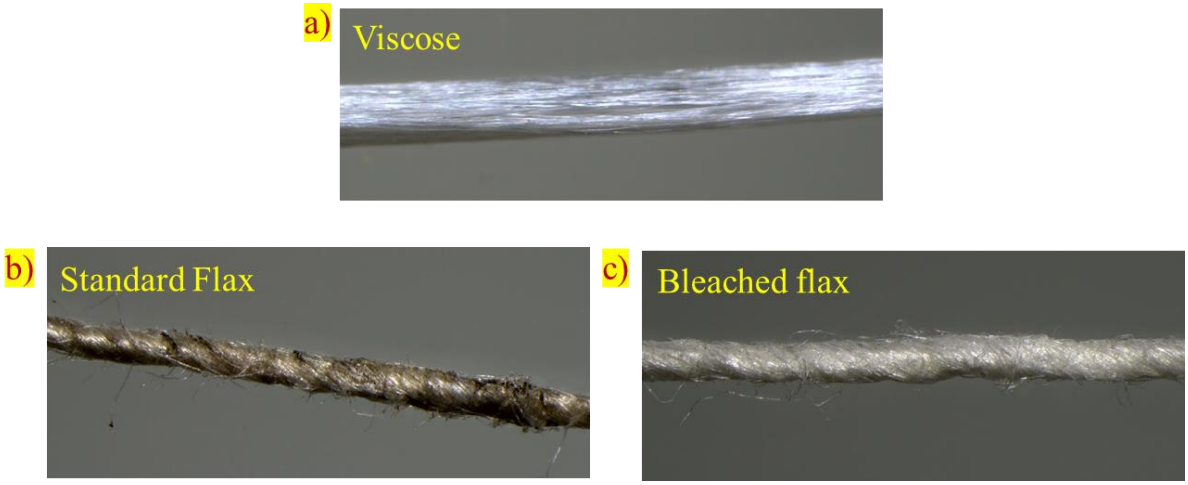

Figure 30 Images of reinforcement yarns a) Viscose b) Standard flax c) Bleached flax

SEM images of yarns and single fibres of viscose, standard flax, and bleached flax reinforcements are shown in Figure 31. Viscose yarn and fibre presented a smooth, homogenous surface similar to the lower magnification images. Standard flax yarn and fibre displayed the presence of non-cellulosic substances such as pectin, lignin, and hemicellulose that hold the flax fibres together in the yarn [291–293]. In contrast, the bleached flax yarn and fibre images exhibit considerably lower amounts of these non-cellulosic materials. The bleached flax yarn also has separation between the fibres without fibre junctions compared to the standard flax yarn [294].

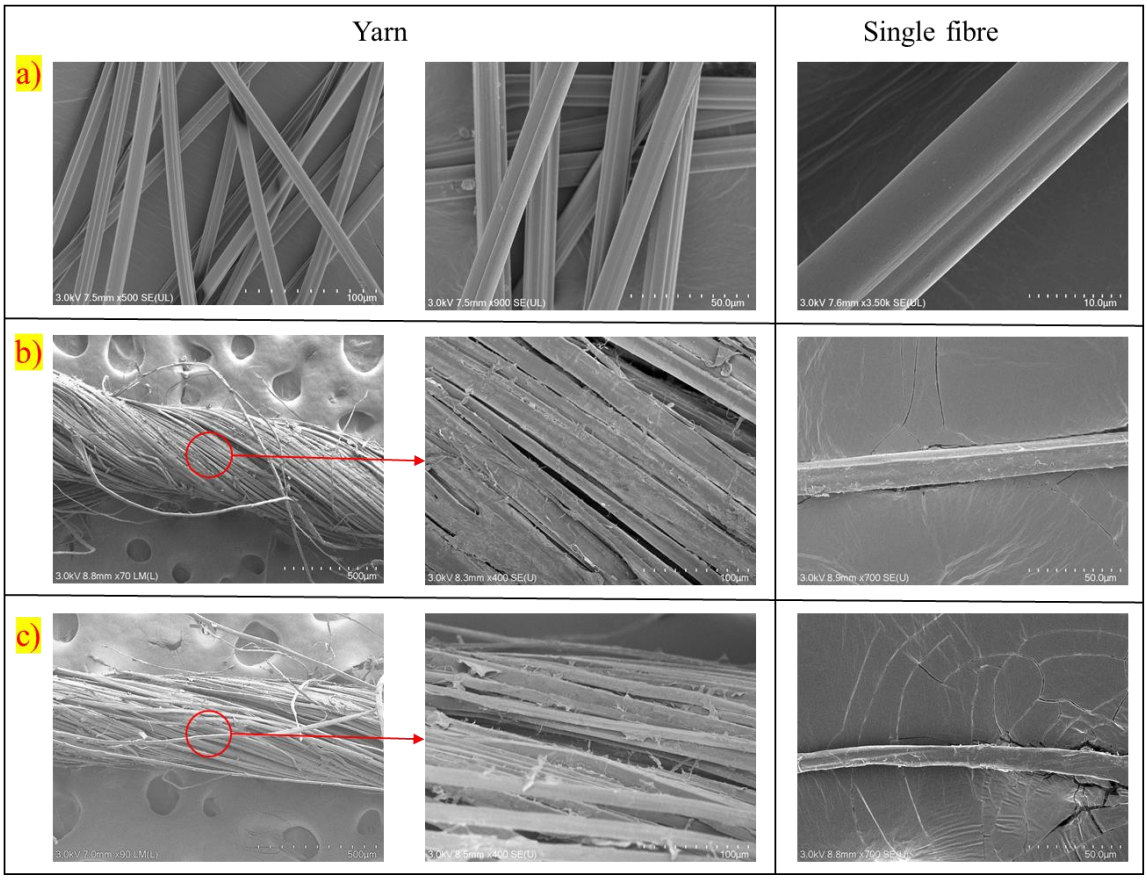

Figure 31 SEM images of reinforcement yarns and single fibres a) Viscose b) Standard flax c) Bleached flax

3.3.2 Single Fibre Tensile Properties

Table 12 summarises the tensile strength, Young's modulus, and elongation at the break of viscose, standard flax, and bleached flax fibres. The stress-strain curves of the single fibres are shown in Figure 32. The highest tensile strength (921.6 ± 30.7) was observed for bleached flax fibres, the highest Young's modulus (31.8 ± 10.7) was obtained for standard flax fibres, and the highest elongation at break (13.2 ± 4.2) was achieved for the viscose fibres. The single fibre properties obtained in this study were similar to those reported in the literature for these fibres, as seen in Table 1. The Young's modulus observed for the flax fibres compared to literature values was slightly lower, which can be attributed to regional and processing variations. Differences in soil, climate, and agricultural practices affect fibre properties, and specific processing methods such as retting and scutching also impact the mechanical performance [295].

As mentioned earlier in the literature review (chapter 2), viscose fibres have a cellulose II structure compared to the cellulose I structure of flax fibres. The main difference between these two structures is that cellulose I contains parallel chains without intersheet hydrogen bonding, and cellulose II contains anti-parallel chains with intersheet hydrogen bonding, which affects the degree of polymerisation and

crystallinity of these fibres [124,125,296,297]. The degree of polymerisation of cellulose II is only 400-700 compared to 5000-10000 for cellulose I. Longer polymer chains provide a more continuous and stronger structure, contributing to better load-bearing capabilities, and this is one of the reasons standard flax and bleached flax have higher tensile strength and modulus compared to viscose [297]. A higher degree of polymerisation often leads to increased crystallinity, high tensile strength and low elongation at break in cellulose fibres. This is because high crystallinity means the inter-chain hydrogen bonding is more significant, and the polymer chains are closer together, increasing the force required for Brownian motion [298]. Viscose has lower crystallinity [299] than other regenerated cellulose fibres and plant fibres, which explains the higher elongation at break but lower tensile strength for these fibres [300–302].

Table 12 Tensile properties of single fibres

Fibre	**Tensile Strength (MPa)**	**Young's Modulus (GPa)**	**Elongation at break (%)**
Viscose	724.2±187.8	22.8±5.9	13.2±4.2
Standard Flax	821.3±287.6	31.8±10.8	2.8±1
Bleached Flax	921.6±320.2	30.7±12.2	3.3±1.6

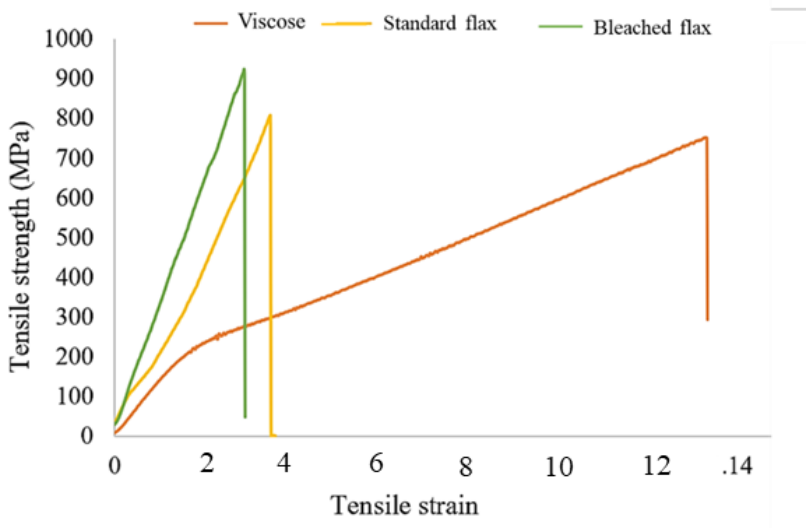

Figure 32 Stress vs strain curves of viscose, standard flax, and bleached flax single fibres.

Mechanical properties of cellulose fibres such as viscose and flax can vary significantly due to the higher probability for weaker parts as the length of fibre sections tested increases [303]. As explained earlier, this size-dependent behaviour of brittle materials can be explained using Griffith's weakest link theory [303]. As the gauge length increases, the number of areas with thinner places in the fibre

increases, and it has been shown in the literature that fibre failures tend to occur at the position of minimum diameter [304]. Figures 33,34, and 35 show box plots to highlight the tensile properties obtained for each gauge length tested and a decrease in tensile properties was observed with an increase in gauge length for all the fibres. Weibull's statistics is a commonly used method for statistical size effects. Bast fibres such as flax are often analysed using Weibull statistics, and an apparent decrease in tensile properties was observed with an increase in fibre volume in multiple studies [305–308]. Regenerated cellulose fibres such as viscose have also been analysed using Weibull statistics by multiple authors in the recent past [309–311]. It was observed that a fair agreement between Weibull strength and experimental data was found at higher sample numbers [311]. A Weibull statistical analysis has not been done on the results obtained in this experiment, as a small sample size was used. The current goal was to understand the relationship between the structure and properties of reinforcements and predict the influence of reinforcements on PLA biocomposites.

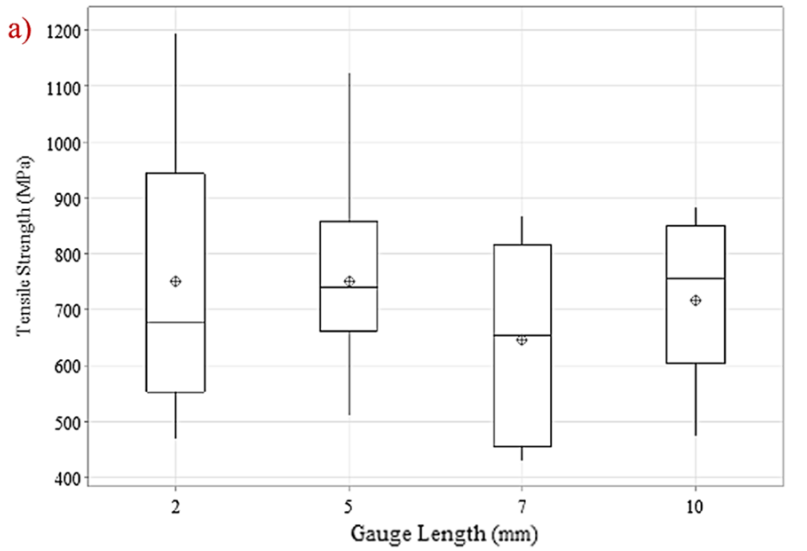

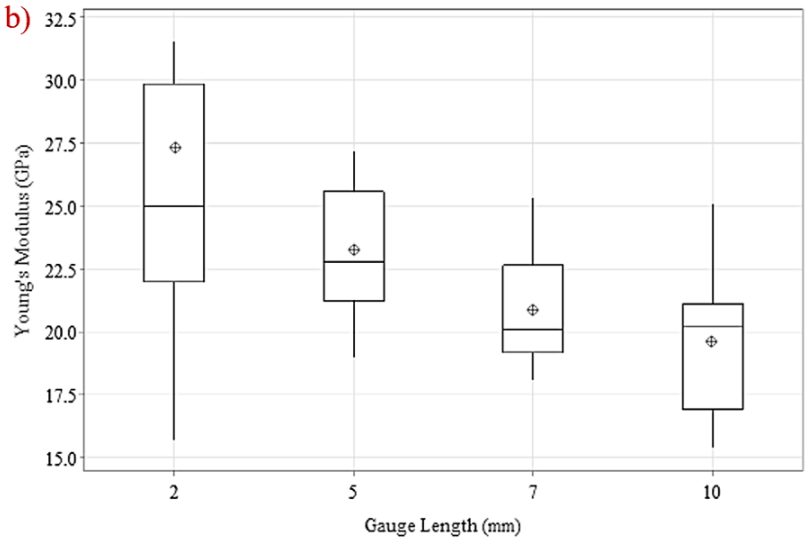

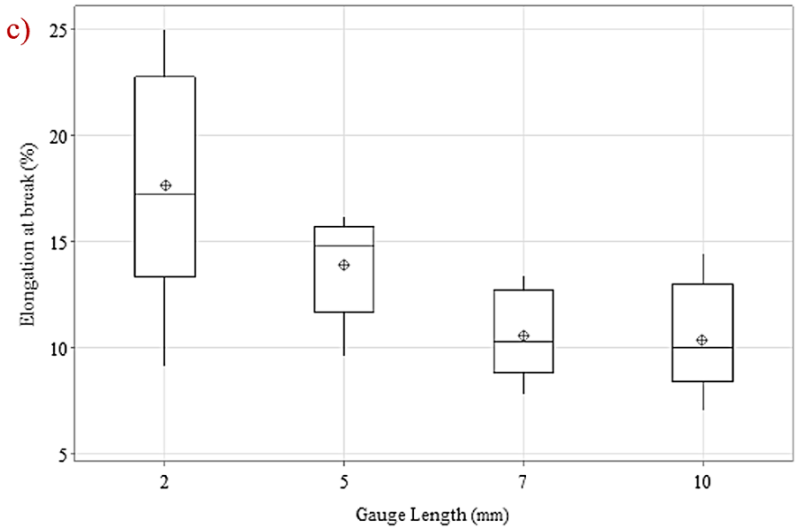

Figure 33 Box plot of tensile properties of viscose single fibres a) Tensile strength b) Young's modulus c) Elongation at break

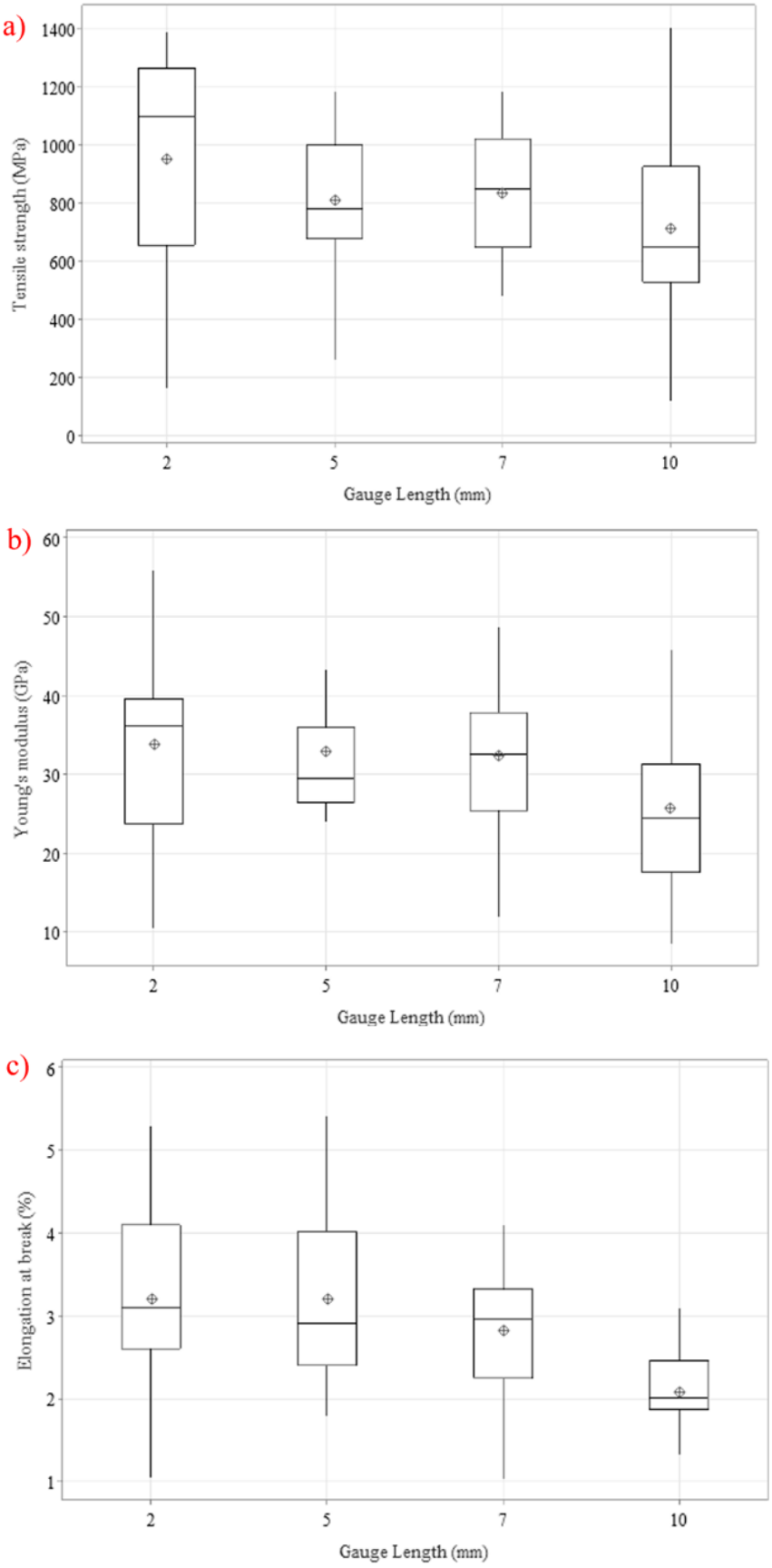

Figure 34 Box plot of tensile properties of standard flax single fibres a) Tensile strength b) Young's modulus c) Elongation at break

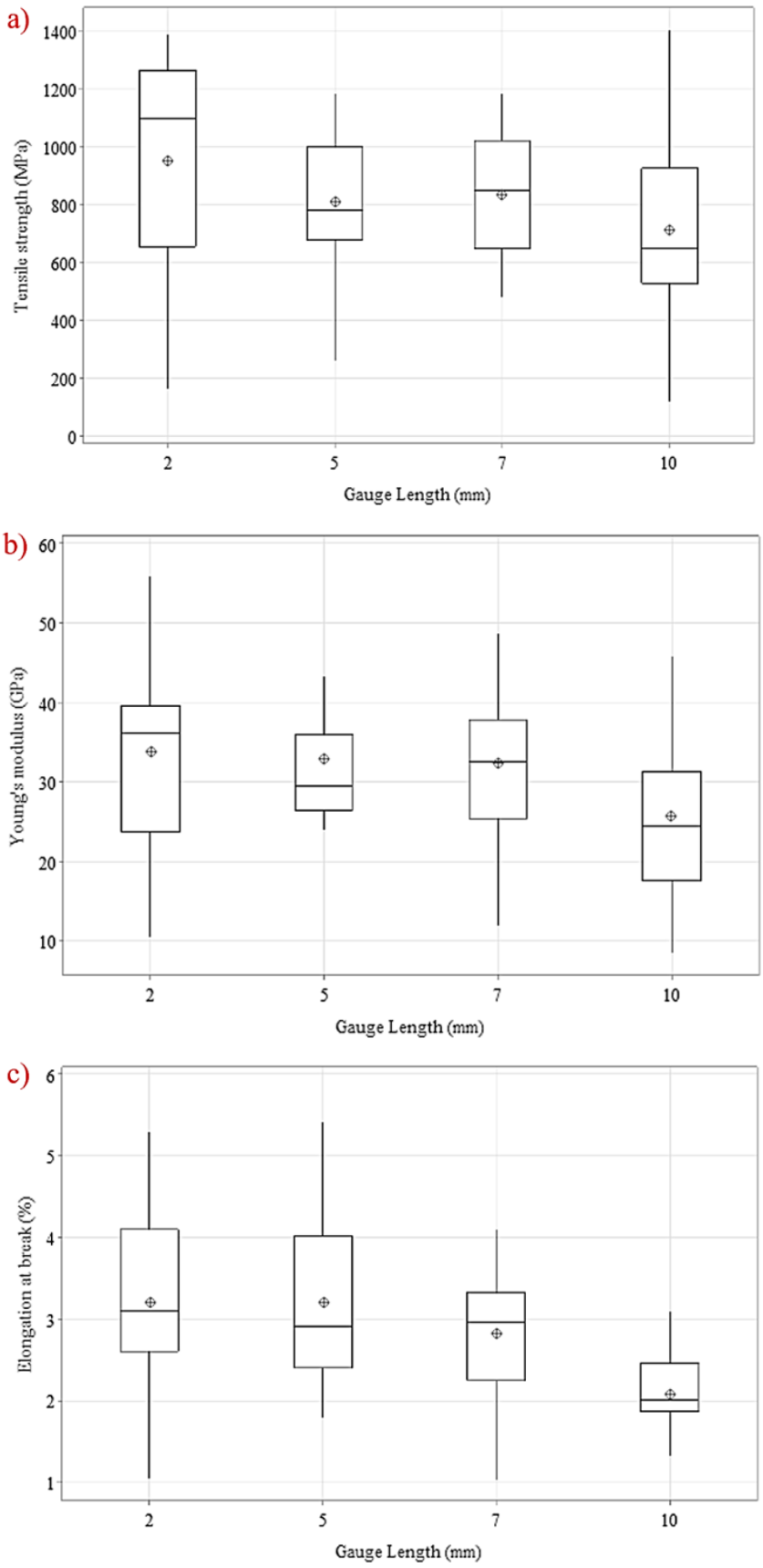

Figure 35 Box plot of tensile properties of bleached flax single fibres a) Tensile strength b) Young's modulus c) Elongation at break

3.3.3 Tensile Properties of Matrix

A comparison of experimental and supplier-provided tensile properties [312,313] of PLA 2003D and PL1005 is given in Table 13. The values from the supplier-provided data sheets are highlighted in parentheses. The experimental properties obtained for PLA 2003D were similar to the supplier-provided values. The experimental tensile strength obtained for PL1005 was significantly higher than the supplier-provided value. This is because of the difference in material processing and testing. According to the technical data sheet, the tensile strength of PL1005 was obtained by testing a PLA sheet obtained from drying the emulsion at 180°C. The experimental tensile strength of PL1005 was obtained in this research after extracting the PLA powder from the emulsion, producing filaments, and performing the tensile strength. Although the tensile strength of PL1005 obtained experimentally differed from the supplier-provided value, it was similar to the experimentally obtained value in the literature [314].

Table 13 Properties of PLA 2003D and PL1005 (supplier-provided values are highlighted in parentheses; NA – not available)

Material	**Tensile strength (MPa)**	**Young's modulus (GPa)**	**Elongation at break (%)**
PLA 2003D	59.8±3.1 (60)	3.7±0.8 (3.5)	3.9±0.6 (6)
PL1005	49.2±4.4 (10)	2.9±0.2 (NA)	3.5±0.9 (NA)

3.3.4 Fracture Surface Analysis of Single Fibres and Matrix

SEM images of fracture surfaces of tensile-tested single viscose, standard flax, and bleached flax fibres are shown in Figures 36 (a), 36 (b), and 36 (c), respectively. SEM image of viscose fibre revealed a brittle fracture surface without any signs of necking or pulling, similar to what was observed in the literature [311]. SEM fracture surface images of standard flax and bleached flax fibres show a complex failure mechanism at the microscale. Firstly, on the outer surface, the fibres tend to break in a brittle manner across the width (transverse failure). Secondly, within the fibres, splitting occurs along the length of microfibrils. Literature suggests that this type of failure mechanism in flax fibres is governed by both surface and internal defects [90,315].

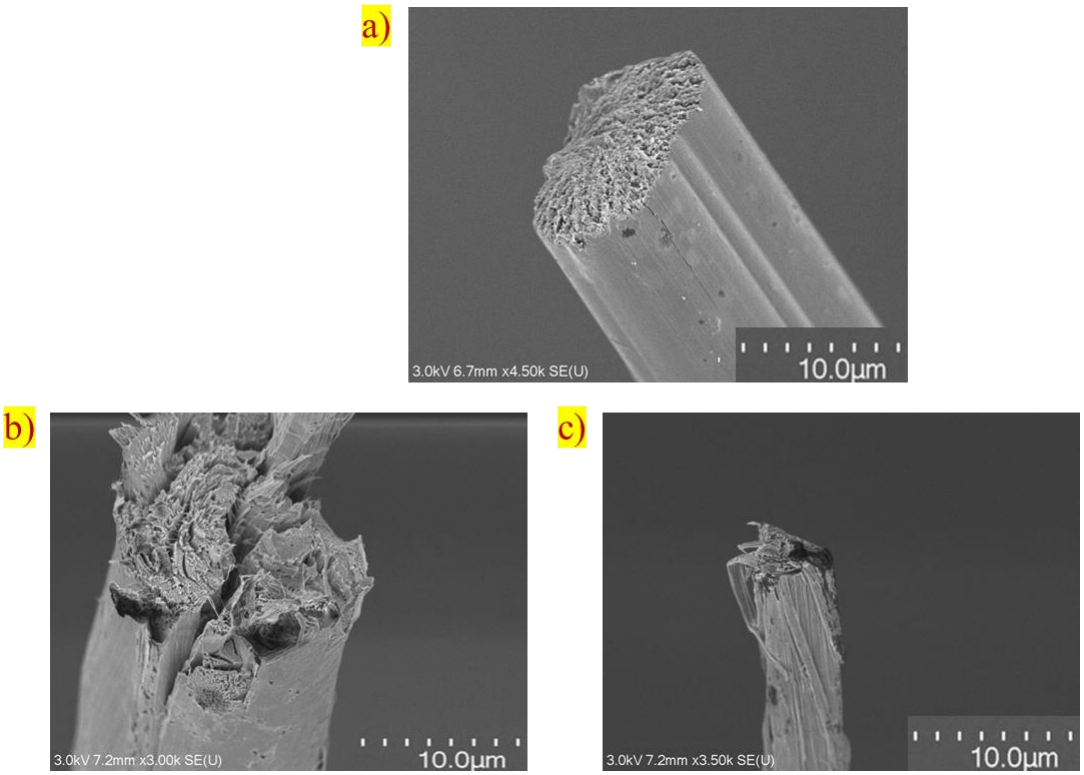

Figure 36 SEM images of fracture surfaces of single fibres a) viscose b) standard flax c) bleached flax

SEM images of fracture surfaces of PLA 2003D and PL 1005 are shown in Figures 37 (a) and 37 (b), respectively. The fracture surface of PLA 2003D shows a smooth and brittle type of failure, resembling the findings reported in the literature [316–319]. PL 1005, on the other hand, displayed porosity along with the typical brittle fracture associated with PLA. PL 1005 was obtained as an emulsion, which was dried to get the powder and further melted and extruded into pellets, from which filament extrusion was done, as explained in section 3.2.3. The porous nature of PL 1005 could be due to the release of air or trapped residual elements released during the extrusion of the filament [320]. The rate of extrusion and cooling could also influence the porosity of the filament. A slower extrusion rate has been proven to reduce voids in the literature. However, degradation of the polymer was observed at slower extrusion rates, due to which it could not be reduced after a certain extent [321,322].

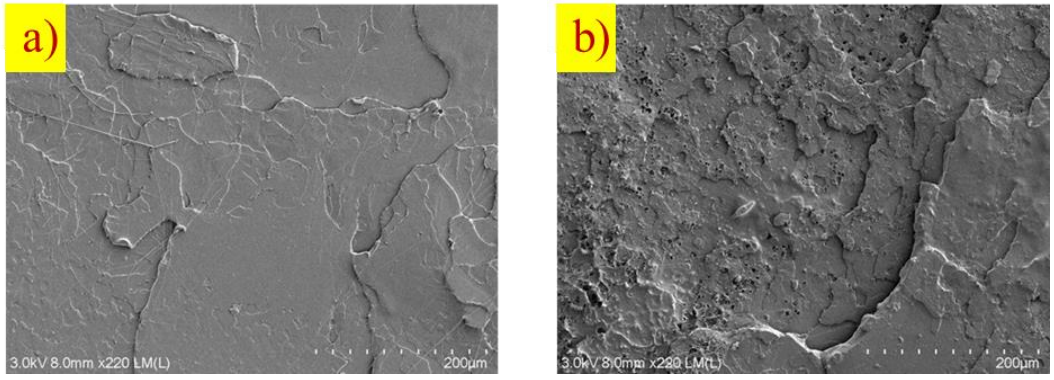

Figure 37 SEM images of fracture surfaces of a) PLA 2003D b) PL1005

3.3.5 Thermal Properties of Matrix and Reinforcements

The TGA and DTG plots of viscose, standard flax, and bleached flax can be seen in Figures 38 (a) and 38 (b). The thermal decomposition behaviour of these bio-derived fibres is characterised by two stages – slow pyrolysis and fast pyrolysis [323]. The slow pyrolysis stage is associated with moisture release and is observed between 50 ºC to 250 ºC. The fast pyrolysis stage occurs from 250 ºC to 350 ºC and is associated with the decomposition of cellulose.

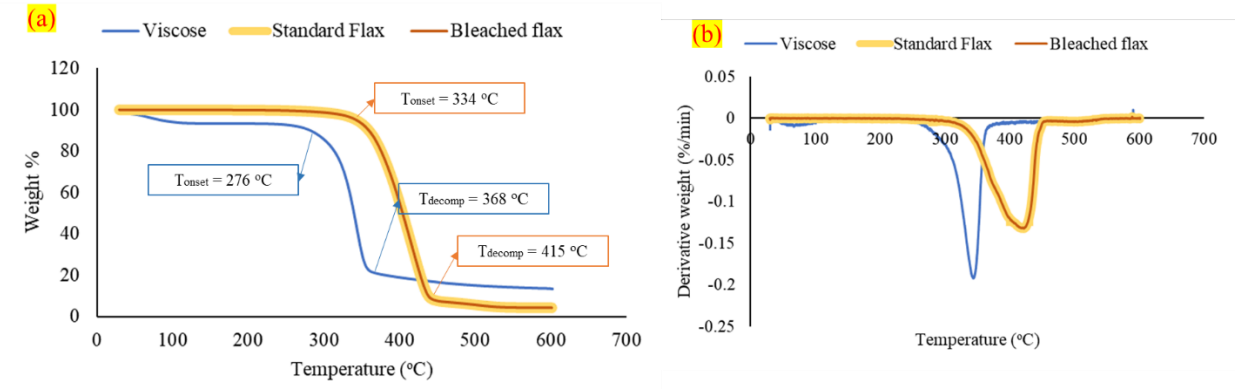

Figure 38 (a) TGA and (b) DTG of standard flax, bleached flax, and viscose fibres

The differences in decomposition profiles and thermal stability between flax and viscose are apparent from the TGA and DTG curves. The cellulose I structure of flax has higher intermolecular bonding and crystallite size compared to the cellulose II structure of viscose. Therefore, flax has higher thermal stability than viscose due to more ordered and packed cellulose regions [324]. The onset temperature for the standard and bleached flax fibres was 334 ºC and 276 ºC for the viscose fibres. The values for all the reinforcements were similar to those presented in the literature [325,326]. Although not seen here, treated flax fibres have been seen to display slightly improved thermal stability, considered to be due to increased crystallinity [326–328]. The absence of improvement in thermal stability could be due to the process followed by the manufacturer to bleach the fibres. Hydrogen peroxide and chlorine

bleaching are the most commonly used bleaching methods for flax fibres [329–332]. Commercial bleaching methods like these primarily focus on achieving lighter colours and improving the crystallinity of flax fibres. While no changes may be observed in the thermal stability of flax following the bleaching process, an improvement in tensile properties was observed, as mentioned earlier, and an increase in crystallinity and surface roughness has also been mentioned as the effects of bleaching in the literature [330–333].

Figures 39 (a) and 39 (b) show the TGA and DTG curves of PLA 2003D and PL1005. The onset and decomposition temperatures of both PLA grades are given in Table 14. PL 1005 displays a higher decomposition temperature than PLA 2003D. PL 1005 also displays higher residue content than PLA 2003D, which could be due to some residual chemicals from the production of PL1005 emulsion. The thermal degradation behaviour of PLA usually depends on the molecular weight and crystallinity [334]. The molecular weight of both PLA grades, as obtained from the manufacturers, is almost similar (around 180000 g/mol), so the crystallinity of these PLA grades needs to be studied further using DSC to understand the differences in behaviour. However, TGA results support that both the PLA grades should be stable in the intended processing temperature range of 190 °C to 220 °C.

Table 14 Onset and decomposition temperatures of PLA 2003D and PL1005

Material	**T_{onset} (°C)**	**T_{decomp} (°C)**
PLA 2003D	295.0	347.5
PL1005	286.2	372.4

DSC thermograms of PLA 2003D and PL 1005 are shown in Figure 39 (c). T_g, T_m, T_{cc}, and degree of crystallinity X_c are given in Table 15. Crystallisation occurred in the PLA 2003D sample between 106 °C and 137 °C, with a peak temperature of 123 °C. Crystallisation enthalpy ΔH_c was calculated as -21.61J/g based on the exotherm heat flow. The degree of crystallinity X_c was calculated to be 0.48% using 93J/g as the melting enthalpy of PLA of infinite crystal size. The DSC results of PLA 2003D were similar to what has been reported in the literature [335]. There was no melting or crystallisation peak observed for PL1005, indicating its amorphous nature. The DSC thermogram of PL1005 is similar to those reported for fully amorphous PLA grades with more than 10–12% D-isomer contents [336,337]. Amorphous PLA tends to have lower strength and higher elongation at break than semi-crystalline PLA, which also agrees with the tensile test results.

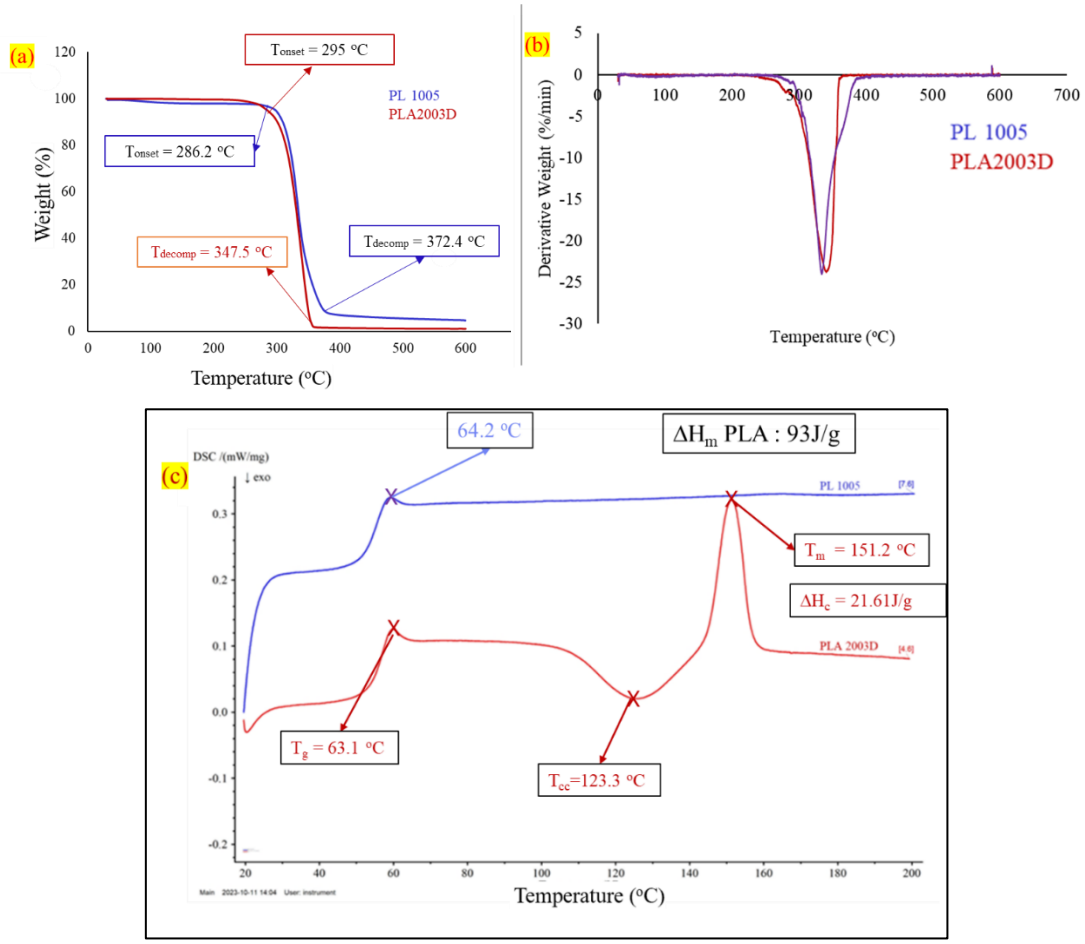

Figure 39 a) TGA of PLA 2003D and PL1005 b) DTG of PLA 2003D and PL1005 c) DSC of neat PLA 2003D and PL1005

Table 15 Summary of DSC results for neat PLA

Material	T_g (°C)	T_m (°C)	T_{cc} (°C)	X_c (%)
PLA 2003D	63.1	151.2	123.3	0.48
PL1005	64.2	-	-	-

3.4 Conclusions

The raw materials used to develop bio-derived fibre-reinforced composites were characterised in this chapter. Tensile test results of single fibres of standard flax, bleached flax, and viscose fibres fitted within the expected range compared to literature values. Viscose fibres demonstrated an average tensile strength of 724.2 MPa, a Young's Modulus of 22.8 GPa, and an elongation at break of 13.2%. Standard flax fibres exhibited an average tensile strength of 821.3 MPa, a Young's Modulus of 31.8 GPa, and an elongation at break of 2.8%. Bleached flax fibres displayed the highest average tensile strength at 921.6

MPa, a Young's Modulus of 30.7 GPa, and an elongation at break of 3.3%. The data indicates that bleached flax possesses the highest tensile strength among the tested fibres, while viscose exhibits the highest elongation at break. Out of the two grades of PLA tested, the semi-crystalline PLA 2003D grade displayed better tensile properties than the amorphous PL1005. TGA of fibres and matrices was done to obtain stable temperature ranges for processing the materials. Both bio-derived reinforcement and matrix were stable up to 250 ^{o}C. DSC of PLA 2003D and PL1005 revealed their semi-crystalline and amorphous natures, respectively.

Chapter 4: Long/Continuous Bio-Derived Fibre Reinforced PLA Composite Filaments Produced by Solution Impregnation

4.1 Introduction

In this chapter, the process of solution impregnation and the resulting properties are detailed. As mentioned earlier, achieving good interfacial adhesion is crucial to producing high-performance composites. The impregnation process was optimised to achieve the best possible fibre wetting to support interfacial adhesion. The solution impregnation process development, effect of impregnation parameters, resulting mechanical properties, and SEM of fracture surfaces are included in detail.

4.2 Materials

Viscose, flax, and bleached flax fibre yarns mentioned in Chapter 3 were used as reinforcements. PLA 2003D grade was used for preparing the PLA solution. Dichloromethane (DCM) supplied by Sigma Aldrich (New Zealand) was used as a solvent.

4.3 Methods

4.3.1 Solution Impregnation and Consolidation

Impregnation: The process started with vacuum drying PLA at 45 ^{o}C for four hours and the yarns at 100 ^{o}C for 24 hours. The next step was to prepare PLA solution by dissolving the desired concentration of PLA in DCM for at least 4 hours. Initially, a single impregnation bath was used, as shown in Figure 40, which was later updated to have two baths in tandem, as shown in Figure 41. Two different concentrations of PLA solution were used for six different formulations, including single and tandem impregnation systems, as summarised in Table 16.

A yarn spooler was used to feed the yarn directly to the impregnation bath (manufactured at the University of Waikato, New Zealand), which consisted of squeezing rollers. Wing nuts were used to adjust the squeezing rollers in the impregnation bath, ensuring the gap was just wide enough for the impregnated yarn to pass through. The solution in the impregnation bath is kept agitated using a magnetic stirrer. Rollers in the impregnation bath enable the splaying of fibres, thereby increasing the chances of wetting through the thickness of the yarn. The excess resin is removed by passing through a 1mm diameter nozzle at the exit of the impregnation bath. The impregnated filament passes through the solvent evaporation zone and is collected onto the winding mandrel. The solvent was evaporated by using heated air from two blow dryers. If the SEM results show that the matrix was homogeneously dispersed within the yarn, the filament is approved for consolidation. If the matrix dispersion in the yarn is poor or limited to the edges, another impregnation cycle is run, and the process is repeated until the

desired impregnation is achieved or no further improvement is observed after a certain number of cycles.

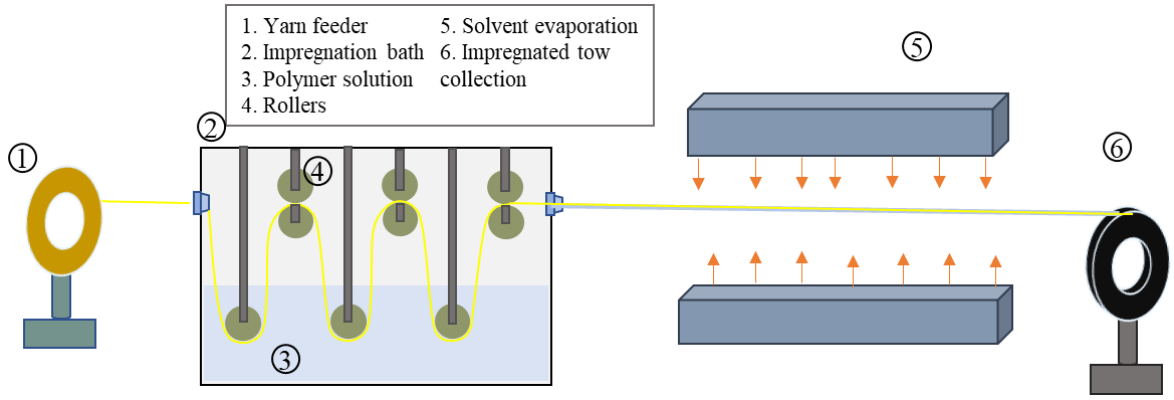

Figure 40 Solution impregnation process with a single impregnation bath

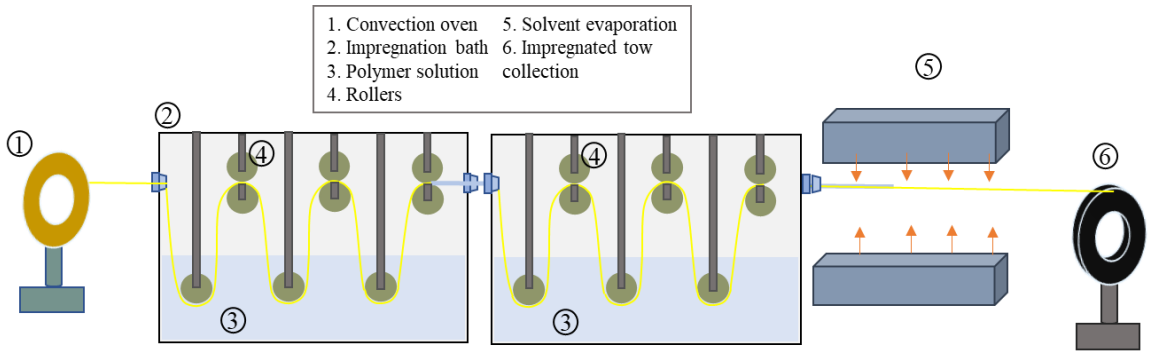

Figure 41 Solution impregnation process with two impregnation baths in tandem.

Table 16 Solution impregnation formulations

Serial No	**Solution Impregnation Formulation**
1	10wt% x1 – Single impregnation cycle with 10wt% PLA/DCM solution
2	10wt% x2 – two single impregnation cycles with 10wt% PLA/DCM solution
3	7wt% x2 – two single impregnation cycles with 7wt% PLA/DCM solution
4	7wt% x3 – three single impregnation cycles with 7wt% PLA/DCM solution
5	7wt% x1 (tandem) – one tandem impregnation cycle with 7wt% PLA/DCM solution

6	7wt% x2 (tandem) – two tandem impregnation cycles with 7wt% PLA/DCM solution

Consolidation: The impregnated yarn undergoes consolidation to enhance the bonding between the matrix and fibre and eliminate voids. The impregnated filament is dried at 80°C in a vacuum oven for six hours and passed through a heated consolidation die. The dimensions of the consolidation die, and the calculation of the exit nozzle area are shown in Figure 42. The entrance and exit of the die are tapered to prevent void formation, and the temperature of the die is between 210 °C to 215 °C.

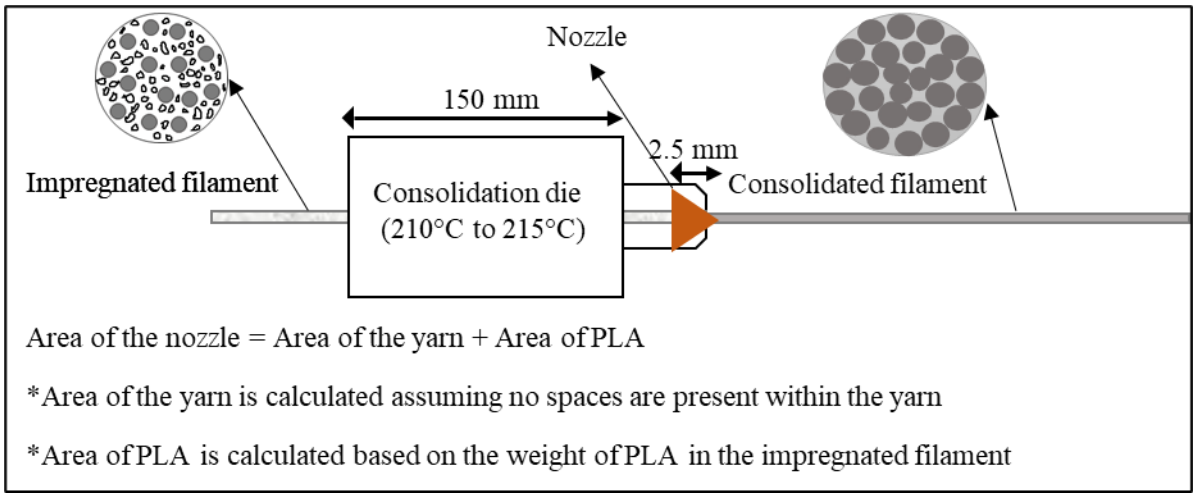

Figure 42 Consolidation process of impregnated filaments

4.3.2 Optical Microscopy

Optical microscopy images of cross-sections of consolidated filaments after each impregnation formulation were captured using an Olympus BX53 microscope. The samples for microscopy were prepared by manually mounting the samples in a silicon mould and pouring the epoxy resin into the mould. Specimens were removed from the mould after 24 hours of curing at room temperature and then ground and polished to reveal the cross-sections of the filaments. The embedded composite filaments can be seen in Figure 43. A series of rough and fine abrasive papers starting from 320 followed by 500, 1000, 2000 and 4000 grit were used for grinding. Polishing was performed using a Tegramin-25 auto-polishing machine and OP-U oxide polishing suspension supplied by Struers.

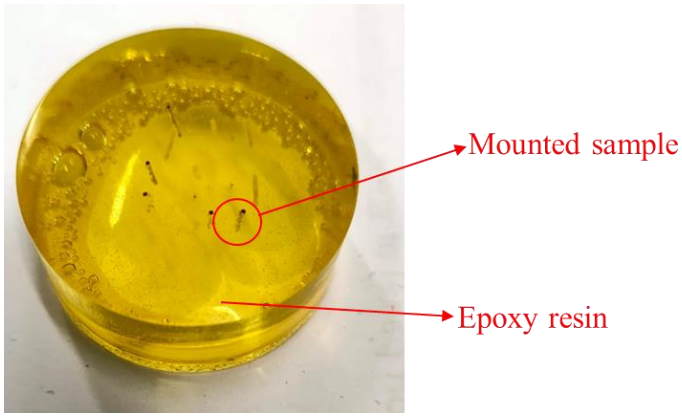

Figure 43 Composite filaments mounted in epoxy resin for optical microscopy.

4.3.3 Porosity and Reinforcement Weight Percentage Analysis

The porosity of the composite filaments was estimated using ASTM D792 standard. In this method, experimental and theoretical densities of the composite filament are used to determine the porosity. The experimental density of the composite filament can be found by using Archimedes' principle given by equation 1[338].

$$\rho_{ce} = \frac{M_a}{(M_a - M_w)} * \rho_w \quad (1)$$

ρ_{ce} is the experimental density of the composite filament sample. M_a is the mass of the composite filament in air, M_w is the mass of the composite filament in water, ρ_w is the density of water.

Theoretical calculation of the density of the composite filament can be done using the rule of mixtures given by equation 2 [339].

$$\rho_{ct} = \rho_f V_f + \rho_m V_m \quad (2)$$

ρ_{ct} is the theoretical density of the composite sample. ρ_f, ρ_m are the densities of fibre and matrix, respectively, and V_f, V_m are the volume fractions of fibre and matrix, respectively. The theoretical density of the PLA matrix (1.24 g/cm^3) and viscose fibres (1.5 g/cm^3) was provided by the supplier, whereas the densities of the flax fibres (1.4 g/cm^3) [340] were obtained from literature because the supplier data did not include the information.

Using the theoretical and experimental values of composite density, the porosity percentage can be evaluated using equation 3 [341].

$$\%\, porosity = \{(\rho_{ct} - \rho_{ce}) \div \rho_{ct}\} \times 100\% \quad (3)$$

A weight analysis was performed to evaluate the amount of PLA impregnated into the yarns. Five sections of 1 metre each were selected for each reinforcement and impregnation method to perform this analysis. Each section was individually weighed in a dry state before and after impregnation. The recorded weights were used to calculate reinforcement percentages.

4.3.4 Tensile Testing

The tensile properties of the composite were evaluated both theoretically and experimentally.

Theoretical calculation of tensile strength and Young's modulus in the longitudinal direction of the composite will be calculated using the rule of mixtures equations below:

$$\sigma_l = \sigma_m(1-V_f) + \sigma_f V_f \quad (4)$$

Where σ_l is the tensile strength in the longitudinal direction, σ_m, is the stress in the matrix at fibre failure, σ_f is the ultimate tensile strength of the fibre, and V_f is the fibre volume fraction.

$$E_l = E_m(1-V_f) + E_f V_f \quad (5)$$

E_l is Young's modulus in the longitudinal direction, E_m is Young's modulus of the matrix, E_f is Young's modulus of the fibre, and V_f is the fibre volume fraction [342].

Experimental tensile testing of the composite filaments was conducted by mounting the composite filaments in 3D printed tabs. These tabs were designed to have a groove with a diameter of 0.5 mm, as shown in Figure 44 (a). A commercial neat PLA filament was used for 3D printing of the tabs. The composite filament was placed in the groove, and epoxy was used to seal two tabs together with the filament in the centre. An adhesive tape was used to hold the tabs together until the epoxy was cured, as shown in Figure 44 (b). The specimens were cured for 24 hours under a pressure of 0.5 tons using a hydraulic press at room temperature. The cured samples were conditioned in a climatic chamber (Binder GmbH, Model KMF 115, Tuttlingen, DE) for 48 h at 23 ºC and 50% relative humidity before testing. An Instron® (model 5982) universal testing machine with a 500 N load cell was used. The diameters of the filaments were measured using an Olympus BX60F5 optical microscope. The diameter of each filament was measured at five different points, and the average value was used for testing and calculations. All the samples were tested at a 5 mm/min crosshead displacement rate and a gauge length of 30 ± 2 mm.

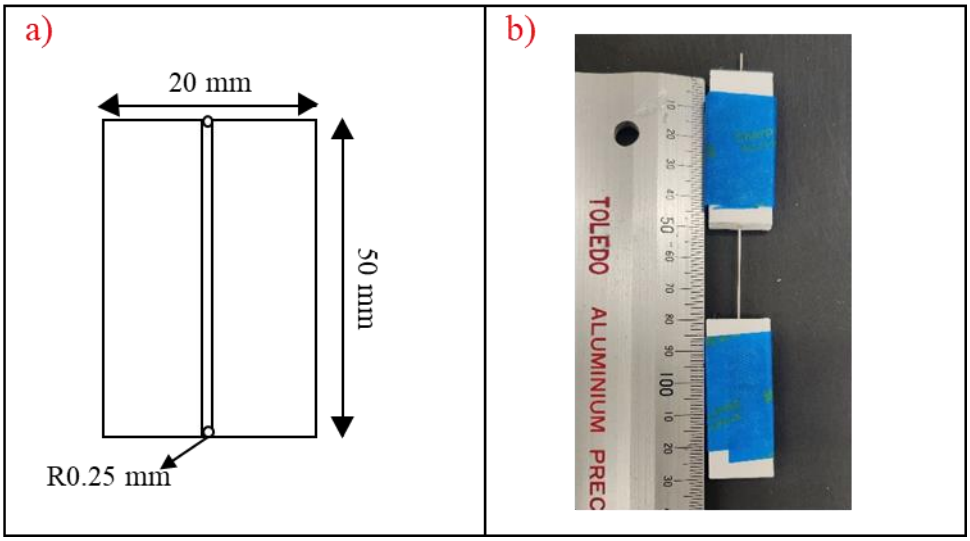

Figure 44 a) Dimensions of the tensile testing tab b) Mounting of composite filament using 3D printed tabs.

4.3.5 SEM of Fracture Surfaces

A Hitachi S-4000 field emission scanning electron microscope, operated at 3 kV, was used to inspect the cryofracture surfaces of impregnated and consolidated filaments and the fracture behaviour of the composite filaments. The samples were mounted on aluminium tabs with the help of carbon tape and sputtered with platinum before the observation, similar to the method described in section 3.2.4.

4.4 Results and Discussion

4.4.1 Assessment of Impregnation and Consolidation Process

The impregnation process is aimed at achieving the wetting of fibres in the yarn by PLA. A homogeneous filling of the yarn is essential to achieve wetting of all the fibres in the yarn. Multiple formulations were tested to find the optimum impregnation parameters. The first impregnation cycle was performed using a 10wt% PLA/DCM solution. PLA/viscose filaments displayed a homogenous distribution of polymer when compared to the PLA/standard flax and PLA/bleached flax filaments, which displayed pooling of polymer at the edges of the filament and little to no polymer at the centre, as shown in Figure 45. The twisted nature of flax yarns could be the reason for the lack of polymer reaching the centre of the filament. However, mechanical interlocking between the polymer and the fibre appeared higher for PLA/standard flax and PLA/bleached flax filaments than for the PLA/viscose filament, as highlighted by yellow arrows in Figure 46. This could be due to the rougher surface of the flax fibres creating more sites for mechanical interlocking compared to the smooth viscose fibres. Polymer content within the filament was noticeably low in all three filaments, which created empty spaces or voids within the filament.

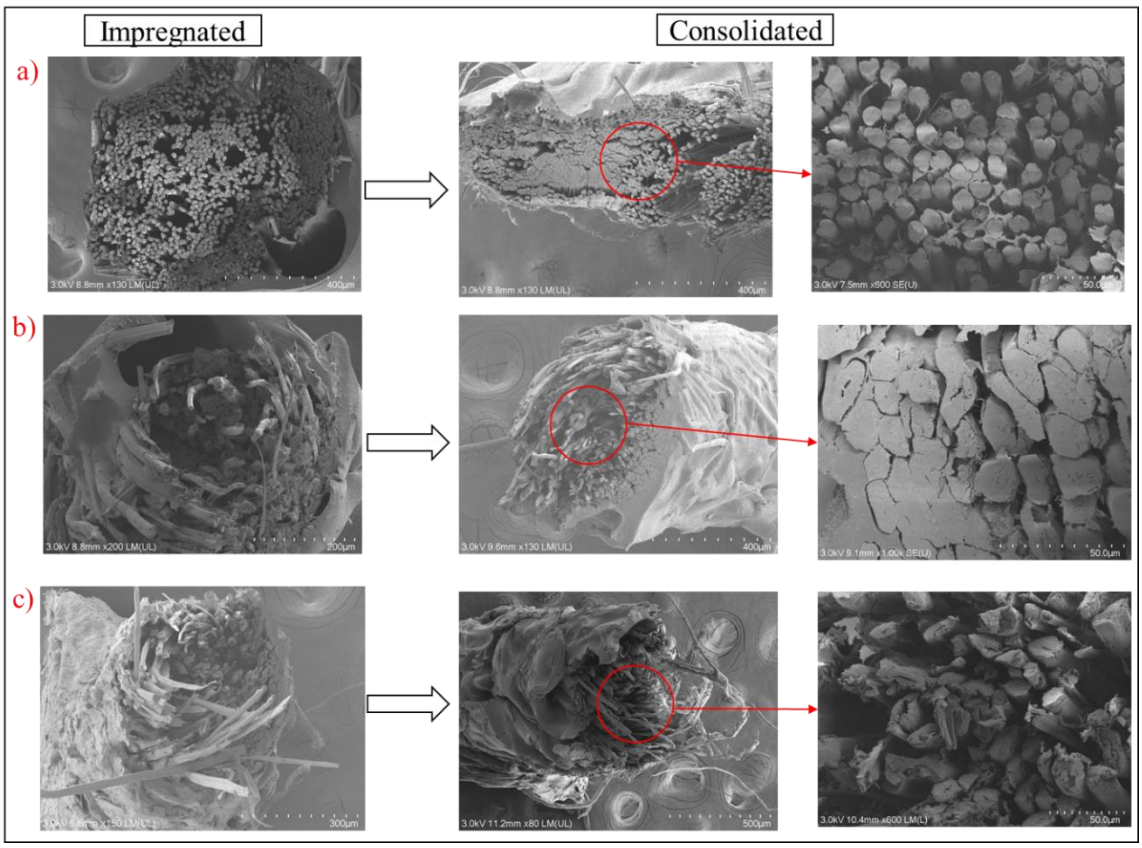

Figure 45 SEM images of cryofracture surfaces of impregnated and consolidated filaments using 10wt%x1 formulation a) PLA/viscose b) PLA/standard flax c) PLA/bleached flax.

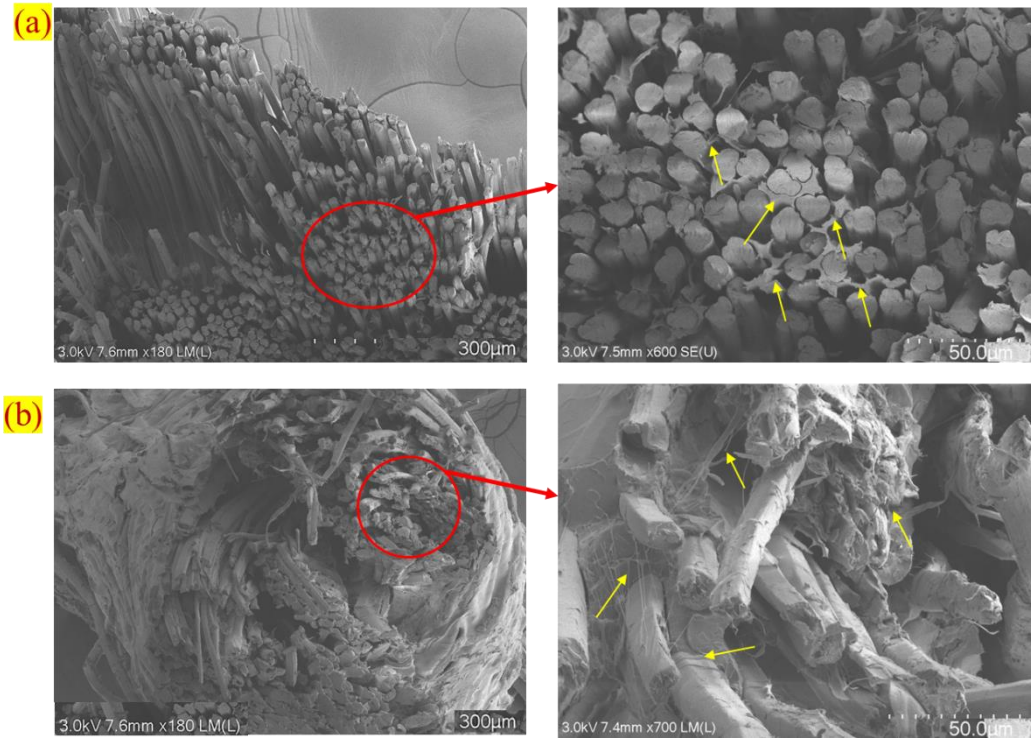

Figure 46 SEM images of cryofracture surfaces depicting mechanical interlocking between PLA and fibres a) PLA/viscose b) PLA/bleached flax as an example of solution impregnation.

A second impregnation cycle was performed using the same parameters to improve the uptake of polymer into the yarns and promote further wetting. A slight increase in polymer content was observed for all three filaments, but a significant improvement could not be seen in polymer distribution within the PLA/standard flax and PLA/bleached flax filaments.

The viscosity of the PLA/DCM solution was reduced to 7wt% to help the polymer reach the centre and improve fibre wetting. The formulation with two impregnation cycles performed with 7 wt% PLA/DCM solution improved wetting central fibres for PLA/standard flax and PLA/bleached flax filaments. However, voids were still prominent in all three filaments due to lower polymer content (SEM images of cryofracture surfaces of all formulations after impregnation and consolidation are given in Appendix 1). So, a third cycle was performed to enhance the polymer uptake. While a noticeable difference could not be observed for PLA/viscose filaments, PLA/standard flax and PLA/bleached flax filaments displayed an improvement in polymer penetration to the centre of the yarn and reduction in voids, especially after consolidation, as shown in Figure 47.

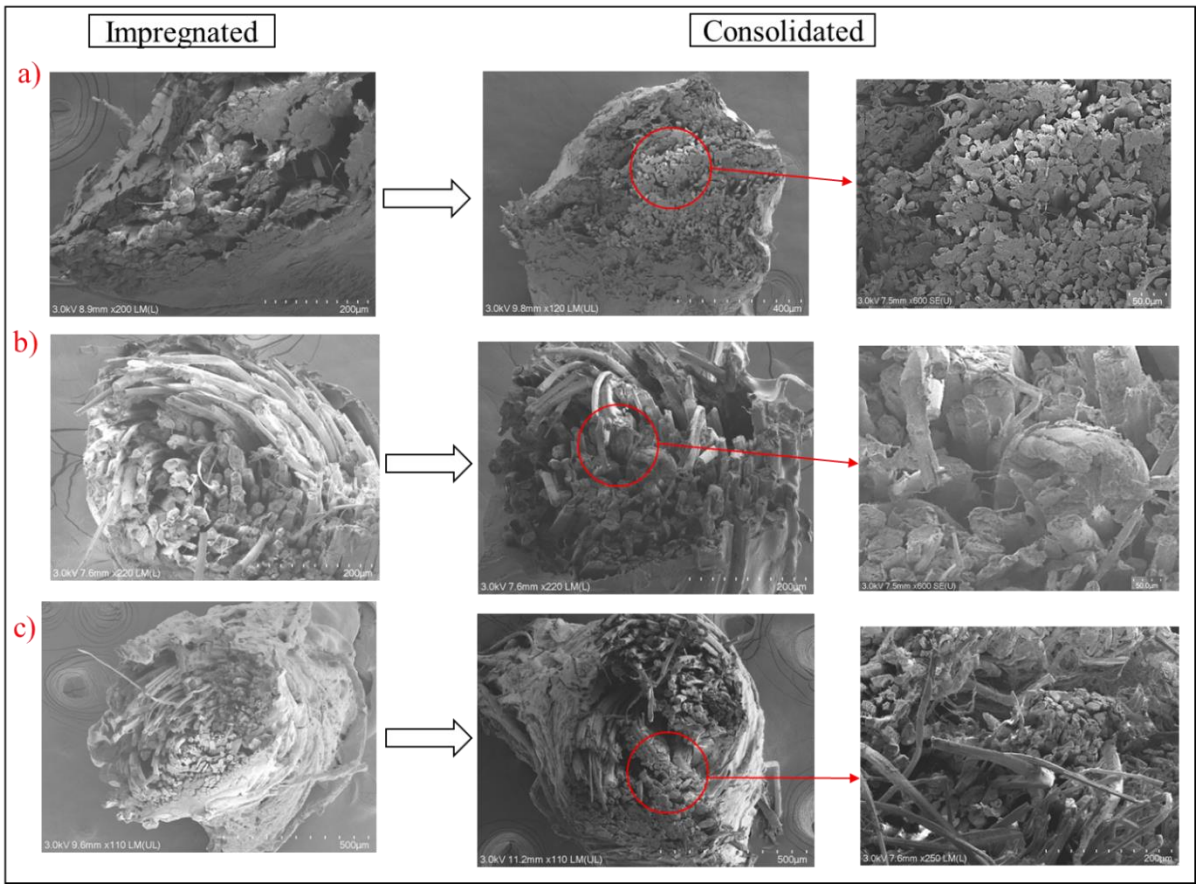

Figure 47 SEM images of cryofracture surfaces of impregnated and consolidated filaments using 7wt%x3 formulation a) PLA/viscose b) PLA/standard flax c) PLA/bleached flax.

Further, a tandem impregnation method was implemented where two impregnation baths were used in tandem. Samples were prepared with 7 wt% PLA/DCM solution at one and two tandem impregnation

cycles. It was observed that the samples with three single impregnation cycles (7wt%x3) and two tandem impregnation cycles (7wt%x2 (tandem)) had the highest polymer content and homogeneous polymer distribution compared to all the other formulations.

Optical microscope images of consolidated filaments of all solution impregnation formulations of PLA/viscose, PLA/standard flax, and PLA/bleached flax can be seen in Figures 48, 49, and 50, respectively. The cross-sectional views of the filaments display an irregular shape and porosity due to voids. These voids are classified into impregnation, interface, and fibre porosity, as highlighted in Figure 51 [343]. Voids caused by impregnation porosity appear dominantly in all the filaments in the form of cracks. Insufficient polymer impregnation is the cause of these crack-like voids. Interface porosity, on the other hand, is caused due to poor interfacial adhesion and was observed to be more dominant in PLA/viscose filaments [343]. Fibre porosity is related to the porosity due to the lumen of the bio-derived fibre. Since viscose fibres do not have a lumen, this is observed only for standard flax and bleached flax reinforced filaments.

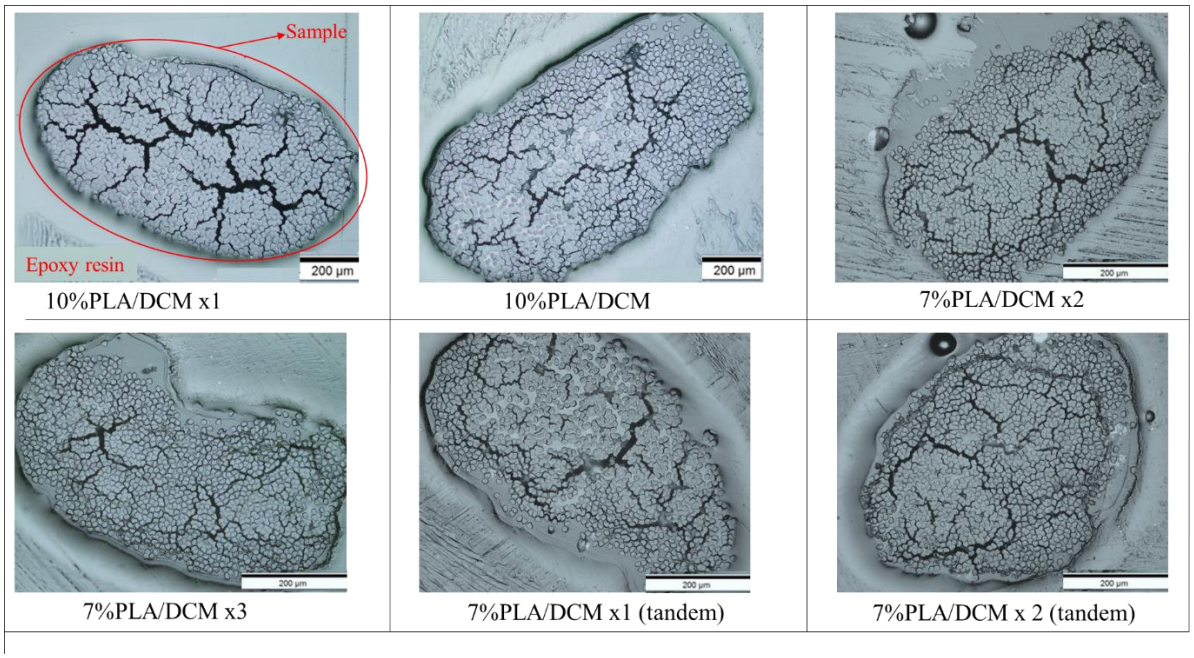

Figure 48 Optical microscope images of consolidated filaments for different formulations – PLA/viscose

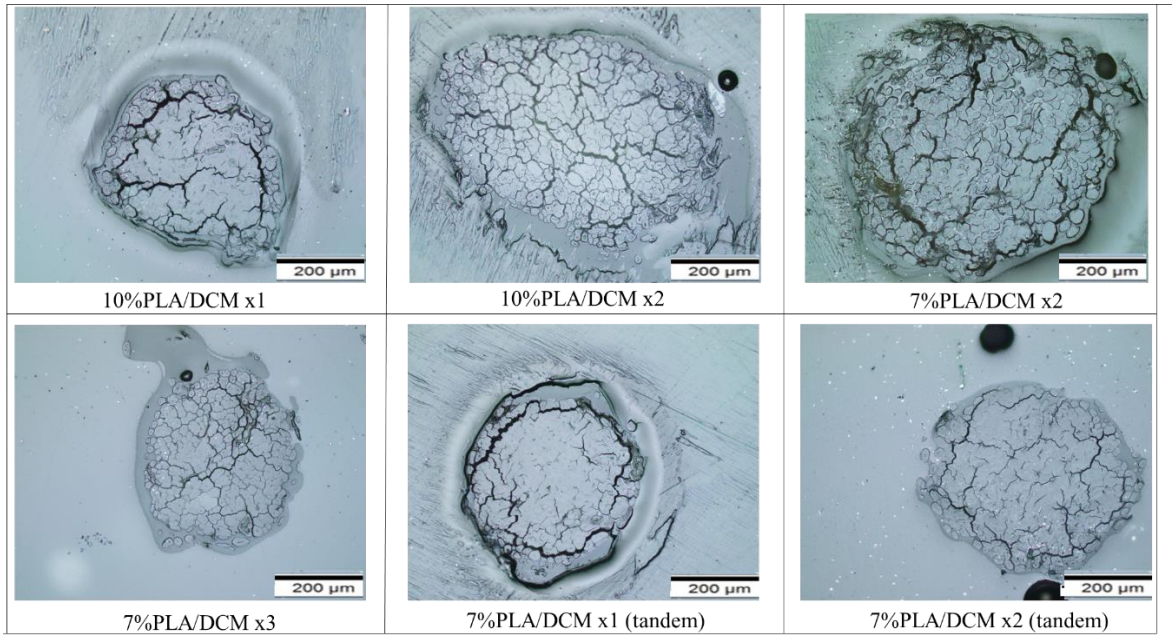

Figure 49 Optical microscope images of consolidated filaments for different formulations - PLA/standard flax

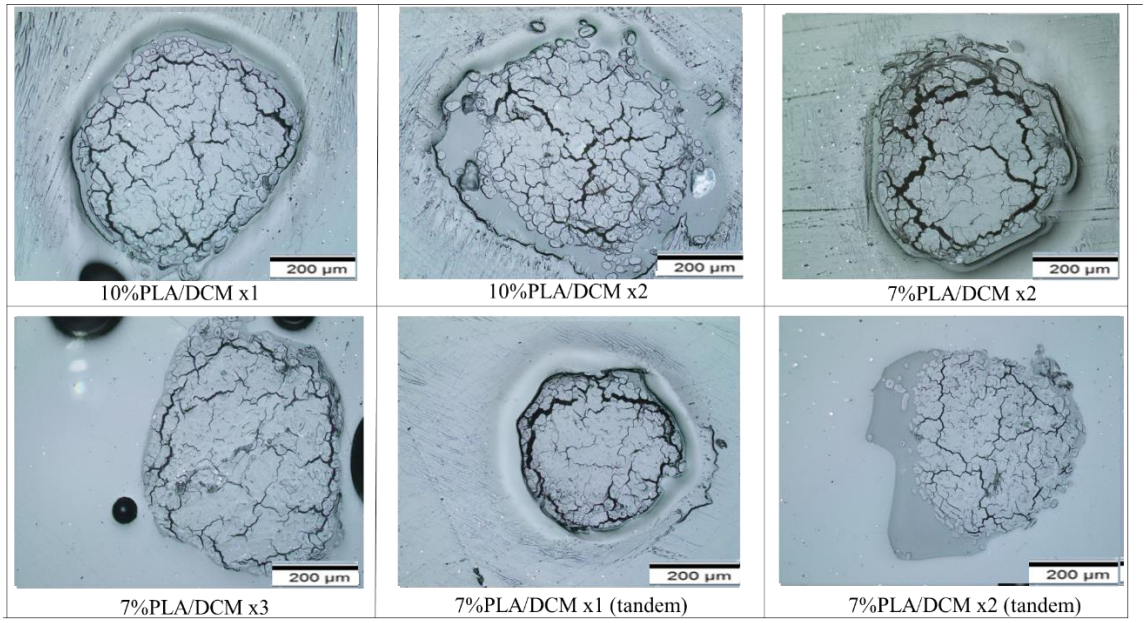

Figure 50 Optical microscope images of consolidated filaments for different formulations - PLA/bleached flax

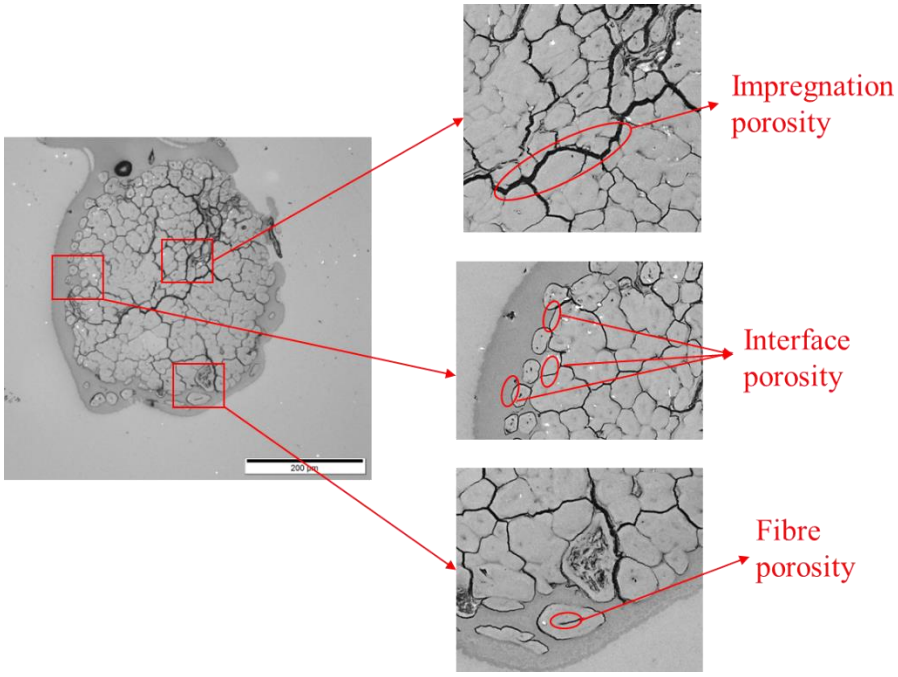

Figure 51 Types of porosities observed in optical microscope images of consolidated filaments.

Impregnation and interface porosity in the PLA/viscose filaments did not change significantly with multiple cycles. In contrast, PLA/standard flax and PLA/bleached flax filaments display a reduction in impregnation porosity and improvement in polymer distribution with an increasing number of impregnation cycles and a reduction in viscosity. In literature, impregnation and interface porosity were reported in flax yarn reinforced filaments produced from melt and solution impregnation techniques [37,217,344][206]. An increase in consolidation pressure (>1.5 MPa) using compression moulding displayed a reduction in porosity and an improvement in tensile strength and modulus in solution-impregnated flax composites [345,346].

The irregular shape of the filaments is assumed to be related to the low polymer content in the filaments. During the consolidation process, a circular-shaped nozzle is used. However, in the filaments with less polymer content, the shape of the filament could be affected by the absence of enough polymer to form the circular shape. It can be observed from the optical microscope images that the filaments with multiple impregnation cycles develop a more circular shape due to higher polymer content.

4.4.2 Porosity and Reinforcement Weight Percentage Analysis

The percentage of reinforcement by weight and porosity for all the formulations of solution impregnation are given in Table 17. The results agreed with the microscope image analysis, where the amount of polymer in the filament has increased with an increase in the number of impregnation cycles. The porosity percentage was higher than 15% in formulations with lower than 25% polymer content. The lowest porosity values were recorded for 7wt%x2 (tandem) formulation with 8.0±3.2 % for

PLA/Viscose, 7.2±2.1 for PLA/standard flax, and 6.2±3.1 for PLA/bleached flax composite filaments. A significant difference was not observed for single impregnation and tandem formulations, as seen in Table 17 for 7wt%x2 and 7wt%x1(tandem) formulations where average reinforcement and porosity percentages were similar. The general trend observed was that the porosity percentage decreased as the polymer content increased, similar to what was reported in the literature. An increase in porosity (> 6.8%) in flax yarn reinforced composites with a high fibre content (>50 wt%) was reported in the literature [347,348]. An experimental model based on unidirectional flax composites showed that porosity content in flax fibre/thermoplastic composites increases significantly above a fibre wt % of 61%, and the optimum combination of low porosity and high fibre wt% is around 61% [343].

Table 17 Fibre and polymer weight percentage and porosity percentage of composite filaments produced using solution impregnation and consolidation method.

Solution impregnation formulation	**Composite Filament**	**Weight % of Reinforcement**	**Weight % of Polymer**	**Porosity (%)**
10wt%x1	PLA/Viscose	76.8±0.2	23.2 ± 0.2	19.8±1.8
	PLA/Standard flax	82.1±1.5	17.9 ± 1.5	17.9±3.7
	PLA/Bleached Flax	77.8±0.2	22.2 ± 0.2	14.5±4.6
10wt%x2	PLA/Viscose	63.2±0.9	36.8 ± 0.9	20.2±2.4
	PLA/Standard flax	73.80±0.2	26.20 ± 0.2	15.0±4.5
	PLA/Bleached Flax	72.2±1.2	27.8 ± 1.2	14.9±4.2
7wt%x2	PLA/Viscose	65.5±2.0	34.5 ± 2.0	14.2±4.5
	PLA/Standard flax	74.20±0.2	25.80 ± 0.2	19±3.5
	PLA/Bleached Flax	74.80±1.4	25.20 ± 1.4	12.8±9.3
7wt%x3	PLA/Viscose	68.1±0.6	31.9 ± 0.6	9.5±3.6

	PLA/Standard flax	66.7±0.3	33.3 ± 0.3	8.0±2.4
	PLA/Bleached Flax	64.3±0.1	35.7 ± 0.1	6.5±3.7
7wt%x1 (tandem)	PLA/Viscose	70.8±0.6	29.2 ± 0.6	14.7±2.6
	PLA/Standard flax	72.2±0.4	27.8 ± 0.4	16.6±3.5
	PLA/Bleached Flax	69.2±0.2	30.8 ± 0.2	13.3±8.4
7wt%x2 (tandem)	PLA/Viscose	64.3±1.0	35.7 ± 1.0	8.0±3.2
	PLA/Standard flax	62.1±0.3	37.9 ± 0.3	7.2±2.1
	PLA/Bleached Flax	60±0.2	40 ± 0.2	6.2±3.1

4.4.3 Tensile Properties of Composite Filaments

A summary of experimental and theoretical tensile properties of composite filaments produced from different formulations of solution impregnation and consolidation is given in Table 18. The theoretical tensile properties calculated using the rule of mixtures formulae are highlighted in parentheses for comparison. Theoretically, the tensile properties of a composite increase with the increasing fibre content because the reinforcing fibres typically have higher properties than the matrix, and the calculations assume that there are no defects or voids within the composite. The experimentally obtained tensile properties for PLA/standard flax and PLA/bleached flax varied significantly from the theoretical values. This could be attributed to the high linear density of bleached flax yarns, which leads to a high twist and reduced mechanical properties in the composite. The linear density of bleached flax yarns used in the present study is 2083 dtex, corresponding to an approximate twist angle of 17º according to the mathematical model for the effect of increasing yarn linear density (tex) on yarn structure presented by Darshil *et al*. The study also reported a decrease of composite tensile strength by approximately 50% at a twist angle of 17º for flax yarn reinforced composites, which aligns with the results obtained in the current study [349]. Interestingly, the experimental properties obtained for PLA/standard flax and PLA/bleached flax composites with low polymer content formulations (10wt%x1, 10wt%2, 7wt%x2) were similar to the literature values reported for tensile properties of flax yarns. This is because the tested specimen behaved like the textile yarn rather than the composite, which

points towards inadequate wetting and poor interfacial adhesion [315,350,351]. For PLA/standard flax and PLA/bleached flax filaments, as the polymer content increased, an increase in experimental tensile properties was observed until an optimum point was reached for 7wt%x3 and 7wt%x2 (tandem) formulations, where a further reduction in fibre content started to have a negative effect on the properties. On the other hand, PLA/viscose composites did not display significant differences in polymer content or tensile properties with an increase in the number of impregnation cycles and changes in solution viscosity. This was because the viscose yarn does not have any twist and, therefore, does not require additional cycles to push the polymer into the centre of the yarn.

The experimental results were consistent with the porosity analysis, where the formulations with lower porosity exhibited higher tensile properties, especially for PLA/standard flax and PLA/bleached flax. Increasing the number of impregnation cycles resulted in increased polymer content in the filament and increased possible sites of mechanical interlocking. Among the formulations, the highest tensile strength is observed in the 7wt%x3 formulation with PLA/bleached flax (356.1±6.8 MPa), the highest Young's modulus was obtained for the 7wt%x2 (tandem) formulation with PLA/bleached flax (17.6±0.8 GPa), and the highest elongation at break was obtained for the 10wt%x2 formulation with PLA/viscose (15.6±3.2) as can be seen in Table 18. The stress-strain curves of these filaments are shown in Figure 52. The elongation at break of PLA/viscose filaments is noticeably higher than the single viscose fibres, and the reason for this could be the sliding of fibres within the filament due to separation caused by reduced fibre diameter during tensile testing. Viscose fibres tend to reduce more in diameter than flax fibres upon tensile testing, which can cause separation and sliding of fibres, resulting in higher elongation at break values. Figure 53 shows the difference between the diameters of standard flax and viscose single fibres before and after the tensile test to highlight the viscose fibre diameter reduction.

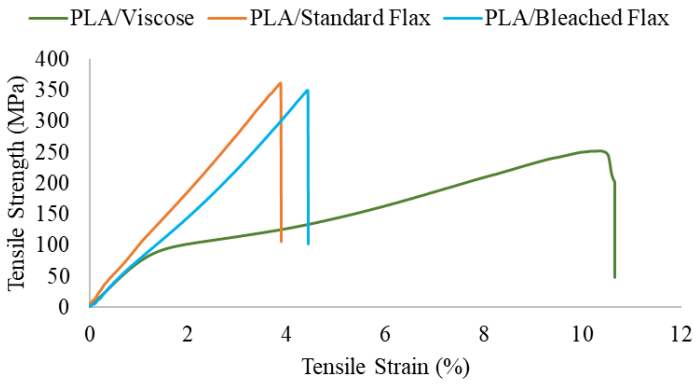

Figure 52 Stress-strain curves of composite filaments produced using solution impregnation.

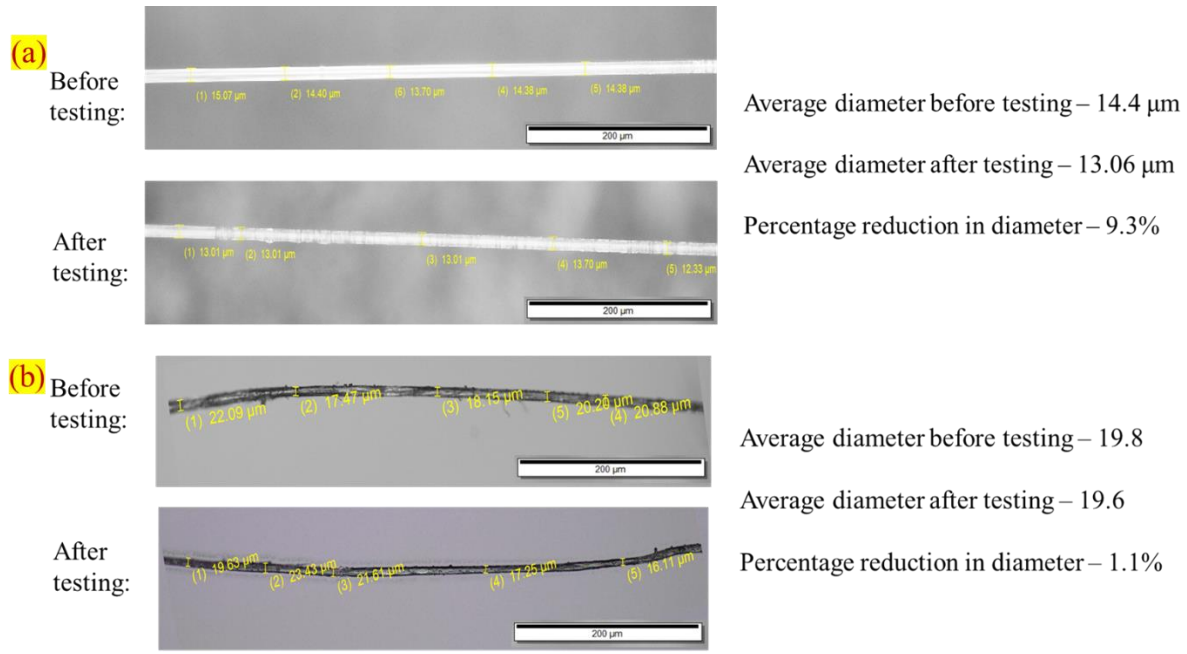

Figure 53 Analysis of percentage reduction in (a) viscose and (b) bleached flax fibre diameters.

Table 18 Tensile properties of composite filaments produced from solution impregnation and consolidation method. The values highlighted in parentheses are theoretically calculated using the rule of mixtures.

Solution impregnation formulation	**Composite Filament**	**Weight % of Reinforcement**	**Tensile Strength (MPa)**	**Young's Modulus (GPa)**	**Elongation at break (%)**
10wt%x1	PLA/Viscose	76.8±0.2	230.6±16.1 (546.4)	6.7±0.4 (17.7)	10.7±1.6
	PLA/Standard flax	82.1±1.5	219.6±19.9 (665.9)	6.5±1.4 (26.1)	4.0±1.2
	PLA/Bleached Flax	77.80±0.2	215.9±12.8 (706.2)	7.3±3.2 (24)	4.2±1.4
10wt%x2	PLA/Viscose	63.2±0.9	235.3±10.1 (449.8)	7.2±1.7 (14.9)	15.6±3.2

	PLA/Standard flax	73.80±0.2	211.1±14.2 (598.2)	9.6±1.1 (23.6)	3.4±0.7
	PLA/Bleached Flax	72.2±1.2	219.6±28.1 (654.5)	8.5±2.1 (22.3)	4.1±0.4
7wt%x2	PLA/Viscose	65.5±2.0	230.8±24.6 (483.7)	7.9±1.5 (15.9)	15.4±2.5
	PLA/Standard flax	74.20±0.2	270.5±20.8 (601.2)	11.0±2.0 (23.7)	2.7±0.1
	PLA/Bleached Flax	74.80±1.4	293.1±28.0 (677.8)	10.6±1.2 (23.1)	4.1±0.6
7wt%x3	PLA/Viscose	63.1±0.6	233.8±16.2 (444.5)	7.5±1.2 (14.8)	12.4±2.3
	PLA/Standard flax	66.7±0.3	351.7±21.6 (540.3)	12.3±1.3 (21.4)	3.5±0.2
	PLA/Bleached Flax	64.3±0.1	356.1±6.8 (582.1)	11.6±1.8 (20.1)	4.2±0.4
7wt%x1 (tandem)	PLA/Viscose	70.8±0.6	245.1±7.6 (502.9)	6.9±1.5 (16.4)	12.9±1.8
	PLA/Standard flax	72.2±0.4	298.1±13.8 (584.5)	11.8±2.2 (23.1)	3.4±0.2
	PLA/Bleached Flax	69.2±0.2	302.7±11.3 (626.9)	10.4±2.8 (21.5)	3.8±0.3

7wt%x2 (tandem)	PLA/Viscose	64.3±1.0	233.0±8.1 (457.1)	7.3±1.0 (15.1)	14.8±1.2
	PLA/Standard flax	62.1±0.3	344.8±9.2 (503.8)	15.3±2.6 (20.1)	3.2±0.4
	PLA/Bleached Flax	60±0.2	326.1±15.5 (544.2)	17.6±0.8 (18.9)	3.2±0.3

Multiple studies have reported the 3D printed composite properties, but the characterisation of the filament has not been focused on widely, and only two studies in the literature have reported filament characterisation for long/continuous bio-derived fibre reinforced composites [352][198]. However, as a composite, the highest tensile strength obtained in this study (356.1±6.8 MPa with 64.3 fibre wt% for PLA/bleached flax) is the highest reported tensile strength for PLA/flax composites when compared to the existing literature [29,57][217]. As mentioned earlier, the highest Young's modulus obtained in the current study was for 7wt%x2 (tandem) formulation for PLA/bleached flax composite with a value of 17.6±0.8 GPa. Higher Young's modulus values have been reported in the literature (Table 7) for lower reinforcement percentages than in the present study, which could be due to the negative effect of high twist, as explained earlier. A common trend of using a low-twist flax yarn was also emphasised in recent works that reported high Young's modulus values [198,206]. The highest tensile strength (245.0±7.6 MPa with 64.3 wt% fibre for 7wt%x1 (tandem) formulation) and Young's modulus (7.9±1.5 MPa with 71.5 wt% fibre for 7wt%x2 formulation) obtained for PLA/Viscose composites in this study are also the highest reported values compared to all the PLA/viscose fibre reinforced composites in literature [73,135,349,353–358] [73] [135,353,354] [355–357] [358].

4.4.4 Fracture Surface Analysis of Composite Filaments

Cross-sectional views were not available for PLA/viscose samples as the failure occurred due to the separation and pull-out of fibres with some of the filament intact, as shown in Figure 54. So, the SEM images of the failure surface were captured instead of the cross-sectional view, as shown in Figure 55. SEM images of fracture surfaces of PLA/standard flax and PLA/bleached flax filaments are shown in Figures 56 and 57, respectively. Similar to the trend in tensile properties for PLA/viscose filaments, a significant difference was not observed in the failure surfaces. The 7wt%x2 (tandem) formulation displayed slightly higher polymer content than the others. All the PLA/viscose failure surfaces showed a combination of debonding and fibre pullout. The areas of polymer debonding and the presence of polymer in the form of strings have been highlighted by yellow arrows in the SEM images.

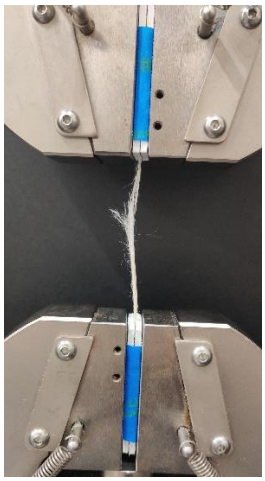

Figure 54 Failure of tensile-tested PLA/viscose composite filaments

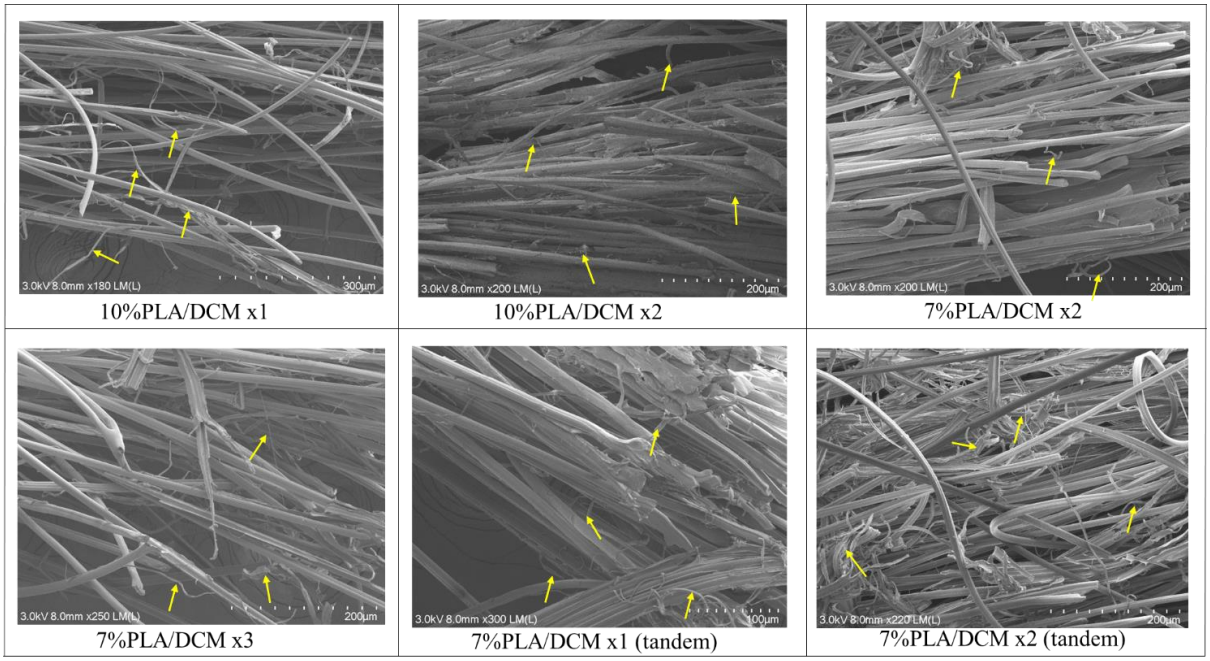

Figure 55 SEM of fracture surfaces of PLA/viscose composite filaments produced using solution impregnation. Yellow arrows highlight the regions of fibre debonding.

The failure surfaces of PLA/standard flax and PLA/bleached flax were similar. The fracture surfaces of 10wt%x1, 10wt%x2, 7wt%x2, and 7wt%x1 (tandem) formulations displayed a high amount of fibre pull-outs corresponding to debonding between the fibre and matrix [206,212]. On the other hand, 7wt%x3 and 7wt%2 (tandem) formulations displayed fewer fibre pull-outs and more fibre breakage, demonstrating strong interfacial bonding between the reinforcement and matrix [359]. Examples of fibre pull-out and fibre breakage regions are highlighted in yellow in Figure 56. This behaviour agrees with the tensile test results, as the highest tensile properties were obtained for the 7wt%x3 and 7wt%x2

(tandem) formulations. Another significant observation from the SEM images of fracture surfaces was the flax yarn's twist, which led to insufficient polymer impregnation and fibre pull-outs.

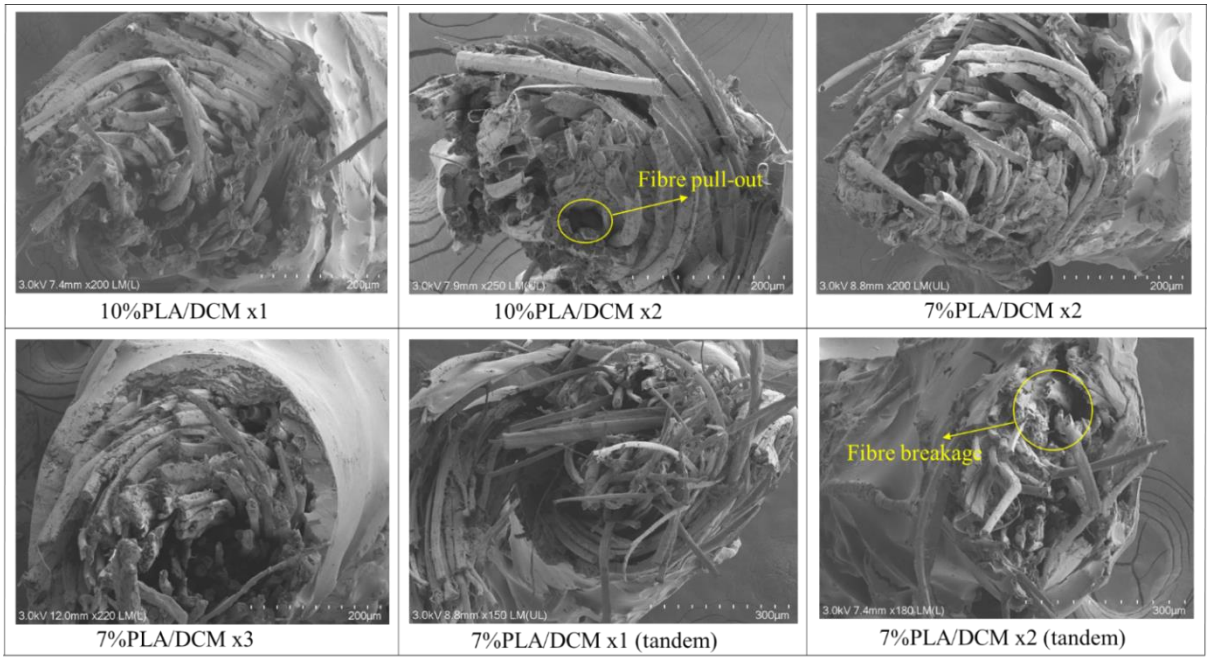

Figure 56 SEM of fracture surfaces of PLA/standard flax composite filaments produced from solution impregnation.

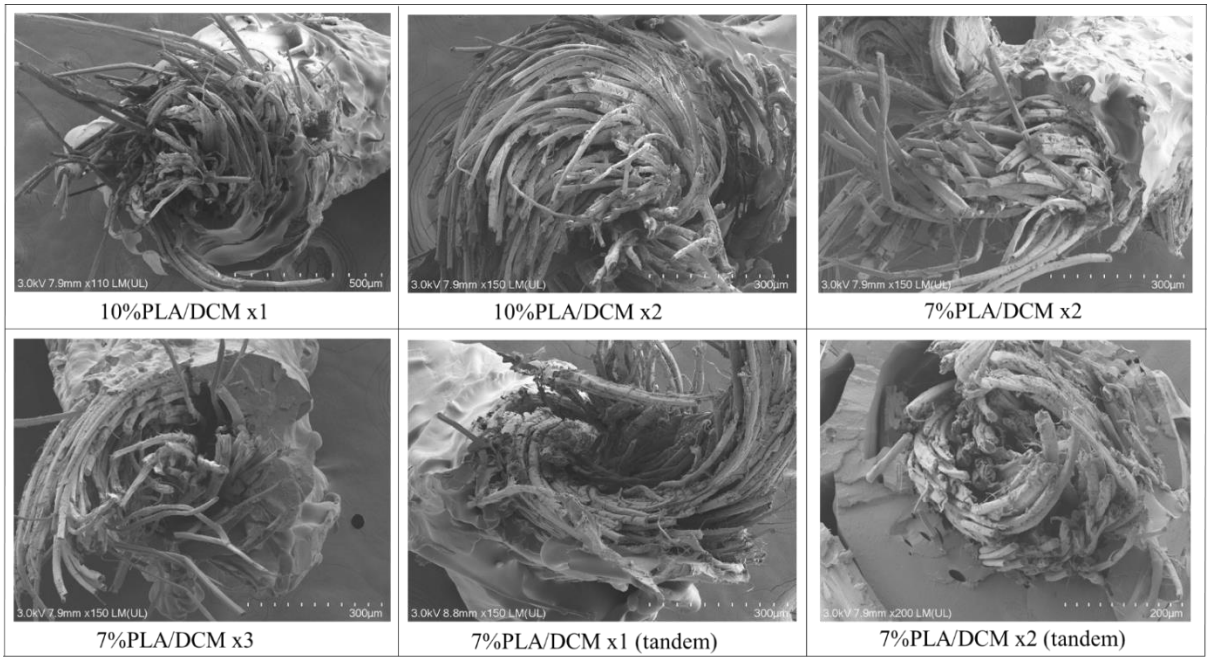

Figure 57 SEM of fracture surfaces of PLA/bleached flax composite filaments produced from solution impregnation.

4.5 Conclusions

The solution impregnation and consolidation steps were performed to achieve fibre wetting by PLA and homogenous polymer distribution. Filaments reinforced with viscose, standard flax, and bleached flax yarn underwent impregnation and consolidation. While PLA/viscose filaments exhibited a uniform polymer distribution, PLA/standard flax and PLA/bleached flax filaments displayed polymer pooling at the edges due to the twisted nature of flax yarns. Additional impregnation cycles, viscosity reduction, and tandem impregnation methods were explored, showing improved polymer distribution, reduced voids, and enhanced wetting, especially for PLA/standard flax and PLA/bleached flax filaments. PLA/bleached flax formulation for 7wt%x2(tandem) formulation achieved the highest tensile strength of 356.1±6.8 MPa, which was higher than the literature values for long/continuous bio-derived fibre reinforced composites. The PLA/viscose composites also achieved the highest reported values for tensile strength (245.0±7.6 MPa with 64.3 wt% fibre in the 7wt%x1 tandem formulation) and Young's modulus (7.9±1.5 MPa with 71.5 wt% fibre in the 7wt%x2 formulation) among all PLA/viscose fibre-reinforced composites documented in the literature. SEM images of fracture surfaces of the composite filaments were analysed, and the formulations with low porosity and high tensile strength displayed less fibre pull-outs and more fibre breakage compared to the low tensile strength and high porosity formulations. Overall, the solution impregnation formulation was optimised to achieve the highest possible tensile properties.

Chapter 5: Long/Continuous Bio-Derived Fibre Reinforced PLA Composite Filaments Produced by Emulsion Impregnation

5.1 Introduction

In the solvent impregnation process discussed in Chapter 4, DCM, a chlorinated organic solvent was used to dissolve PLA. Using some chlorinated solvents like DCM in large amounts can pose health risks and harm the environment if the solvent is not recovered during the process. A water-based PLA emulsion was explored as an alternative to the PLA/DCM solution.

In this chapter, the process of emulsion impregnation and the resulting properties are detailed. The impregnation process was optimised to achieve the best fibre wetting and interfacial adhesion possible. The emulsion impregnation process development, effects of impregnation parameters, resulting mechanical properties, and SEM images of fracture surfaces are given in detail. A comparison of results obtained from solution and impregnation methods is also included.

5.2 Materials

Viscose, flax, and bleached flax fibre yarns mentioned in Chapter 3 were used as reinforcements. A commercial 40 wt% PLA/water emulsion (PL1005), mentioned in Chapter 3, was used for the impregnation process.

5.3 Methods

5.3.1 Emulsion Impregnation and Consolidation

Impregnation: The emulsion impregnation process uses the same setup as the solvent impregnation process shown in Figures 40 and 41 and involves drawing the fibre yarns through the PLA emulsion using the impregnation bath. Fibre yarns pass through the emulsion, contacting the micro-PLA particles which adhere to the fibre surfaces. The excess emulsion is removed by passing through the 1mm die at the exit of the impregnation bath. The impregnated yarn passes through a drying zone, where the filament is dried using heated air from two blow dryers and then collected onto a winding mandrel. Five formulations, including single and tandem impregnation systems, were used, as summarised in Table 19.

Table 19 Emulsion impregnation formulations

Serial No	Emulsion Impregnation Formulation
1	Emulsionx1 – Single impregnation cycle with 40wt% PLA/water emulsion
2	Emulsionx2 – Two single impregnation cycles with 40wt% PLA/water emulsion
3	Emulsionx3 – Three single impregnation cycles with 40wt% PLA/water emulsion
4	Emulsionx1 (tandem) – One tandem impregnation cycle with 40wt% PLA/water emulsion
5	Emulsionx2 (tandem) – Two tandem impregnation cycles with 40wt% PLA/water emulsion

Consolidation: The consolidation process is the same as explained in section 4.3.1.

5.3.2 Optical Microscopy

Optical microscopy samples were prepared and analysed following the method detailed in section 4.3.2.

5.3.3 Porosity and Reinforcement Weight Percentage Analysis

The porosity and weight percentage analysis methods are the same as in section 4.3.3. The literature value of theoretical density was chosen for PL1005 (1.25 g/cm^3) grade based on the extensive literature available for amorphous PLA grades, as the supplier data was not available [145,360–363].

5.3.4 Tensile Testing

The theoretical and experimental tensile properties were evaluated based on the methods explained in section 4.3.4.

5.3.5 SEM of Fracture Surfaces

SEM images were captured following the method explained in section 4.3.5.

5.4 Results and Discussion

5.4.1 Assessment of Impregnation and Consolidation Process

The first emulsion impregnation cycle was performed by passing the yarn through a single impregnation bath. Figure 58 shows SEM images of impregnated and consolidated filaments after the first cycle. PLA/viscose filaments displayed a homogenous distribution of PLA, and the matrix surrounded all the fibres. PLA/ standard flax and PLA/bleached flax filaments displayed matrix pooling at the edges with

little to no polymer at the centre of the filament. The texture of consolidated polymer in the filaments was also observed to be porous, similar to neat PL 1005 filaments. The porosity observed in the composites has been reported earlier in similar aqueous suspension based impregnation approaches. The porosity is created by the sintering process during consolidation, where voids may be created if the viscosity of the polymer is higher and the polymer does not flow and impregnate the fibres thoroughly [364,365].

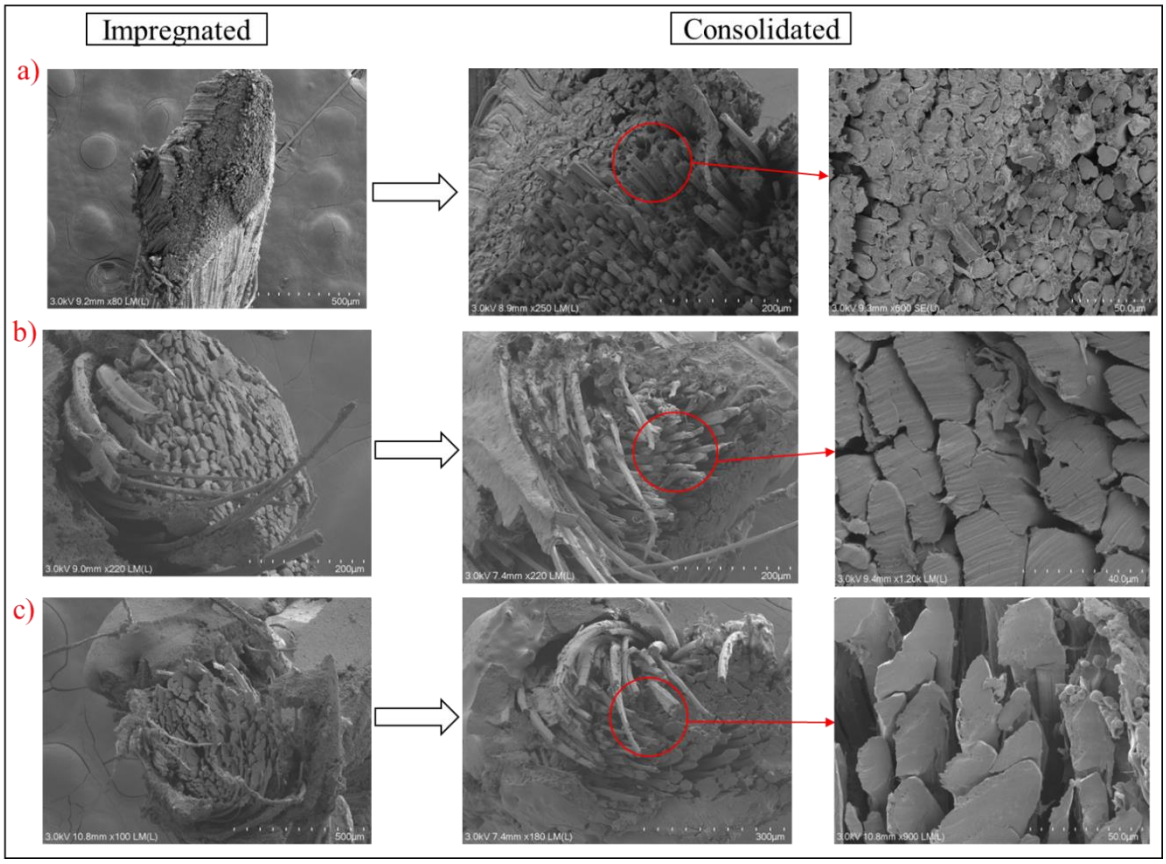

Figure 58 SEM images of cryofracture surfaces of emulsion impregnated and consolidated filaments for Emulsionx1 formulation.

A second impregnation cycle was conducted to facilitate emulsion penetration towards the filament centre and enhance fibre wetting. Cryofracture surface analysis revealed increased matrix accumulation at the filament edges, especially for PLA/standard flax and PLA/bleached flax filaments. PLA/viscose filaments displayed a more uniformly distributed matrix around the fibres.

A third impregnation cycle led to substantial matrix coverage around the central fibres in PLA/standard flax and PLA/bleached flax filaments, while matrix pooling at the edges persisted and increased with additional cycles, as shown in Figure 59. PLA/viscose filaments exhibited minimal changes with increasing impregnation cycles. Tandem impregnation also resulted in similar matrix pooling around the edges for PLA/standard flax and PLA/bleached flax, as the cycle count increased. Similar to solution

impregnation, PLA/viscose filaments displayed reduced mechanical interlocking (interface porosity) compared to PLA/standard flax and PLA/bleached flax filaments, as depicted in Figure 60.

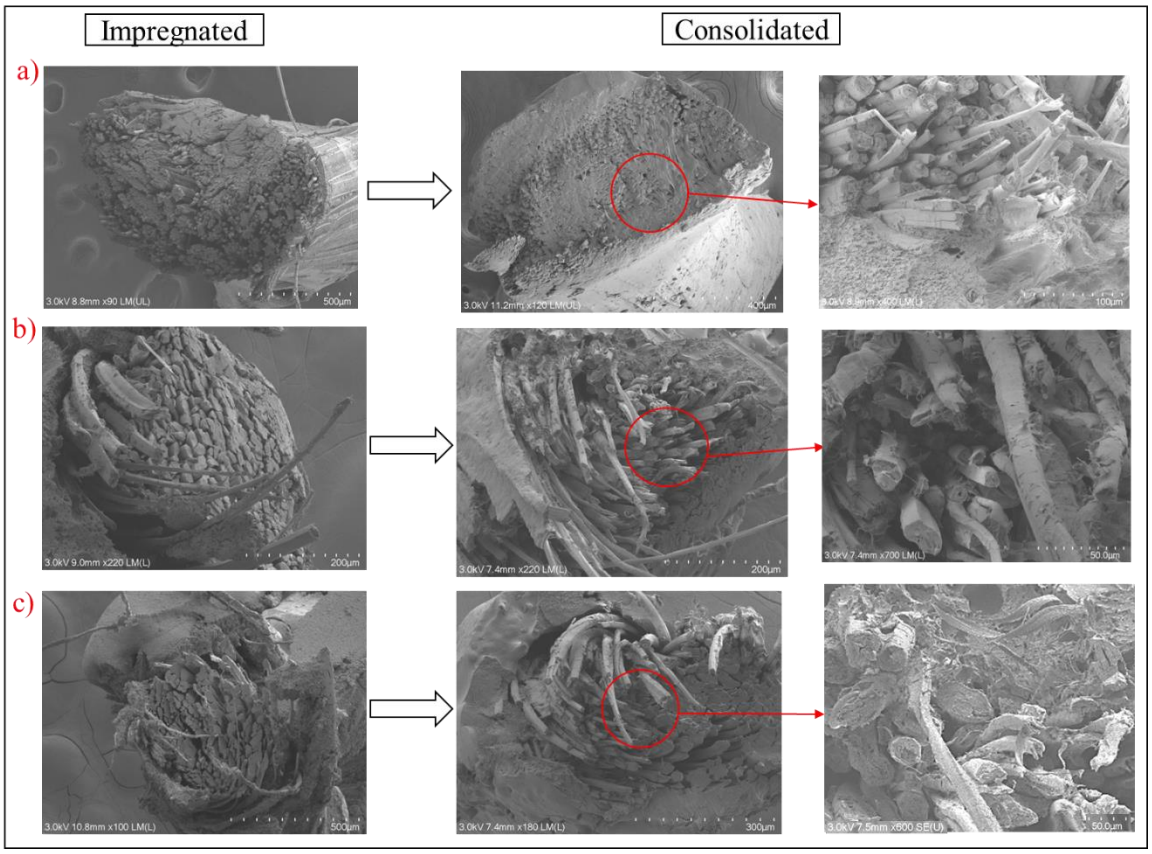

Figure 59 SEM images of cryofracture surfaces of emulsion impregnated and consolidated filaments for Emulsionx3 formulation. a) PLA/viscose b) PLA/standard flax c) PLA/bleached flax

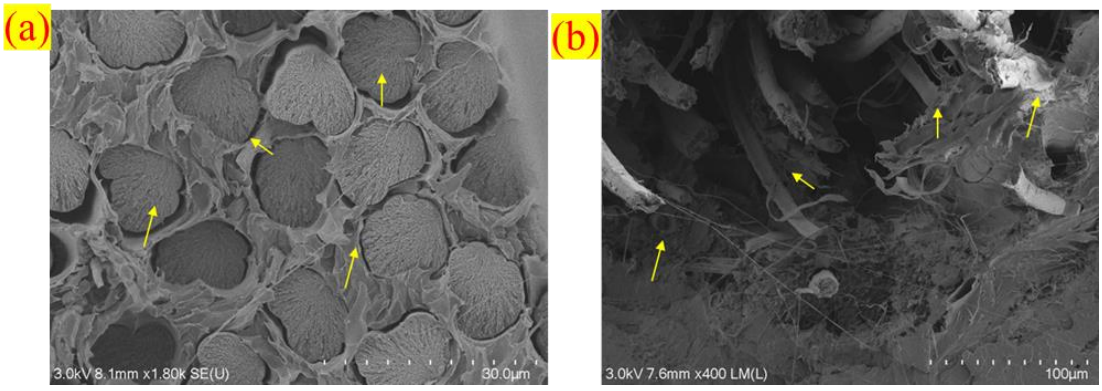

Figure 60 SEM images of cryofracture surfaces depicting mechanical interlocking between PLA and fibres a) PLA/viscose b) PLA/standard flax as an example for emulsion impregnation.

Figures 61, 62, and 63 show optical microscopy images of all the emulsion impregnation formulations studied in this work for PLA/viscose, PLA/standard flax, and PLA/bleached flax filaments, respectively. Optical microscopy images in Figure 61 show decreased crack-like voids due to

impregnation porosity in PLA/viscose filaments after two impregnation cycles and a homogenous polymer distribution in all the formulations. Figures 62 and 63 show the increase in matrix pooling around the edges of PLA/standard flax and PLA/bleached flax filaments with increased impregnation cycles. It can also be observed that the appearance of impregnation porosities was only reduced in Emulsionx2 (tandem) formulations for PLA/standard flax and PLA/bleached flax filaments, in which the yarn was passed through the impregnation bath for a total of four times.

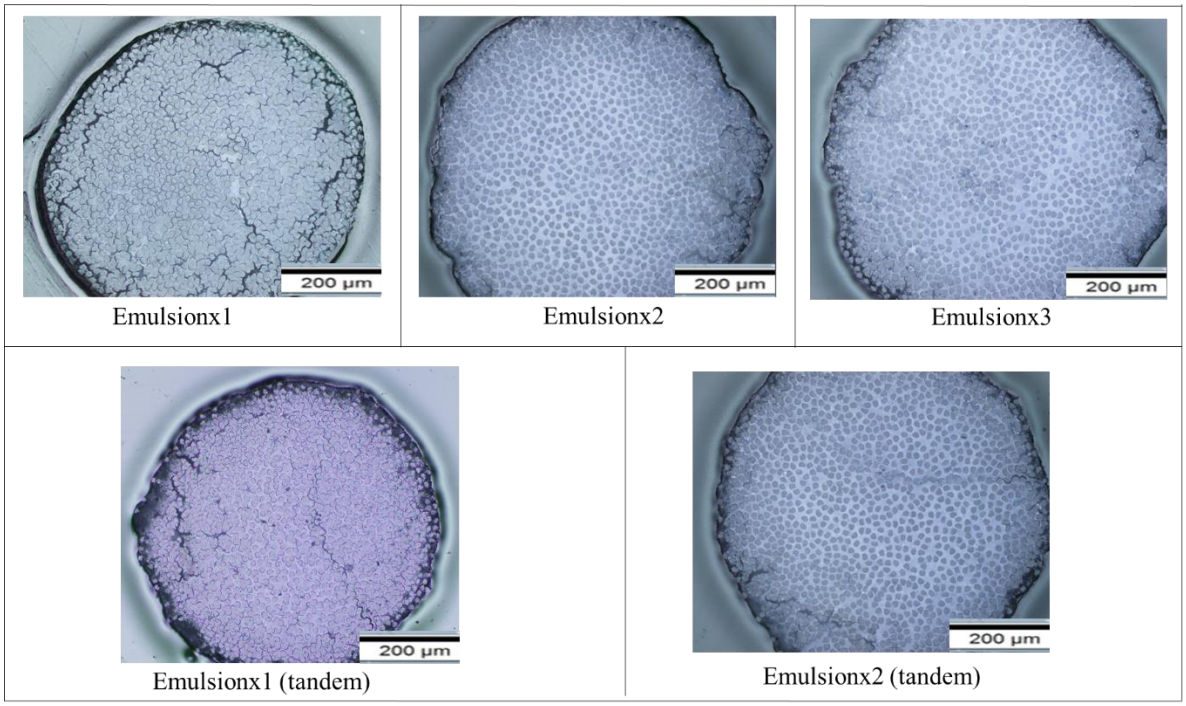

Figure 61 Optical microscopy images of consolidated filaments for different emulsion impregnation formulations – PLA/viscose

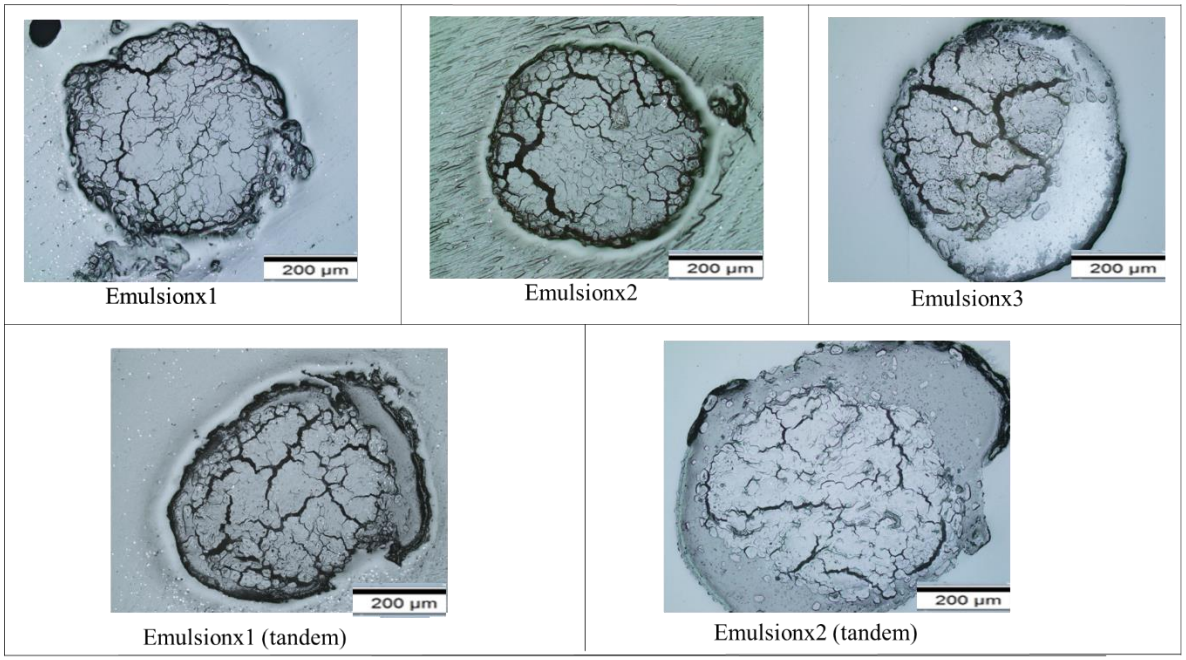

Figure 62 Optical microscopy images of consolidated filaments for different emulsion impregnation formulations – PLA/standard flax

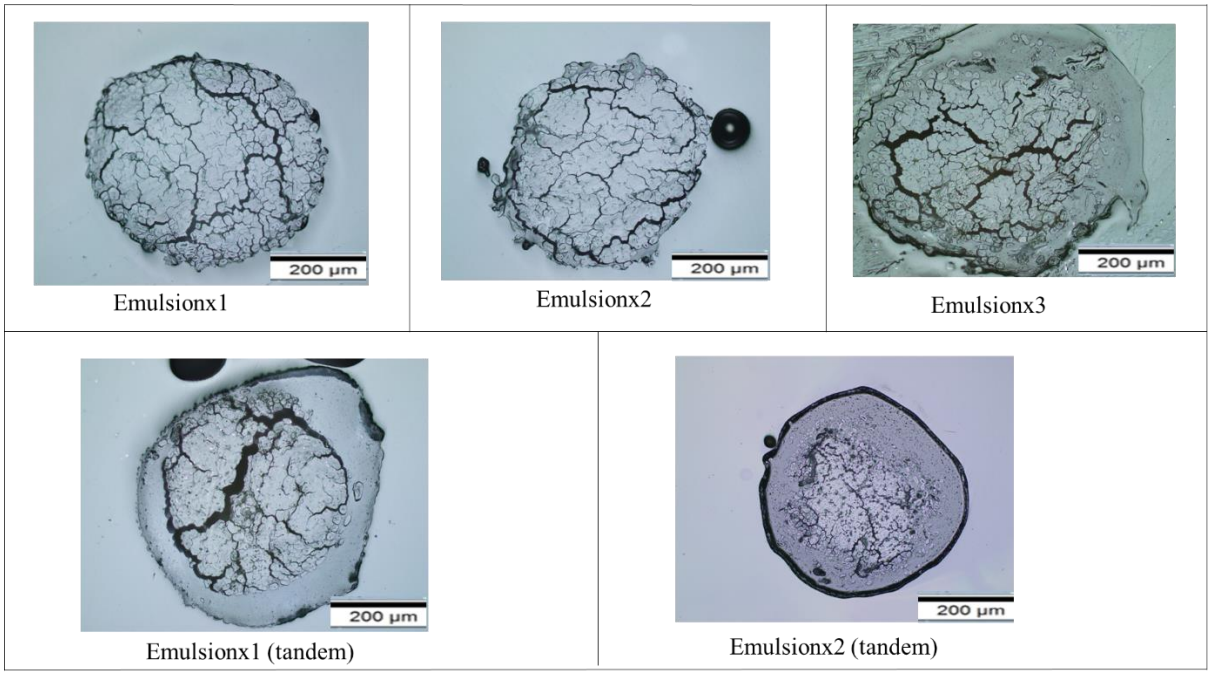

Figure 63 Optical microscopy images of consolidated filaments for different emulsion impregnation formulations – PLA/bleached flax

Compared to solution impregnation and consolidation, a key difference observed in the optical microscopy images was the amount of PLA in the filaments. The emulsion has 40wt% PLA, whereas the solution consisted of 10wt% or 7wt% PLA, depending on the formulation, leading to more PLA

being impregnated into the yarns. Differences in the polarity of water and DCM could also be a reason for higher matrix content. Water exhibits higher polarity compared to DCM due to a greater electronegativity difference between hydrogen and oxygen (1.24 for water) in contrast to carbon and chlorine (0.61 for DCM) [366,367]. The polar nature of water facilitates strong hydrogen bonding with the hydroxyl groups in cellulose, leading to absorption and swelling of the fibres [368]. In contrast, the lack of significant polar interactions results in lower affinity and absorption of DCM by flax fibres compared to water. Since the wetting of fibres by water is higher than the wetting of fibres by DCM, there could be higher chances of deposition of PLA particles onto the fibre surface by the PLA/water emulsion compared to the PLA/DCM solution. This is observed in the PLA/viscose filaments, where higher PLA amounts could be seen around each fibre (Figure 61). However, the twist in flax yarns increases the complexity of the impregnation mechanism. Although the amount of polymer impregnated is higher for PLA/standard flax and PLA/bleached flax filaments, it is essential that the polymer penetrates through the twist of the yarn and wets the fibres homogeneously. A complete analysis of tensile properties and fracture surfaces is required to conclude which impregnation method is better.

5.4.2 Porosity and Reinforcement Weight Percentage Analysis

The percentage of porosity and reinforcement by weight for all the formulations of solution impregnation are given in Table 20. Porosity was the lowest for PLA/Viscose filaments, with Emulsionx3 formulation having the lowest porosity of 4.0±2.5%. The highest porosity was observed for the Emulsionx1 formulation for all the filaments. Porosity decreases with increasing number of impregnation cycles for all the filaments, similar to the solution impregnation results. The lowest porosity for PLA/standard flax (10.3±2.4%) and PLA/bleached flax (7.8±4.0) filaments was observed for the formulation with the highest number of impregnation cycles – Emulsionx2 (tandem). Compared to solution impregnation formulations, PLA/viscose filaments displayed lower porosity and PLA/standard flax, and PLA/bleached flax filaments displayed higher porosity. This is because the PLA/viscose filaments from emulsion impregnation displayed a more homogenous matrix distribution, and a higher amount of matrix surrounded all the fibres than the solution impregnated ones. The porosity values for solution and emulsion impregnation are relatively lower compared to the literature where 7% to 30% porosity has been reported for bio-derived fibre reinforced filaments [369–372].

Table 20 Fibre and polymer weight percentage and porosity percentage of composite filaments produced using emulsion impregnation and consolidation method.

Emulsion impregnation formulation	Composite Filament	Weight % of Reinforcement	Weight % of Polymer	Porosity
Emulsionx1	PLA/Viscose	48±1.4	52.0±1.4	10.3±3.0
	PLA/Standard flax	70.2±0.2	29.8±0.2	16.8±3.9
	PLA/Bleached Flax	69.5±0.3	30.5±0.3	17.0±2.0
Emulsionx2	PLA/Viscose	41.2±1.3	58.8±1.3	7.4±1.6
	PLA/Standard flax	64.5±0.2	35.5±0.2	11.3±2.4
	PLA/Bleached Flax	68.1±1.1	31.9±1.1	8.9±3.0
Emulsionx3	PLA/Viscose	40.0±0.2	60.0±0.2	4.0±2.5
	PLA/Standard flax	56.2±0.2	43.8±0.2	10.4±4.0
	PLA/Bleached Flax	58±0.4	42.0±0.2	9.3±5.7
Emulsionx1 (tandem)	PLA/Viscose	42.1±0.8	57.9±0.8	5.1±2.1
	PLA/Standard flax	68.3±0.7	31.7±0.7	11.7±3.6
	PLA/Bleached Flax	69.7±1.3	30.3±1.3	9.8±4.3
Emulsionx2 (tandem)	PLA/Viscose	40.00±1.4	60.0±1.4	4.7±2.3
	PLA/Standard flax	43.9±0.8	56.1±0.8	10.3±2.4
	PLA/Bleached Flax	41±0.5	59.0±0.5	7.8±4.0

For PLA/viscose filaments, the weight percentage of reinforcement did not change significantly with an increase in the number of impregnation cycles after the second impregnation cycle and remained at a constant of around 40wt%. PLA/standard flax and PLA/bleached flax filaments showed a proportional increase in the amount of polymer with the increasing number of impregnation cycles. A significant difference was not observed in weight percentage or porosity between single and tandem impregnation formulations.

5.4.3 Tensile Properties of Composite Filaments

A summary of tensile properties obtained from theoretical and experimental processes for emulsion impregnation formulations is given in Table 21. The theoretical tensile properties calculated using the rule of mixtures formulae are highlighted in parentheses for comparison. Typical stress-strain curves of the composite filaments obtained from emulsion impregnation are shown in Figure 64. Similar to solution impregnation, PLA/viscose filaments display a higher elongation at break than single viscose fibres –phenomena due to the sliding of viscose fibres during tensile testing, as explained in section 4.4.3.

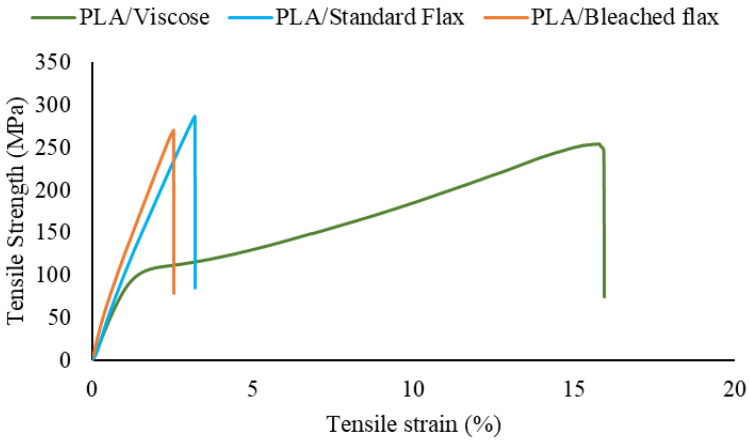

Figure 64 Stress-strain curves of composite filaments produced using emulsion impregnation.

Table 21 Tensile properties of composite filaments produced using emulsion impregnation and consolidation method.

Emulsion impregnation formulation	Composite Filament	Weight % of Polymer	Tensile Strength (MPa)	Young's Modulus (GPa)	Elongation at break (%)
Emulsionx1	PLA/Viscose	52.0±2.4	246.5±17.4 (373.2)	7.5.0±1.4 (12.5)	12.5±4.8
	PLA/Standard flax	29.8±0.4	210.2±27.7 (591.2)	6.2±2.4 (23.2)	4.2±0.5
	PLA/Bleached Flax	30.5±0.6	215.9±16.8 (655.5)	6.4±1.9 (22.2)	4.4±0.9

Emulsionx2	PLA/Viscose	58.8±2.4	254.7±15.3 (327.3)	9.1±0.4 (11.1)	14.7±2.1
	PLA/Standard flax	35.5±0.4	225.7±13.7 (547.2)	6.6±2.4 (21.6)	3.5±1.2
	PLA/Bleached Flax	31.9±2.2	227.8±15.2 (643.3)	7.0±1.9 (21.8)	3.8±0.6
Emulsionx3	PLA/Viscose	60.0±0.4	250.8±15.4 (319.2)	8.1±1.2 (10.9)	11.7±1.9
	PLA/Standard flax	43.8±0.4	262.7±35.0 (483.1)	10.2±2.7 (19.2)	3.3±0.4
	PLA/Bleached Flax	42.0±0.8	291.6±19.8 (555.2)	12.3±1.3 (19.0)	3.1±0.2
Emulsionx1 (tandem)	PLA/Viscose	57.9±1.6	247.2±18.8 (333.3)	8.4±0.7 (11.3)	15.2±1.4
	PLA/Standard flax	31.7±1.4	239.6±16.3 (576.5)	9.3±1.5 (22.6)	3.5±0.3
	PLA/Bleached Flax	30.3±2.6	251.1±15.1 (657.3)	9.2±1.9 (22.3)	3.1±0.5
Emulsionx2 (tandem)	PLA/Viscose	60.0±2.8	241.8±19.6 (319.2)	8.1±1.6 (10.9)	14.3±4.6
	PLA/Standard flax	56.1±1.6	282.7±20.3 (388.1)	12.3±1.9 (15.6)	3.1±0.4
	PLA/Bleached Flax	59.0±1.0	296.2±22.1 (411.3)	12.6±1.1 (14.5)	3.2±0.3

The tensile strength and Young's modulus of PLA/viscose samples increased with an increase in polymer content for the Emulsionx2 formulation and showed a trend of decreasing with a further increase in polymer content. The latter trend agrees with the theoretical results, but the experimental results are lower than the theoretical values because the actual composite performance is influenced by the fibre-matrix interface and porosity [342]. An optimum polymer content of 58.8% for Emulsionx2 formulation resulted in the highest tensile strength of 254.7±15.3 MPa and Young's modulus of 9.1±0.4 GPa for PLA/Viscose. These properties were higher than those obtained for solution impregnation formulations and the PLA/viscose composites reported in the literature [73] [135,353,354] [355–357] [358].

PLA/standard flax and PLA/bleached flax composite filaments displayed increased tensile properties with increased polymer content and tandem impregnation, resulting in better properties than single impregnation. Tandem impregnation gives better results using emulsion because when a wet yarn passes through an impregnation bath for the second time, the possibility of matrix penetration is higher. In a single impregnation process, when an impregnated yarn is passed through the bath for the second time, the particles on the surface are solidified and might create a barrier for complete wetting. The best tensile strength and stiffness were obtained for the Emulsionx2 (tandem) formulation for PLA/standard flax (tensile strength of 282.7±20.3 MPa and Young's modulus of 12.3±1.9 GPa) and PLA/bleached flax filaments (tensile strength of 296.2±22.1 MPa and Young's modulus of 12.6±1.1 GPa). These properties were lower than those obtained for solution impregnation, but it should be noted that the polymer content was also higher than solution impregnation formulations.

Figure 65 shows a comparison between tensile properties obtained for solution and emulsion impregnation formulations. PLA/Viscose filaments displayed better results with emulsion impregnation, and PLA/standard flax and PLA/bleached flax filaments displayed better results with solution impregnation. The main reason for this could be the ability of the solution to impregnate the twisted flax yarns better than the emulsion. Since the viscose yarns have no twist, a higher amount of polymer content in the emulsion could homogenously distribute within the yarn and reduce voids.

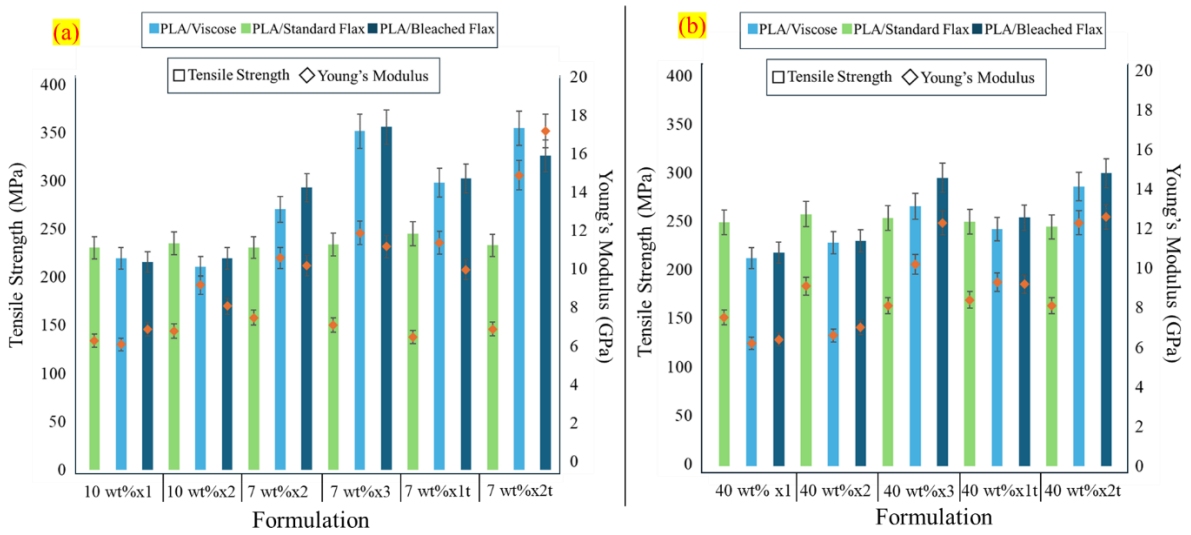

Figure 65 Summary of tensile properties obtained from all the solution and emulsion impregnation formulations a) solution impregnation b) emulsion impregnation. The error bars display standard deviation.

5.4.4 Fracture Surface Analysis of Composite Filaments

SEM images of fracture surfaces of PLA/viscose filaments for all the emulsion impregnation formulations are shown in Figure 66. Fracture surfaces revealed that some of the viscose fibres were still embedded in the matrix, suggesting good stress transfer, while some of the fibres pulled out, as highlighted in Figure 67. Brittle failure surfaces of viscose fibres could also be observed, along with some areas where the fibre impressions could be seen on the matrix. These features indicated that the interfacial bonding could be further improved [356,373]. The fracture surfaces of the filaments were similar to what has been reported in the literature for continuous viscose-reinforced composites [73] [374]

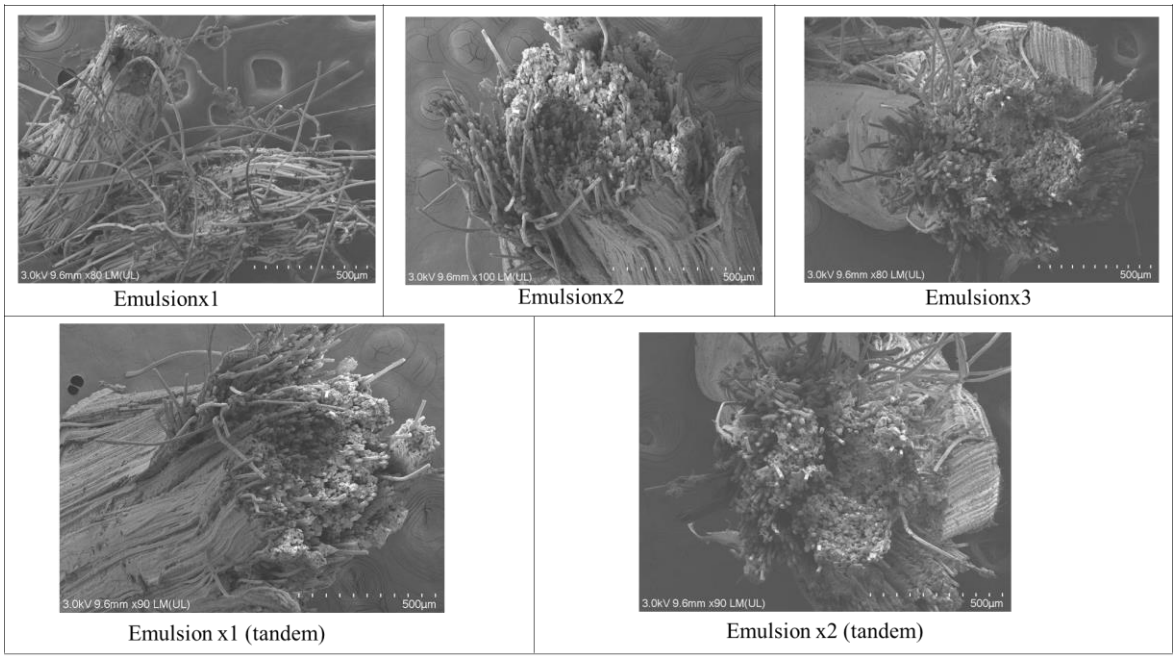

Figure 66 SEM of fracture surfaces of PLA/viscose composite filaments produced using emulsion impregnation.

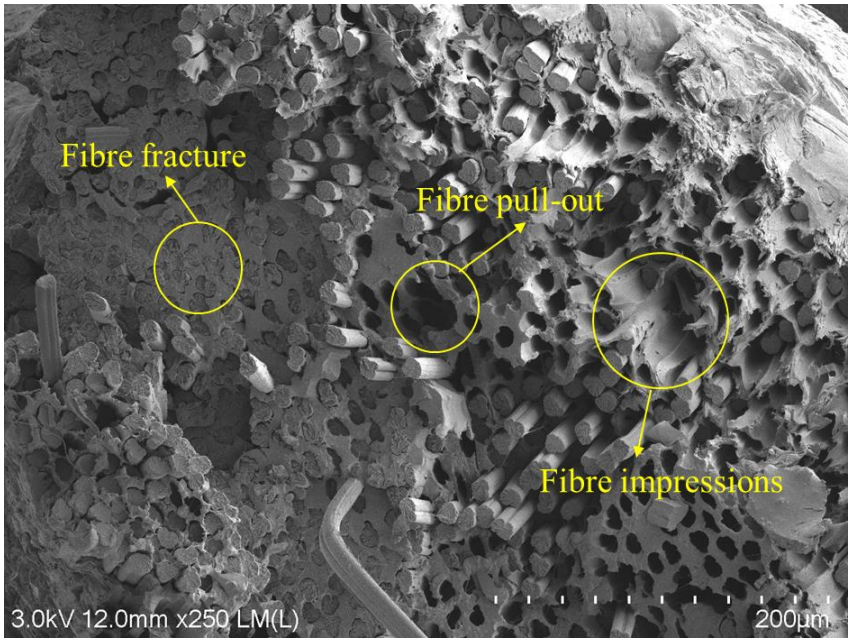

Figure 67 SEM of PLA/Viscose (Emulsionx2) with features highlighted.

SEM images of fracture surfaces of PLA/standard flax and PLA/bleached flax filaments are shown in Figures 68 and 69, respectively. Compared to solution impregnation, the emulsion impregnation filaments displayed high fibre pullouts and debonding, as highlighted in Figure 68. This indicates a poor fibre-matrix interface and a lack of matrix impregnation, especially at the centre of the yarn [375]. A similar fracture behaviour was observed in the literature for flax yarn reinforced PLA

composites[217,218,376][216]. Flax fibre treatment with silane coupling agents was found to slightly reduce the fibre pullouts and increase tensile strength by 11% [216]. Some filaments also displayed matrix cracking, as highlighted in Figure 69. Matrix cracking typically occurs due to voids or inclusions in the matrix [377].

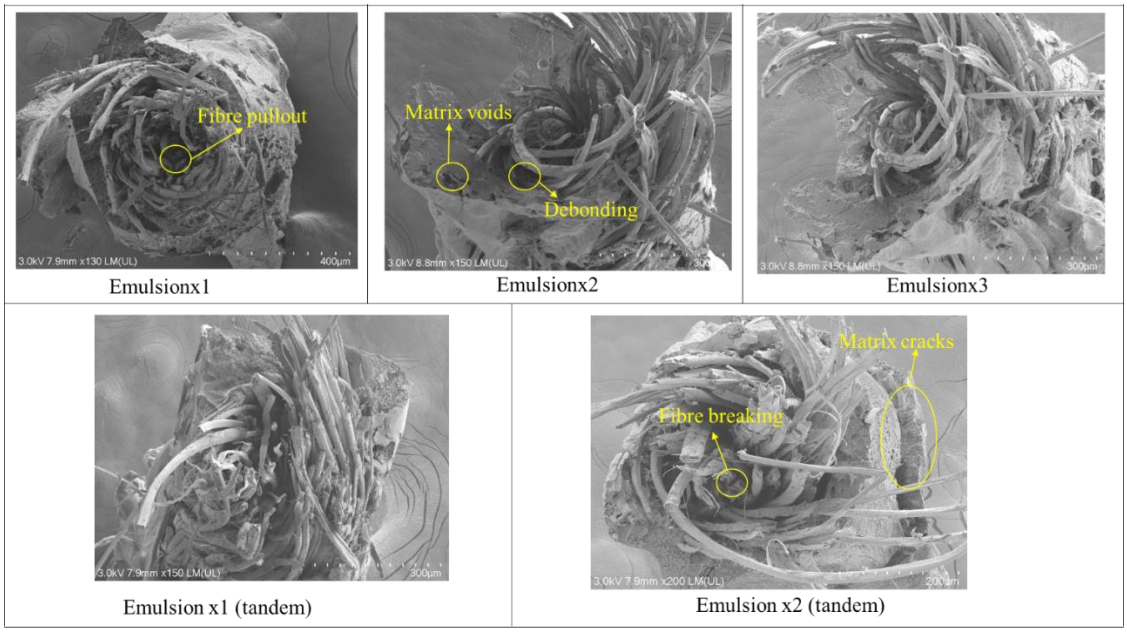

Figure 68 SEM of fracture surfaces of PLA/standard flax composite filaments produced using emulsion impregnation.

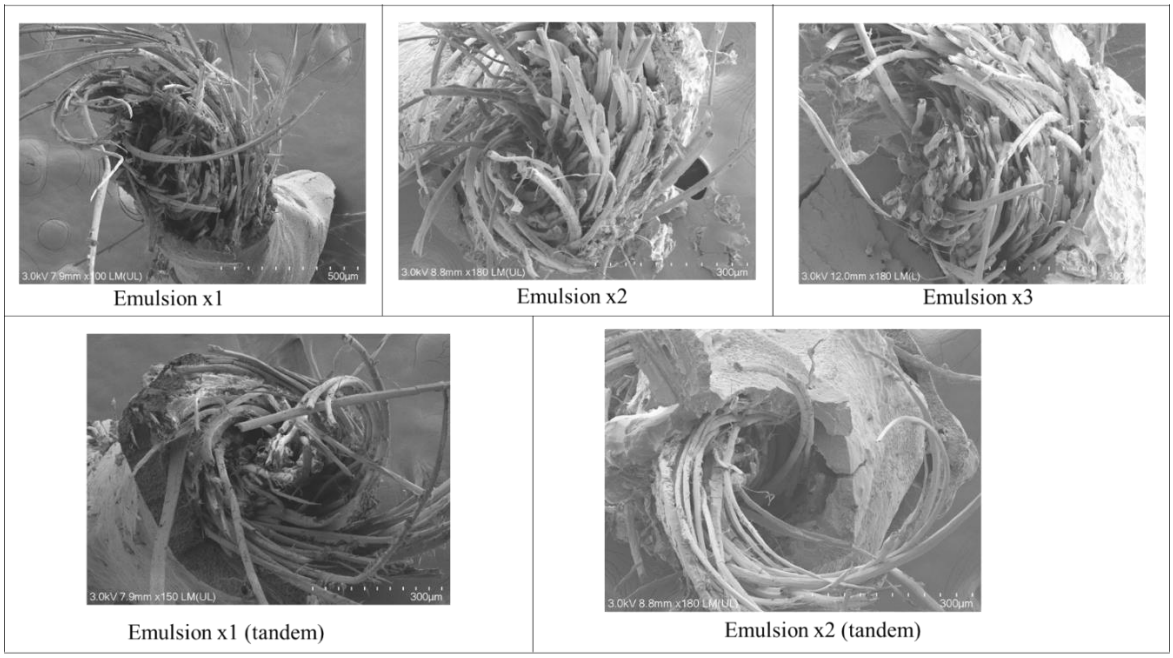

Figure 69 SEM of fracture surfaces of PLA/bleached flax composite filaments produced using emulsion impregnation.

5.5 Conclusions

Filaments of five different formulations were produced by emulsion impregnation and consolidation and characterised by mechanical and microstructural analyses. These results were then compared to the solution impregnation outcomes from Chapter 4. Emulsion impregnation notably improved the tensile properties and reduced porosity in PLA/viscose composites when compared to the solution impregnation process. Conversely, PLA/standard flax and PLA/bleached flax filaments exhibited weaker interfacial adhesion, higher porosity, and decreased tensile properties in comparison to solution impregnation. The polymer content in emulsion impregnated filaments was higher than solution impregnated filaments, attributed to the higher polarity of water in opposition to DCM, which facilitated polymer uptake. However, achieving uniform polymer distribution in twisted yarns like flax was easier with the solution impregnation method due to its fully liquid nature, unlike emulsion with solid PLA particles dispersed in water.

Chapter 6: 3D Printing Long/Continuous Bio-Derived Fibre Reinforced PLA Composites

6.1 Introduction

This chapter focuses on producing 3D printing filaments and 3D printing using the impregnated filaments developed in Chapters 4 and 5 that are compatible with commercial FDM 3D printers. Commercially available FDM 3D printers are typically designed for filament diameters of 1.75 mm and 2.85 mm, and the minimum printable diameter is 1.4 mm of the Makergear® printer used in the current study [378] [379]. With the composite filaments from earlier chapters averaging 0.45 mm in diameter, combining multiple filaments and melt impregnation with additional polymer was employed to achieve an optimized average diameter of 1.45 mm, ensuring printability with a commercial 3D printer.

6.2 Materials

The impregnation formulations that resulted in the highest tensile properties were chosen to produce 3D printing filaments as given in Table 22. PLA 2003D granules were used for impregnating additional polymer into the filaments.

Table 22 Impregnation formulations selected for the production of filaments.

Solution impregnation	
PLA/Viscose	7wt% x2
PLA/Standard Flax	7wt%x2 (tandem)
PLA/Bleached Flax	7wt%x2 (tandem)
Emulsion impregnation	
PLA/Viscose	Emulsionx2
PLA/Standard Flax	Emulsionx2 (tandem)
PLA/Bleached Flax	Emulsionx2 (tandem)

6.3 Methods

6.3.1 Production of Long/Continuous Bio-Derived Fibre Reinforced PLA Composite Filaments for FDM 3D Printing

Three filaments were combined into one wider filament using pultrusion and the consolidation procedure similar to that shown in Section 4.3.1. Commercial Filabot extruder nozzles with modified diameters were used for consolidation. These nozzles were selected for their extended tapered section

length, in contrast to the nozzles employed in Chapters 4 and 5, aiming to minimize porosity through prolonged consolidation duration [218]. The schematic of the consolidation die and the calculation of the exit nozzle area are shown in Figure 70.

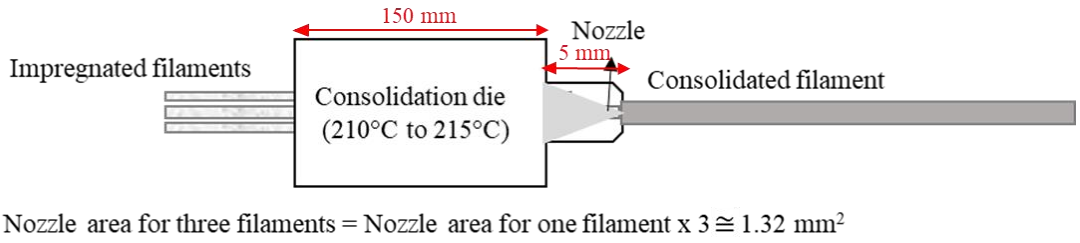

Figure 70 Consolidation process of three filaments into one filament.

The consolidated filament obtained by combining three filaments into one did not meet the minimum filament diameter of 1.4 mm required for compatibility with the commercial 3D printer. This smaller filament diameter, combined with the high fibre contents (60% to 70%), would lead to nozzle clogging and poor printing. Therefore, an additional melt impregnation step was employed to optimize the filament's diameter and fibre content. Figure 71 shows the production line where the combined filament is fed to the crosshead die attached to the Filabot single-screw extruder. The temperature of the crosshead die was maintained at 190 °C. Molten PLA is squeezed into the crosshead die, where the filament is impregnated with the polymer continuously. The impregnated filament passes through the filament cooler (Filabot Airpath), where it is cooled, and then is collected onto the filament creel using a spooling system. Extrusion and filament spooling speeds were controlled to achieve a uniform 1.45 ± 0.5 mm diameter.

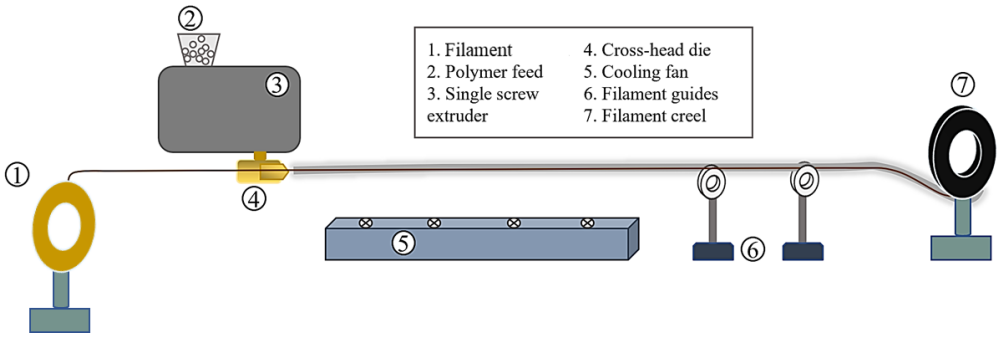

Figure 71 Production of 3D printing filaments via melt-impregnation of pre-consolidated filaments.

6.3.2 FDM 3D Printing

A MakerGear® M2 desktop printer was used for 3D printing samples for tensile, flexure, and impact testing. Samples were cut from 3D printed rectangles according to the required dimensions for mechanical testing. The dimensions of the samples and the standards followed are summarised in Table

23. Figure 72 shows 3D printing in progress. The samples were printed with 100 % infill density using a nozzle of 1.5 mm, raster angle of 0°, layer height of 0.8 mm, bed temperature of 60 °C, nozzle temperature of 190°C, and a printing speed of 300 mm/min. At the end of printing, the filament was manually cut to avoid traction and movement of the printed sample. Some studies have also reported modifying the 3D printer to have a filament cutter in case of printing complicated shapes where the filament needs to be cut multiple times [34].

Table 23 Dimensions of FDM 3D Printing samples for mechanical testing.

Test	Sample dimensions (lxbxh) (mm)	Standard
Tensile	10x125x2	ISO 527-4
Flexure	80x10x2	ASTM D790
Impact	80x10x4	ISO 179

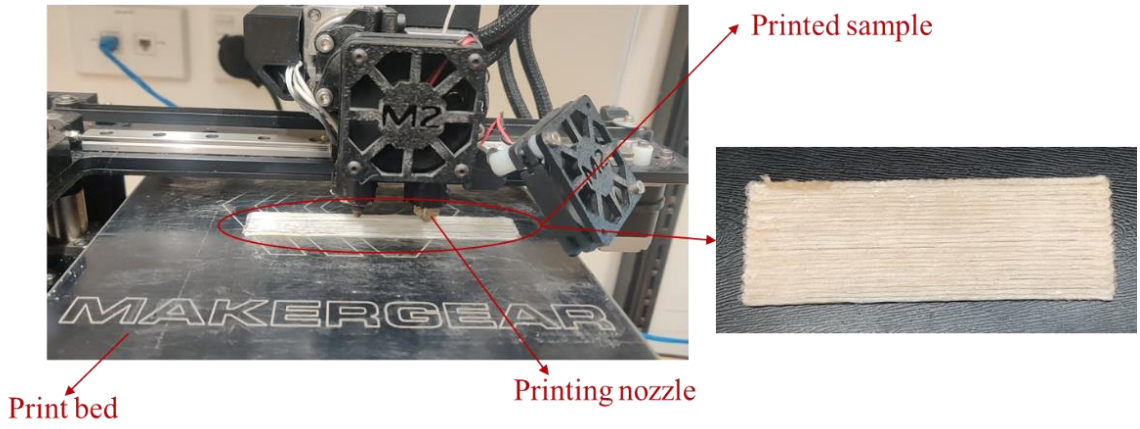

Figure 72 FDM 3D printing of long/continuous bio-derived fibre reinforced PLA composite

6.3.3 Optical Microscopy

Optical microscopy images of cross-sections of multiple consolidated filaments, 3D printing filaments, and 3D printed samples were captured using an Olympus BX53 microscope. The samples were prepared following the protocol mentioned in section 4.3.2.

6.3.4 Porosity and Reinforcement Weight Percentage Analysis

Porosity and weight percentage analysis was performed for multiple consolidated filaments, 3D printing filaments, and the 3D printed samples following the procedure detailed in section 4.3.3.

6.3.5 Tensile Testing

Experimental and theoretical tensile properties of the filaments and the 3D printed specimens were evaluated. The multiple consolidated filaments and the 3D printing filaments were tested using the method described in section 4.3.4. The 3D printed specimens were tested using end tabs according to ISO 527-4 standards. The tensile testing was performed using an Instron® 5982 tensile tester with a 5 kN load cell. Aluminium end tabs were used, and epoxy (Araldite) was used to mount the specimens to the end tabs, as shown in Figure 73. The specimens were tested with a crosshead displacement rate set at 5 mm/min. The tensile strain was measured using a 10 mm clip-on extensometer. Five specimens were tested for each composite type.

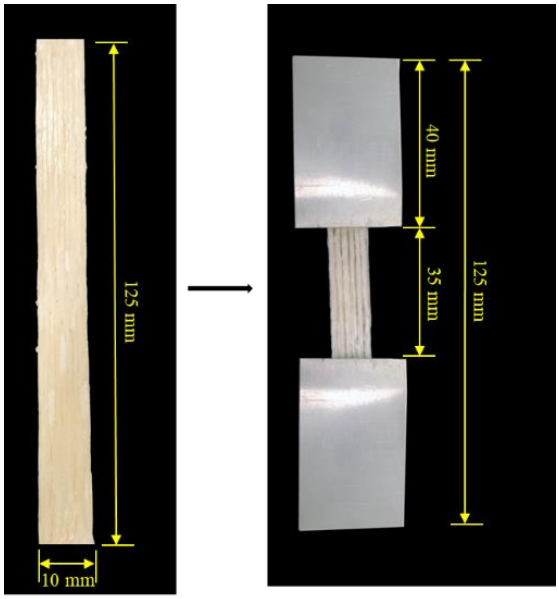

Figure 73 3D printed tensile specimen (left), mounted specimen for tensile testing (right)

6.3.6 SEM of Fracture Surfaces

A Hitachi S-4000 field emission scanning electron microscope, operated at 3 kV, was used to inspect the fracture surfaces of the composite filaments and the 3D printed specimens. The samples were mounted on aluminium tabs with the help of carbon tape and sputtered with platinum before the observation, similar to the method described in section 3.2.4.

6.3.7 Three-Point Bending Test

Three-point bending test of the 3D printed composites was done using an Instron® 5982 tensile tester with a 5 kN load cell. A span length of 55 mm (Figure 74) was used for the bending test, and five replicates for each composite type were tested according to ASTM D790 standards. The samples were conditioned in a climatic chamber at 23°C and relative humidity of 50% for 48 hours before testing.

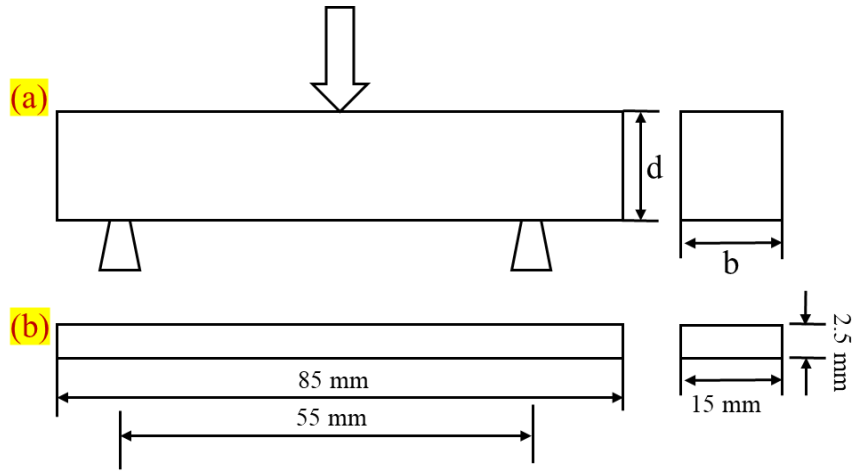

Figure 74 (a) Three-point bending test ASTM D790, (b) Size of bending test specimen

6.3.8 Impact Testing

The Charpy impact strength of the 3D printed composites was tested according to ISO 179 standards. Unnotched, rectangular specimens (80 mm × 10 mm × 4 mm), as shown in Figure 75 were used for testing. Five specimens were tested for each composite type.

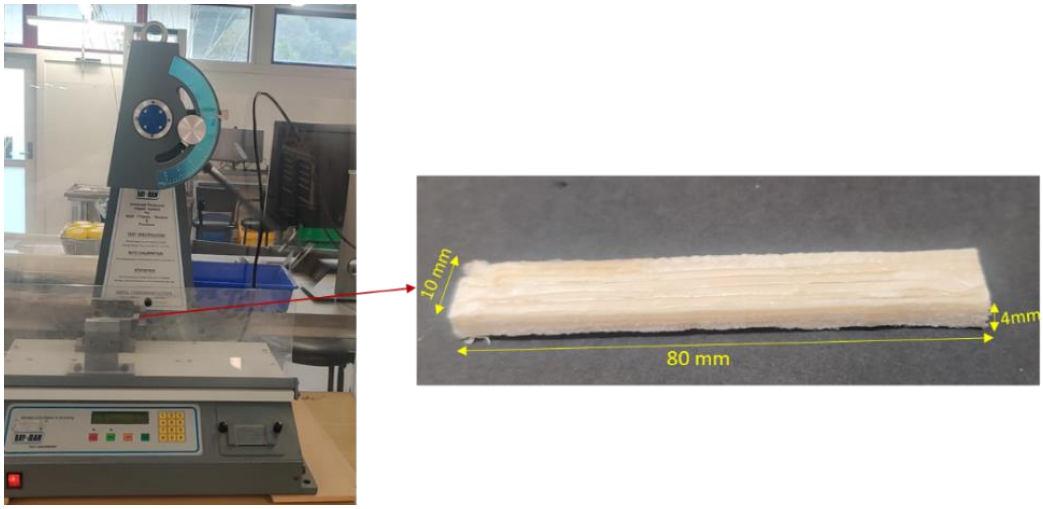

Figure 75 Impact testing machine and sample dimensions. Ray-Ran universal pendulum impact tester with a hammer weight of 1.19 kg and a test speed of 2.9m/s.

6.3.9 DSC

The calorimetric measurements of the 3D printing filaments and the printed samples were recorded using a Netzsch DSC3500 Sirius differential scanning calorimeter using aluminium crucibles from 20-200 ^{o}C at 10 ^{o}C/min with a Nitrogen flow of 60 mL/min. The glass transition (T_g), melting (T_m), and cold crystallisation (T_{cc}) temperatures were obtained from the DSC scans.

6.4 Results and Discussion

6.4.1 Morphology of Multiple Consolidated and FDM 3D Printing Composite Filaments

Figure 76 illustrates the cross-sections of the multiple consolidated filaments, which resulted from combining three filaments using selected formulations of both solution and emulsion impregnation. PLA/viscose filaments displayed good adhesion between individual filaments in both impregnation methods, with the appearance of minimal voids. However, PLA/viscose filaments impregnated with emulsion exhibited fusion of individual filaments only in the boundaries without complete merging, in contrast to the solution impregnated ones where the complete merging of filaments was observed. This is due to the sintering effect caused by emulsion particles, as elaborated in section 6.4.1, resulting in reduced viscosity and melt flow rate of the polymer [380]. Solution impregnated PLA/standard flax filaments exhibited poor adhesion among individual filaments (Figure 76), which could be due to insufficient polymer content for bonding and limited interaction between the fibres of each filament. Solution impregnated PLA/bleached flax filaments, on the other hand, demonstrated improved bonding between filaments compared to PLA/standard flax. This difference arises from the more fibrillated nature of the bleached flax yarn, which lacks non-cellulosic components present in the standard flax yarn that prevent effective interaction with neighbouring filaments [378,381]. Both PLA/standard flax and PLA/bleached flax displayed irregularly shaped translucent voids within the composite, as depicted in Figure 76, attributed to inadequate drying or trapped moisture [382]. Emulsion impregnated PLA/standard flax and PLA/bleached flax filaments appeared similar and exhibited an increased presence of matrix-rich regions compared to their solution-impregnated counterparts, owing to a higher matrix content in single filaments.

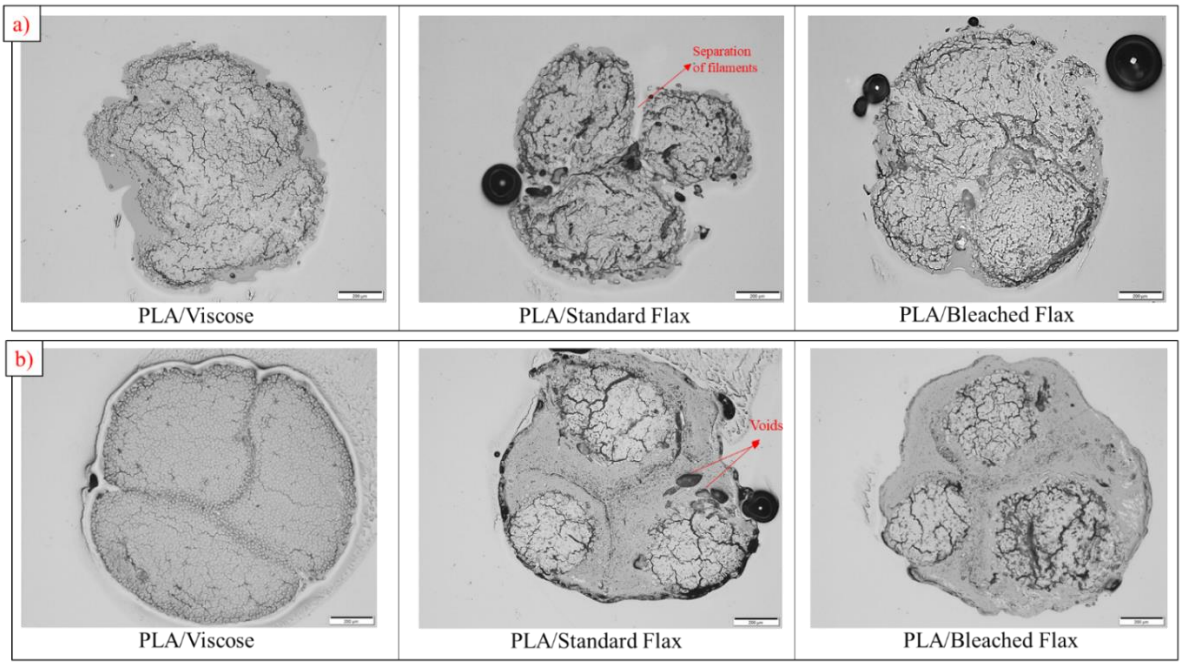

Figure 76 Optical microscope images of cross-sections of multiple consolidated filaments a) Solution impregnation b) Emulsion impregnation

PLA/Viscose and PLA/bleached flax filaments were selected to produce 3D printing filaments for both solution and emulsion impregnation formulations as viscose and bleached flax reinforced filaments were better consolidated than the standard flax ones. Figure 77 illustrates the cross-sections of the 3D printing filaments. The melt impregnation process, while appearing to introduce additional polymer around the filaments, did not result in an improvement in fibre distribution within the filaments. This inability to enhance fibre impregnation and distribution through the melt impregnation method may be attributed to inadequate pressure during the impregnation process and the high viscosity of the PLA matrix. It is worth noting that similar challenges in achieving successful impregnation and homogeneous fibre distribution through melt-impregnation have been documented in the existing literature [30,32,34,198,199,205,206,212,383–385]. However, this can be beneficial for improving inter-layer adhesion during the FDM 3D printing process [30,352].

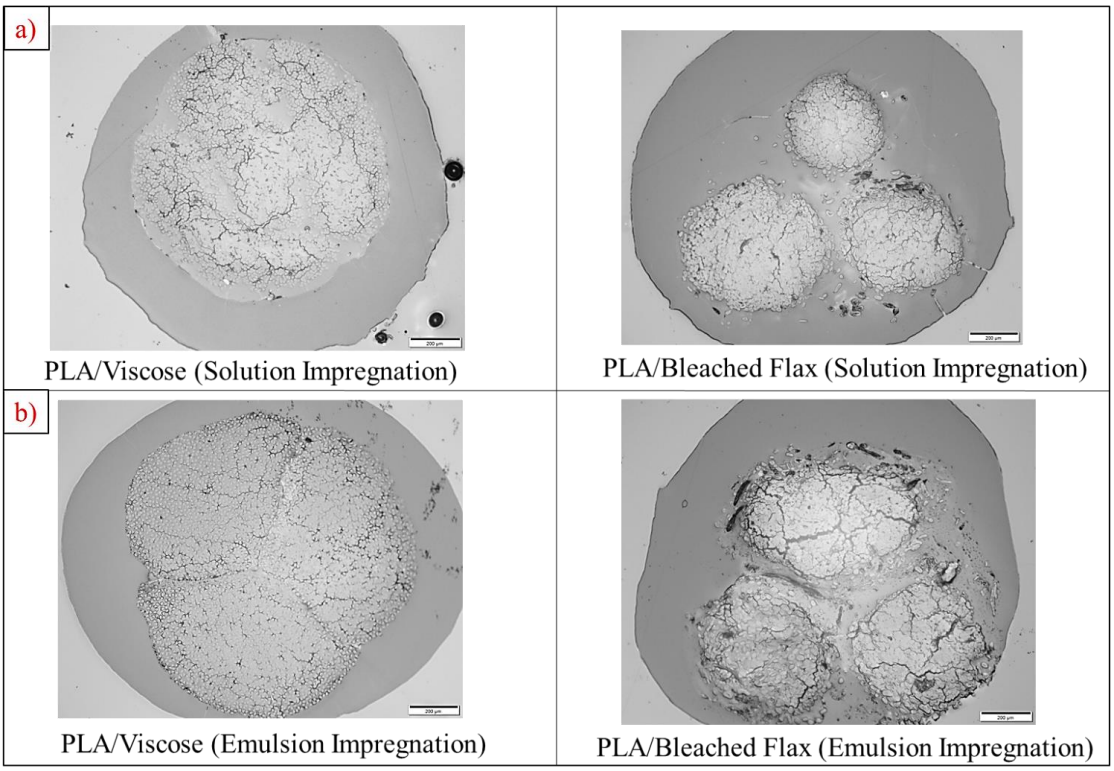

Figure 77 Optical microscope images of cross-sections of melt impregnated 3D printing filaments a) Solution impregnation b) Emulsion impregnation.

6.4.2 Porosity and Reinforcement Weight Percentage of Multiple Consolidated and Melt Impregnated FDM 3D Printing Filaments

The fibre and polymer weight and porosity percentages of the multiple consolidated and 3D printing filaments are given in Tables 24 and 25, respectively. Consolidating three filaments into one resulted in a slight increase in fibre wt% for all the composites compared to the single filaments. The increase in fibre wt% could be due to the application of pressure and heat leading to the squeezing out of some polymer from the composite structure into the consolidation die. A similar tendency of increase in fibre wt% by 1% to 10% during consolidation has been observed for consolidation processes such as pultrusion and compression [386,387]. However, the impact of this increased fibre wt% on composite mechanical properties depends on the homogeneity of fibre distribution and porosity. An increase in fibre content combined with insufficient polymer around the fibres leads to an increase in porosity, resulting in a loss of tensile performance [388].

Among the multiple consolidated filaments, PLA/viscose filaments displayed lower porosity values compared to PLA/standard flax and PLA/bleached flax filaments for both solution and emulsion impregnation methods, similar to the trends observed for single filaments. Interestingly, the porosity values for PLA/viscose filaments were lower than the single filaments, which shows that the consolidation process resulted in the elimination of impregnation porosities in PLA/viscose. The

porosity values of the multiple consolidated PLA/standard flax and PLA/bleached flax, on the other hand, increased compared to the single filaments. This is attributed to the twist in flax filaments, unlike viscose. During consolidation, the non-twisted viscose filaments can interact with neighbouring filaments, forming a cohesive structure. In contrast, the twist in flax filaments could hinder inter-filament interactions during consolidation [344].

After performing melt impregnation to increase the filament diameter, all the 3D printing filaments displayed lower porosity values ranging from 4.5% to 5.5%. This decrease in porosity could be due to the lower porosity of the matrix, leading to a reduction in the average porosity of the filament. The application of heat and pressure during the melt-impregnation process could also release any trapped moisture or air and could lead to the removal of voids.

Table 24 Fibre and polymer weight percentage and porosity percentage of multiple consolidated filaments.

Impregnation Type	Composite Filament	Fibre wt%	Polymer wt%	Porosity (%)
Solution impregnation	PLA/Viscose	71.4±2.3	28.6±2.3	9.5±2.7
	PLA/Standard Flax	73.5±4.8	26.5±4.8	17.2±2.2
	PLA/Bleached Flax	70.3±5.9	29.7±5.9	16.7±1.4
Emulsion impregnation	PLA/Viscose	62.4±2.9	37.6±2.9	6.0±2.2
	PLA/Standard Flax	56.9±1.9	43.1±1.9	10.5±0.6
	PLA/Bleached Flax	54.2±2.0	45.8±2.0	10.0±1.5

Table 25 Fibre and polymer weight percentage and porosity percentage of melt impregnated 3D printing filaments.

Impregnation type	Composite Filament	Fibre wt%	Polymer wt%	Porosity (%)
Solution impregnation	PLA/Viscose	33.4±1.3	66.6±1.3	4.4±1.8
	PLA/Bleached Flax	27.8±2.1	72.2±2.1	5.2±0.6
Emulsion impregnation	PLA/Viscose	32.8±0.9	67.2±0.9	5.0±2.1
	PLA/Bleached Flax	26.4±2.8	73.6±2.8	5.5±1.9

6.4.3 Tensile Properties of Multiple Consolidated and Melt Impregnated FDM 3D Printing Composite Filaments

Tensile Properties of Multiple Consolidated Composite Filaments

The experimental and theoretical tensile properties of multiple consolidated filaments are summarised in Table 26. Theoretical calculations using the rule of mixtures gave higher tensile properties with reduced polymer content, but the experimental testing revealed lower tensile properties in all composite filaments. This can be attributed to defects caused by porosity within the filament structure caused by insufficient polymer to surround all the fibres.

Compared to single filaments, solution impregnated PLA/viscose demonstrated increased tensile strength (251.2±15.2 MPa) and Young's modulus (8.8±0.8 GPa) for multiple consolidated filaments by approximately 8.8% and 11.4%, respectively. This aligns with the microscopic and porosity analysis, where an increase in fibre content was observed without an increase in porosity. The elongation at break of PLA/viscose was higher than single viscose fibres, which could be due to the sliding mechanism of viscose fibres, as explained in section 4.2.2. PLA/standard flax displayed significant reductions in both tensile strength (258.2±19.6 MPa) and Young's modulus (12.2±2.8 GPa), indicating a decrease of approximately 25% and 20.9%, respectively. PLA/bleached flax also demonstrated decreased tensile strength (305.7±23.8 MPa) and Young's modulus (15.5±2.2) of about 6% and 11.4%, respectively. An increase in porosity was observed after the consolidation of multiple filaments for both PLA/standard flax and PLA/bleached flax filaments. Poor adhesion between the individual filaments and porosity-induced defects could be the contributing factors to the loss of tensile properties [95,389,390].

For emulsion impregnation, all the filaments showed reduced tensile properties for multiple consolidated filaments compared to single filaments. Although the porosity of multiple consolidated PLA/viscose was slightly lower than the single filament, as mentioned earlier, a small reduction in tensile strength (245.3±13 MPa) and Young's modulus (7.5±0.5 GPa), with reductions of approximately 3.8% and 17.6%, respectively were observed. This may be attributed to thermal degradation resulting from a decrease in molecular weight due to exposure to multiple melt processing cycles, a phenomenon that can be verified through any significant reductions in T_g via DSC analysis [391–393]. The reduction could also be due to any stress concentrations developed during consolidation near the edges where the individual filaments meet, as observed in Figure 77 (b). Emulsion impregnated PLA/standard flax exhibited a substantial decrease in both tensile strength (151±10.6 MPa) and Young's modulus (7.2±1.4 GPa), with decreases of approximately 58.6% and 28%, respectively. PLA/bleached flax also decreased tensile strength (215.9±12.8 MPa) and Young's modulus (9.8±0.9 GPa), with reductions of about 27% and 13.8%, respectively. The reduced tensile properties could be attributed to an increase in fibre content and porosity after consolidation.

Table 26 Tensile properties of multiple consolidated filaments. The values highlighted in parentheses are theoretically calculated using the rule of mixtures.

Impregnation Type	Composite Filament	Fibre wt%	Tensile Strength (MPa)	Young's Modulus (GPa)	Elongation at break (%)
Solution impregnation	PLA/Viscose	71.4±2.3	251.2±15.2 (506.9)	8.8±0.8 (16.5)	21.2±3.9
	PLA/Standard flax	73.5±4.8	258.2±19.6 (601.2)	12.2±2.8 (23.7)	3.5±0.2
	PLA/Bleached Flax	70.3±5.9	305.7±23.8 (643.3)	15.5±2.2 (22)	4.0±0.5
Emulsion impregnation	PLA/Viscose	62.4±2.9	245.3±13 (439.3)	7.5±0.5 (14.4)	25.8±4.5
	PLA/Standard flax	56.9±1.9	151±10.6 (465.3)	7.2±1.4 (18.5)	3.3±1.2
	PLA/Bleached Flax	54.2±2.0	215.9±12.8 (496)	9.8±0.9 (17.1)	3.3±0.4

Tensile Properties of FDM 3D Printing Composite Filaments

PLA/viscose and PLA/bleached flax filaments were selected for the production of 3D printing filaments based on their mechanical properties. Table 27 summarises the experimental and theoretical tensile properties of the composite 3D printing filaments. The addition of PLA via melt impregnation reduced theoretical and experimental tensile properties for all the composites, which is expected as the composite properties generally tend to reduce with an increase in matrix content [394]. Compared to the multiple consolidated filaments, PLA/viscose filaments exhibited a lesser reduction in tensile properties than PLA/bleached flax. This difference could be attributed to the difference in fibre wt% between PLA/viscose and PLA/bleached flax filaments. PLA/viscose filaments have an average fibre wt% of 33.4, while PLA/bleached flax filaments averaged 27.8% after melt-impregnation, resulting in a more significant decrease in tensile properties for the latter.

In the case of solution impregnation, PLA/viscose 3D printing filaments demonstrated a reduction of approximately 19.8% in tensile strength and 22.7% in Young's modulus. On the other hand, PLA/bleached flax exhibited more substantial reductions of 40.8% in tensile strength and 37.4% in Young's modulus. Similarly, for emulsion impregnation, PLA/viscose 3D printing filaments showed a

decrease of around 22.4% in tensile strength and a marginal 1.3% reduction in Young's modulus. On the other hand, PLA/bleached flax displayed reductions of 28.2% in tensile strength and 6.1% in Young's modulus. Apart from lower fibre content, higher porosity content in PLA/bleached flax filaments also contributed to higher reductions in tensile properties, as the presence of voids leads to premature fracture [395].

Table 27 Tensile properties of 3D printing filaments. The values highlighted in parentheses are theoretically calculated using the rule of mixtures.

Impregnation Type	Material	Fibre wt%	Tensile Strength (MPa)	Young's Modulus (GPa)	Elongation at break (%)
Solution impregnation	PLA/Viscose	33.4±1.3	201.8±19.6 (254.5)	6.8±3.6 (9.3)	17.5±2.8
	PLA/Bleached flax	27.8±2.1	180.9±7.4 (278.8)	9.6±5.3 (10.6)	3.0±0.2
Emulsion impregnation	PLA/Viscose	32.8±0.9	190.2±15.9 (242.9)	7.4±1.7 (8.6)	22.1±3.9
	PLA/Bleached flax	26.4±2.8	154.7±16 (259.5)	9.2±5.5 (9.6)	3.4±0.9

6.4.4 Fracture Surface Analysis of Multiple Consolidated Filament and Melt Impregnated FDM 3D Printing Composite Filament

SEM images of fracture surfaces of multiple consolidated filaments of solution and emulsion impregnated filaments are shown in Figures 78 (a) and 78 (b), respectively. PLA/viscose filaments did not undergo fracture by fibre breakage, as shown in Figure 78, so fracture surfaces were obtained from the failure region. In solution impregnated PLA/viscose, debonding of fibre and matrix and fibre breakage were similar to the single filament failure mechanism. PLA/standard flax and PLA/bleached flax composites showed fibre-rich areas, fibre pull-outs, and filament separation in solution-impregnated filaments [316–319].

In emulsion impregnation, PLA/viscose exhibited separation of consolidated filaments and fibre breakage, indicating good bonding between fibre and matrix but poor adhesion between individual filaments. PLA/standard flax filaments displayed complete pull-out of the central yarn portion,

suggesting insufficient impregnation and fibre wetting [356,373]. PLA/bleached flax observations included fibre pull-outs and brittle fracture surfaces in matrix-rich areas [316–319].

Figures 80 (a) and 80 (b) show the macroscopic failure surfaces of PLA/viscose and the SEM images of fracture surfaces of all tensile-tested 3D printing filaments of solution and emulsion impregnation, respectively. Macroscopic failure surfaces of solution and emulsion impregnated PLA/viscose reveals the separation of surrounding polymer and fibre, suggesting weak adhesion between melt-impregnated PLA and viscose fibres. SEM images show debonding, fibre breakage, and fibre pullouts in both solution and emulsion impregnated PLA/viscose filaments associated with interface porosity [396]. PLA/bleached flax, on the other hand, displayed a combination of fibre pull-outs and brittle fracture surface of the matrix for both solution and emulsion impregnated filaments, indicating poor impregnation and interfacial adhesion [30,397].

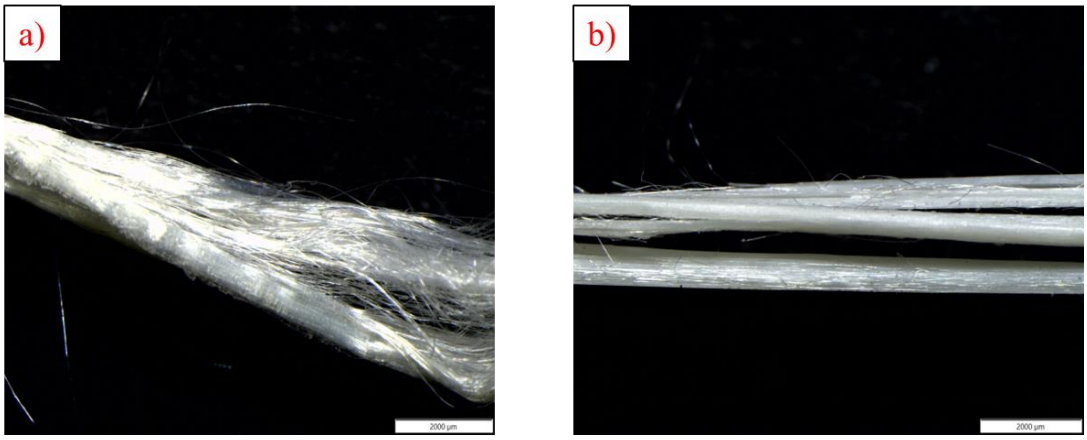

Figure 78 Macroscopic failure surfaces of multiple consolidated PLA/viscose filaments a) Solution impregnation b) Emulsion impregnation

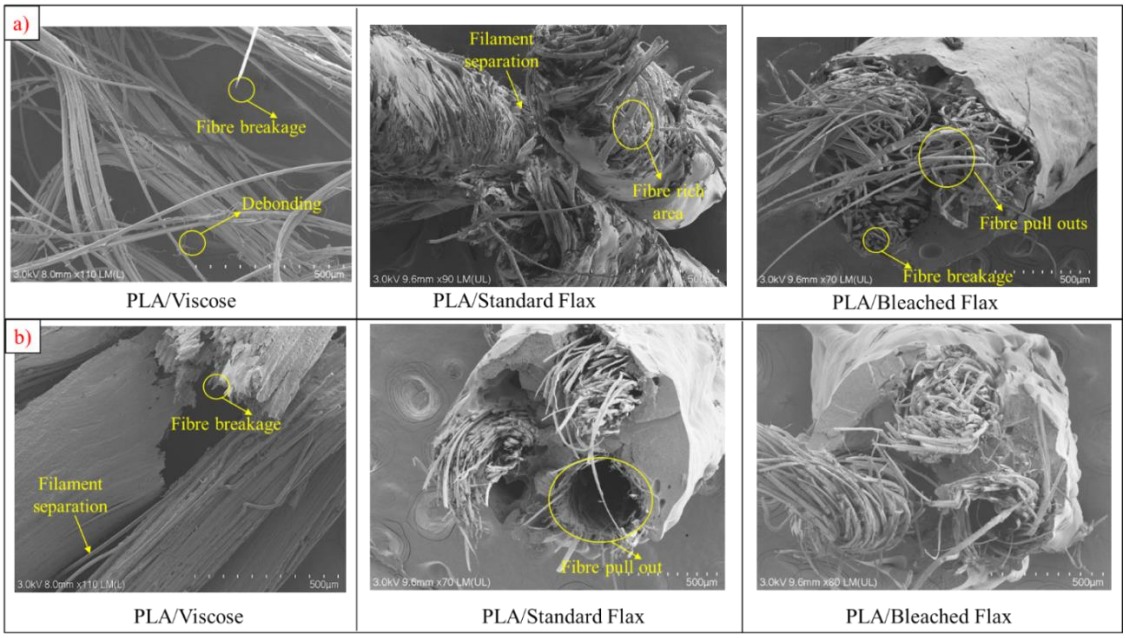

Figure 79 SEM images of fracture surfaces of multiple consolidated filaments a) Solution impregnation b) Emulsion impregnation

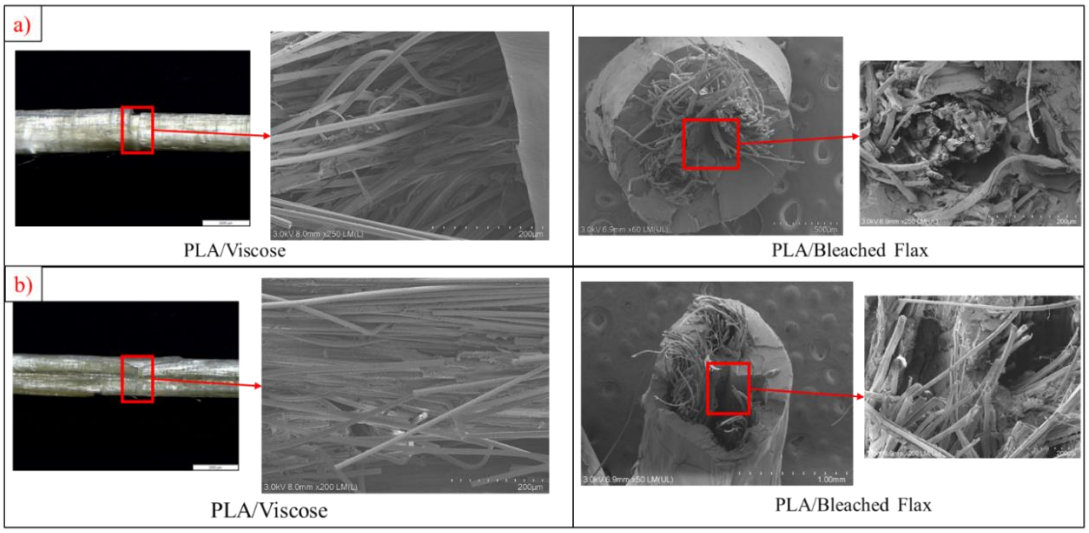

Figure 80 SEM images of fracture surfaces of 3D printing filaments a) Solution impregnation b) Emulsion impregnation.

6.4.5 Thermal Properties of FDM 3D Printing Composite Filament

DSC thermograms of solution and emulsion impregnated 3D printing composite filaments are shown in Figures 81 (a) and 81 (b). Table 28 presents T_g, T_m, T_{cc}, and degree of crystallinity (X_c). DSC thermograms of solution impregnated PLA/viscose, PLA/bleached flax, and emulsion impregnated PLA/bleached flax display sharp, high enthalpy melting peaks similar to those of semi-crystalline PLA

2003D. Emulsion impregnated bleached flax filament, on the other hand, displays a broader glass transition peak and a small melting peak, similar to the amorphous PL1005. Solution impregnated filaments were entirely produced from PLA 2003D grade, while emulsion impregnated filaments initially use PL1005 and are further melt-impregnated with PLA 2003D. The reason for emulsion impregnated PLA/bleached flax to have more semi-crystalline behaviour could be due to higher PLA 2003D content in emulsion impregnated PLA/bleached flax compared to PLA/viscose.

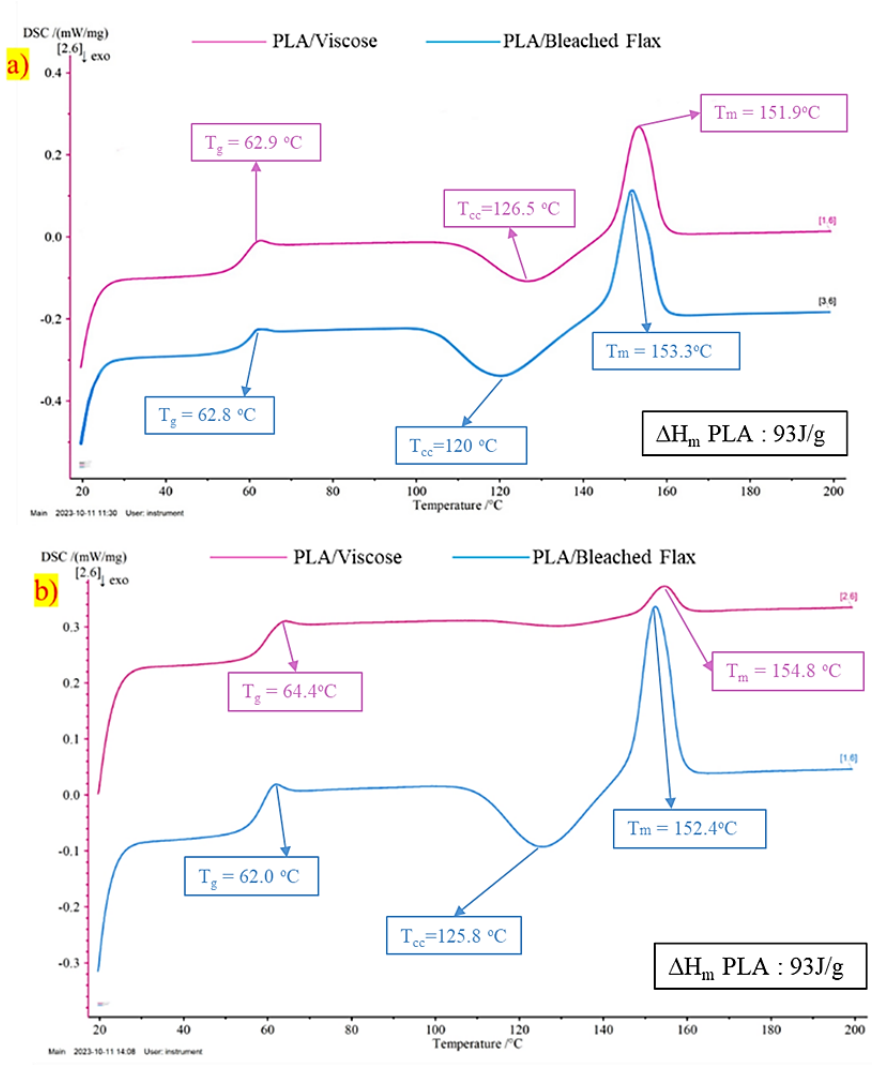

Figure 81 DSC thermograms of 3D printing composite filaments a) Solution impregnation b) Emulsion impregnation.

T_g, T_m, and T_{cc} values remain similar to neat PLA, with an increased crystallinity (Xc) percentage observed in all composite filaments. Literature indicates that bio-derived fibres promote crystallization by serving as nucleating agents [398]. The highest crystallinity (24.3%) is found in solution-impregnated viscose, which also exhibits the highest mechanical properties. This is attributed to enhanced molecular orientation in crystalline regions, leading to increased stiffness and strength along the alignment direction [399,400]. Although an increase in crystallisation is shown to improve

mechanical properties in composites, achieving significant improvements also requires strong interfacial adhesion between fibres and the matrix for effective load transfer [401–403].

Table 28 Summary of DSC for 3D printing composite filaments

Impregnation Type	Composite Filament	T_g (°C)	T_m (°C)	T_{cc} (°C)	X_c (%)
Solution Impregnation	PLA/Viscose	62.9	151.9	126.5	24.3
	PLA/Bleached Flax	62.8	153.3	120	19.2
Emulsion Impregnation	PLA/Viscose	64.4	154.8	-	-
	PLA/Bleached Flax	62.0	152.4	125.8	21.2

6.4.6 FDM 3D Printing

Composite filaments measuring 1.45 ± 0.5 mm were utilized for 3D printing, and printing parameters, including nozzle diameter, printing temperature, layer height, and printing speed, were optimised to improve printing quality. A nozzle diameter smaller than the filament caused filament dragging due to nozzle clogging, as shown in Figure 82 (a). Hence, a nozzle diameter of 1.5 mm was chosen. Lower printing temperatures (180°C –190°C) exhibited poor inter-layer adhesion, while higher temperatures (210°C – 220°C) resulted in poor dimensional tolerance. The optimal printing temperature was determined to be 200°C, which was similar to literature values for 3D printing continuous bio-derived fibre reinforced composites [404][405]. High printing speeds (>400 mm/min) led to the pulling out of fibres due to the drag force applied by the nozzle, as shown in Figure 82 (b), and lower printing speeds led to excess material deposition and distortion of the printed specimen [30,406,407]. An optimum printing speed of 300 mm/min was chosen for achieving printing without distortions. Layer heights less than 0.8 mm also resulted in fibre pulling and uneven printing, causing the printed specimen to be lifted from the print bed, as highlighted in Figure 82 (c). Increasing layer height has been reported to increase inter-layer voids, so a minimum printable layer height of 0.8 mm was chosen [404][408]. The g-code for 3D printing is provided in Appendix B.

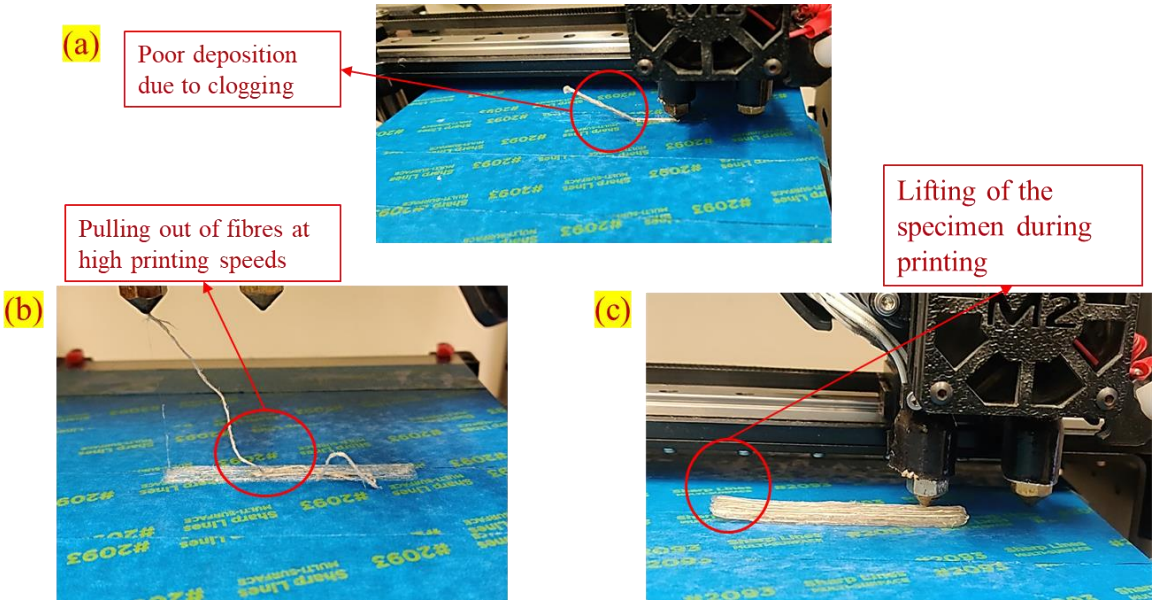

Figure 82 Problems occurred during the optimisation of FDM 3D Printing parameters.

6.4.7 Morphology of FDM 3D Printed Composite

Optical microscopy images of the cross-sections of solution and emulsion impregnated 3D printed composites are shown in Figures 83 (a) and 83 (b), respectively. The reinforcing yarns were observed to be positioned on the upper part of the printing layer for all the composites except for emulsion impregnated PLA/viscose. As explained earlier, the drag force of the nozzle responsible for the pulling of the fibres causes this positioning of reinforcing yarns. A similar feature has been reported in multiple studies based on 3D printing of long/continuous fibre reinforced composites [30,32,34,384]. The absence of fibres pushed to the surface in emulsion impregnated PLA/viscose indicates efficient matrix impregnation and good interfacial bonding, preventing the yarn from getting dragged out of the matrix [212].

The morphology of the 3D printed composites also revealed porosity created by inter-layer voids, as highlighted in Figure 81. High layer heights create these voids and have been shown to negatively affect the tensile properties of 3D printed composites [408][30]. An adaptive extrusion model was suggested in the literature to fill these gaps by modifying the 3D printer to introduce additional polymer via the co-extrusion method, which reduced porosity by 54.4% [408]. A post-consolidation method using compression moulding was also reported to reduce inter-layer voids and porosity by 6% to 10% [404].

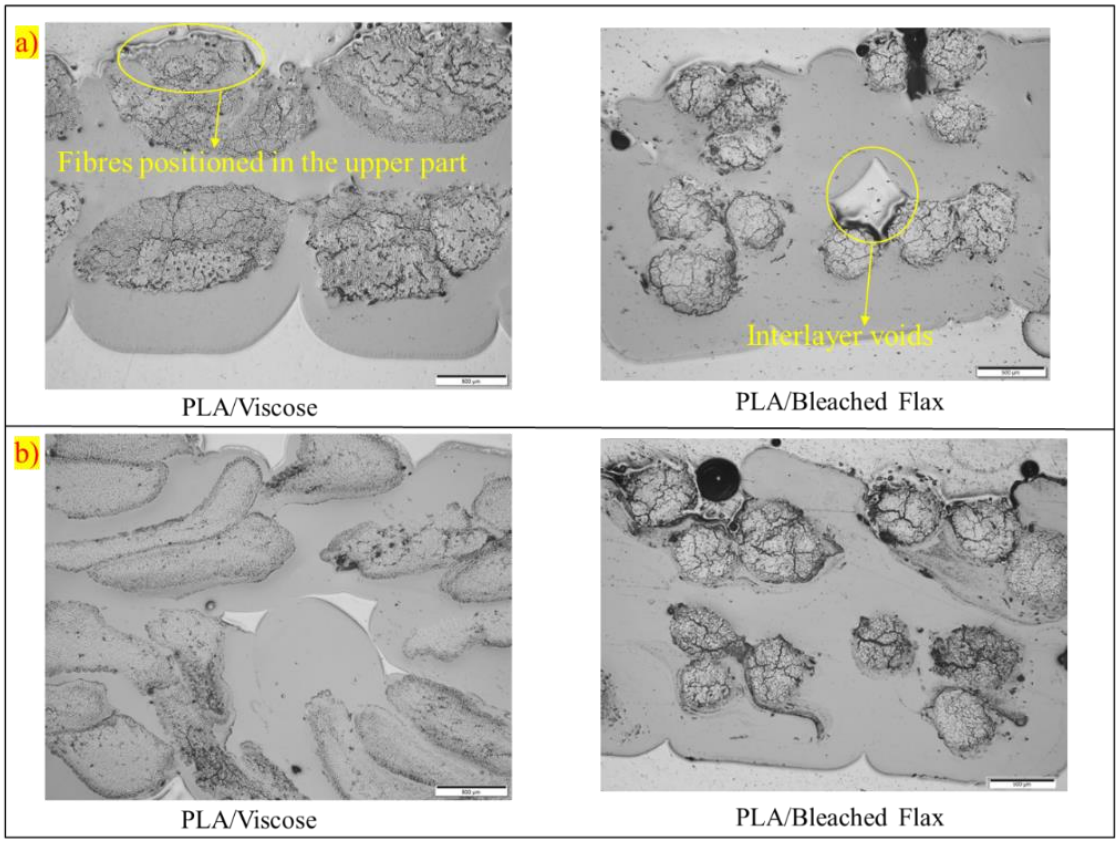

Figure 83 Optical microscope images of 3D printed composites produced from a) Solution impregnation and b) Emulsion impregnation.

6.4.7 Porosity and Reinforcement Weight Percentage of FDM 3D Printed Composites

Table 29 presents the porosity and fibre weight % of the 3D printed composites. The fibre wt% is the same as that of the filaments. A minor increase in porosity was observed for all the printed specimens compared to the 3D printing filaments. The increase in porosity is due to the defects introduced by the printing process. As observed in Figure 83, inter-layer voids created due to the fibres being pulled to the surface during printing cause porosity. As mentioned earlier, in-situ impregnation and post-printing consolidation can reduce these voids [408] [404].

Table 29 Fibre and polymer weight percentage and porosity percentage of 3D printed composite specimens.

Impregnation type	Composite Filament	Fibre wt%	Polymer wt%	Porosity (%)
Solution impregnation	PLA/Viscose	33.4±1.3	66.6±2.3	6.3±3.4
	PLA/Bleached Flax	27.8±2.1	72.2±4.2	8.8±1.2
Emulsion impregnation	PLA/Viscose	32.8±0.9	67.2±1.8	7.0±2.4
	PLA/Bleached Flax	26.4±2.8	73.6±5.6	9.2±0.5

6.4.8 Tensile Properties of FDM 3D Printed Composites

A summary of the experimental tensile properties of the 3D printed composites and a comparison of % decrease compared to 3D printing filaments is given in Table 30. Significant reductions were observed in all the tensile properties of the printed samples. The reduction in tensile properties of the 3D printed composites compared to the filaments is due to the defects induced by the printing process. Modifying the 3D printing equipment to print with lower layer heights and filament diameters is required to minimise the loss in tensile properties [16,409].

A comparison of tensile strength and Young's modulus of all the 3D printed long/continuous fibre reinforced PLA composites in the literature with this study is shown in Figure 84. This is the first study to 3D print PLA/continuous viscose composites, but PLA/flax yarn composites have been used for FDM 3D printing in multiple studies. Studies that reported higher tensile properties highlighted the following aspects:

1. Untwisting of flax yarns allows for better impregnation and avoids high fibre/fibre friction [218].
2. Modification of the 3D printer to allow for printing with lower layer heights [217] [215].
3. Surface treatment of flax fibre yarn to improve impregnation [217].
4. In-situ impregnation of PLA to improve inter-layer adhesion and avoid pulling of reinforcing fibres to the surface [217].
5. 3D printing with higher fibre wt% between 30% to 45% [215][217][218].

Table 30 Tensile properties of 3D printed composite specimens and percentage decrease compared to 3D printing filaments (highlighted in parentheses).

Impregnation Type	Material	Fibre wt%	Tensile Strength (MPa) (% Decrease)	Young's Modulus (GPa) (% Decrease)	Elongation at break (%) (% Decrease)
Solution impregnation	PLA/Viscose	33.4±1.3	139.9 (↓30.7%)	5.9 (↓13.2%)	7.5 (↓57.1%)
	PLA/Bleached flax	27.8±2.1	127.3 (↓29.6%)	7.2 (↓25.0%)	3.9 (↓23.0%)
Emulsion impregnation	PLA/Viscose	32.8±0.9	158.0 (↓17.0%)	6.9 (↓6.8%)	8.3 (↓62.3%)
	PLA/Bleached flax	26.4±2.8	108.4 (↓29.9%)	5.8 (↓36.5%)	3.2 (↓5.9%)

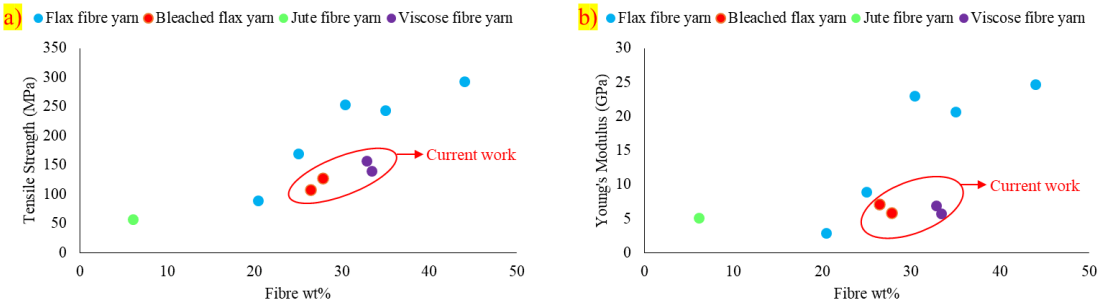

Figure 84 Comparison of tensile strength and Young's modulus obtained in the current work with the literature for 3D printed long/continuous bio-derived fibre reinforced PLA composites.

6.4.9 Fracture Surface Analysis of FDM 3D Printed Composites

Fibre pull-outs and seperation of melt impregnated polymer were visible in all specimens. SEM images of fracture surfaces of neat PLA and the composite specimens are shown in Figure 85. Neat PLA displayed a characteristic brittle failure surface. Interlayer voids formed due to high layer height were visible in the fracture surface of neat PLA. Solution impregnated PLA/viscose, and PLA/bleached flax exhibited fibre pull-outs and some fibre breakages similar to the 3D printing filaments. Emulsion impregnated PLA/viscose displayed lesser fibre pull-outs than the rest of the composites and more fibre breakage, which agrees with its high tensile properties [410,411]. Emulsion impregnated PLA/bleached

flax displayed a similar fracture behaviour to the 3D printing filament with a high number of fibre pull-outs and brittle fracture of the surrounding matrix.

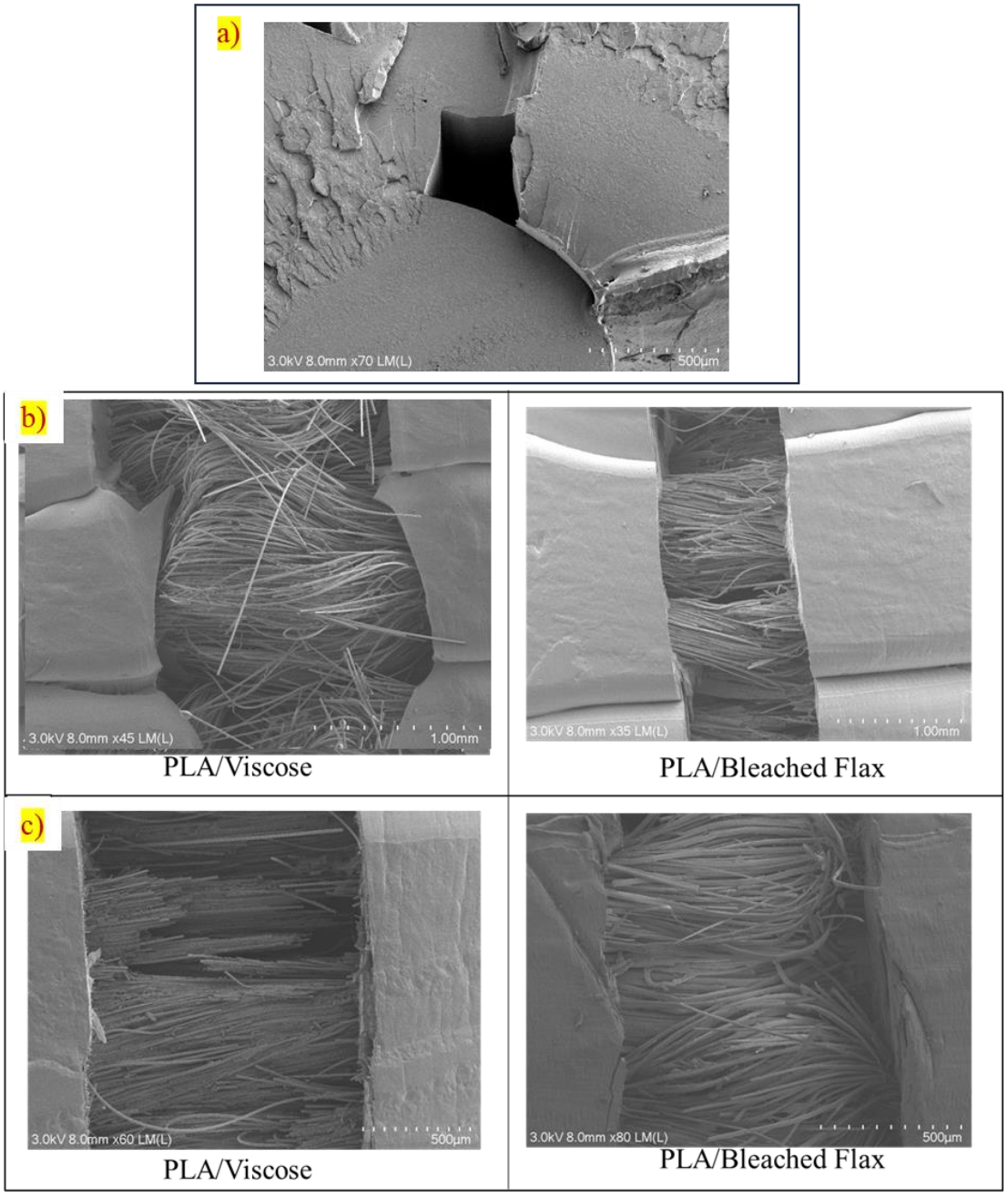

Figure 85 SEM images of fracture surfaces of 3D printed specimens a) Neat PLA b) Solution impregnation c) Emulsion impregnation.

6.4.10 Flexural Properties of FDM 3D Printed Composites

Flexural properties of FDM 3D printed composites are summarised in Table 31. The stress vs strain curves obtained for flexural testing are shown in Figure 86. Neat PLA displayed a linear stress-strain behaviour followed by an abrupt fracture due to its brittle nature [412]. On the other hand, the composite

specimens displayed a linear stress-strain behaviour with a subsequent slow decrease in strength with increasing strain associated with the onset of fibre/matrix interface debonding until failure [413–415]. Flexural properties of PLA/viscose showed higher improvement with emulsion impregnation, whereas PLA/bleached flax performed better with solution impregnation, similar to what was observed for tensile properties. The highest increase in flexural properties compared to neat PLA was obtained for emulsion-impregnated PLA/viscose, with an increase of 80% in bending strength and 212% in bending modulus, respectively.

It was observed that the bending modulus was higher than Young's modulus in composite materials. This could be due to the effect of uneven distribution of stress in bending tests, and it is only maximum at outermost fibres, by which internal flaws become comparatively less effective as in the case of the tensile test, where the stress is uniform throughout the cross-section. Fibre alignment and impregnation quality also play critical roles where fibres well-aligned in the direction of bending and well-impregnated contribute significantly to bending stiffness [416]. The flexural properties of long/continuous bio-derived fibre reinforced 3D printed composites have not been reported in the literature, but the properties obtained in this study were comparable to those reported for 3D printed continuous carbon fibre reinforced composites [417].

Table 31 Flexural properties of FDM 3D printed composites.

Impregnation Type	**Material**	**Bending Strength (MPa)**	**Bending Modulus (GPa)**
None	Neat PLA	91.0±5.5	3.0±0.2
Solution impregnation	PLA/Viscose	154.3±20.3	7.9±2.1
	PLA/Bleached flax	127.0±20.3	8.9±1.0
Emulsion impregnation	PLA/Viscose	163.8±20	9.8±1.1
	PLA/Bleached flax	122.4±17.5	8.5±1.4

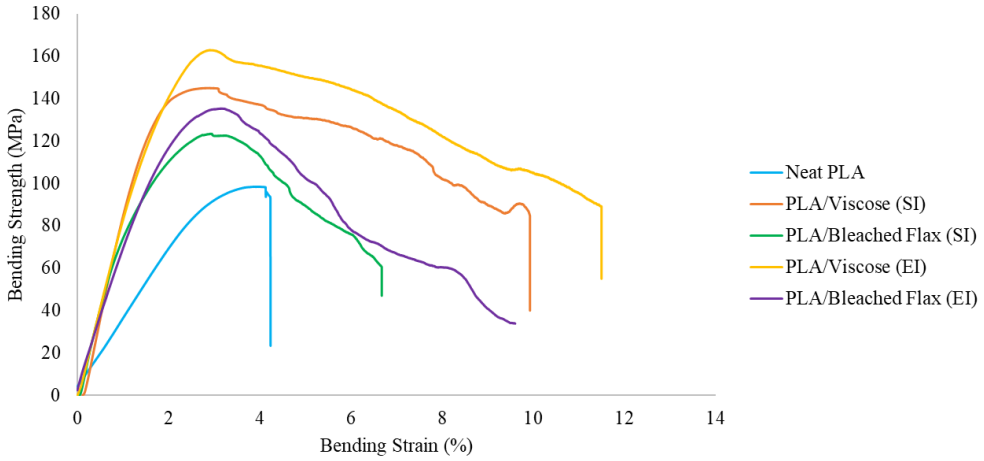

Figure 86 Stress vs Strain for flexural testing of 3D printed composites; SI - Solution impregnation; EI - Emulsion impregnation.

6.4.11 Impact Strength of FDM 3D Printed Composite

The impact strength of FDM 3D printed composites is summarised in Table 32. Solution-impregnated PLA/viscose composites displayed exceptional impact strength with an increase of 500% compared to neat PLA. Solution and emulsion impregnated PLA/bleached flax composites displayed similar impact strengths with an increase of 213.4% and 221.5% compared to neat PLA, respectively. The impact strength of the emulsion-impregnated PLA/viscose samples exceeded the Charpy impact testing machine's upper limit; hence, the impact strength is mentioned as >127KJ/m2 in Table 32. A comparison of the Charpy impact strength values of PLA composites in literature and current work is presented in Figure 87. According to the current research findings, the Charpy impact strengths obtained in the present work are higher than any reported values for bio-derived fibre-reinforced PLA composites, to the best of our knowledge.

The energy absorption mechanisms can explain the higher impact strength of the PLA/viscose composites during impact. It has been hypothesised that fibres pull out rather than break; this pull-out process tends to be energy intensive. More energy dissipates through debonding at the interface and frictional sliding between the fibre and the matrix. The weak interfaces have the effect of deflection on the crack, introducing longer crack path length and, therefore, the much-needed energy for crack propagation. The matrix also deforms plastically or undergoes microcracking, which absorbs more energy [136]. Hence, the fibre pull-out, debonding, crack deflection, frictional sliding, and matrix deformation lead to multiple energy dissipation mechanisms that, in turn, enhance the impact strength of the composite. [374,418].

Table 32 Impact strength of FDM 3D printed composites.

Impregnation Type	Material	Impact Strength (KJ/m^2)
None	Neat PLA	20.9±4.5
Solution impregnation	PLA/Viscose	125.8±2.1
	PLA/Bleached flax	65.6±5.1
Emulsion impregnation	PLA/Viscose	>127
	PLA/Bleached flax	67.2±5.0

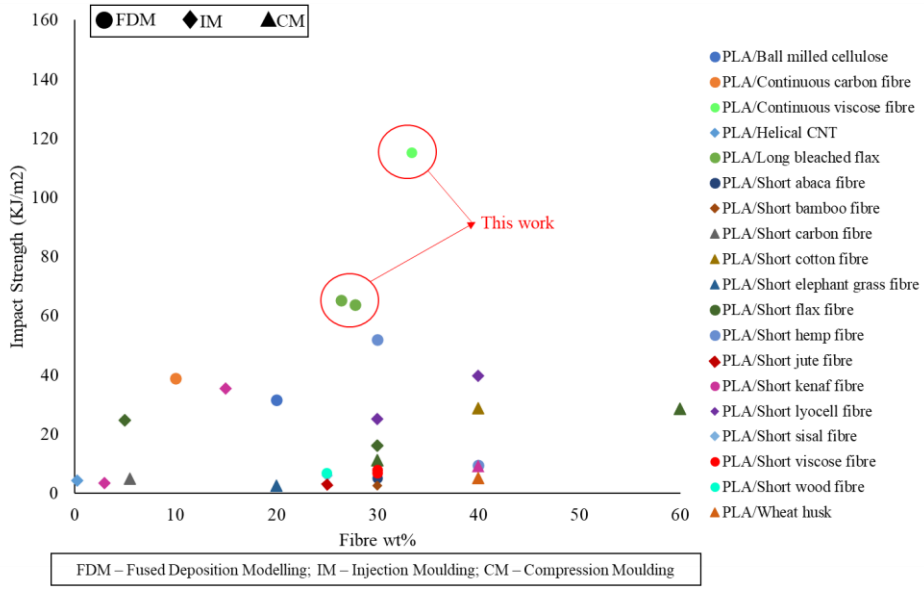

Figure 87 Comparison of Charpy impact strength for PLA composites reported across literature with current work [111,135,213,419–438].

6.4.12 Thermal Properties of FDM 3D Printed Composite

DSC thermograms of solution and emulsion impregnated 3D printed composites are shown in Figures 88 (a) and 88 (b), respectively. T_g, T_m, T_{cc}, and degree of crystallinity X_c are given in Table 33. T_g, T_m, and T_{cc} values remained relatively similar to the 3D printing filaments. However, a decrease in crystallinity values was observed. The decrease in crystallinity resulted from the 3D printing process, during which a higher layer height (0.8 mm) and heated build platform (60 °C) were used. It has been observed that printing with higher layer heights on a heated build platform reduces the molecular orientation during the deposition, leading to the formation of lesser stable δ form crystallites of PLA, which results in a reduction of crystallinity [405]. A post-printing heat treatment has been proven to improve the crystallinity and mechanical properties of PLA composites [439–441].

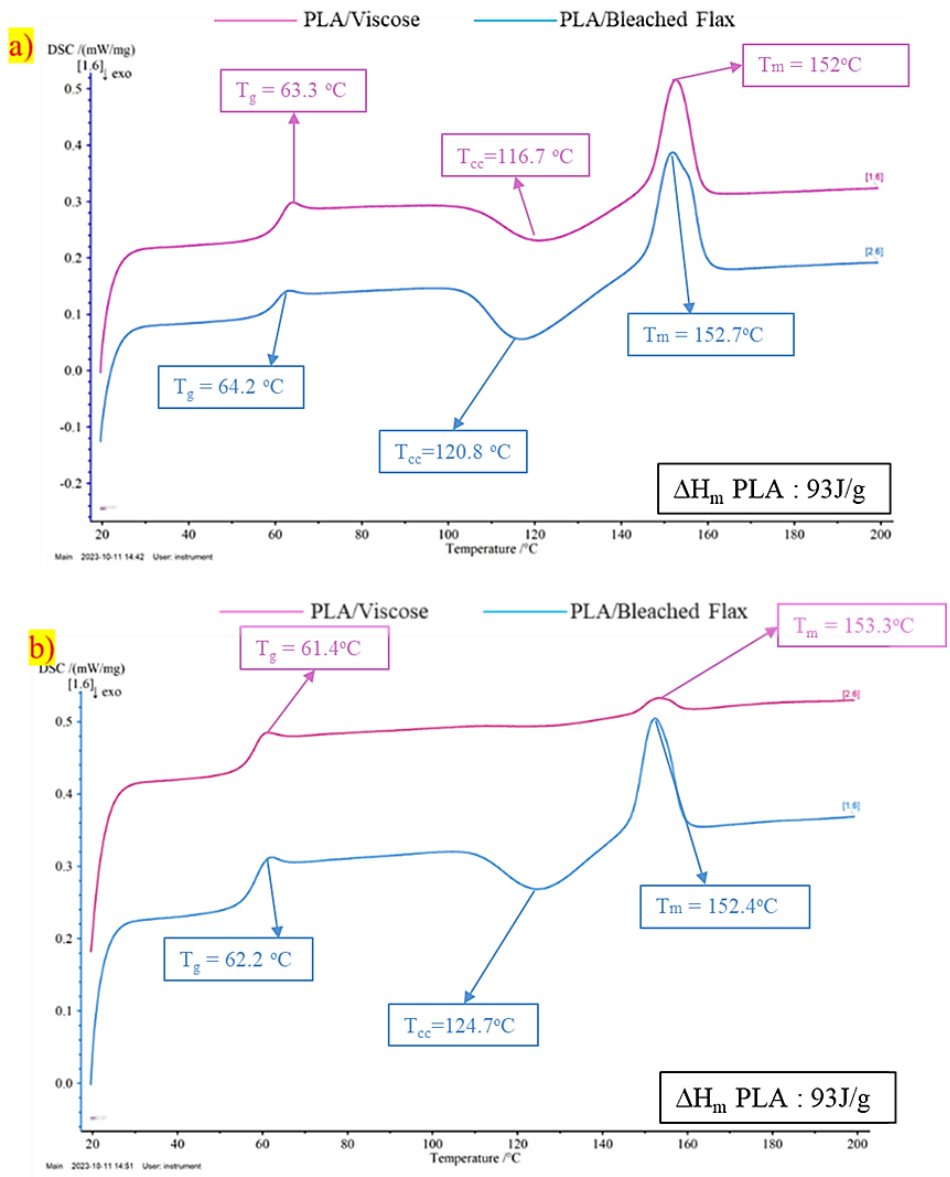

Figure 88 DSC thermograms of FDM 3D printed composites a) Solution impregnation b) Emulsion impregnation

Table 33 Summary of DSC of 3D printed composites.

Impregnation Type	3DP Composite	T_g (°C)	T_m (°C)	T_{cc} (°C)	X_c (%)
Solution Impregnation	PLA/Viscose	63.3	152	116.7	19.7
	PLA/Bleached Flax	64.2	152.7	120.8	14.2
Emulsion Impregnation	PLA/Viscose	61.4	153.3	-	-
	PLA/Bleached Flax	62.2	152.4	124.7	10.5

6.5 Conclusions

In producing 3D printing filaments, three impregnated filaments were consolidated into one, and the additional polymer was introduced through melt impregnation to achieve an average filament diameter of 1.45 mm. Based on their mechanical performance, PLA/viscose and PLA/bleached flax were chosen for 3D printing. Multiple consolidated filaments exhibited increased fibre weight percentage compared to single filaments. With further polymer content increase via melt impregnation, a reduction in porosity, fibre wt%, and tensile properties was observed. The reduction in tensile properties was less pronounced for PLA/viscose compared to PLA/bleached flax, especially with emulsion impregnation, because of a stronger affinity between viscose fibres and water-based PLA emulsion. Additionally, DSC analysis revealed improved crystallinity in all the 3D printing filaments, with the highest crystallinity (24.3%) observed in solution impregnated viscose, contributing to enhanced mechanical properties.

3D printed PLA/viscose and PLA/bleached flax composites were characterized for porosity, tensile, flexural, impact, and thermal properties. The composites exhibited higher porosity than the 3D printing filaments, primarily due to printing-induced defects like inter-layer voids and fibre migration to the surface. Emulsion impregnated PLA/viscose showed superior fibre distribution and tensile properties within the printed composites. However, the tensile properties in this study were lower than reported in the literature, where studies recommended untwisting yarns, surface treatment of flax fibre yarns, in-situ PLA impregnation, and using higher fibre weight percentages to achieve higher tensile properties. Similar trends were observed in flexural properties, with viscose reinforced composites outperforming bleached flax reinforced composites. Impact strengths achieved for the composites in this study outperformed available literature, with the highest impact strength of greater than 127KJ/m^2 for emulsion impregnated PLA/viscose. DSC analysis revealed decreased crystallinity in the 3D printed composites compared to the filaments, attributed to δ form crystallite formation during deposition.

Chapter 7 Conclusions

1. Processes for solution and emulsion impregnation and consolidation were successfully developed, resulting in the production of composite filaments.
2. Emulsion impregnated composites demonstrated higher polymer uptake due to the improved affinity between water and bio-derived fibres. In contrast, solution-impregnated composites exhibited better polymer distribution, especially in twisted flax-reinforced filaments, due to the efficient impregnation of the PLA/DCM solution.
3. In PLA/viscose composites, emulsion impregnation led to higher tensile strength (254.7 MPa) and Young's modulus (9.1 GPa), surpassing values reported in the literature. The solution-impregnated PLA/bleached flax, for the 7wt% x 3 formulation, achieved the highest tensile strength (356.1 MPa), also exceeding values reported in the existing literature for PLA/flax composites.
4. The production of 3D printing filaments by combining multiple filaments resulted in a loss of tensile properties due to the addition of polymer via melt-impregnation to achieve printability. Additionally, the 3D printing process increased porosity and decreased tensile properties.
5. The highest tensile and flexural properties were observed in emulsion-impregnated PLA/viscose composites, highlighting the importance of efficient impregnation. These composites also displayed an impact strength greater than 127 KJ/m², which is higher than reported values for any PLA biocomposite in the literature.

Chapter 8 Recommendations and Future Work

The outcomes of this research provide a crucial foundation for enhancing the mechanical properties of long/continuous bio-derived fibre reinforced PLA composites for 3D printing. Several suggestions for future investigations are outlined below:

1. The solution and emulsion impregnation processes used in this research proved effective in the impregnation of continuous viscose fibre yarns. However, it was observed that flax fibre yarns need an untwisting mechanism, either before or during impregnation, to reduce impregnation porosity and ensure homogeneous polymer distribution. A combination of untwisting and impregnation could result in improved wetting of flax fibres.
2. Viscose-reinforced filaments exhibited interface porosities, which resulted in fibre pull-outs. This issue can be attributed to the smooth surface of viscose fibres, which limits mechanical interlocking. Potential solutions to enhance the mechanical properties of PLA/viscose composites include applying a suitable surface treatment to viscose fibres or incorporating compatibilisers.
3. This research primarily highlighted enhancing fibre wettability and elevating the mechanical performance of composite materials. To extend the high tensile properties achieved with single yarn reinforced filaments to 3D printing filaments and printed specimens, it is imperative to prioritize modifications to the printing equipment, such as incorporating a dual nozzle system for in-situ polymer impregnation and adjustable filament feeder to accommodate long/continuous fibre-reinforced filaments with smaller diameters and higher fibre wt%.
4. Post-printing heat treatment or compression moulding can enhance interlayer adhesion, minimize porosity, and improve mechanical performance. Combining 3D printing for material deposition with subsequent compression moulding can eliminate voids and defects, resulting in high-performance composites.

References

1. Peltola SM., Melchels FPW., Grijpma DW., Kellomäki M. A review of rapid prototyping techniques for tissue engineering purposes. Annals of Medicine. 2008. 268–280 p. Available at: DOI:10.1080/07853890701881788

2. Peppas NA., Brannon-Peppas L. Drug Delivery Biomaterials. In: Buschow KHJ, Cahn RW, Flemings MC, Ilschner B, Kramer EJ, Mahajan S, et al. (eds.) Encyclopedia of Materials: Science and Technology. Oxford: Elsevier; 2001. pp. 2351–2355. Available at: DOI:https://doi.org/10.1016/B0-08-043152-6/00414-9

3. Hexpol. Biobased vs Biodegradable. 2020. Available at: https://www.hexpol.com/tpe/resources/sustainability-insights/biobased-vs-biodegradable/ (Accessed: 18 July 2022)

4. Niaounakis M. Chapter 1 - Introduction. In: Niaounakis M (ed.) Biopolymers: Processing and Products. Oxford: William Andrew Publishing; 2015. pp. 1–77. Available at: DOI:https://doi.org/10.1016/B978-0-323-26698-7.00001-5

5. Kerni L., Singh S., Patnaik A., Kumar N. A review on natural fiber reinforced composites. Materials Today: Proceedings. Elsevier Ltd.; 2020; 28: 1616–1621. Available at: DOI:10.1016/j.matpr.2020.04.851

6. Müssig J., Graupner N. Test methods for fibre/matrix adhesion in cellulose fibre-reinforced thermoplastic composite materials: A critical review. Reviews of Adhesion and Adhesives. 2020; 8(2): 68–129. Available at: DOI:10.7569/RAA.2020.097306

7. Vincent JFV. Unified nomenclature for plant fibres for industrial use. Applied Composite Materials. 2000; 7(5–6): 269–271. Available at: DOI:10.1023/A:1026516105382

8. Sayed MA. Definition Of Yarn | Classification Of Yarn. TEXTILE APEX. Available at: https://textileapex.blogspot.com/2013/11/yarn-classification.html (Accessed: 20 September 2022)

9. Bartl A. Chapter 10 - Textiles production and end-of-life management options. In: Letcher TM (ed.) Plastic Waste and Recycling. Academic Press; 2020. pp. 251–279. Available at: DOI:https://doi.org/10.1016/B978-0-12-817880-5.00010-4

10. Count UY., Uses THE., Australian OF., Spinning WHY., Love M., Cotton A., et al. FACT SHEET UNDERSTANDING YARN COUNTS. Available at: https://australiancotton.com.au/assets/downloads/Australian_Cotton_Fact_Sheet_-

_Understanding_Yarn_Counts.pdf

11. Mwema FM., Akinlabi ET. Basics of Fused Deposition Modelling (FDM). Fused Deposition Modeling: Strategies for Quality Enhancement. Cham: Springer International Publishing; 2020. pp. 1–15. Available at: DOI:10.1007/978-3-030-48259-6_1

12. van Wijk A., van Wijk I. 3D printing with biomaterials: Towards a sustainable and circular economy. 3D Printing with Biomaterials: Towards a Sustainable and Circular Economy. 2015. 1–85 p. Available at: DOI:10.3233/978-1-61499-486-2-i

13. Saheb DN., Jog JP. Natural fiber polymer composites: A review. Advances in Polymer Technology. John Wiley & Sons, Ltd; 1 December 1999; 18(4): 351–363. Available at: DOI:https://doi.org/10.1002/(SICI)1098-2329(199924)18:4<351::AID-ADV6>3.0.CO;2-X

14. Rothen-Weinhold A., Besseghir K., Vuaridel E., Sublet E., Oudry N., Kubel F., et al. Injection-molding versus extrusion as manufacturing technique for the preparation of biodegradable implants. European Journal of Pharmaceutics and Biopharmaceutics. 1999; 48(2): 113–121. Available at: DOI:https://doi.org/10.1016/S0939-6411(99)00034-X

15. Hsissou R., Seghiri R., Benzekri Z., Hilali M., Rafik M., Elharfi A. Polymer composite materials: A comprehensive review. Composite Structures. 2021; 262: 113640. Available at: DOI:https://doi.org/10.1016/j.compstruct.2021.113640

16. Rahim TNAT., Abdullah AM., Md Akil H. Recent Developments in Fused Deposition Modeling-Based 3D Printing of Polymers and Their Composites. Polymer Reviews. Taylor & Francis; 2019; 59(4): 589–624. Available at: DOI:10.1080/15583724.2019.1597883

17. Road B. a Review : Fused Deposition Modeling – a Rapid Prototyping Process. International Research Journal of Engineering and Technology(IRJET). 2017; 4(9): 5–9. Available at: https://irjet.net/archives/V4/i9/IRJET-V4I989.pdf

18. Tran TN., Heredia-Guerrero J., Frugone M., Lagomarsino M., Maggio F., Athanassiou A. Cocoa Shell Waste Biofilaments for 3D Printing Applications. Macromolecular Materials and Engineering. 2017; 302: 1700219. Available at: DOI:10.1002/mame.201700219

19. Hao W., Liu Y., Zhou H., Chen H., Fang D. Preparation and characterization of 3D printed continuous carbon fiber reinforced thermosetting composites. Polymer Testing. 2018; 65: 29–34. Available at: DOI:https://doi.org/10.1016/j.polymertesting.2017.11.004

20. Gezer FH., Sahin I. Improving the mechanical properties of Polylactic Acid (PLA) based 3D printing materials: Current methods and applications. Selcuk University Journal of Engineering

Sciences. 2023; 22(02): 80–88. Available at: http://sujes.selcuk.edu.tr

21. Ambade V V., Rajurkar SW., Awari GK. Optimization of process parameters affecting performance of part characteristics in fused deposition modeling (FDM) 3D printing: A critical review. AIP Conference Proceedings. 2023; 2800(1): 20072. Available at: DOI:10.1063/5.0162925

22. Sawant DA., Shinde BM., Raykar SJ. Post processing techniques used to improve the quality of 3D printed parts using FDM: State of art review and experimental work. Materials Today: Proceedings. 2023; Available at: DOI:https://doi.org/10.1016/j.matpr.2023.09.202

23. Pickering KL., Efendy MGA., Le TM. A review of recent developments in natural fibre composites and their mechanical performance. Composites Part A: Applied Science and Manufacturing. 2016; 83: 98–112. Available at: DOI:10.1016/j.compositesa.2015.08.038

24. Ramamoorthy SK., Skrifvars M., Persson A. A review of natural fibers used in biocomposites: Plant, animal and regenerated cellulose fibers. Polymer Reviews. 2015; 55(1): 107–162. Available at: DOI:10.1080/15583724.2014.971124

25. Gauss C., Pickering KL., Muthe LP. The use of cellulose in bio-derived formulations for 3D/4D printing: A review. Composites Part C: Open Access. Elsevier B.V.; 2021; 4(December 2020): 100113. Available at: DOI:10.1016/j.jcomc.2021.100113

26. Worldwide most used 3D printing materials, as of July 2018*. statista. 2018. Available at: https://www.statista.com/statistics/800454/worldwide-most-used-3d-printing-materials/#:~:text=This statistic shows the worldwide,most used 3D printing material. (Accessed: 2 September 2020)

27. Mukherjee T., Kao N. PLA Based Biopolymer Reinforced with Natural Fibre: A Review. Journal of Polymers and the Environment. 2011; 19(3): 714–725. Available at: DOI:10.1007/s10924-011-0320-6

28. Getme AS., Patel B. A review: Bio-fiber's as reinforcement in composites of polylactic acid (PLA). Materials Today: Proceedings. Elsevier Ltd.; 2019; 26: 2116–2122. Available at: DOI:10.1016/j.matpr.2020.02.457

29. Muthe LP., Pickering K., Gauss C. A Review of 3D/4D Printing of Poly-Lactic Acid Composites with Bio-Derived Reinforcements. Composites Part C: Open Access. Elsevier B.V.; 2022; 8(April): 100271. Available at: DOI:10.1016/j.jcomc.2022.100271

30. Cheng P., Wang K., Chen X., Wang J., Peng Y., Ahzi S., et al. Interfacial and mechanical

properties of continuous ramie fiber reinforced biocomposites fabricated by in-situ impregnated 3D printing. Industrial Crops and Products. Elsevier B.V.; 2021; 170(March): 113760. Available at: DOI:10.1016/j.indcrop.2021.113760

31. Zhuo P., Li S., Ashcroft I., Jones A., Pu J. 3D printing of continuous fibre reinforced thermoplastic composites. ICCM International Conferences on Composite Materials. 2017; 2017-Augus(August): 20–25.

32. Matsuzaki R., Ueda M., Namiki M., Jeong TK., Asahara H., Horiguchi K., et al. Three-dimensional printing of continuous-fiber composites by in-nozzle impregnation. Scientific Reports. Nature Publishing Group; 2016; 6(December 2015): 1–7. Available at: DOI:10.1038/srep23058

33. Le Duigou A., Chabaud G., Matsuzaki R., Castro M. Tailoring the mechanical properties of 3D-printed continuous flax/PLA biocomposites by controlling the slicing parameters. Composites Part B: Engineering. 2020; 203: 108474. Available at: DOI:https://doi.org/10.1016/j.compositesb.2020.108474

34. Tian X., Todoroki A., Liu T., Wu L., Hou Z., Ueda M., et al. 3D Printing of Continuous Fiber Reinforced Polymer Composites: Development, Application, and Prospective. Chinese Journal of Mechanical Engineering: Additive Manufacturing Frontiers. 2022; 1(1): 100016. Available at: DOI:https://doi.org/10.1016/j.cjmeam.2022.100016

35. Le Duigou A., Chabaud G., Matsuzaki R., Castro M. Tailoring the mechanical properties of 3D-printed continuous flax/PLA biocomposites by controlling the slicing parameters. Composites Part B: Engineering. Elsevier Ltd; 2020; 203(July): 108474. Available at: DOI:10.1016/j.compositesb.2020.108474

36. Chen K., Yu L., Cui Y., Jia M., Pan K. Optimization of printing parameters of 3D-printed continuous glass fiber reinforced polylactic acid composites. Thin-Walled Structures. Elsevier Ltd.; 2021; 164(November 2020): 107717. Available at: DOI:10.1016/j.tws.2021.107717

37. Long Y., Zhang Z., Fu K., Li Y. Efficient plant fibre yarn pre-treatment for 3D printed continuous flax fibre/poly(lactic) acid composites. Composites Part B: Engineering. 2021; 227: 109389. Available at: DOI:https://doi.org/10.1016/j.compositesb.2021.109389

38. McGregor OPL., Duhovic M., Somashekar AA., Bhattacharyya D. Pre-impregnated natural fibre-thermoplastic composite tape manufacture using a novel process. Composites Part A: Applied Science and Manufacturing. 2017; 101: 59–71. Available at: DOI:https://doi.org/10.1016/j.compositesa.2017.05.025

39. Baley C., Kervoëlen A., Lan M., Cartié D., Le Duigou A., Bourmaud A., et al. Flax/PP manufacture by automated fibre placement (AFP). Materials & Design. 2016; 94: 207–213. Available at: DOI:https://doi.org/10.1016/j.matdes.2016.01.011

40. George Cornel Dumitrescu IAT. 3D Printing – A New Industrial Revolution. Knowledge Horizons. Economics. 2016; 8(1): 32–39. Available at: https://econpapers.repec.org/article/khejournl/v_3a8_3ay_3a2016_3ai_3a1_3ap_3a32-39.htm

41. Pereira T., Kennedy J V., Potgieter J. A comparison of traditional manufacturing vs additive manufacturing, the best method for the job. Procedia Manufacturing. Elsevier B.V.; 2019; 30: 11–18. Available at: DOI:10.1016/j.promfg.2019.02.003

42. Gurung D. Technological comparison of 3D and 4D printing. Arcada University of Applied Sciences; 2017. Available at: https://www.theseus.fi/bitstream/handle/10024/130325/Thesis_Dilip.pdf?sequence=1

43. Sundaram S. 3D-printing Form and Function. MASSACHUSETTS INSTITUTE OF TECHNOLOGY; 2018. Available at: https://dspace.mit.edu/handle/1721.1/120416

44. Zhang Z., Demir KG., Gu GX. Developments in 4D-printing: a review on current smart materials, technologies, and applications. International Journal of Smart and Nano Materials. Taylor & Francis; 2019; 10(3): 205–224. Available at: DOI:10.1080/19475411.2019.1591541

45. Oxman N., Laucks J., Kayser M., Tsai E., Firstenberg M. Freeform 3D printing: Towards a sustainable approach to additive manufacturing. Green Design, Materials and Manufacturing Processes - Proceedings of the 2nd International Conference on Sustainable Intelligent Manufacturing, SIM 2013. 2013; : 479–483.

46. Kuka Partner Publishes Video on Using Freeform 3D Printing for the Future of Construction. 3D Printing Media Network. 2016. Available at: https://www.3dprintingmedia.network/kuka-releases-video-using-robotic-arm-additive-building-construction/#:~:text=Freeform printing in open space,or highly controlled build environments. (Accessed: 26 August 2020)

47. Wonjin Jo,* Kyung Sung Chu, Heon Ju Lee M-WM. 3D and 4D Printing Technologies: An Overview. Material Matters. 2016; 11.2. Available at: https://www.sigmaaldrich.com/technical-documents/articles/material-matters/3d-and-4d-printing-technologies.html#:~:text=3D printing can involve different,the design process more important.

48. Ligon SC., Liska R., Stampfl J., Gurr M., Mülhaupt R. Polymers for 3D Printing and Customized Additive Manufacturing. Chemical Reviews. 2017; 117(15): 10212–10290. Available at: DOI:10.1021/acs.chemrev.7b00074

49. Campbell TA., Tibbits S., Garrett B. The next wave : 4D printing - programming the material world. Atlantic Council. 2014; (January): 1–15. Available at: https://www.atlanticcouncil.org/wp-content/uploads/2014/05/The_Next_Wave_4D_Printing_Programming_the_Material_World.pdf

50. Bogue R. Smart materials: A review of capabilities and applications. Assembly Automation. 2014; 34(1): 16–22. Available at: DOI:10.1108/AA-10-2013-094

51. Nkomo NZ. A review of 4D printing technology and future trends. 11th South African Conference on Computational and Applied Mechanics, SACAM 2018. National University of Science and Technology, Zimbabwe; 2018. Available at: https://www.researchgate.net/publication/328162917%0AA

52. Columbus L. The State of 3D Printing, 2018. Forbes. 2018. Available at: https://www.forbes.com/sites/louiscolumbus/2018/05/30/the-state-of-3d-printing-2018/?sh=70f203a97b0a (Accessed: 10 November 2020)

53. Chhabra D. Comparison and analysis of different 3d printing techniques. International Journal of Latest Trends in Engineering and Technology. 2017; 8(41): 264–272. Available at: DOI:10.21172/1.841.44

54. saasworthy. 3D Printing Statistics for 2023. 2023. Available at: https://www.saasworthy.com/blog/3d-printing-statistics (Accessed: 25 October 2023)

55. Gkartzou E., Koumoulos EP., Charitidis CA. Production and 3D printing processing of bio-based thermoplastic filament. Manufacturing Review. 2017; 4. Available at: DOI:10.1051/mfreview/2016020

56. Eda HT., Husnu YE. Extrusion-Based 3D Printing Applications of PLA Composites: A Review. Coatings. 2021; 11(4): 1–42. Available at: https://doi.org/10.3390/coatings11040390

57. Le Duigou A., Correa D., Ueda M., Matsuzaki R., Castro M. A review of 3D and 4D printing of natural fibre biocomposites. Materials and Design. The Authors; 2020; 194: 108911. Available at: DOI:10.1016/j.matdes.2020.108911

58. Vengatesan MR., Mittal V. Nanoparticle- and Nanofiber-Based Polymer Nanocomposites: An Overview. Spherical and Fibrous Filler Composite. 2016. pp. 1–38. Available at: DOI:https://doi.org/10.1002/9783527670222.ch1

59. WOODINGS C. 1 - A brief history of regenerated cellulosic fibres. In: Woodings C (ed.)

Regenerated Cellulose Fibres. Woodhead Publishing; 2001. pp. 1–21. Available at: DOI:https://doi.org/10.1533/9781855737587.1

60. Fibres CC. Properties of regenerated fibres. 2015;

61. LÖNNBERG B. 2 - Industrial cellulose. In: Woodings C (ed.) Regenerated Cellulose Fibres. Woodhead Publishing; 2001. pp. 22–36. Available at: DOI:https://doi.org/10.1533/9781855737587.22

62. Sayyed AJ., Deshmukh NA., Pinjari D V. A critical review of manufacturing processes used in regenerated cellulosic fibres: viscose, cellulose acetate, cuprammonium, LiCl/DMAc, ionic liquids, and NMMO based lyocell. Cellulose. Springer Netherlands; 2019; 26(5): 2913–2940. Available at: DOI:10.1007/s10570-019-02318-y

63. Pickering KL., Aruan Efendy MG. Preparation and mechanical properties of novel bio-composite made of dynamically sheet formed discontinuous harakeke and hemp fibre mat reinforced PLA composites for structural applications. Industrial Crops and Products. Elsevier B.V.; 2016; 84: 139–150. Available at: DOI:10.1016/j.indcrop.2016.02.005

64. Hassan E. Plant Fibers Reinforced Poly (Lactic Acid) (Pla) As a Green Composites : Review. International Journal of Engineering Science and Technology. 2012; 4(10): 4429–4439.

65. Ejaz M., Azad MM., Shah AUR., Afaq SK., Song J il. Mechanical and Biodegradable Properties of Jute/Flax Reinforced PLA Composites. Fibers and Polymers. 2020; 21(11): 2635–2641. Available at: DOI:10.1007/s12221-020-1370-y

66. Sawpan MA., Pickering KL., Fernyhough A. Improvement of mechanical performance of industrial hemp fibre reinforced polylactide biocomposites. Composites Part A: Applied Science and Manufacturing. 2011; 42(3): 310–319. Available at: DOI:https://doi.org/10.1016/j.compositesa.2010.12.004

67. Anuar H., Zuraida A., Kovacs JG., Tabi T. Improvement of mechanical properties of injection-molded polylactic acid-kenaf fiber biocomposite. Journal of Thermoplastic Composite Materials. 2012; 25(2): 153–164. Available at: DOI:10.1177/0892705711408984

68. Gauss C., Pickering KL., Graupner N., Müssig J. 3D-printed polylactide composites reinforced with short lyocell fibres – Enhanced mechanical properties based on bio-inspired fibre fibrillation and post-print annealing. Additive Manufacturing. 2023; 77: 103806. Available at: DOI:https://doi.org/10.1016/j.addma.2023.103806

69. Yuan R., Wu K., Fu Q. 3D printing of all-regenerated cellulose material with truly 3D

configuration: The critical role of cellulose microfiber. Carbohydrate Polymers. 2022; 294: 119784. Available at: DOI:https://doi.org/10.1016/j.carbpol.2022.119784

70. Gauss C., Pickering K., Barbier M., Miller T. Additive manufacturing of hygromorphic structures using regenerated cellulose/PLA biocomposites. Materials Today: Proceedings. 2023; Available at: DOI:https://doi.org/10.1016/j.matpr.2023.04.227

71. Gauss C., Pickering KL., Tshuma J., McDonald-Wharry J. Production and Assessment of Poly(Lactic Acid) Matrix Composites Reinforced with Regenerated Cellulose Fibres for Fused Deposition Modelling. Polymers. 2022; 14(19). Available at: DOI:10.3390/polym14193991

72. Ismail K., YAP TC., Ahmed R. 3D-Printed Fiber-Reinforced Polymer Composites by Fused Deposition Modelling (FDM): Fiber Length and Fiber Implementation Techniques. Polymers. 2022; 14: 4659. Available at: DOI:10.3390/polym14214659

73. Touchard F., Marchand D., Chocinski-Arnault L., Fournier T., Magro C. 3D printing of continuous cellulose fibre composites: microstructural and mechanical characterisation. Rapid Prototyping Journal. Emerald Publishing Limited; 1 January 2023; 29(9): 1879–1887. Available at: DOI:10.1108/RPJ-04-2023-0121

74. Adusumali RB., Reifferscheid M., Weber H., Roeder T., Sixta H., Gindl W. Mechanical properties of regenerated cellulose fibres for composites. Macromolecular Symposia. 2006; 244: 119–125. Available at: DOI:10.1002/masy.200651211

75. Adusumalli RB., Müller U., Weber H., Roeder T., Sixta H., Gindl W. Tensile testing of single regenerated cellulose fibres. Macromolecular Symposia. 2006; 244: 83–88. Available at: DOI:10.1002/masy.200651207

76. Gomes A., Matsuo T., Goda K., Ohgi J. Development and effect of alkali treatment on tensile properties of curaua fiber green composites. Composites Part A: Applied Science and Manufacturing. 2007; 38: 1811–1820. Available at: DOI:10.1016/j.compositesa.2007.04.010

77. Spinacé M a S., Lambert CS., Fermoselli KKG., De Paoli M a. Characterization of lignocellulosic curaua fibres. Carbohydrate Polymers. Elsevier Ltd; 2009; 77(1): 47–53. Available at: DOI:10.1016/j.carbpol.2008.12.005

78. Baley C., Bourmaud A., Davies P. Eighty years of composites reinforced by flax fibres: A historical review. Composites Part A: Applied Science and Manufacturing. 2021; 144: 106333. Available at: DOI:https://doi.org/10.1016/j.compositesa.2021.106333

79. Ramesh M. Flax (Linum usitatissimum L.) fibre reinforced polymer composite materials: A

review on preparation, properties and prospects. Progress in Materials Science. 2019; 102: 109–166. Available at: DOI:https://doi.org/10.1016/j.pmatsci.2018.12.004

80. Dhirhi N., Shukla R., Patel NB., Sahu H., Mehta N. Extraction method of flax fibre and its uses. 2015; 15: 711–716.

81. Baley C., Gomina M., Breard J., Bourmaud A., Drapier S., Ferreira M., et al. Specific features of flax fibres used to manufacture composite materials. International Journal of Material Forming. 2019; 12(6): 1023–1052. Available at: DOI:10.1007/s12289-018-1455-y

82. Yan L., Chouw N., Jayaraman K. Flax fibre and its composites – A review. Composites Part B: Engineering. 2014; 56: 296–317. Available at: DOI:https://doi.org/10.1016/j.compositesb.2013.08.014

83. Baley C., Gomina M., Breard J., Bourmaud A., Davies P. Variability of mechanical properties of flax fibres for composite reinforcement. A review. Industrial Crops and Products. 2020; 145: 111984. Available at: DOI:https://doi.org/10.1016/j.indcrop.2019.111984

84. Moon RJ., Martini A., Nairn J., Simonsen J., Youngblood J. Cellulose nanomaterials review: Structure, properties and nanocomposites. Chemical Society Reviews. 2011. 3941–3994 p. Available at: DOI:10.1039/c0cs00108b

85. O'SULLIVAN AC. Cellulose: the structure slowly unravels. Cellulose. 1997; 4(3): 173–207. Available at: DOI:10.1023/A:1018431705579

86. Heinze T. Cellulose: Structure and Properties. In: Rojas OJ (ed.) Cellulose Chemistry and Properties: Fibers, Nanocelluloses and Advanced Materials. Cham: Springer International Publishing; 2016. pp. 1–52. Available at: DOI:10.1007/12_2015_319

87. Rahman MZ. Mechanical and Damping Performances of Flax Fibre Composites – A Review. 2021; 4. Available at: DOI:10.1016/j.jcomc.2020.100081

88. Malik K., Ahmad F., Gunister E., Nakato T., Mouri E., Muhammad M., et al. A Review of Flax Fiber Reinforced Thermoset Polymer Composites: Structure and Mechanical Performance. Journal of Natural Fibers. 2021; 19: 1–25. Available at: DOI:10.1080/15440478.2021.1990182

89. Baley C. Analysis of the flax fibres tensile behaviour and analysis of the tensile stiffness increase. Composites Part A: Applied Science and Manufacturing. 2002; 33(7): 939–948. Available at: DOI:https://doi.org/10.1016/S1359-835X(02)00040-4

90. Andersons J., Spārniņš E., Joffe R., Wallström L. Strength distribution of elementary flax fibres. Composites Science and Technology. 2005; 65(3): 693–702. Available at:

DOI:https://doi.org/10.1016/j.compscitech.2004.10.001

91. Richely E., Bourmaud A., Placet V., Guessasma S., Beaugrand J. A critical review of the ultrastructure, mechanics and modelling of flax fibres and their defects. Progress in Materials Science. 2022; 124: 100851. Available at: DOI:https://doi.org/10.1016/j.pmatsci.2021.100851

92. Charlet K., Eve S., Jernot JP., Bréard J. Tensile deformation of a flax fiber. Procedia Engineering. 2009; 1: 233–236. Available at: DOI:10.1016/j.proeng.2009.06.055

93. Li H., Tang R., Dai J., Wang Z., Meng S., Zhang X., et al. Recent Progress in Flax Fiber-Based Functional Composites. Advanced Fiber Materials. 2022; 4(2): 171–184. Available at: DOI:10.1007/s42765-021-00115-6

94. Omrani F., Wang P., Soulat D., Ferreira M. Mechanical properties of flax-fibre-reinforced preforms and composites: Influence of the type of yarns on multi-scale characterisations. Composites Part A: Applied Science and Manufacturing. 2017; 93: 72–81. Available at: DOI:https://doi.org/10.1016/j.compositesa.2016.11.013

95. Baley C., Gomina M., Breard J., Bourmaud A., Drapier S., Ferreira M., et al. Specific features of flax fibres used to manufacture composite materials. International Journal of Material Forming. International Journal of Material Forming; 2019; 12(6): 1023–1052. Available at: DOI:10.1007/s12289-018-1455-y

96. Monti A., El Mahi A., Jendli Z., Guillaumat L. Mechanical behaviour and damage mechanisms analysis of a flax-fibre reinforced composite by acoustic emission. Composites Part A: Applied Science and Manufacturing. Elsevier Ltd; 2016; 90: 100–110. Available at: DOI:10.1016/j.compositesa.2016.07.002

97. Rajesh M., Pitchaimani J. Mechanical Properties of Natural Fiber Braided Yarn Woven Composite: Comparison with Conventional Yarn Woven Composite. Journal of Bionic Engineering. 2017; 14(1): 141–150. Available at: DOI:https://doi.org/10.1016/S1672-6529(16)60385-2

98. Bernaoui A., Lebrun G., Ruiz E. High performance natural fiber composites from mat and UD flax reinforcements backed with a mat Binder: A study of mat fiber surface fibrillation. Composites Part A: Applied Science and Manufacturing. 2022; 160: 107064. Available at: DOI:https://doi.org/10.1016/j.compositesa.2022.107064

99. Kanakannavar S., Pitchaimani J. Fabrication and mechanical properties of braided flax fabric polylactic acid bio-composites. The Journal of The Textile Institute. Taylor & Francis; 4 May 2022; 113(5): 833–845. Available at: DOI:10.1080/00405000.2021.1907958

100. Kuschmitz S., Schirp A., Busse J., Watschke H., Schirp C., Vietor T. Development and Processing of Continuous Flax and Carbon Fiber-Reinforced Thermoplastic Composites by a Modified Material Extrusion Process. Materials (Basel, Switzerland). Switzerland; April 2021; 14(9). Available at: DOI:10.3390/ma14092332

101. Huang G., Liu L. Research on properties of thermoplastic composites reinforced by flax fabrics. Materials & Design. 2008; 29(5): 1075–1079. Available at: DOI:https://doi.org/10.1016/j.matdes.2007.03.027

102. Woigk W., Fuentes CA., Rion J., Hegemann D., van Vuure AW., Kramer E., et al. Fabrication of flax fibre-reinforced cellulose propionate thermoplastic composites. Composites Science and Technology. 2019; 183: 107791. Available at: DOI:https://doi.org/10.1016/j.compscitech.2019.107791

103. Muthe LP., Pickering K., Gauss C. A Review of 3D/4D Printing of Poly-Lactic Acid Composites with Bio-Derived Reinforcements. Composites Part C: Open Access. 2022; 8: 100271. Available at: DOI:https://doi.org/10.1016/j.jcomc.2022.100271

104. Rabbi MS., Islam T., Islam GMS. Injection-molded natural fiber-reinforced polymer composites–a review. International Journal of Mechanical and Materials Engineering. 2021; 16(1): 15. Available at: DOI:10.1186/s40712-021-00139-1

105. Aly M., Hashmi M s. J., Olabi AG., Benyounis K., Messeiry M., Hussain AI., et al. Optimization of Alkaline Treatment Conditions of Flax Fiber Using Box–Behnken Method. Journal of Natural Fibers. 2013; 9. Available at: DOI:10.1080/15440478.2012.738036

106. Frącz W., Janowski G., Bąk Ł. Influence of the Alkali Treatment of Flax and Hemp Fibers on the Properties of PHBV Based Biocomposites. Polymers. Switzerland; June 2021; 13(12). Available at: DOI:10.3390/polym13121965

107. Narayana V., Rao L. A brief review on the effect of alkali treatment on mechanical properties of various natural fiber reinforced polymer composites. Materials Today: Proceedings. 2021; 44. Available at: DOI:10.1016/j.matpr.2020.12.117

108. Li X., Tabil LG., Panigrahi S. Chemical Treatments of Natural Fiber for Use in Natural Fiber-Reinforced Composites: A Review. Journal of Polymers and the Environment. 2007; 15(1): 25–33. Available at: DOI:10.1007/s10924-006-0042-3

109. Gupta US., Dhamarikar M., Dharkar A., Chaturvedi S., Kumrawat A., Giri N., et al. Plasma modification of natural fiber: A review. Materials Today: Proceedings. 2021; 43: 451–457. Available at: DOI:https://doi.org/10.1016/j.matpr.2020.11.973

110. Bozaci E., Sever K., Sarikanat M., Seki Y., Demir A., Ozdogan E., et al. Effects of the atmospheric plasma treatments on surface and mechanical properties of flax fiber and adhesion between fiber–matrix for composite materials. Composites Part B: Engineering. 2013; 45(1): 565–572. Available at: DOI:https://doi.org/10.1016/j.compositesb.2012.09.042

111. Xia X., Liu W., Zhou L., Hua Z., Liu H., He S. Modification of flax fiber surface and its compatibilization in polylactic acid/flax composites. Iranian Polymer Journal. 2016; 25(1): 25–35. Available at: DOI:10.1007/s13726-015-0395-3

112. Zubair NA., Moawia RM., Nasef MM., Hubbe M., Zakeri M. A Critical Review on Natural Fibers Modifications by Graft Copolymerization for Wastewater Treatment. Journal of Polymers and the Environment. 2022; 30(4): 1199–1227. Available at: DOI:10.1007/s10924-021-02269-1

113. Samanth M., Subrahmanya Bhat K. Conventional and unconventional chemical treatment methods of natural fibres for sustainable biocomposites. Sustainable Chemistry for Climate Action. 2023; 3: 100034. Available at: DOI:https://doi.org/10.1016/j.scca.2023.100034

114. Wang W., Fu R., Deng Q., Wang X., Wang Y., Zhang Z., et al. Surface Modification of Flax Fibers with Isocyanate and Its Effects on Fiber/Epoxy Interfacial Properties. Fibers and Polymers. 2020; 21(12): 2888–2895. Available at: DOI:10.1007/s12221-020-9722-1

115. De Prez J., Van Vuure AW., Ivens J., Aerts G., Van de Voorde I. Effect of enzymatic treatment of flax on fineness of fibers and mechanical performance of composites. Composites Part A: Applied Science and Manufacturing. 2019; 123: 190–199. Available at: DOI:https://doi.org/10.1016/j.compositesa.2019.05.007

116. Sharma HSS., Whiteside L., Kernaghan K. Enzymatic treatment of flax fibre at the roving stage for production of wet-spun yarn. Enzyme and Microbial Technology. 2005; 37(4): 386–394. Available at: DOI:https://doi.org/10.1016/j.enzmictec.2004.10.007

117. De Prez J., Van Vuure AW., Ivens J., Aerts G., Van de Voorde I. Flax treatment with strategic enzyme combinations: Effect on chemical fiber composition and ease of fiber extraction. Biotechnology Reports. 2019; 23: e00358. Available at: DOI:https://doi.org/10.1016/j.btre.2019.e00358

118. Biswas S. Chemistry of the Viscose Process. 2020. Available at: DOI:10.13140/RG.2.2.16243.35363

119. Sayyed AJ., Deshmukh NA., Pinjari D V. A critical review of manufacturing processes used in regenerated cellulosic fibres: viscose, cellulose acetate, cuprammonium, LiCl/DMAc, ionic

liquids, and NMMO based lyocell. Cellulose. 2019; 26(5): 2913–2940. Available at: DOI:10.1007/s10570-019-02318-y

120. Sharma A., Nagarkar S., Thakre S., Kumaraswamy G. Structure–property relations in regenerated cellulose fibers: comparison of fibers manufactured using viscose and lyocell processes. Cellulose. 2019; 26. Available at: DOI:10.1007/s10570-019-02352-w

121. Solhi L., Guccini V., Heise K., Solala I., Niinivaara E., Xu W., et al. Understanding Nanocellulose-Water Interactions: Turning a Detriment into an Asset. Chemical reviews. 1 February 2023; 123. Available at: DOI:10.1021/acs.chemrev.2c00611

122. Wohlert M., Benselfelt T., Wågberg L., Furó I., Berglund LA., Wohlert J. Cellulose and the role of hydrogen bonds: not in charge of everything. Cellulose. 2022; 29(1): 1–23. Available at: DOI:10.1007/s10570-021-04325-4

123. Djafari Petroudy SR. 3 - Physical and mechanical properties of natural fibers. In: Fan M, Fu F (eds.) Advanced High Strength Natural Fibre Composites in Construction. Woodhead Publishing; 2017. pp. 59–83. Available at: DOI:https://doi.org/10.1016/B978-0-08-100411-1.00003-0

124. Jiang G., Huang W., Li L., Wang X., Pang F., Zhang Y., et al. Structure and properties of regenerated cellulose fibers from different technology processes. Carbohydrate Polymers. 2012; 87(3): 2012–2018. Available at: DOI:https://doi.org/10.1016/j.carbpol.2011.10.022

125. Kroon-Batenburg LMJ., Kroon J. The crystal and molecular structures of cellulose I and II. Glycoconjugate Journal. 1997; 14(5): 677–690. Available at: DOI:10.1023/A:1018509231331

126. Sullivan ACO. Cellulose : the structure slowly unravels. 1997; : 173–207.

127. Revol B., Thomassey M., Ruch F., Nardin M. Influence of the sample number for the prediction of the tensile strength of high tenacity viscose fibres using a two parameters Weibull distribution. Cellulose. 1 August 2016; 23. Available at: DOI:10.1007/s10570-016-0974-2

128. Northolt MG., Baltussen JJM. The tensile and compressive deformation of polymer and carbon fibers. Journal of Applied Polymer Science. 2001; 83(3): 508–538. Available at: DOI:10.1002/app.2256

129. Gindl W., Reifferscheid M., Adusumalli R-B., Weber H., Röder T., Sixta H., et al. Anisotropy of the modulus of elasticity in regenerated cellulose fibres related to molecular orientation. Polymer. 2008; 49(3): 792–799. Available at: DOI:https://doi.org/10.1016/j.polymer.2007.12.016

130. Gindl W., Keckes J. Strain hardening in regenerated cellulose fibres. Composites Science and Technology. 2006; 66(13): 2049–2053. Available at: DOI:10.1016/j.compscitech.2005.12.019

131. Ganster J., Fink H-P., Pinnow M. High-tenacity man-made cellulose fibre reinforced thermoplastics – Injection moulding compounds with polypropylene and alternative matrices. Composites Part A: Applied Science and Manufacturing. 2006; 37(10): 1796–1804. Available at: DOI:https://doi.org/10.1016/j.compositesa.2005.09.005

132. Graupner N., Müssig J. Regenerated Cellulose Fibres: Properties, Pros and Cons for Composite Applications. 1st International Conference on Cellulose Fibres. 2020.

133. Wang S., Lu A., Zhang L. Recent advances in regenerated cellulose materials. Progress in Polymer Science. Elsevier Ltd; 2016; 53: 169–206. Available at: DOI:10.1016/j.progpolymsci.2015.07.003

134. Feldmann M., Verheyen F. Impact Behavior of Continuous Biaxial Reinforced Composites Based on Bio-Polyamides and Man-Made Cellulose Fibres. International Polymer Processing. 2016; 31: 198–206. Available at: https://api.semanticscholar.org/CorpusID:138217322

135. Bax B., Müssig J. Impact and tensile properties of PLA/Cordenka and PLA/flax composites. Composites Science and Technology. 2008; 68(7–8): 1601–1607. Available at: DOI:10.1016/j.compscitech.2008.01.004

136. Navaranjan N., Neitzert T. Impact Strength of Natural Fibre Composites Measured by Different Test Methods: A Review. MATEC Web of Conferences. 2017; 109: 1003. Available at: DOI:10.1051/matecconf/201710901003

137. Shanmugam V., Rajendran DJJ., Babu K., Rajendran S., Veerasimman A., Marimuthu U., et al. The mechanical testing and performance analysis of polymer-fibre composites prepared through the additive manufacturing. Polymer Testing. 2021; 93: 106925. Available at: DOI:https://doi.org/10.1016/j.polymertesting.2020.106925

138. Bugnicourt E., Cinelli P., Lazzeri A., Alvarez V. Polyhydroxyalkanoate (PHA): Review of synthesis, characteristics, processing and potential applications in packaging. Express Polymer Letters. 2014; 8(11): 791–808. Available at: DOI:10.3144/expresspolymlett.2014.82

139. S. Pratt, B. Laycock, L. P. Halley, P. Lant LV. PHA Bioplastics. Available at: https://d2cax41o7ahm5l.cloudfront.net/cs/speaker-ppts/steven-pratt-the-university-of-queensland-australia.pptx

140. Filgueira D., Holmen S., Melbø JK., Moldes D., Echtermeyer AT., Chinga-Carrasco G. 3D

printable filaments made of biobased polyethylene biocomposites. Polymers. 2018; 10(3). Available at: DOI:10.3390/polym10030314

141. Kucherov F., Gordeev E., Kashin A., Ananikov V. 3D printing with biobased PEF for carbon neutral manufacturing. Angewandte Chemie International Edition. 2017; 56. Available at: DOI:10.1002/anie.201708528

142. Park SJ., Lee JE., Lee HB., Park J., Lee NK., Son Y., et al. 3D printing of bio-based polycarbonate and its potential applications in ecofriendly indoor manufacturing. Additive Manufacturing. Elsevier; 2020; 31(October 2019): 100974. Available at: DOI:10.1016/j.addma.2019.100974

143. sculpteo. Ultrasint® PA11 3D printing material. 2017. Available at: https://www.sculpteo.com/en/materials/sls-material/pa11/ (Accessed: 25 January 2020)

144. Dubey SP., Thakur VK., Krishnaswamy S., Abhyankar HA., Marchante V., Brighton JL. Progress in environmental-friendly polymer nanocomposite material from PLA: Synthesis, processing and applications. Vacuum. Elsevier Ltd; 2017; 146: 655–663. Available at: DOI:10.1016/j.vacuum.2017.07.009

145. Farah S., Anderson DG., Langer R. Physical and mechanical properties of PLA, and their functions in widespread applications — A comprehensive review. Advanced Drug Delivery Reviews. 2016; 107: 367–392. Available at: DOI:https://doi.org/10.1016/j.addr.2016.06.012

146. Bezerra EB., de França DC., de Souza Morais DD., dos Santo Silva ID., Siqueira DD., Araújo EM., et al. Compatibility and characterization of Bio-PE/PCL blends. Polimeros. 2019; 29(2). Available at: DOI:10.1590/0104-1428.02518

147. Patrycja Bazan *, Dariusz Mierzwi ´nski RB and SK. Bio-Based Polyethylene Composites with Natural Fiber: Mechanical, Thermal, and Ageing Properties. Materials. 2020; 13(11). Available at: DOI:https://doi.org/10.3390/ma13112595

148. Wang G., Jiang M., Zhang Q., Wang R., Zhou G. Biobased copolyesters: synthesis, crystallization behavior, thermal and mechanical properties of poly(ethylene glycol sebacate-co-ethylene glycol 2,5-furan dicarboxylate). RSC Advances. Royal Society of Chemistry; 2017; 7(23): 13798–13807. Available at: DOI:10.1039/c6ra27795k

149. Hauenstein O., Agarwal S., Greiner A. Bio-based polycarbonate as synthetic toolbox. Nature Communications. Nature Publishing Group; 2016; 7(May): 1–7. Available at: DOI:10.1038/ncomms11862

150. Choi YH., Lyu MY. Comparison of Rheological Characteristics and Mechanical Properties of Fossil-Based and Bio-Based Polycarbonate. Macromolecular Research. 2020; 28(4): 299–309. Available at: DOI:10.1007/s13233-020-8093-1

151. Pappu A., Pickering KL., Thakur VK. Manufacturing and characterization of sustainable hybrid composites using sisal and hemp fibres as reinforcement of poly (lactic acid) via injection moulding. Industrial Crops and Products. Elsevier; 2019; 137(May): 260–269. Available at: DOI:10.1016/j.indcrop.2019.05.040

152. Garlotta D. A Literature Review of Poly(Lactic Acid). Journal of Polymers and the Environment. Vol. 9(No. 2). Available at: DOI:10.1023/A:1020200822435

153. Kimura*a KM and Y. PLA Synthesis. From the Monomer to the Polymer. oly(lactic acid) Science and Technology: Processing, Properties, Additives and Applications. 2014. pp. 1–36. Available at: DOI:10.1039/9781782624806-00001

154. Murariu M., Dubois P. PLA composites: From production to properties. Advanced Drug Delivery Reviews. Elsevier B.V.; 2016; 107: 17–46. Available at: DOI:10.1016/j.addr.2016.04.003

155. Hartmann MH. High Molecular Weight Polylactic Acid Polymers. In: Kaplan DL (ed.) Biopolymers from Renewable Resources. Berlin, Heidelberg: Springer Berlin Heidelberg; 1998. pp. 367–411. Available at: DOI:10.1007/978-3-662-03680-8_15

156. Madhavan Nampoothiri K., Nair NR., John RP. An overview of the recent developments in polylactide (PLA) research. Bioresource Technology. Elsevier Ltd; 2010; 101(22): 8493–8501. Available at: DOI:10.1016/j.biortech.2010.05.092

157. Ali W., Ali H., Gillani S., Zinck P., Souissi S. Polylactic acid synthesis, biodegradability, conversion to microplastics and toxicity: a review. Environmental Chemistry Letters. Springer International Publishing; 2023; 21(3): 1761–1786. Available at: DOI:10.1007/s10311-023-01564-8

158. Shekhar N., Mondal A. Synthesis, properties, environmental degradation, processing, and applications of Polylactic Acid (PLA): an overview. Polymer Bulletin. 2024; Available at: DOI:10.1007/s00289-024-05252-7

159. Kliem S., Kreutzbruck M., Bonten C. Review on the Biological Degradation of Polymers in Various Environments. Materials. 2020; 13(20). Available at: DOI:10.3390/ma13204586

160. Wayman C., Niemann H. The fate of plastic in the ocean environment-a minireview.

Environmental Science: Processes and Impacts. Royal Society of Chemistry; 2021; 23(2): 198–212. Available at: DOI:10.1039/d0em00446d

161. AVPlastics. 3D Printing History [Online]. AZTEC Mouldings. Available at: http://www.avplastics.co.uk/3d-printing-history (Accessed: 12 August 2020)

162. Ning F., Cong W., Wei J., Wang S., Zhang M. Additive Manufacturing of CFRP Composites Using Fused Deposition Modeling: Effects of Carbon Fiber Content and Length. 2015; (March). Available at: DOI:10.1115/msec2015-9436

163. Liu Z., Wang Y., Wu B., Cui C., Guo Y., Yan C. A critical review of fused deposition modeling 3D printing technology in manufacturing polylactic acid parts. International Journal of Advanced Manufacturing Technology. The International Journal of Advanced Manufacturing Technology; 2019; 102(9–12): 2877–2889. Available at: DOI:10.1007/s00170-019-03332-x

164. Popescu D., Zapciu A., Amza C., Baciu F., Marinescu R. FDM process parameters influence over the mechanical properties of polymer specimens: A review. Polymer Testing. 2018; 69(April): 157–166. Available at: DOI:10.1016/j.polymertesting.2018.05.020

165. Akhoundi B., Behravesh AH. Effect of Filling Pattern on the Tensile and Flexural Mechanical Properties of FDM 3D Printed Products. Experimental Mechanics. 2019; 59(6): 883–897. Available at: DOI:10.1007/s11340-018-00467-y

166. Samykano M., Selvamani SK., Kadirgama K., Ngui WK., Kanagaraj G., Sudhakar K. Mechanical property of FDM printed ABS: influence of printing parameters. International Journal of Advanced Manufacturing Technology. The International Journal of Advanced Manufacturing Technology; 2019; 102(9–12): 2779–2796. Available at: DOI:10.1007/s00170-019-03313-0

167. Mazzanti V., Malagutti L., Mollica F. FDM 3D printing of polymers containing natural fillers: A review of their mechanical properties. Polymers. 2019; 11(7). Available at: DOI:10.3390/polym11071094

168. Luo C. Modeling the temperature profile of an extrudate in material extrusion additive manufacturing. Materials Letters. Elsevier B.V.; 2020; 270: 127742. Available at: DOI:10.1016/j.matlet.2020.127742

169. Solomon IJ., Sevvel P., Gunasekaran J. A review on the various processing parameters in FDM. Materials Today: Proceedings. Elsevier Ltd.; 2020; 37(Part 2): 509–514. Available at: DOI:10.1016/j.matpr.2020.05.484

170. Domingo-Espin M., Puigoriol-Forcada JM., Garcia-Granada A-A., Llumà J., Borros S., Reyes G. Mechanical property characterization and simulation of fused deposition modeling Polycarbonate parts. Materials & Design. 2015; 83: 670–677. Available at: DOI:https://doi.org/10.1016/j.matdes.2015.06.074

171. Smith WC., Dean RW. Structural characteristics of fused deposition modeling polycarbonate material. Polymer Testing. 2013; 32(8): 1306–1312. Available at: DOI:https://doi.org/10.1016/j.polymertesting.2013.07.014

172. Jin Y., Wan Y., Zhang B., Liu Z. Modeling of the chemical finishing process for polylactic acid parts in fused deposition modeling and investigation of its tensile properties. Journal of Materials Processing Technology. 2017; 240: 233–239. Available at: DOI:https://doi.org/10.1016/j.jmatprotec.2016.10.003

173. Wu W., Ye W., Wu Z., Geng P., Wang Y., Zhao J. Influence of layer thickness, raster angle, deformation temperature and recovery temperature on the shape-memory effect of 3D-printed polylactic acid samples. Materials. 2017; 10(8). Available at: DOI:10.3390/ma10080970

174. Wu W., Geng P., Li G., Zhao D., Zhang H., Zhao J. Influence of layer thickness and raster angle on the mechanical properties of 3D-printed PEEK and a comparative mechanical study between PEEK and ABS. Materials. 2015; 8(9): 5834–5846. Available at: DOI:10.3390/ma8095271

175. Dizon JRC., Espera AH., Chen Q., Advincula RC. Mechanical characterization of 3D-printed polymers. Additive Manufacturing. 2018; 20: 44–67. Available at: DOI:https://doi.org/10.1016/j.addma.2017.12.002

176. Maurya NK., Rastogi V., Singh P. An overview of mechanical properties and form error for rapid prototyping. CIRP Journal of Manufacturing Science and Technology. 2020; 29: 53–70. Available at: DOI:https://doi.org/10.1016/j.cirpj.2020.02.003

177. Dudescu C., Racz L. Effects of Raster Orientation, Infill Rate and Infill Pattern on the Mechanical Properties of 3D Printed Materials. ACTA Universitatis Cibiniensis. 2018; 69(1): 23–30. Available at: DOI:10.1515/aucts-2017-0004

178. Ouhsti M., El Haddadi B., Belhouideg S. Effect of printing parameters on the mechanical properties of parts fabricated with open-source 3D printers in PLA by fused deposition modeling. Mechanics and Mechanical Engineering. 2018; 22(4): 895–907. Available at: DOI:10.2478/mme-2018-0070

179. Mohan N., Senthil P., Vinodh S., Jayanth N. A review on composite materials and process parameters optimisation for the fused deposition modelling process. Virtual and Physical

Prototyping. Taylor & Francis; 2017; 12(1): 47–59. Available at: DOI:10.1080/17452759.2016.1274490

180. Yang T-C., Yeh C-H. Morphology and Mechanical Properties of 3D Printed Wood Fiber/Polylactic Acid Composite Parts Using Fused Deposition Modeling (FDM): The Effects of Printing. Polymers. 2020; Available at: DOI:10.3390/polym12061334

181. Geng P., Zhao J., Wu W., Ye W., Wang Y., Wang S., et al. Effects of extrusion speed and printing speed on the 3D printing stability of extruded PEEK filament. Journal of Manufacturing Processes. 2019; 37: 266–273. Available at: DOI:https://doi.org/10.1016/j.jmapro.2018.11.023

182. Miazio Ł. Impact of Print Speed on Strength of Samples Printed in FDM Technology. Agricultural Engineering. 2019; 23(2): 33–38. Available at: DOI:10.1515/agriceng-2019-0014

183. David Stoof, Kim Pickering YZ. Fused Deposition Modelling of Natural Fibre/Polylactic Acid Composites. Journal of Composites Science. 2017; 1(2): 8. Available at: DOI:10.3390/jcs1010008

184. Wang Q., Ji C., Sun L., Sun J., Liu J. Cellulose nanofibrils filled poly(lactic acid) biocomposite filament for FDM 3D printing. Molecules. 2020; 25(10). Available at: DOI:10.3390/molecules25102319

185. Gonzalo M., Gauss C., Fangueiro R. Potential of Cellulose Microfibers for PHA and PLA Biopolymers Reinforcement. Molecules. 2020; 25(20): 4653. Available at: DOI:10.3390/molecules25204653

186. Mariotti C., Alimenti F., Roselli L., Tentzeris MM. High-Performance RF Devices and Components on Flexible Cellulose Substrate by Vertically Integrated Additive Manufacturing Technologies. IEEE Transactions on Microwave Theory and Techniques. IEEE; 2017; 65(1): 62–71. Available at: DOI:10.1109/TMTT.2016.2615934

187. Tanase-Opedal M., Espinosa E., Rodríguez A., Chinga-Carrasco G. Lignin: A biopolymer from forestry biomass for biocomposites and 3D printing. Materials. 2019; 12(18): 1–15. Available at: DOI:10.3390/ma12183006

188. Depuydt D., Balthazar M., Hendrickx K., Six W., Ferraris E., Desplentere F., et al. Production and characterization of bamboo and flax fiber reinforced polylactic acid filaments for fused deposition modeling (FDM). Polymer Composites. 2019; 40(5): 1951–1963. Available at: DOI:10.1002/pc.24971

189. Liu H., He H., Peng X., Huang B., Li J. Three-dimensional printing of poly(lactic acid) bio-

based composites with sugarcane bagasse fiber: Effect of printing orientation on tensile performance. Polymers for Advanced Technologies. 2019; 30. Available at: DOI:10.1002/pat.4524

190. Rubio-López A., Olmedo A., Díaz-Álvarez A., Santiuste C. Manufacture of compression moulded PLA based biocomposites: A parametric study. Composite Structures. 2015; 131: 995–1000. Available at: DOI:https://doi.org/10.1016/j.compstruct.2015.06.066

191. Akindoyo JO., Pickering K., Beg MD., Mucalo M. Combined digestion and bleaching of New Zealand flax /harakeke fibre and its effects on the mechanical, thermal, and dynamic mechanical properties of poly(lactic) acid matrix composites. Composites Part A: Applied Science and Manufacturing. 2023; 164: 107326. Available at: DOI:https://doi.org/10.1016/j.compositesa.2022.107326

192. Graupner N., Ziegmann G., Wilde F., Beckmann F., Müssig J. Procedural influences on compression and injection moulded cellulose fibre-reinforced polylactide (PLA) composites: Influence of fibre loading, fibre length, fibre orientation and voids. Composites Part A: Applied Science and Manufacturing. 2016; 81: 158–171. Available at: DOI:https://doi.org/10.1016/j.compositesa.2015.10.040

193. Baghaei B., Skrifvars M., Rissanen M., Ramamoorthy SK. Mechanical and thermal characterization of compression moulded polylactic acid natural fiber composites reinforced with hemp and lyocell fibers. Journal of applied polymer science. Baghaei, B. Hoboken, NJ: Blackwell Publishing Ltd; 2014; 131(15): np-n/a.

194. Ahmad Adlie Shamsuri *. Important Criteria for Preparation of 3D Printer Filaments from Polymer Biocomposites. SVOA Materials Science & Technology. 2019; 1(1): 1–3. Available at: https://sciencevolks.com/materials-science/pdf/SVOA-MST-MR-01.pdf

195. Tarrés Q., Melbø JK., Delgado-Aguilar M., Espinach FX., Mutjé P., Chinga-Carrasco G. Bio-polyethylene reinforced with thermomechanical pulp fibers: Mechanical and micromechanical characterization and its application in 3D-printing by fused deposition modelling. Composites Part B: Engineering. Elsevier; 2018; 153(April): 70–77. Available at: DOI:10.1016/j.compositesb.2018.07.009

196. M. Milosevic DS and KLP. Characterizing the Mechanical Properties of Fused Deposition Modelling Natural Fiber Recycled Polypropylene Composites. Journal of Composites Science. 2017; 1(1): 7. Available at: DOI:10.3390/jcs1010007

197. Yao Y., Li M., Lackner M., Herfried L. A continuous fiber-reinforced additive manufacturing

processing based on PET fiber and PLA. Materials. 2020; 13(14). Available at: DOI:10.3390/ma13143044

198. Zhang H., Liu D., Huang T., Hu Q., Lammer H. Three-dimensional printing of continuous flax fiber-reinforced thermoplastic composites by five-axis machine. Materials. 2020; 13(7). Available at: DOI:10.3390/ma13071678

199. Hu Q., Duan Y., Zhang H., Liu D., Yan B., Peng F. Manufacturing and 3D printing of continuous carbon fiber prepreg filament. Journal of Materials Science. Springer US; 2018; 53(3): 1887–1898. Available at: DOI:10.1007/s10853-017-1624-2

200. Brooks H. Title : 3D printing of continuous Kevlar fibre reinforced composites. 2019. Available at: https://www.researchgate.net/publication/336216483

201. Yang C., Tian X., Liu T., Cao Y., Li D. 3D printing for continuous fiber reinforced thermoplastic composites: Mechanism and performance. Rapid Prototyping Journal. 2017; 23(1): 209–215. Available at: DOI:10.1108/RPJ-08-2015-0098

202. Li N., Li Y., Liu S. Rapid prototyping of continuous carbon fiber reinforced polylactic acid composites by 3D printing. Journal of Materials Processing Technology. Elsevier B.V.; 2016; 238: 218–225. Available at: DOI:10.1016/j.jmatprotec.2016.07.025

203. Mei H., Ali Z., Yan Y., Ali I., Cheng L. Influence of mixed isotropic fiber angles and hot press on the mechanical properties of 3D printed composites. Additive Manufacturing. 2019; 27(February): 150–158. Available at: DOI:10.1016/j.addma.2019.03.008

204. Mark Two The powerful professional Continuous Carbon Fiber 3D printer for aluminum-strength parts. Available at: https://markforged.com/3d-printers/mark-two?mfa=ga-search&adg=40301838887&kw=markforged&device=c&gclid=EAIaIQobChMInLeUioSI4QIVzrftCh0GaglPEAAYASAAEgKxnfD_BwE (Accessed: 15 October 2020)

205. Suteja J., Firmanto H., Soesanti A., Christian C. Properties investigation of 3D printed continuous pineapple leaf fiber-reinforced PLA composite. Journal of Thermoplastic Composite Materials. 2020; Available at: DOI:10.1177/0892705720945371

206. Le Duigou A., Barbé A., Guillou E., Castro M. 3D printing of continuous flax fibre reinforced biocomposites for structural applications. Materials and Design. The Authors; 2019; 180: 107884. Available at: DOI:10.1016/j.matdes.2019.107884

207. Montalvo JIN., Hidalgo MA. 3D printing with natural fiber reinforced filament. Proceedings - 26th Annual International Solid Freeform Fabrication Symposium - An Additive Manufacturing

Conference, SFF 2015. 2020; : 922–934.

208. Reverte JM., Caminero M ángel., Chacón JM., García-Plaza E., Núñez PJ., Becar JP. Mechanical and geometric performance of PLA-based polymer composites processed by the fused filament fabrication additive manufacturing technique. Materials. 2020; 13(8). Available at: DOI:10.3390/MA13081924

209. Li X., Ni Z., Bai S., Lou B. Preparation and Mechanical Properties of Fiber Reinforced PLA for 3D Printing Materials. IOP Conference Series: Materials Science and Engineering. 2018; 322(2). Available at: DOI:10.1088/1757-899X/322/2/022012

210. Liu Z., Lei Q., Xing S. Mechanical characteristics of wood, ceramic, metal and carbon fiber-based PLA composites fabricated by FDM. Journal of Materials Research and Technology. The Authors; 2019; 8(5): 3743–3753. Available at: DOI:10.1016/j.jmrt.2019.06.034

211. Heidari-Rarani M., Rafiee-Afarani M., Zahedi AM. Mechanical characterization of FDM 3D printing of continuous carbon fiber reinforced PLA composites. Composites Part B: Engineering. Elsevier Ltd; 2019; 175(July): 107147. Available at: DOI:10.1016/j.compositesb.2019.107147

212. Tian X., Liu T., Yang C., Wang Q., Li D. Interface and performance of 3D printed continuous carbon fiber reinforced PLA composites. Composites Part A: Applied Science and Manufacturing. Elsevier Ltd; 2016; 88: 198–205. Available at: DOI:10.1016/j.compositesa.2016.05.032

213. Tian X., Liu T., Wang Q., Dilmurat A., Li D., Ziegmann G. Recycling and remanufacturing of 3D printed continuous carbon fiber reinforced PLA composites. Journal of Cleaner Production. Elsevier Ltd; 2017; 142: 1609–1618. Available at: DOI:10.1016/j.jclepro.2016.11.139

214. Sang L., Han S., Li Z., Yang X., Hou W. Development of short basalt fiber reinforced polylactide composites and their feasible evaluation for 3D printing applications. Composites Part B: Engineering. Elsevier; 2019; 164(October 2018): 629–639. Available at: DOI:10.1016/j.compositesb.2019.01.085

215. Le Duigou A., Barbé A., Guillou E., Castro M. 3D printing of continuous flax fibre reinforced biocomposites for structural applications. Materials & Design. 2019; 180: 107884. Available at: DOI:https://doi.org/10.1016/j.matdes.2019.107884

216. Long Y., Zhang Z., Fu K., Li Y. Efficient plant fibre yarn pre-treatment for 3D printed continuous flax fibre/poly(lactic) acid composites. Composites Part B: Engineering. Elsevier Ltd; 2021; 227(September): 109389. Available at: DOI:10.1016/j.compositesb.2021.109389

217. Long Y., Zhang Z., Fu K., Yang Z., Li Y. Design and fabrication of high-performance 3D printed continuous flax fibre/PLA composites. Journal of Manufacturing Processes. 2023; 99: 351–361. Available at: DOI:https://doi.org/10.1016/j.jmapro.2023.05.044

218. Yang Z., Zhang Z., Long Y., Fu K., Li Y. Process optimization of continuous flax fiber/polylactic acid prepreg filaments toward high performance 3D-printed composites. Polymer Composites. 2023; 44(9): 6242–6253. Available at: DOI:10.1002/pc.27559

219. Jose AS., Athijayamani A., Jani SP. A review on the mechanical properties of bio waste particulate reinforced polymer composites. Materials Today: Proceedings. Elsevier Ltd.; 2020; 37(Part 2): 1757–1760. Available at: DOI:10.1016/j.matpr.2020.07.360

220. Senvol Database. Available at: http://senvol.com/5_material-results/?appSession=710Z80HT59I6G23F8K98R7CBSGVIF0223ZGWFAJ11EA79088K725Q48FO011Q6J4U3I62D516D373WUJI72DQETUM63U89HF230GOB20CIL71JL01XA21HTRLU9IMK31&PageID=2&PrevPageID=2&cpipage=2&CPISortType=&CPIorderBy=&cbCurrentPageSize=25 (Accessed: 31 August 2020)

221. Senvol LLC. Senvol 3D Printing Materials Database. Available at: http://senvol.com/material-search/ (Accessed: 15 July 2020)

222. Kariz M., Sernek M., Kuzman MK. Effect of humidity on 3D-printed specimens from wood-pla filaments. Wood Research. 2018; 63(5): 917–922.

223. Guessasma S., Belhabib S., Nouri H. Microstructure and mechanical performance of 3D printed wood-PLA/PHA using fused deposition modelling: Effect of printing temperature. Polymers. 2019; 11(11). Available at: DOI:10.3390/polym11111778

224. Wang Q., Sun J., Yao Q., Ji C., Liu J., Zhu Q. 3D printing with cellulose materials. Cellulose. Springer Netherlands; 2018; 25(8): 4275–4301. Available at: DOI:10.1007/s10570-018-1888-y

225. Yang TC. Effect of extrusion temperature on the physico-mechanical properties of unidirectional wood fiber-reinforced polylactic acid composite (WFRPC) components using fused depositionmodeling. Polymers. 2018; 10(9). Available at: DOI:10.3390/polym10090976

226. Kuzman MK., Ayrilmis N., Sernek M., Kariz M. Effect of selected printing settings on viscoelastic behaviour of 3D printed polymers with and without wood. Materials Research Express. IOP Publishing; 2019; 6(10). Available at: DOI:10.1088/2053-1591/ab411c

227. Ayrilmis N. Effect of layer thickness on surface properties of 3D printed materials produced from wood flour/PLA filament. Polymer Testing. 2018; 71(July): 163–166. Available at:

DOI:10.1016/j.polymertesting.2018.09.009

228. Ecker JV., Haider A., Burzic I., Huber A., Eder G., Hild S. Mechanical properties and water absorption behaviour of PLA and PLA/wood composites prepared by 3D printing and injection moulding. Rapid Prototyping Journal. 2019; 25(4): 672–678. Available at: DOI:10.1108/RPJ-06-2018-0149

229. Ayrilmis N., Kariz M., Kwon JH., Kitek Kuzman M. Effect of printing layer thickness on water absorption and mechanical properties of 3D-printed wood/PLA composite materials. International Journal of Advanced Manufacturing Technology. 2019; 102(5–8): 2195–2200. Available at: DOI:10.1007/s00170-019-03299-9

230. Bhagia S., Lowden RR., Erdman D., Rodriguez M., Haga BA., Solano IRM., et al. Tensile properties of 3D-printed wood-filled PLA materials using poplar trees. Applied Materials Today. Elsevier Ltd; 2020; 21: 100832. Available at: DOI:10.1016/j.apmt.2020.100832

231. Bhagia S., Bornani K., Agarwal R., Satlewal A., Ďurkovič J., Lagaňa R., et al. Critical review of FDM 3D printing of PLA biocomposites filled with biomass resources, characterization, biodegradability, upcycling and opportunities for biorefineries. Applied Materials Today. 2021; 24: 101078. Available at: DOI:10.1016/j.apmt.2021.101078

232. Kariz M., Sernek M., Obućina M., Kuzman MK. Effect of wood content in FDM filament on properties of 3D printed parts. Materials Today Communications. 2018; 14(December 2017): 135–140. Available at: DOI:10.1016/j.mtcomm.2017.12.016

233. Coppola B., Garofalo E., Di Maio L., Scarfato P., Incarnato L. Investigation on the use of PLA/hemp composites for the fused deposition modelling (FDM) 3D printing. AIP Conference Proceedings. 2018; 1981(July 2018): 1–5. Available at: DOI:10.1063/1.5045948

234. Wang C., Smith LM., Zhang W., Li M., Wang G., Shi SQ., et al. Reinforcement of polylactic acid for fused deposition modeling process with nano particles treated bamboo powder. Polymers. 2019; 11(7). Available at: DOI:10.3390/polym11071146

235. Cisneros-López EO., Pal AK., Rodriguez AU., Wu F., Misra M., Mielewski DF., et al. Recycled poly(lactic acid)–based 3D printed sustainable biocomposites: a comparative study with injection molding. Materials Today Sustainability. 2020; 7–8: 1–12. Available at: DOI:10.1016/j.mtsust.2019.100027

236. Vigneshwaran K., Venkateshwaran N. Statistical analysis of mechanical properties of wood-PLA composites prepared via additive manufacturing. International Journal of Polymer Analysis and Characterization. Taylor & Francis; 2019; 24(7): 584–596. Available at:

DOI:10.1080/1023666X.2019.1630940

237. Koo JM., Kang J., Shin SH., Jegal J., Cha HG., Choy S., et al. Biobased thermoplastic elastomer with seamless 3D-Printability and superior mechanical properties empowered by in-situ polymerization in the presence of nanocellulose. Composites Science and Technology. Elsevier Ltd; 2020; 185(October 2019): 107885. Available at: DOI:10.1016/j.compscitech.2019.107885

238. Phanthong P., Reubroycharoen P., Hao X., Xu G., Abudula A., Guan G. Nanocellulose: Extraction and application. Carbon Resources Conversion. KeAi Communications Co., Ltd; 2018; 1(1): 32–43. Available at: DOI:10.1016/j.crcon.2018.05.004

239. Moon RJ., Martini A., Nairn J., Simonsen J., Youngblood J. Cellulose nanomaterials review: structure{,} properties and nanocomposites. Chem. Soc. Rev. The Royal Society of Chemistry; 2011; 40(7): 3941–3994. Available at: DOI:10.1039/C0CS00108B

240. Dong J., Li M., Zhou L., Lee S., Mei C., Xu X., et al. The influence of grafted cellulose nanofibers and postextrusion annealing treatment on selected properties of poly(lactic acid) filaments for 3D printing. Journal of Polymer Science, Part B: Polymer Physics. 2017; 55(11): 847–855. Available at: DOI:10.1002/polb.24333

241. Rigotti D., Dorigato A., Cataldi A., Fambri L., Pegoretti A. Nanocellulose as reinforcing agent for biodegradable polymers in 3D printing fused deposition modeling. ECCM 2018 - 18th European Conference on Composite Materials. 2020; (June): 24–28.

242. Frone AN., Batalu D., Chiulan I., Oprea M., Gabor AR., Nicolae CA., et al. Morpho-structural, thermal and mechanical properties of PLA/PHB/Cellulose biodegradable nanocomposites obtained by compression molding, extrusion, and 3d printing. Nanomaterials. 2020; 10(1). Available at: DOI:10.3390/nano10010051

243. Li L., Chen Y., Yu T., Wang N., Wang C., Wang H. Preparation of polylactic acid/TEMPO-oxidized bacterial cellulose nanocomposites for 3D printing via Pickering emulsion approach. Composites Communications. Elsevier Ltd; 2019; 16(September): 162–167. Available at: DOI:10.1016/j.coco.2019.10.004

244. Tekinalp HL., Meng X., Lu Y., Kunc V., Love LJ., Peter WH., et al. High modulus biocomposites via additive manufacturing: Cellulose nanofibril networks as “microsponges”. Composites Part B: Engineering. Elsevier Ltd; 2019; 173(May 2018): 106817. Available at: DOI:10.1016/j.compositesb.2019.05.028

245. Ambone T., Torris A., Shanmuganathan K. Enhancing the mechanical properties of 3D printed polylactic acid using nanocellulose. Polymer Engineering and Science. 2020; (February): 1842–

1855. Available at: DOI:10.1002/pen.25421

246. Gauss C., Pickering KL. A new method for producing polylactic acid biocomposites for 3D printing with improved tensile and thermo-mechanical performance using grafted nanofibrillated cellulose. Additive Manufacturing. 2023; 61: 103346. Available at: DOI:https://doi.org/10.1016/j.addma.2022.103346

247. Mohan D., Teong ZK., Bakir AN., Sajab MS., Kaco H. Extending cellulose-based polymers application in additive manufacturing technology: A review of recent approaches. Polymers. 2020; 12(9). Available at: DOI:10.3390/POLYM12091876

248. Ghasemlou M., Daver F., Ivanova EP., Habibi Y., Adhikari B. Surface modifications of nanocellulose: From synthesis to high-performance nanocomposites. Progress in Polymer Science. Elsevier B.V.; 2021; 119: 101418. Available at: DOI:10.1016/j.progpolymsci.2021.101418

249. Lamm ME., Wang L., Kishore V., Tekinalp H., Kunc V., Wang J., et al. Material Extrusion Additive Manufacturing of Wood and Lignocellulosic Filled Composites.

250. Tang Z., Zhang C., Liu X. The crystallization behavior and mechanical properties of polylactic acid in the presence of a crystal nucleating agent. Journal of Applied Polymer Science. 2012; 125. Available at: DOI:10.1002/app.34799

251. Dai J., Yang Q., Liu B. Crystallization Behavior of PLA/PEG/Nucleating Agent Blends. Advanced Materials Research. 2013; 807–809: 578–581. Available at: DOI:10.4028/www.scientific.net/AMR.807-809.578

252. Aliotta L., Cinelli P., Coltelli M., Righetti MC., Gazzano M., Lazzeri A. Effect of nucleating agents on crystallinity and properties of Poly (lactic acid) (PLA). European Polymer Journal. 2017; Available at: DOI:10.1016/j.eurpolymj.2017.04.041

253. Levenhagen NP., Dadmun MD. Bimodal molecular weight samples improve the isotropy of 3D printed polymeric samples. Polymer. Elsevier Ltd; 2017; 122: 232–241. Available at: DOI:10.1016/j.polymer.2017.06.057

254. Shaffer S., Yang K., Vargas J., Di Prima MA., Voit W. On reducing anisotropy in 3D printed polymers via ionizing radiation. Polymer. Elsevier Ltd; 2014; 55(23): 5969–5979. Available at: DOI:10.1016/j.polymer.2014.07.054

255. Lee CH., Khalina A., Lee SH. Importance of interfacial adhesion condition on characterization of plant-fiber-reinforced polymer composites: A review. Polymers. 2021; 13(3): 1–22. Available

at: DOI:10.3390/polym13030438

256. Petinakis E., Yu L., Edward G., Dean K., Liu H., Scully AD. Effect of matrix-particle interfacial adhesion on the mechanical properties of poly(lactic acid)/wood-flour micro-composites. Journal of Polymers and the Environment. 2009; 17(2): 83–94. Available at: DOI:10.1007/s10924-009-0124-0

257. Hao M., Wu H., Qiu F., Wang X. Interface bond improvement of sisal fibre reinforced polylactide composites with added epoxy oligomer. Materials. 2018; 11(3). Available at: DOI:10.3390/ma11030398

258. Fuentes Rojas CA. Interfacial Adhesion in Natural and Synthetic Fibre Composites: a Physical-Chemical-Mechanical Approach. 2014. 1–168 p. Available at: DOI:10.13140/RG.2.2.36823.52647

259. Olonisakin K., fan M., Xin-Xiang Z., Ran L., Lin WS., Zhang W., et al. Key Improvements in Interfacial Adhesion and Dispersion of Fibers/Fillers in Polymer Matrix Composites; Focus on PLA Matrix Composites. Composite Interfaces. Taylor & Francis; 2021; 00(00): 1–50. Available at: DOI:10.1080/09276440.2021.1878441

260. Singhvi MS., Zinjarde SS., Gokhale D V. Polylactic acid: synthesis and biomedical applications. Journal of Applied Microbiology. 2019; 127(6): 1612–1626. Available at: DOI:10.1111/jam.14290

261. Bayart M., Adjallé K., Diop A., Ovlaque P., Barnabé S., Robert M., et al. PLA/flax fiber bio-composites: effect of polyphenol-based surface treatment on interfacial adhesion and durability. Composite Interfaces. Taylor & Francis; 2020; 28(3): 1–22. Available at: DOI:10.1080/09276440.2020.1773179

262. Siakeng R., Jawaid M., Asim M., Saba N., Sanjay MR., Siengchin S., et al. Alkali treated coir/pineapple leaf fibres reinforced pla hybrid composites: Evaluation of mechanical, morphological, thermal and physical properties. Express Polymer Letters. 2020; 14(8): 717–730. Available at: DOI:10.3144/expresspolymlett.2020.59

263. Yang Z., Feng X., Xu M., Rodrigue D. Properties of poplar fiber/PLA composites: Comparison on the effect of maleic anhydride and KH550 modification of poplar fiber. Polymers. 2020; 12(3): 1–13. Available at: DOI:10.3390/polym12030729

264. Ramesh P., Prasad BD., Narayana KL. Influence of Montmorillonite Clay Content on Thermal, Mechanical, Water Absorption and Biodegradability Properties of Treated Kenaf Fiber/ PLA-Hybrid Biocomposites. Silicon. Silicon; 2021; 13(1): 109–118. Available at:

DOI:10.1007/s12633-020-00401-9

265. Khieomuang J., Thongpin C. Fabrication of non-woven hybrid natural fiber/poly(lactic acid) composite via prepreg lamination. IOP Conference Series: Materials Science and Engineering. 2020; 965(1). Available at: DOI:10.1088/1757-899X/965/1/012017

266. Li FJ., Yu XT., Huang Z., Liu DF. Interfacial improvements in cellulose nanofibers reinforced polylactide bionanocomposites prepared by in situ reactive extrusion. Polymers for Advanced Technologies. 2021; 32(6): 2352–2366. Available at: DOI:10.1002/pat.5264

267. Yin Y., Lucia LA., Pal L., Jiang X., Hubbe MA. Lipase-catalyzed laurate esterification of cellulose nanocrystals and their use as reinforcement in PLA composites. Cellulose. Springer Netherlands; 2020; 27(11): 6263–6273. Available at: DOI:10.1007/s10570-020-03225-3

268. Lee JH., Park SH., Kim SH. Surface alkylation of cellulose nanocrystals to enhance their compatibility with polylactide. Polymers. 2020; 12(1): 1–16. Available at: DOI:10.3390/polym12010178

269. Jing H., He H., Liu H., Huang B., Zhang C. Study on properties of polylactic acid/lemongrass fiber biocomposites prepared by fused deposition modeling. Polymer Composites. 2021; 42(2): 973–986. Available at: DOI:10.1002/pc.25879

270. Wang FY., Dai L., Ge TT., Yue CB., Song YM. A-Methylstyrene-Assisted Maleic Anhydride Grafted Poly(Lactic Acid) As an Effective Compatibilizer Affecting Properties of Microcrystalline Cellulose/Poly(Lactic Acid) Composites. Express Polymer Letters. 2020; 14(6): 530–541. Available at: DOI:10.3144/expresspolymlett.2020.43

271. Liao J., Brosse N., Hoppe S., Du G., Zhou X., Pizzi A. One-step compatibilization of poly(lactic acid) and tannin via reactive extrusion. Materials and Design. The Authors; 2020; 191: 108603. Available at: DOI:10.1016/j.matdes.2020.108603

272. Arbelaiz A., Txueka U., Mezo I., Orue A. Biocomposites Based on Poly(Lactic Acid) Matrix and Reinforced with Lignocellulosic Fibers: The Effect of Fiber Type and Matrix Modification. Journal of Natural Fibers. Taylor & Francis; 2020; 00(00): 1–14. Available at: DOI:10.1080/15440478.2020.1726247

273. Trinh BM., Ogunsona EO., Mekonnen TH. Thin-structured and compostable wood fiber-polymer biocomposites: Fabrication and performance evaluation. Composites Part A: Applied Science and Manufacturing. Elsevier Ltd; 2021; 140(October 2020): 106150. Available at: DOI:10.1016/j.compositesa.2020.106150

274. Rajendran Royan NR., Leong JS., Chan WN., Tan JR., Shamsuddin ZSB. Current state and challenges of natural fibre-reinforced polymer composites as feeder in fdm-based 3d printing. Polymers. 2021; 13(14). Available at: DOI:10.3390/polym13142289

275. Guessasma S., Belhabib S., Nouri H. Understanding the microstructural role of bio-sourced 3D printed structures on the tensile performance. Polymer Testing. 2019; 77(May). Available at: DOI:10.1016/j.polymertesting.2019.105924

276. Figueroa-Velarde V., Diaz-Vidal T., Cisneros-López EO., Robledo-Ortiz JR., López-Naranjo EJ., Ortega-Gudiño P., et al. Mechanical and Physicochemical Properties of 3D-Printed Agave Fibers/Poly(lactic) Acid Biocomposites. Materials. 2021; 14(11): 3111. Available at: DOI:10.3390/ma14113111

277. Sun Q., Rizvi G., Bellehumeur C., Gu P. Effect of processing conditions on the bonding quality of FDM polymer filaments. Rapid Prototyping Journal. 2008; 14: 72–80. Available at: https://doi.org/10.1108/13552540810862028

278. Bellehumeur C., Li L., Sun Q., Gu P. Modeling of Bond Formation Between Polymer Filaments in the Fused Deposition Modeling Process. Journal of Manufacturing Processes. 2004; 6(2): 170–178. Available at: DOI:https://doi.org/10.1016/S1526-6125(04)70071-7

279. Sabyrov N., Abilgaziyev A., Ali MH. Enhancing interlayer bonding strength of FDM 3D printing technology by diode laser-assisted system. International Journal of Advanced Manufacturing Technology. 2020; 108(1–2): 603–611. Available at: DOI:10.1007/s00170-020-05455-y

280. Ravi AK., Deshpande A., Hsu KH. An in-process laser localized pre-deposition heating approach to inter-layer bond strengthening in extrusion based polymer additive manufacturing An in-process laser localized pre-deposition heating approach to inter-layer bond strengthening in extrusion . Journal of Manufacturing Processes. The Society of Manufacturing Engineers; 2016; 24(October): 179–185. Available at: DOI:10.1016/j.jmapro.2016.08.007

281. Kishore V., Ajinjeru C., Nycz A., Post B., Lindahl J., Kunc V., et al. Infrared preheating to improve interlayer strength of big area additive manufacturing (BAAM) components. Additive Manufacturing. Elsevier B.V.; 2017; 14(May 2020): 7–12. Available at: DOI:10.1016/j.addma.2016.11.008

282. Butt J., Bhaskar R. Investigating the effects of annealing on the mechanical properties of FFF-printed thermoplastics. Journal of Manufacturing and Materials Processing. 2020; 4(2): 1–20. Available at: DOI:10.3390/jmmp4020038

283. Wach R., Wolszczak P., Adamus-Włodarczyk A. Enhancement of Mechanical Properties of FDM-PLA Parts via Thermal Annealing. Macromolecular Materials and Engineering. 2018; 303. Available at: DOI:10.1002/mame.201800169

284. Suder J., Bobovsky Z., Zeman Z., Mlotek J., Vocetka M. The influence of annealing temperature on tensile strength of polylactic acid. MM Science Journal. 2020; 2020(November): 4132–4137. Available at: DOI:10.17973/MMSJ.2020_11_2020048

285. Wang S., Lu A., Zhang L. Recent advances in regenerated cellulose materials. Progress in Polymer Science. Elsevier Ltd; 2016; 53: 169–206. Available at: DOI:10.1016/j.progpolymsci.2015.07.003

286. Thomason JL., Carruthers J., Kelly J., Johnson G. Fibre cross-section determination and variability in sisal and flax and its effects on fibre performance characterisation. Composites Science and Technology. 2011; 71(7): 1008–1015. Available at: DOI:https://doi.org/10.1016/j.compscitech.2011.03.007

287. Bunsell AR., Joannès S., Marcellan A. 2 - Testing and characterization of fibers. In: Bunsell AR (ed.) Handbook of Properties of Textile and Technical Fibres (Second Edition). Second Edi. Woodhead Publishing; 2018. pp. 21–55. Available at: DOI:https://doi.org/10.1016/B978-0-08-101272-7.00002-X

288. ASTM International. Standard Test Method for Tensile Strength and Young's Modulus for High-Modulus Single-Filament Materials. System. 2000.

289. Stuart T., McCall RD., Sharma HSS., Lyons G. Modelling of wicking and moisture interactions of flax and viscose fibres. Carbohydrate Polymers. 2015; 123: 359–368. Available at: DOI:https://doi.org/10.1016/j.carbpol.2015.01.053

290. Ding J., Liang L., Meng X., Yang F., Pu Y., Ragauskas AJ., et al. The physiochemical alteration of flax fibers structuring components after different scouring and bleaching treatments. Industrial Crops and Products. 2021; 160: 113112. Available at: DOI:https://doi.org/10.1016/j.indcrop.2020.113112

291. Amiri A., Ulven CA., Huo S. Effect of chemical treatment of flax fiber and resin manipulation on service life of their Composites using time-temperature superposition. Polymers. 2015; 7(10): 1965–1978. Available at: DOI:10.3390/polym7101493

292. Amiri A., Ulven C., Huo S. Effect of Chemical Treatment of Flax Fiber and Resin Manipulation on Service Life of Their Composites Using Time-Temperature Superposition. Polymers. 2015; 7: 1965–1978. Available at: DOI:10.3390/polym7101493

293. Lazic BD., Janjic SD., Rijavec T., Kostic MM. Effect of chemical treatments on the chemical composition and properties of flax fibers. Journal of the Serbian Chemical Society. 2017; 82(1): 83–97. Available at: DOI:10.2298/JSC160707106L

294. Zhang H., Ming R., Yang G., Li Y., Li Q., Shao H. Influence of alkali treatment on flax fiber for use as reinforcements in polylactide stereocomplex composites. Polymer Engineering \& Science. 2015; 55(11): 2553–2558. Available at: DOI:https://doi.org/10.1002/pen.24147

295. Bourmaud A., Morvan C., Bouali A., Placet V., Perré P., Baley C. Relationships between micro-fibrillar angle, mechanical properties and biochemical composition of flax fibers. Industrial Crops and Products. 2013; 44: 343–351. Available at: DOI:10.1016/j.indcrop.2012.11.031

296. Eichhorn SJ., Davies GR. Modelling the crystalline deformation of native and regenerated cellulose. Cellulose. 2006; 13(3): 291–307. Available at: DOI:10.1007/s10570-006-9046-3

297. Sharma A., Nagarkar S., Thakre S., Kumaraswamy G. Structure–property relations in regenerated cellulose fibers: comparison of fibers manufactured using viscose and lyocell processes. Cellulose. Springer Netherlands; 2019; 26(6): 3655–3669. Available at: DOI:10.1007/s10570-019-02352-w

298. Ward K. Crystallinity of Cellulose and Its Significance for the Fiber Properties. Textile Research Journal. 1950; 20(6): 363–372. Available at: DOI:10.1177/004051755002000601

299. Kalia S., Kaith BS. Synthesis of flax-g-copolymers under pressure for use in phenolic composites as reinforcement. Journal of the Chilean Chemical Society. 2009; 54(2): 108–112. Available at: DOI:10.4067/S0717-97072009000200002

300. Eichhorn YRJ. The young's modulus of a microcrystalline cellulose. Cellulose. 2001; 8(3): 197–207. Available at: DOI:10.1023/A:1013181804540

301. Matsuo M., Sawatari C., Iwai Y., Ozaki F. Effect of Orientation Distribution and Crystallinity on the Measurement by x-ray Diffraction of the Crystal Lattice Moduli of Cellulose i and ii. Macromolecules. 1990; 23(13): 3266–3275. Available at: DOI:10.1021/ma00215a012

302. Moryganov AP., Zavadskii AE., Stokozenko VG. Special Features of X-ray Analysis of Cellulose Crystallinity and Content in Flax Fibres. Fibre Chemistry. 2018; 49(6): 382–387. Available at: DOI:10.1007/s10692-018-9904-4

303. Sutherland LS., Shenoi RA., Lewis SM. Size and scale effects in composites: I. Literature review. Composites Science and Technology. 1999; 59(2): 209–220. Available at: DOI:https://doi.org/10.1016/S0266-3538(98)00065-7

304. Morton WE., Hearle JWS. Physical Properties of Textile Fibres: Fourth Edition. Physical Properties of Textile Fibres: Fourth Edition. 2008. 1–776 p. Available at: DOI:10.1533/9781845694425

305. Amroune S., Belaadi A., Bourchak M., Makhlouf A., Satha H. Statistical and Experimental Analysis of the Mechanical Properties of Flax Fibers. Journal of Natural Fibers. 2020; Available at: DOI:10.1080/15440478.2020.1775751

306. Joffe R., Andersons J., Sparniņš E. Applicability of Weibull strength distribution for cellulose fibers with highly non-linear behaviour. ICCM International Conferences on Composite Materials. 2009;

307. Zafeiropoulos N., Baillie C. A study of the effect of surface treatments on the tensile strength of flax fibres: Part II. Application of Weibull statistics. Composites Part A-applied Science and Manufacturing - COMPOS PART A-APPL SCI MANUF. 2007; 38: 629–638. Available at: DOI:10.1016/j.compositesa.2006.02.005

308. Amroune S., Belaadi A., Bourchak M., Makhlouf A., Satha H. Statistical and Experimental Analysis of the Mechanical Properties of Flax Fibers. Journal of Natural Fibers. Taylor & Francis; 2022; 19(4): 1387–1401. Available at: DOI:10.1080/15440478.2020.1775751

309. Revol BP., Thomassey M., Ruch F., Nardin M. Influence of the sample number for the prediction of the tensile strength of high tenacity viscose fibres using a two parameters Weibull distribution. Cellulose. Springer Netherlands; 2016; 23(4): 2701–2713. Available at: DOI:10.1007/s10570-016-0974-2

310. Johannes G., Fink H-P., Uihlein K., Zimmerer B. Cellulose man-made fibre reinforced polypropylene - Correlations between fibre and composite properties. Cellulose. 2008; 15: 561–569. Available at: DOI:10.1007/s10570-008-9204-x

311. Graupner N., Basel S., Müssig J. Size effects of viscose fibres and their unidirectional epoxy composites: application of least squares Weibull statistics. Cellulose. 2018; 25(6): 3407–3421. Available at: DOI:10.1007/s10570-018-1819-y

312. Fat, Miyoshi Oil & Fat Co. L. pl1005 technical data sheet.pdf. 2020. Available at: https://www.miyoshi-yushi.co.jp/en/business-information/pdf/06_landyPL_en202210.pdf

313. NatureWorks. Ingeo™ Biopolymer 2003D Technical Data Sheet. Available at: https://www.natureworksllc.com/~/media/Technical_Resources/Technical_Data_Sheets/TechnicalDataSheet_2003D_FFP-FSW_pdf.pdf

314. Nakagaito AN., Kanzawa S., Takagi H. Polylactic acid reinforced with mixed cellulose and chitin nanofibers—effect of mixture ratio on the mechanical properties of composites. Journal of Composites Science. 2018; 2(2). Available at: DOI:10.3390/jcs2020036

315. Aldroubi S., Kasal B., Yan L., Bachtiar EV. Multi-scale investigation of morphological, physical and tensile properties of flax single fiber, yarn and unidirectional fabric. Composites Part B: Engineering. Elsevier Ltd; 2023; 259(April): 110732. Available at: DOI:10.1016/j.compositesb.2023.110732

316. Dong X., Wu Z., Wang Y., Li T., Zhang X., Yuan H., et al. Toughening polylactide using epoxy-functionalized core-shell starch nanoparticles. Polymer Testing. 2021; 93: 106926. Available at: DOI:10.1016/j.polymertesting.2020.106926

317. Shen H., Hu Y., Lin Z., Meng F., Ju G. Mechanical Properties, Crystallization Behaviors and Phase Morphologies of PLA/GTR Blends by Reactive Compatibilization. Materials. 2022; 15: 7095. Available at: DOI:10.3390/ma15207095

318. Chu W., Yan S., Cai Z., Yang S., Hu X., Yin X. Poly(lactic acid) toughen by aromatic sulfonamide toward balanced rheology processing and mechanical properties. Materials Research Express. 2022; 9. Available at: DOI:10.1088/2053-1591/ac7b73

319. Carlsson J., Isaksson P. Dynamic crack propagation in wood fibre composites analysed by high speed photography and a dynamic phase field model. International Journal of Solids and Structures. 1 April 2018; 144–145. Available at: DOI:10.1016/j.ijsolstr.2018.04.015

320. Damptey R., Torres S., Cummings L., Mohan R V. Synthesis and characterization of polylactic acid microspheres via emulsion-based processing. MRS Advances. 2023; 8(17): 982–987. Available at: DOI:10.1557/s43580-023-00634-x

321. Singh B., Sharma C., Sharma S. Fundamentals of Extrusion processing. 2017. pp. 1–46.

322. Wolfson SA., Nikolskii VG. Powder extrusion: Fundamentals and different applications. Polymer Engineering \& Science. 1997; 37(8): 1294–1300. Available at: DOI:https://doi.org/10.1002/pen.11775

323. Yeng LC., Wahit MU., Othman N. Thermal and flexural properties of regenerated cellulose(RC)/poly(3- hydroxybutyrate)(PHB)biocomposites. Jurnal Teknologi. 2015; 75(11): 107–112. Available at: DOI:10.11113/jt.v75.5338

324. Matheus Poletto, Vinícios Pistor AJZ. Structural Characteristics and Thermal Properties of Native Cellulose. Cellulose-Fundamental aspects. 2013; 11: 13. Available at:

DOI:10.5772/50452

325. Ramadevi P., Dhanalakshmi S., Bennehalli B., Ranganagowda RP., Venkateshappa SC. NATURAL ARECA FIBER: SURFACE MODIFICATION AND SPECTRAL STUDIES. Journal of Advances in Chemistry. 2014; 10(1): 2146–2161.

326. Pereira P., Ferreira DP., Araújo JC., Ferreira A., Fangueiro R. The potential of graphene nanoplatelets in the development of smart and multifunctional ecocomposites. Polymers. 2020; 12(10). Available at: DOI:10.3390/POLYM12102189

327. Xiao X., Zhong Y., Cheng M., Sheng L., Wang D., Li S. Improved hygrothermal durability of flax/polypropylene composites after chemical treatments through a hybrid approach. Cellulose. Springer Netherlands; 2021; 28(17): 11209–11229. Available at: DOI:10.1007/s10570-021-04179-w

328. Zhu J., Njuguna J., Pacacz J., Abhyankar H., Pielichowski K., Zhu H., et al. Effects of chemical treatments on physical properties of flax fibres. 5th International Seminar on Modern Polymeric Materials for Environmental Applications,. 2013; (1–9).

329. Ahmed-Haras MR., Kao N., Islam MS., Ward L. An Overview of Recent Developments in Hetero-Catalytic Conversion of Cellulosic Biomass. Research Communication in Engineering Science & Technology. 2020; 4: 43–54. Available at: DOI:10.22597/rcest.v4.65

330. Li Z., Yu T., Yu L. Study on the scouring-bleaching technology of Xinjiang scutched flax. Journal of Engineered Fibers and Fabrics. 2020; 15(118). Available at: DOI:10.1177/1558925020957650

331. Duchemin B., Thuault A., Vicente A., Rigaud B., Fernandez C., Eve S. Ultrastructure of cellulose crystallites in flax textile fibres. Cellulose. 2012; 19(6): 1837–1854. Available at: DOI:10.1007/s10570-012-9786-1

332. Ding J., Liang L., Meng X., Yang F., Pu Y., Ragauskas AJ., et al. The physiochemical alteration of flax fibers structuring components after different scouring and bleaching treatments. Industrial Crops and Products. 2021; 160: 1–45. Available at: DOI:10.1016/j.indcrop.2020.113112

333. J. Acera Fernandez, N. Le Moigne, A. S. Caro-Bretelle, Roland El Hage, A. Le Duc, M. Lozachmeur, P. Bono AB. Role of flax cell wall components on the microstructure and transverse mechanical behaviour of flax fabrics reinforced epoxy biocomposites. Industrial Crops and Products. 2016; : 93–108. Available at: 10.1016/j.indcrop.2016.02.047

334. Tsuji H., Iguchi K., Tashiro K., Arakawa Y. Crystallization behavior{,} structure{,} morphology{,} and thermal properties of crystalline and amorphous stereo diblock copolymers{,} poly(l-lactide)-b-poly(dl-lactide). Polym. Chem. The Royal Society of Chemistry; 2020; 11(36): 5711–5724. Available at: DOI:10.1039/D0PY01115K

335. Cao X., Mohamed A., Gordon SH., Willett JL., Sessa DJ. DSC study of biodegradable poly(lactic acid) and poly(hydroxy ester ether) blends. Thermochimica Acta. 2003; 406(1–2): 115–127. Available at: DOI:10.1016/S0040-6031(03)00252-1

336. Greco A., Ferrari F. Thermal behavior of PLA plasticized by commercial and cardanol-derived plasticizers and the effect on the mechanical properties. Journal of Thermal Analysis and Calorimetry. 2021; 146(1): 131–141. Available at: DOI:10.1007/s10973-020-10403-9

337. Albuquerque R., Brütting C., Standau T., Ruckdäschel H. A machine learning investigation of low-density polylactide batch foams. e-Polymers. 17 March 2022; 22: 318–331. Available at: DOI:10.1515/epoly-2022-0031

338. Wei Z. Mechanical and Microstructural Characteristics of the Fiber-Reinforced Composite Materials. 2016; (August): 6–7. Available at: DOI:10.20944/preprints201608.0220.v1

339. Composite Materials , Microstructural. Composites. 1999;

340. Le Gall M., Davies P., Martin N., Baley C. Recommended flax fibre density values for composite property predictions. Industrial Crops and Products. 2018; 114: 52–58. Available at: DOI:https://doi.org/10.1016/j.indcrop.2018.01.065

341. Fatile OB., AkinruliI J fedayo., Amori AA. Microstructure and Mechanical Behaviour of Stir-Cast Al-Mg-Sl Alloy Matrix Hybrid Composite Reinforced with Corn Cob Ash and Silicon Carbide. International Journal of Engineering and Technology Innovation. 2014; 4(4): 251–259. Available at: https://doaj.org/article/3ff98d13a11042498fb5fe293ccaae35%0Ahttp://ojs.imeti.org/index.php/IJETI/article/view/42

342. Callister W. Material Science and Engineering. Materials Science and Engineering B. 2018.

343. Madsen B., Gamstedt K. Wood versus Plant Fibers: Similarities and Differences in Composite Applications. Advances in Materials Science and Engineering. 2013; 2013. Available at: DOI:10.1155/2013/564346

344. Rask M., Madsen B. Twisting of fibres in yarns for natural fibre composites. ICCM International Conferences on Composite Materials. 2011;

345. McGregor OPL. Manufacture and Characterisation of Natural Fibre Thermoplastic Composite Tapes. 2014.

346. Rasyid MFA., Salim MS., Akil HM., Ishak ZAM. Optimization of Processing Conditions Via Response Surface Methodology (RSM) of Nonwoven Flax Fibre Reinforced Acrodur Biocomposites. Procedia Chemistry. Elsevier Ltd.; 2016; 19: 469–476. Available at: DOI:10.1016/j.proche.2016.03.040

347. Hou Z., Tian X., Zheng Z., Zhang J., Zhe L., Li D., et al. A constitutive model for 3D printed continuous fiber reinforced composite structures with variable fiber content. Composites Part B: Engineering. 2020; 189: 107893. Available at: DOI:https://doi.org/10.1016/j.compositesb.2020.107893

348. Zhang H., Huang T., Jiang Q., He L., Bismarck A., Hu Q. Recent progress of 3D printed continuous fiber reinforced polymer composites based on fused deposition modeling: a review. Journal of Materials Science. 2021; 56(23): 12999–13022. Available at: DOI:10.1007/s10853-021-06111-w

349. Shah DU., Schubel PJ., Clifford MJ. Modelling the effect of yarn twist on the tensile strength of unidirectional plant fibre yarn composites. Journal of Composite Materials. 2013; 47(4): 425–436. Available at: DOI:10.1177/0021998312440737

350. Belaadi A., Amroune S., Bourchak M. Effect of eco-friendly chemical sodium bicarbonate treatment on the mechanical properties of flax fibres: Weibull statistics. International Journal of Advanced Manufacturing Technology. The International Journal of Advanced Manufacturing Technology; 2020; 106(5–6): 1753–1774. Available at: DOI:10.1007/s00170-019-04628-8

351. Chabba S., Matthews GF., Netravali AN. 'Green' composites using cross-linked soy flour and flax yarns. Green Chemistry. 2005; 7(8): 576–581. Available at: DOI:10.1039/b410817e

352. Matumoto K., Takemura K., Kitamura R., Katogi H., Tanaka T., Takagi H. Cellulose nanofiber-introduced continuous-ramie yarn-reinforced polylactic acid filament for 3D printing: Novel fabrication process and mechanical properties. Composites Part A: Applied Science and Manufacturing. Elsevier Ltd; 2024; 176(June 2023): 107836. Available at: DOI:10.1016/j.compositesa.2023.107836

353. Faruk O., Bledzki AK., Fink HP., Sain M. Biocomposites reinforced with natural fibers: 2000-2010. Progress in Polymer Science. Elsevier Ltd; 2012; 37(11): 1552–1596. Available at: DOI:10.1016/j.progpolymsci.2012.04.003

354. Ganster J., Fink HP., Pinnow M. High-tenacity man-made cellulose fibre reinforced

thermoplastics - Injection moulding compounds with polypropylene and alternative matrices. Composites Part A: Applied Science and Manufacturing. 2006; 37(10): 1796–1804. Available at: DOI:10.1016/j.compositesa.2005.09.005

355. Bajpai PK., Singh I., Madaan J. Development and characterization of PLA-based green composites: A review. Journal of Thermoplastic Composite Materials. SAGE Publications Ltd STM; 22 March 2012; 27(1): 52–81. Available at: DOI:10.1177/0892705712439571

356. Ganster J., Fink H-P. Novel cellulose fibre reinforced thermoplastic materials. Cellulose. 2006; 13(3): 271–280. Available at: DOI:10.1007/s10570-005-9045-9

357. Reinhardt M., Kaufmann J., Kausch M., Kroll L. PLA-viscose-composites with continuous fibre reinforcement for structural applications. Procedia Materials Science. Elsevier Masson SAS; 2013; 2(Carus 2008): 137–143. Available at: DOI:10.1016/j.mspro.2013.02.016

358. Bledzki AK., Jaszkiewicz A., Scherzer D. Mechanical properties of PLA composites with man-made cellulose and abaca fibres. Composites Part A: Applied Science and Manufacturing. Elsevier Ltd; 2009; 40(4): 404–412. Available at: DOI:10.1016/j.compositesa.2009.01.002

359. Ejaz M., Azad M., Shah A ur R., Afaq S., Song J-I. Mechanical and Biodegradable Properties of Jute/Flax Reinforced PLA Composites. Fibers and Polymers. 1 November 2020; 21: 2635–2641. Available at: DOI:10.1007/s12221-020-1370-y

360. Sharif A., Mondal S., Hoque ME. Polylactic Acid (PLA)-Based Nanocomposites: Processing and Properties. In: Sanyang ML, Jawaid M (eds.) Bio-based Polymers and Nanocomposites : Preparation, Processing, Properties {\&} Performance. Cham: Springer International Publishing; 2019. pp. 233–254. Available at: DOI:10.1007/978-3-030-05825-8_11

361. Kalistratova LF., Mashkov YK., Egorova VA. Calculation of X-ray Density of Amorphous–Crystalline Polymer Taking into Account Degree of Ordering of Amorphous Phase. Inorganic Materials: Applied Research. 2018; 9(4): 687–692. Available at: DOI:10.1134/S2075113318040147

362. Naser AZ., Deiab I., Darras BM. Poly(lactic acid) (PLA) and polyhydroxyalkanoates (PHAs){,} green alternatives to petroleum-based plastics: a review. RSC Adv. The Royal Society of Chemistry; 2021; 11(28): 17151–17196. Available at: DOI:10.1039/D1RA02390J

363. Kholodovych V., Welsh WJ. Densities of Amorphous and Crystalline Polymers. In: Mark JE (ed.) Physical Properties of Polymers Handbook. New York, NY: Springer New York; 2007. pp. 611–617. Available at: DOI:10.1007/978-0-387-69002-5_37

364. Goud V., Singh D., Ramasamy A., Das A., Kalyanasundaram D. Investigation of the mechanical performance of carbon/polypropylene 2D and 3D woven composites manufactured through multi-step impregnation processes. Composites Part A: Applied Science and Manufacturing. 2020; 130: 105733. Available at: DOI:https://doi.org/10.1016/j.compositesa.2019.105733

365. Balakumaran V., Alagirusamy R., Kalyanasundaram D. A multi-scale aqueous dispersion coating technique for manufacturing carbon fiber reinforced PEEK composite. Composites Part A: Applied Science and Manufacturing. 2023; 165: 107314. Available at: DOI:https://doi.org/10.1016/j.compositesa.2022.107314

366. Bell-Young L. What is Dichloromethane? The Chemistry Blog. 2017. Available at: https://www.chemicals.co.uk/blog/what-is-dichloromethane (Accessed: 23 November 2023)

367. Boundless. Biology. 2013. Available at: https://www.goodreads.com/book/show/20940609-biology

368. Alhuthali A., Low IM., Dong C. Characterisation of the water absorption, mechanical and thermal properties of recycled cellulose fibre reinforced vinyl-ester eco-nanocomposites. Composites Part B: Engineering. 2012; 43(7): 2772–2781. Available at: DOI:https://doi.org/10.1016/j.compositesb.2012.04.038

369. Figueroa-Velarde V., Diaz-Vidal T., Cisneros-López EO., Robledo-Ortiz JR., López-Naranjo EJ., Ortega-Gudiño P., et al. Mechanical and Physicochemical Properties of 3D-Printed Agave Fibers/Poly(lactic) Acid Biocomposites. Materials. 2021; 14(11). Available at: DOI:10.3390/ma14113111

370. Scaffaro R., Gulino EF., Citarrella MC., Maio A. Green Composites Based on Hedysarum coronarium with Outstanding FDM Printability and Mechanical Performance. Polymers. 2022; 14(6). Available at: DOI:10.3390/polym14061198

371. Nafis ZAS., Nuzaimah M., Kudus SIA., Yusuf Y., Ilyas RA., Knight VF., et al. Effect of Wood Dust Fibre Treatments Reinforcement on the Properties of Recycled Polypropylene Composite (r-WoPPC) Filament for Fused Deposition Modelling (FDM). Materials. 2023; 16(2). Available at: DOI:10.3390/ma16020479

372. Girdis J., Gaudion L., Proust G., Löschke S., Dong A. Rethinking Timber: Investigation into the Use of Waste Macadamia Nut Shells for Additive Manufacturing. JOM. 2017; 69(3): 575–579. Available at: DOI:10.1007/s11837-016-2213-6

373. Meredith J., Coles SR., Powe R., Collings E., Cozien-Cazuc S., Weager B., et al. On the static and dynamic properties of flax and Cordenka epoxy composites. Composites Science and

Technology. 2013; 80: 31–38. Available at: DOI:https://doi.org/10.1016/j.compscitech.2013.03.003

374. Frackowiak S., Ludwiczak J., Leluk K. Man-Made and Natural Fibres as a Reinforcement in Fully Biodegradable Polymer Composites: A Concise Study. Journal of Polymers and the Environment. 2018; 26(12): 4360–4368. Available at: DOI:10.1007/s10924-018-1301-9

375. Tekinalp HL., Kunc V., Velez-Garcia GM., Duty CE., Love LJ., Naskar AK., et al. Highly oriented carbon fiber–polymer composites via additive manufacturing. Composites Science and Technology. 2014; 105: 144–150. Available at: DOI:https://doi.org/10.1016/j.compscitech.2014.10.009

376. Ramezani Dana H., El Mansori M. Investigations on the mechanical properties of PLA/Flax fibre composites obtained by Fused Filament Fabrication. Plastics, Rubber and Composites. 2022; 51(8): 393–406. Available at: DOI:10.1080/14658011.2022.2110554

377. Luo HA., Chen Y. Matrix Cracking in Fiber-Reinforced Composite Materials. Journal of Applied Mechanics. 1 September 1991; 58(3): 846–848. Available at: DOI:10.1115/1.2897274

378. Haque ANMA., Naebe M. Tensile Properties of Natural Fibre-Reinforced FDM Filaments: A Short Review. Sustainability. 2023; 15(24). Available at: DOI:10.3390/su152416580

379. Kam M., İpekçi A., Şengül Ö. Investigation of the effect of FDM process parameters on mechanical properties of 3D printed PA12 samples using Taguchi method. Journal of Thermoplastic Composite Materials. 2023; 36(1): 307–325. Available at: DOI:10.1177/08927057211006459

380. Nassar MMA., Alzebdeh KI., Pervez T., Al-Hinai N., Munam A., Al-Jahwari F., et al. Polymer powder and pellets comparative performances as bio-based composites. Iranian Polymer Journal. 2021; 30(3): 269–283. Available at: DOI:10.1007/s13726-020-00888-4

381. Souri H., Bhattacharyya D. Electrical conductivity of the graphene nanoplatelets coated natural and synthetic fibres using electrophoretic deposition technique. International Journal of Smart and Nano Materials. 2018; 9: 1–17. Available at: DOI:10.1080/19475411.2018.1476419

382. Oliveira C., Carvalho D., Moura I., Ribeiro B., Ferreira F. 3D Printing Using Natural Fibers -- An Emerging Technology in Sustainable Manufacturing: A Review. In: Guarda T, Portela F, Diaz-Nafria JM (eds.) Advanced Research in Technologies, Information, Innovation and Sustainability. Cham: Springer Nature Switzerland; 2024. pp. 343–356.

383. Reinhardt M., Kaufmann J., Kausch M., Kroll L. PLA-Viscose-Composites with Continuous

Fibre Reinforcement for Structural Applications. Procedia Materials Science. Elsevier Masson SAS; 2013; 2(Carus 2008): 137–143. Available at: DOI:10.1016/j.mspro.2013.02.016

384. Hou Z., Tian X., Zhang J., Li D. 3D printed continuous fibre reinforced composite corrugated structure. Composite Structures. Elsevier; 2018; 184(October 2017): 1005–1010. Available at: DOI:10.1016/j.compstruct.2017.10.080

385. Matsuzaki R., Ueda M., Namiki M., Jeong TK., Asahara H., Horiguchi K., et al. Three-dimensional printing of continuous-fiber composites by in-nozzle impregnation. Scientific Reports. Nature Publishing Group; 2016; 6(April). Available at: DOI:10.1038/srep23058

386. Irfan MS., Harris D., Paget MA., Ma T., Leek C., Machavaram VR., et al. On-site evaluation of a modified pultrusion process: Fibre spreading and resin injection-based impregnation. Journal of Composite Materials. 2021; 55(1): 77–93. Available at: DOI:10.1177/0021998320943268

387. Belnoue JP-H., Nixon-Pearson OJ., Thompson AJ., Ivanov DS., Potter KD., Hallett SR. Consolidation-Driven Defect Generation in Thick Composite Parts. Journal of Manufacturing Science and Engineering. 2018; 140(7): 71006. Available at: DOI:10.1115/1.4039555

388. Yang G., Bi J., Dong Z., Li Y., Liu Y. Experimental Study on Dynamic Tensile Properties of Macro-Polypropylene Fiber Reinforced Cementitious Composites. International Journal of Concrete Structures and Materials. 2022; 16(1): 66. Available at: DOI:10.1186/s40069-022-00559-z

389. Kanakannavar S., Pitchaimani J., Goh K-L. Tensile Behaviour of Double-Edge Notched Flax Braided Yarn Woven Fabric Reinforced PLA Composite. Fibers and Polymers. 2023; 24(10): 3713–3722. Available at: DOI:10.1007/s12221-023-00339-w

390. Mishra S., Parashar V. Experimental analysis of duo-fiber interaction on the tensile strength of surface-modified flax–kenaf-reinforced epoxy composite. Polymer Bulletin. 2023; 80(12): 13159–13179. Available at: DOI:10.1007/s00289-023-04708-6

391. Velghe I., Buffel B., Vandeginste V., Thielemans W., Desplentere F. Review on the Degradation of Poly(lactic acid) during Melt Processing. Polymers. 2023; 15(9). Available at: DOI:10.3390/polym15092047

392. Nascimento L., Gamez-Perez J., Santana OO., Velasco JI., Maspoch ML., Franco-Urquiza E. Effect of the Recycling and Annealing on the Mechanical and Fracture Properties of Poly(Lactic Acid). Journal of Polymers and the Environment. 2010; 18(4): 654–660. Available at: DOI:10.1007/s10924-010-0229-5

393. Żenkiewicz M., Richert J., Rytlewski P., Moraczewski K., Stepczyńska M., Karasiewicz T. Characterisation of multi-extruded poly(lactic acid). Polymer Testing. 2009; 28(4): 412–418. Available at: DOI:https://doi.org/10.1016/j.polymertesting.2009.01.012

394. Shesan OJ., Stephen AC., Chioma AG., Neerish R., Rotimi SE. Fiber-Matrix Relationship for Composites Preparation. In: Pereira AB, Fernandes FAO (eds.) Renewable and Sustainable Composites. Rijeka: IntechOpen; 2019. Available at: DOI:10.5772/intechopen.84753

395. Li Q., Chen Y., Chen Y., Ai S., Fang D. Effects of Void Defects on Fracture Features and Tensile Strength of C/SiC Composites: an Image-based FEM Study. Applied Composite Materials. 2022; 29(3): 1021–1039. Available at: DOI:10.1007/s10443-021-10002-3

396. Le Moigne N., Otazaghine B., Corn S., Angellier-Coussy H., Bergeret A. Interfaces in Natural Fibre Reinforced Composites: Definitions and Roles. Surfaces and Interfaces in Natural Fibre Reinforced Composites: Fundamentals, Modifications and Characterization. Cham: Springer International Publishing; 2018. pp. 23–34. Available at: DOI:10.1007/978-3-319-71410-3_2

397. Gholampour A., Ozbakkaloglu T. A review of natural fiber composites: properties, modification and processing techniques, characterization, applications. Journal of Materials Science. 2020; 55(3): 829–892. Available at: DOI:10.1007/s10853-019-03990-y

398. Ahmed J., Zhang J-X., Song Z., Varshney SK. Thermal properties of polylactides. Journal of Thermal Analysis and Calorimetry. 2009; 95(3): 957–964. Available at: DOI:10.1007/s10973-008-9035-x

399. Pan P., Zhu B., Kai W., Serizawa S., Iji M., Inoue Y. Crystallization behavior and mechanical properties of bio-based green composites based on poly(L-lactide) and kenaf fiber. Journal of Applied Polymer Science. 2007; 105(3): 1511–1520. Available at: DOI:https://doi.org/10.1002/app.26407

400. Nassiopoulos E., Njuguna J. Thermo-mechanical performance of poly(lactic acid)/flax fibre-reinforced biocomposites. Materials & Design. 2015; 66: 473–485. Available at: DOI:https://doi.org/10.1016/j.matdes.2014.07.051

401. Batista NL., Olivier P., Rezende MC., Botelho EC., Talim R. Correlation between degree of crystallinity , morphology and mechanical properties of PPS / carbon fiber laminates. 2016; 19(1): 195–201.

402. Yang H., Du J. Crystallinity, Rheology, and Mechanical Properties of Low-/High-Molecular-Weight PLA Blended Systems. Molecules. 2024; 29(1). Available at: DOI:10.3390/molecules29010169

403. Oksiuta Z., Jalbrzykowski M., Mystkowska J., Romanczuk E., Osiecki T. Mechanical and Thermal Properties of Polylactide (PLA) Composites Modified with Mg, Fe, and Polyethylene (PE) Additives. Polymers. 2020; 12(12). Available at: DOI:10.3390/polym12122939

404. Savandaiah C., Maurer J., Plank B., Steinbichler G., Sapkota J. Rapid Consolidation of 3D Printed Composite Parts Using Compression Moulding for Improved Thermo Mechanical Properties. Rapid Prototyping Journal. 2022; Available at: DOI:10.1108/rpj-11-2021-0311

405. Liao Y., Liu C., Coppola B., Barra G., Di Maio L., Incarnato L., et al. Effect of porosity and crystallinity on 3D printed PLA properties. Polymers. 2019; 11(9): 1–14. Available at: DOI:10.3390/polym11091487

406. Matsuzaki R., Ueda M., Namiki M., Jeong T-K., Asahara H., Horiguchi K., et al. Three-dimensional printing of continuous-fiber composites by in-nozzle impregnation. Scientific Reports. 2016; 6(1): 23058. Available at: DOI:10.1038/srep23058

407. Vigil Fuentes MA., Thakur S., Wu F., Misra M., Gregori S., Mohanty AK. Study on the 3D printability of poly(3-hydroxybutyrate-co-3-hydroxyvalerate)/poly(lactic acid) blends with chain extender using fused filament fabrication. Scientific Reports. 2020; 10(1): 11804. Available at: DOI:10.1038/s41598-020-68331-5

408. Yang J., Ma Y., Chen L., Zhang L., Wu H., Yao Y. An adaptive matrix material extrusion optimization model for in situ impregnated continuous fiber-reinforced 3D printing. The International Journal of Advanced Manufacturing Technology. 2023; 129(3): 1527–1545. Available at: DOI:10.1007/s00170-023-12284-2

409. Hannah Mason GG. 3D printing with continuous fiber: A landscape. Composites world. 2020. Available at: https://www.compositesworld.com/articles/3d-printing-with-continuous-fiber-a-landscape (Accessed: 30 January 2020)

410. Girard H., Doitrand A., Koohbor B., Rinaldi RG., Godin N., Long D., et al. Influence of nearby fiber on fiber–matrix debonding: Coupled Criterion prediction and debonding shape determination. Journal of the Mechanics and Physics of Solids. 2024; 183: 105498. Available at: DOI:https://doi.org/10.1016/j.jmps.2023.105498

411. Xu M., Wagner HD., An B. An analysis of interfacial debonding in beaded fiber composites. International Journal of Fracture. 2023; Available at: DOI:10.1007/s10704-023-00753-4

412. Motru S., Adithyakrishna VH., Bharath J., Guruprasad R. Development and Evaluation of Mechanical Properties of Biodegradable PLA/Flax Fiber Green Composite Laminates. Materials Today: Proceedings. 2020; 24: 641–649. Available at:

DOI:https://doi.org/10.1016/j.matpr.2020.04.318

413. Atakok G., Kam M., Koc HB. Tensile, three-point bending and impact strength of 3D printed parts using PLA and recycled PLA filaments: A statistical investigation. Journal of Materials Research and Technology. 2022; 18: 1542–1554. Available at: DOI:https://doi.org/10.1016/j.jmrt.2022.03.013

414. Ansari AA., Kamil M. Investigation of flexural properties in 3D printed continuous fiber-reinforced polymer composites. IOP Conference Series: Materials Science and Engineering. IOP Publishing; July 2022; 1248(1): 12070. Available at: DOI:10.1088/1757-899X/1248/1/012070

415. Kumar S., Singh R., Singh TP., Batish A. On flexural and pull out properties of 3D printed PLA based hybrid composite matrix. Materials Research Express. IOP Publishing; January 2020; 7(1): 15330. Available at: DOI:10.1088/2053-1591/ab66f4

416. Drahansky M., Paridah M., Moradbak A., Mohamed A., Owolabi F abdulwahab taiwo., Asniza M., et al. We are IntechOpen , the world ' s leading publisher of Open Access books Built by scientists , for scientists TOP 1 %. Intech. 2016; i(tourism): 13. Available at: DOI:http://dx.doi.org/10.5772/57353

417. Kabir SMF., Mathur K., Seyam A-FM. A critical review on 3D printed continuous fiber-reinforced composites: History, mechanism, materials and properties. Composite Structures. 2020; 232: 111476. Available at: DOI:https://doi.org/10.1016/j.compstruct.2019.111476

418. Bax B., Müssig J. Impact and tensile properties of PLA/Cordenka and PLA/flax composites. Composites Science and Technology. 2008; 68(7): 1601–1607. Available at: DOI:https://doi.org/10.1016/j.compscitech.2008.01.004

419. Wang Y., Mei Y., Wang Q., Wei W., Huang F., Li Y., et al. Improved fracture toughness and ductility of PLA composites by incorporating a small amount of surface-modified helical carbon nanotubes. Composites Part B: Engineering. Elsevier; 2019; 162(October 2018): 54–61. Available at: DOI:10.1016/j.compositesb.2018.10.060

420. Wang G., Zhang D., Li B., Wan G., Zhao G., Zhang A. Strong and thermal-resistance glass fiber-reinforced polylactic acid (PLA) composites enabled by heat treatment. International Journal of Biological Macromolecules. 2019; 129: 448–459. Available at: DOI:10.1016/j.ijbiomac.2019.02.020

421. Tawakkal ISMA., Talib RA., Abdan K., Ling CN. Mechanical and physical properties of kenaf-derived cellulose (KDC)-filled polylactic acid (PLA) composites. BioResources. 2012; 7(2): 1643–1655. Available at: DOI:10.15376/biores.7.2.1643-1655

422. Kamaal M., Anas M., Rastogi H., Bhardwaj N., Rahaman A. Effect of FDM process parameters on mechanical properties of 3D-printed carbon fibre–PLA composite. Progress in Additive Manufacturing. Springer International Publishing; 2021; 6(1): 63–69. Available at: DOI:10.1007/s40964-020-00145-3

423. Nuthong W., Uawongsuwan P., Pivsa-Art W., Hamada H. Impact property of flexible epoxy treated natural fiber reinforced PLA composites. Energy Procedia. Elsevier B.V.; 2013; 34: 839–847. Available at: DOI:10.1016/j.egypro.2013.06.820

424. Graupner N., Albrecht K., Ziegmann G., Enzler H., Müssig J. Influence of reprocessing on fibre length distribution, tensile strength and impact strength of injection moulded cellulose fibre-reinforced polylactide (PLA) composites. Express Polymer Letters. 2016; 10(8): 647–663. Available at: DOI:10.3144/expresspolymlett.2016.59

425. Gao H., Qiang T. Fracture surface morphology and impact strength of cellulose/PLA composites. Materials. 2017; 10(6): 1–11. Available at: DOI:10.3390/ma10060624

426. Chen K., Yu L., Cui Y., Jia M., Pan K. Optimization of printing parameters of 3D-printed continuous glass fiber reinforced polylactic acid composites. Thin-Walled Structures. 2021; 164: 107717. Available at: DOI:https://doi.org/10.1016/j.tws.2021.107717

427. Mamun AA., Bledzki AK. Micro fibre reinforced PLA and PP composites: Enzyme modification, mechanical and thermal properties. Composites Science and Technology. 2013; 78: 10–17. Available at: DOI:10.1016/j.compscitech.2013.01.013

428. Motru S., Adithyakrishna VH., Bharath J., Guruprasad R. Development and Evaluation of Mechanical Properties of Biodegradable PLA/Flax Fiber Green Composite Laminates. Materials Today: Proceedings. Elsevier Ltd.; 2020; 24: 641–649. Available at: DOI:10.1016/j.matpr.2020.04.318

429. Yang Z., Feng X., Bi Y., Zhou Z., Yue J., Xu M. Bleached extruder chemi-mechanical pulp fiber-PLA composites: Comparison of mechanical, thermal, and rheological properties with those of wood flour-PLA bio-composites. Journal of Applied Polymer Science. 2016; 133(48): 1–9. Available at: DOI:10.1002/app.44241

430. Bajpai PK., Singh I., Madaan J. Development and characterization of PLA-based green composites: A review. Journal of Thermoplastic Composite Materials. 2014; 27(1): 52–81. Available at: DOI:10.1177/0892705712439571

431. Striemann P., Hülsbusch D., Mrzljak S., Niedermeier M., Walther F. Systematic approach for the characterization of additive manufactured and injection molded short carbon fiber-reinforced

polymers under tensile loading. Materials Testing. 2020; 62: 561–567. Available at: DOI:10.3139/120.111517

432. Graupner N., Herrmann AS., Müssig J. Natural and man-made cellulose fibre-reinforced poly(lactic acid) (PLA) composites: An overview about mechanical characteristics and application areas. Composites Part A: Applied Science and Manufacturing. Elsevier Ltd; 2009; 40(6–7): 810–821. Available at: DOI:10.1016/j.compositesa.2009.04.003

433. Tian X., Liu T., Wang Q., Dilmurat A., Li D., Ziegmann G. Recycling and remanufacturing of 3D printed continuous carbon fiber reinforced PLA composites. Journal of Cleaner Production. 2017; 142: 1609–1618. Available at: DOI:https://doi.org/10.1016/j.jclepro.2016.11.139

434. Shahar FS., Hameed Sultan MT., Safri SNA., Jawaid M., Abu Talib AR., Basri AA., et al. Fatigue and impact properties of 3D printed PLA reinforced with kenaf particles. Journal of Materials Research and Technology. 2022; 16: 461–470. Available at: DOI:https://doi.org/10.1016/j.jmrt.2021.12.023

435. Alimuzzaman S., Gong RH., Akonda M. Impact Property of PLA/Flax Nonwoven Biocomposite. Conference Papers in Materials Science. 2013; 2013: 1–6. Available at: DOI:10.1155/2013/136861

436. Xia X., Shi X., Liu W., He S., Zhu C., Liu H. Effects of gamma irradiation on properties of PLA/flax composites. Iranian Polymer Journal (English Edition). Springer Berlin Heidelberg; 2020; 29(7): 581–590. Available at: DOI:10.1007/s13726-020-00820-w

437. Gunti R., Ratna Prasad A V., Gupta AVSSKS. Mechanical and degradation properties of natural fiber-reinforced PLA composites: Jute, sisal, and elephant grass. Polymer Composites. 2018; 39(4): 1125–1136. Available at: DOI:10.1002/pc.24041

438. Islam MS., Pickering KL., Foreman NJ. Influence of accelerated ageing on the physico-mechanical properties of alkali-treated industrial hemp fibre reinforced poly(lactic acid) (PLA) composites. Polymer Degradation and Stability. Elsevier Ltd; 2010; 95(1): 59–65. Available at: DOI:10.1016/j.polymdegradstab.2009.10.010

439. Zeynivandnejad M., Moradi M., Sadeghi A. Mechanical, physical, and degradation properties of 3D printed PLA + Mg composites. Journal of Manufacturing Processes. 2023; 101: 234–244. Available at: DOI:https://doi.org/10.1016/j.jmapro.2023.05.099

440. Pan P., Zhu B., Kai W., Dong T., Inoue Y. Polymorphic Transition in Disordered Poly(l-lactide) Crystals Induced by Annealing at Elevated Temperatures. Macromolecules. American Chemical Society; 1 June 2008; 41(12): 4296–4304. Available at: DOI:10.1021/ma800343g

441. Zhang J., Duan Y., Sato H., Tsuji H., Noda I., Yan S., et al. Crystal Modifications and Thermal Behavior of Poly(l-lactic acid) Revealed by Infrared Spectroscopy. Macromolecules. American Chemical Society; 1 September 2005; 38(19): 8012–8021. Available at: DOI:10.1021/ma051232r

Appendix A

SEM images of Cryofracture surfaces of Solution Impregnation Formulations

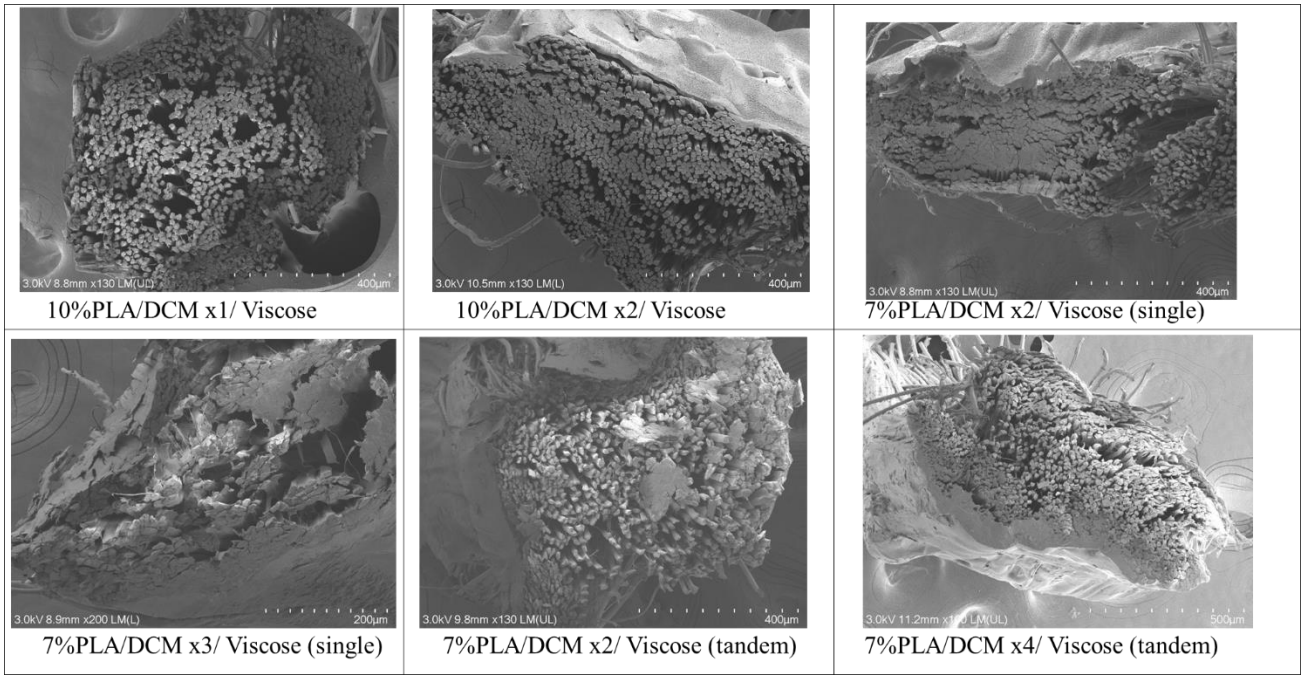

Figure 89 SEM images of cryofracture surfaces of solution impregnated PLA/viscose filaments.

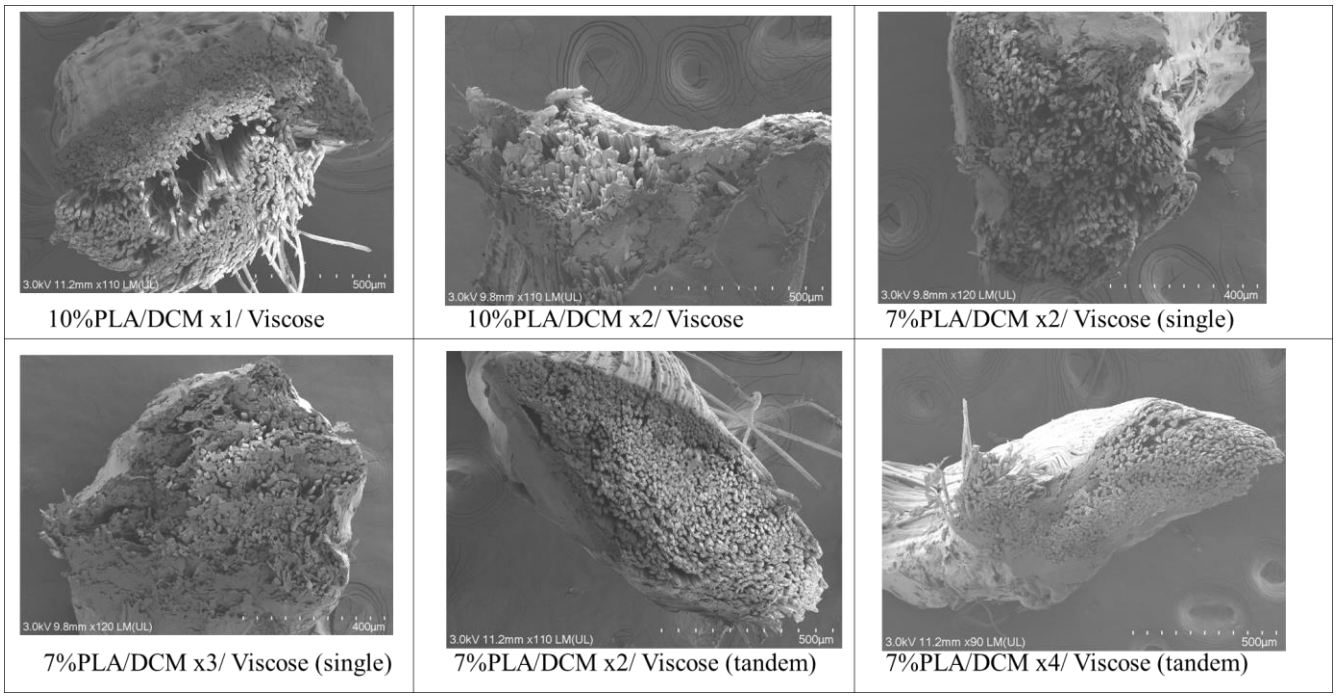

Figure 90 SEM images of cryofracture surfaces of solution impregnated and consolidated PLA/viscose filaments.

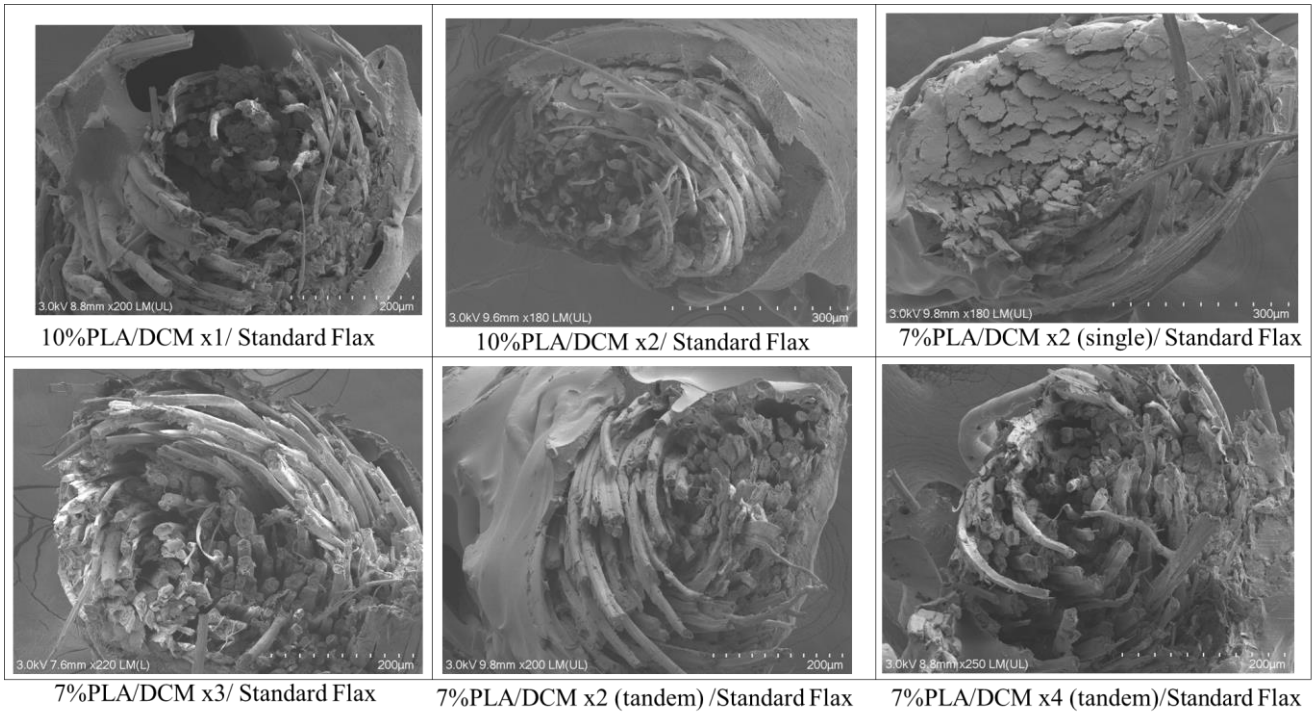

Figure 91 SEM images of cryofracture surfaces of solution impregnated PLA/standard flax filaments.

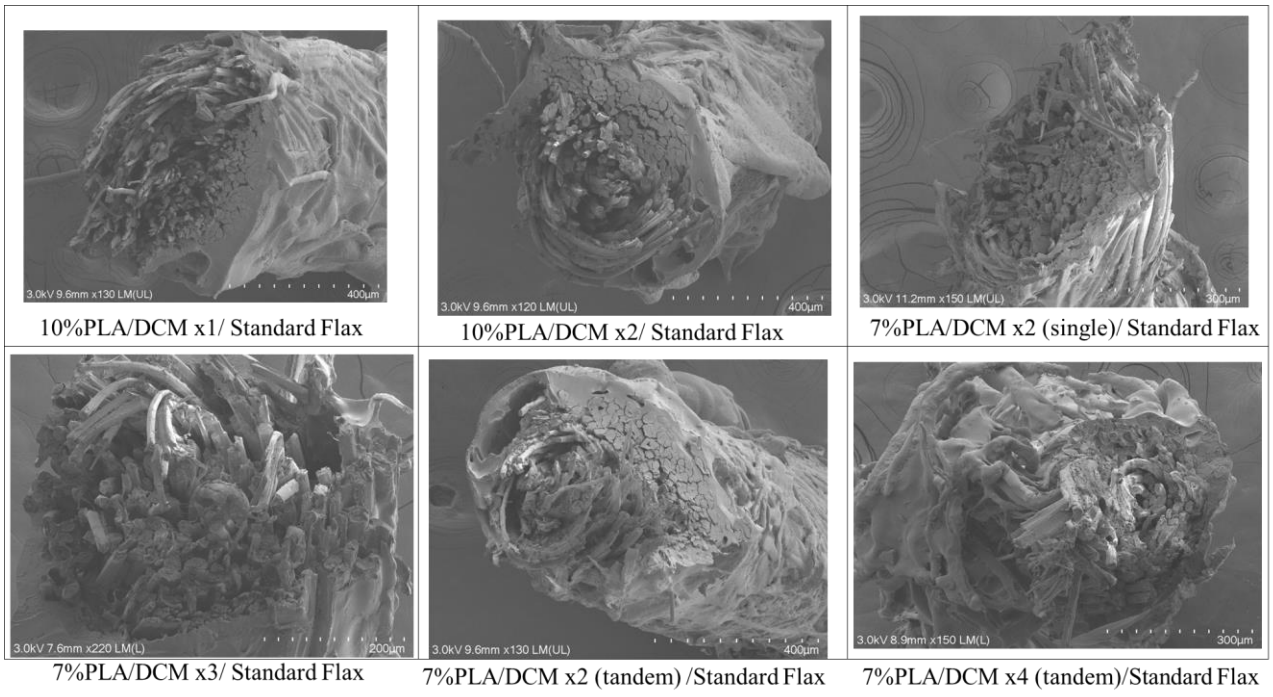

Figure 92 SEM images of cryofracture surfaces of solution impregnated and consolidated PLA/standard flax filaments.

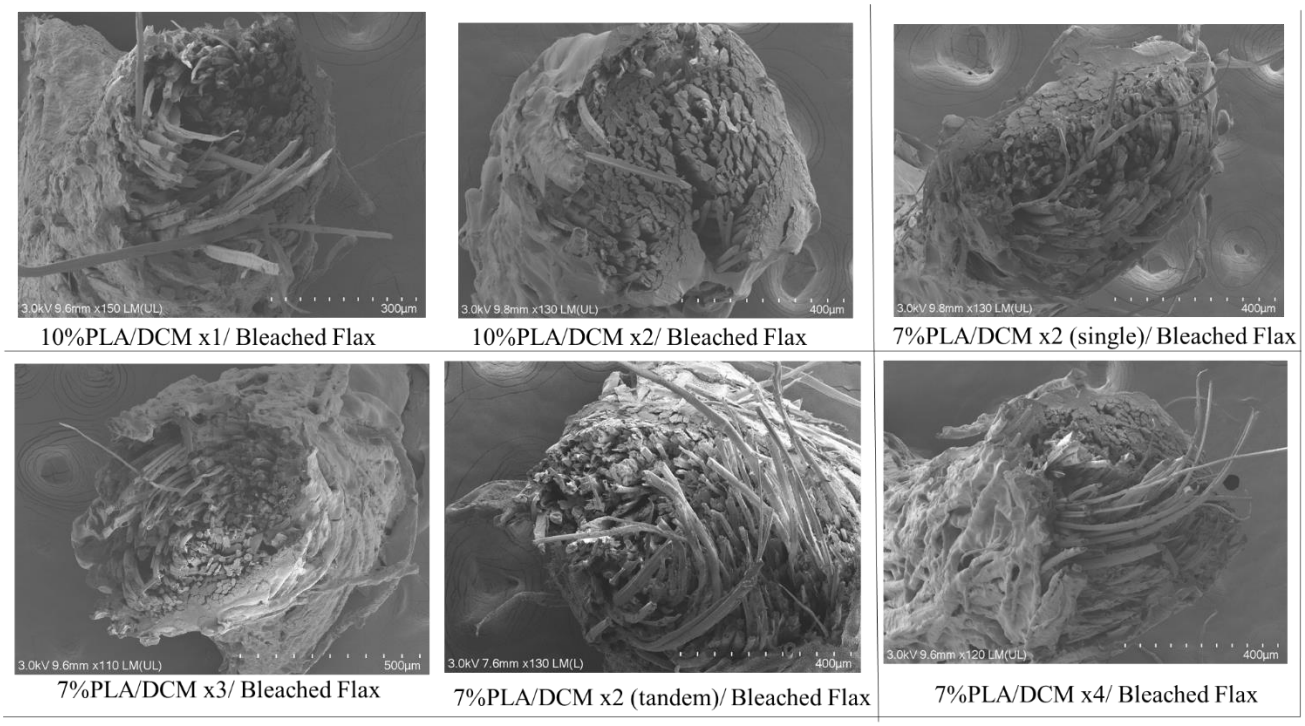

Figure 93 SEM images of cryofracture surfaces of solution impregnated PLA/bleached flax filaments.

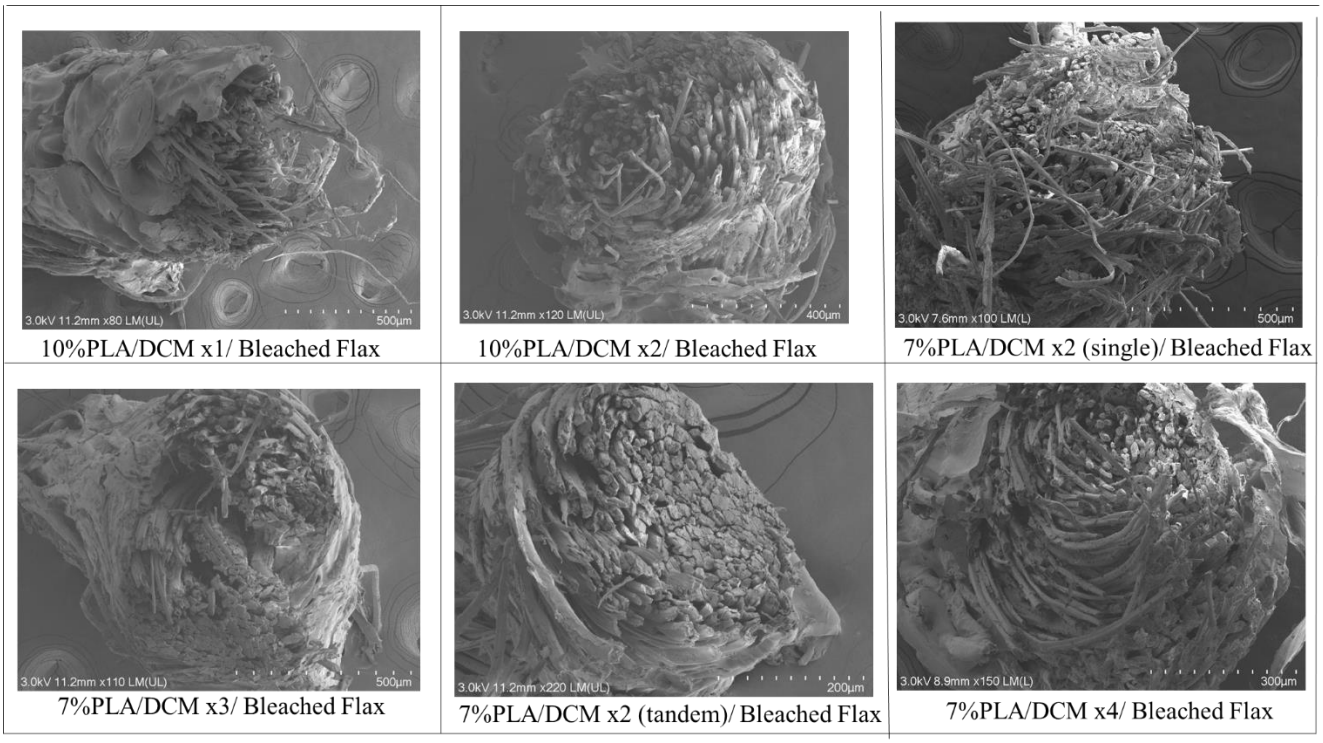

Figure 94 SEM images of cryofracture surfaces of solution impregnated and consolidated PLA/bleached flax filaments.

SEM images of Cryofracture surfaces of Emulsion Impregnation Formulations

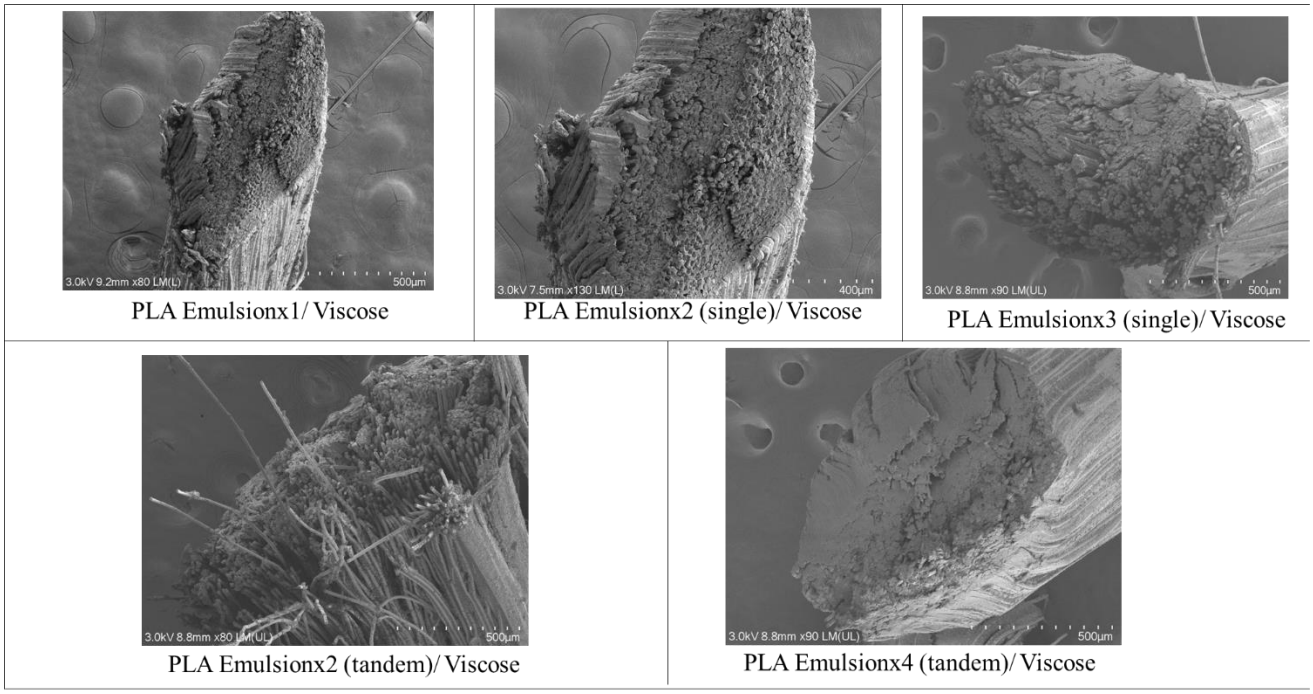

Figure 95 SEM images of cryofracture surfaces of emulsion impregnated PLA/viscose filaments.

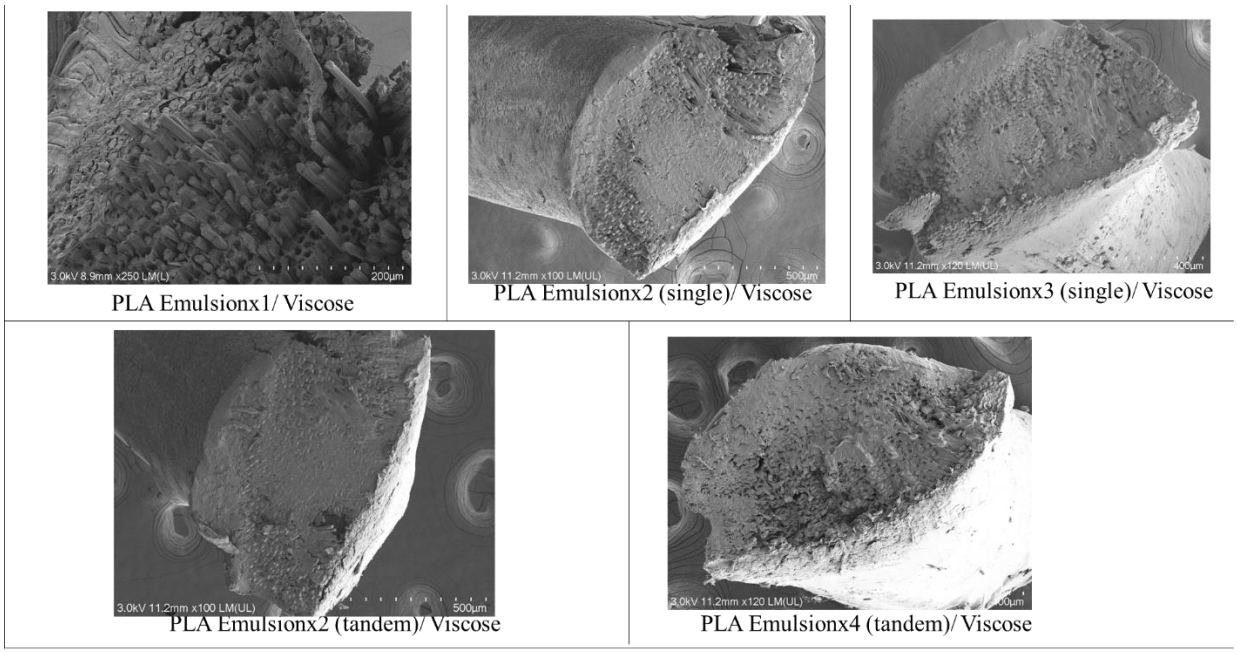

Figure 96 SEM images of cryofracture surfaces of emulsion impregnated and consolidated PLA/viscose filaments.

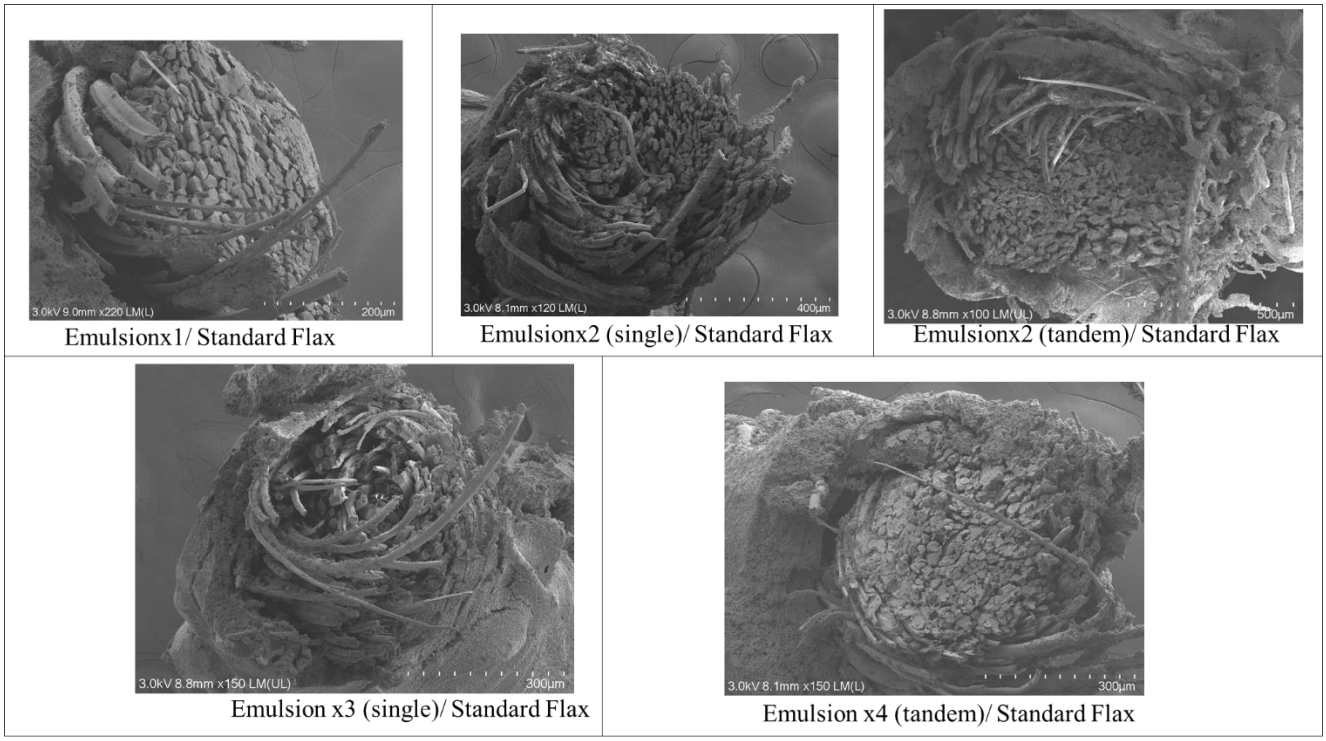

Figure 97 SEM images of cryofracture surfaces of emulsion impregnated PLA/standard flax filaments.

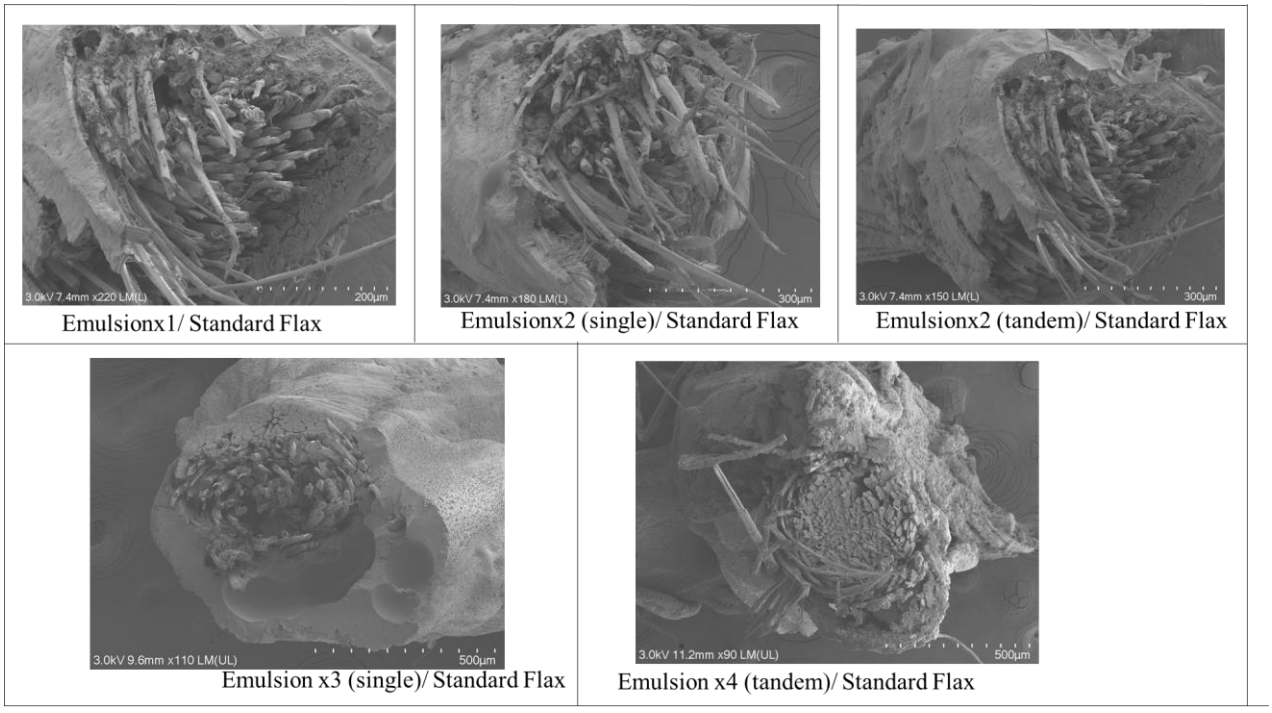

Figure 98 SEM images of cryofracture surfaces of emulsion impregnated and consolidated PLA/standard flax filaments.

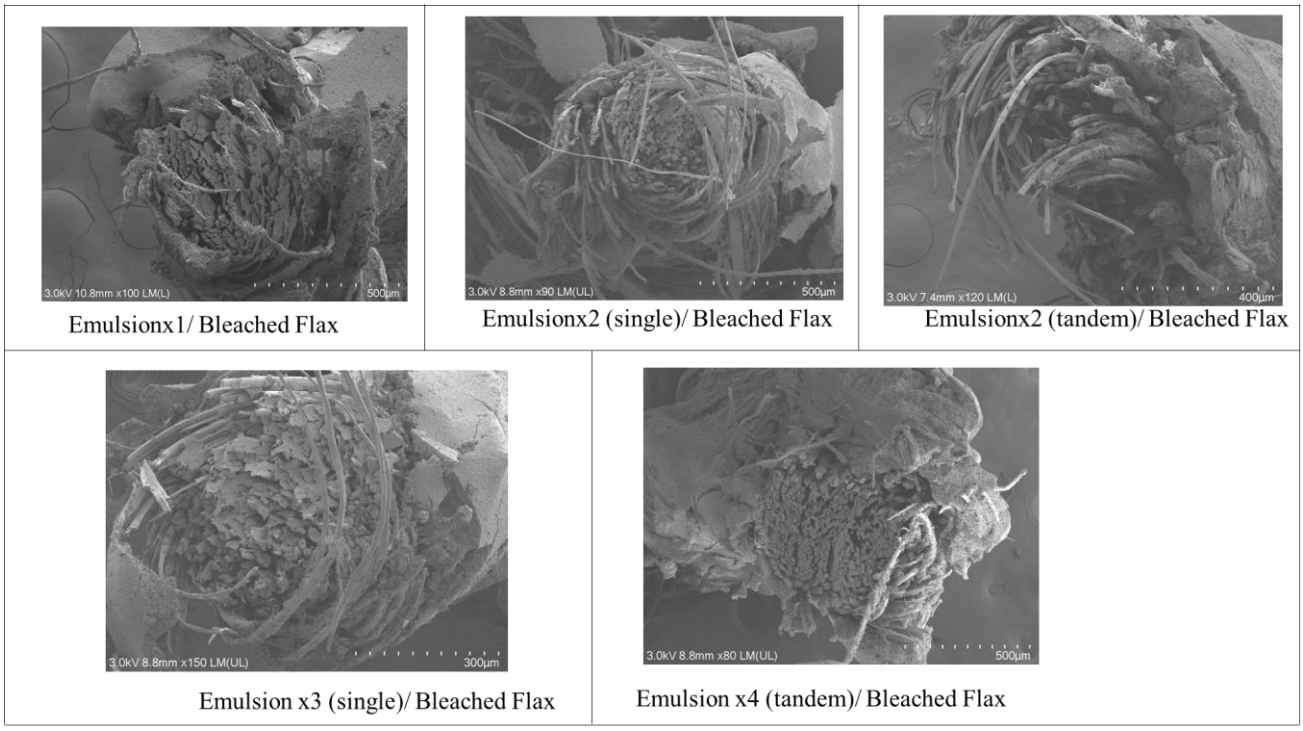

Figure 99 SEM images of cryofracture surfaces of emulsion impregnated PLA/bleached flax filaments.

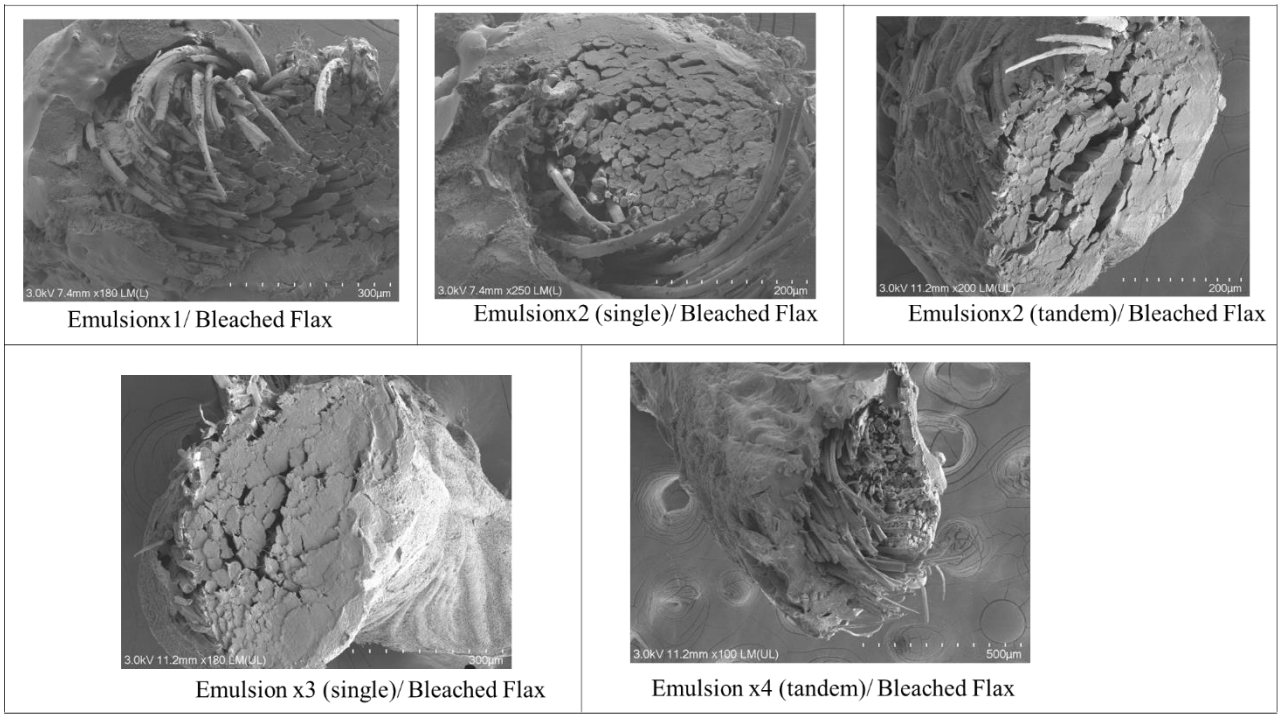

Figure 100 SEM images of cryofracture surfaces of emulsion impregnated and consolidated PLA/bleached flax filaments.

Appendix B

G-Code used for 3D Printing of Composite Specimens

G-Code for tensile and three-point bending test samples

; G-Code generated by Simplify3D(R) Version 3.1.1

; Jun 25, 2024 at 9:24:22 AM

; Settings Summary

; processName,Process1

; applyToModels,150403_D256_45x5x1.5(2)(2)(2)

; profileName,Christian - PLA correct (modified)

; profileVersion,2017-06-27 14:09:50

; baseProfile,MakerGear M2 Dual (modified)

; printMaterial,PLA

; printQuality,Medium

; printExtruders,Right Extruder Only

; extruderName,Right Extruder

; extruderToolheadNumber,1

; extruderDiameter,1.5

; extruderAutoWidth,0

; extruderWidth,1.5

; extrusionMultiplier,0.95

; extruderUseRetract,1

; extruderRetractionDistance,1

; extruderExtraRestartDistance,0

; extruderRetractionZLift,0

; extruderRetractionSpeed,2400

; extruderUseCoasting,0

; extruderCoastingDistance,0.2

; extruderUseWipe,0

; extruderWipeDistance,5

; primaryExtruder,0

; layerHeight,0.8

; topSolidLayers,0

; bottomSolidLayers,0

; perimeterOutlines,0

; printPerimetersInsideOut,1

; startPointOption,2

; startPointOriginX,0

; startPointOriginY,0

; startPointOriginZ,300

; sequentialIslands,0

; spiralVaseMode,0

; firstLayerHeightPercentage,100

; firstLayerWidthPercentage,100

; firstLayerUnderspeed,1

; useRaft,0

; raftExtruder,0

; raftLayers,3

; raftOffset,3

; raftSeparationDistance,0.14

; raftInfill,85

; disableRaftBaseLayers,0

; useSkirt,0

; skirtExtruder,0

; skirtLayers,1

; skirtOutlines,2

; skirtOffset,5

; usePrimePillar,0

; primePillarExtruder,999

; primePillarWidth,12

; primePillarLocation,7

; primePillarSpeedMultiplier,1

; useOozeShield,0

; oozeShieldExtruder,999

; oozeShieldOffset,2

; oozeShieldOutlines,1

; oozeShieldSidewallShape,1

; oozeShieldSidewallAngle,30

; oozeShieldSpeedMultiplier,1

; infillExtruder,0

; internalInfillPattern,Rectilinear

; externalInfillPattern,Rectilinear

; infillPercentage,100

; outlineOverlapPercentage,40

; infillExtrusionWidthPercentage,100

; minInfillLength,0.1

; infillLayerInterval,1

; infillAngles,0

; overlapInfillAngles,0

; generateSupport,0

; supportExtruder,0

; supportInfillPercentage,30

; supportExtraInflation,0

; denseSupportLayers,0

; denseSupportInfillPercentage,70

; supportLayerInterval,1

; supportHorizontalPartOffset,0.3

; supportUpperSeparationLayers,1

; supportLowerSeparationLayers,1

; supportType,0

; supportGridSpacing,4

; maxOverhangAngle,45

; supportAngles,0

; temperatureName,Right Extruder,Left Extruder,Heated Bed

; temperatureNumber,1,0,2

; temperatureSetpointCount,1,1,1

; temperatureSetpointLayers,1,1,1

; temperatureSetpointTemperatures,195,0,60

; temperatureStabilizeAtStartup,1,0,1

; temperatureHeatedBed,0,0,1

; temperatureRelayBetweenLayers,0,0,0

; temperatureRelayBetweenLoops,0,0,0

; fanLayers,1,2

; fanSpeeds,0,50

; blipFanToFullPower,1

; adjustSpeedForCooling,1

; minSpeedLayerTime,15

; minCoolingSpeedSlowdown,20

; increaseFanForCooling,0

; minFanLayerTime,45

; maxCoolingFanSpeed,100

; increaseFanForBridging,0

; bridgingFanSpeed,100

; use5D,1

; relativeEdistances,0

; allowEaxisZeroing,1

; independentExtruderAxes,0

; includeM10123,0

; stickySupport,1

; applyToolheadOffsets,0

; gcodeXoffset,0

; gcodeYoffset,0

; gcodeZoffset,0

; overrideMachineDefinition,1

; machineTypeOverride,0

; strokeXoverride,175

; strokeYoverride,250

; strokeZoverride,200

; originOffsetXoverride,0

; originOffsetYoverride,0

; originOffsetZoverride,0

; homeXdirOverride,-1

; homeYdirOverride,-1

; homeZdirOverride,-1

; flipXoverride,1

; flipYoverride,-1

; flipZoverride,1

; toolheadOffsets,0,0|-31.1,0|0,0|0,0|0,0|0,0

; overrideFirmwareConfiguration,1

; firmwareTypeOverride,RepRap (Marlin/Repetier/Sprinter)

; GPXconfigOverride,r2

; baudRateOverride,115200

; overridePrinterModels,1

; printerModelsOverride,MakerGear_M2Dual.stl

; startingGcode,M108 S255 ; Turn on M2 fans,T1 ; Switch to right extruder offsets for homing,G28 ; Home all axes,T0 ; Switch to left extruder,G1 X0 Y50 Z0.3 F9600 ; Move forward to avoid binder clips,,

; layerChangeGcode,

; retractionGcode,

; toolChangeGcode,

; endingGcode,G91 ; relative mode,G1 Z40 ; lift 10mm,G90 ; absolute mode,G28 X0 ; home X axis,M84 ; disable motors

; exportFileFormat,gcode

; celebration,0

; celebrationSong,Random Song

; postProcessing,

; defaultSpeed,300

; outlineUnderspeed,1

; solidInfillUnderspeed,1

; supportUnderspeed,1

; rapidXYspeed,800

; rapidZspeed,800

; minBridgingArea,50

; bridgingExtraInflation,0

; bridgingExtrusionMultiplier,1

; bridgingSpeedMultiplier,1

; filamentDiameter,1.4

; filamentPricePerKg,46

; filamentDensity,1.25

; useMinPrintHeight,0

; minPrintHeight,0

; useMaxPrintHeight,0

; maxPrintHeight,0

; useDiaphragm,0

; diaphragmLayerInterval,20

; robustSlicing,1

; mergeAllIntoSolid,0

; onlyRetractWhenCrossingOutline,1

; retractBetweenLayers,1

; useRetractionMinTravel,0

; retractionMinTravel,3

; retractWhileWiping,0

; onlyWipeOutlines,1

; avoidCrossingOutline,0

; maxMovementDetourFactor,3

; toolChangeRetractionDistance,12

; toolChangeExtraRestartDistance,-0.5

; toolChangeRetractionSpeed,600

; allowThinWallGapFill,1

; thinWallAllowedOverlapPercentage,10

; horizontalSizeCompensation,0

G90

M82

M106 S0

M140 S60

M190 S60

M104 S195 T1

M104 S0 T0

M109 S195 T1

M108 S255 ; Turn on M2 fans

T1 ; Switch to right extruder offsets for homing

G28 ; Home all axes

T0 ; Switch to left extruder

G1 X0 Y50 Z0.3 F9600 ; Move forward to avoid binder clips

G92 E0

G1 E-1.0000 F2400

G1 Z0.800 F800

; layer 1, Z = 0.8

T1

; tool H0.800 W1.500

; infill

G1 X21.650 Y103.635 F800

G1 E0.0000 F720

G92 E0

G1 X153.350 Y103.635 E97.5314 F300

G1 X153.350 Y105.135 E98.6423

G1 X21.650 Y105.135 E196.1737

G1 X21.650 Y106.635 E197.2845

G1 X153.350 Y106.635 E294.8159

G1 X153.350 Y108.135 E295.9268

G1 X21.650 Y108.135 E393.4582

G1 X21.650 Y109.635 E394.5690

G1 X153.350 Y109.635 E492.1005

G1 X153.350 Y111.135 E493.2113

G1 X21.650 Y111.135 E590.7427

G1 X21.650 Y112.635 E591.8536

G1 X153.350 Y112.635 E689.3850

G1 X153.350 Y114.135 E690.4958

G1 X21.650 Y114.135 E788.0272

G1 X21.650 Y115.635 E789.1381

G1 X153.350 Y115.635 E886.6695

G1 X153.350 Y117.135 E887.7803

G1 X21.650 Y117.135 E985.3118

G1 X21.650 Y118.635 E986.4226

G1 X153.350 Y118.635 E1083.9540

G1 X153.350 Y120.135 E1085.0649

G1 X21.650 Y120.135 E1182.5963

G1 X21.650 Y121.635 E1183.7071

G1 X153.350 Y121.635 E1281.2385

G1 X153.350 Y123.135 E1282.3494

G1 X21.650 Y123.135 E1379.8808

G1 X21.650 Y124.635 E1380.9916

G1 X153.350 Y124.635 E1478.5231

G1 X153.350 Y126.135 E1479.6339

G1 X21.650 Y126.135 E1577.1653

G1 X21.650 Y127.635 E1578.2762

G1 X153.350 Y127.635 E1675.8076

G1 X153.350 Y129.135 E1676.9184

G1 X21.650 Y129.135 E1774.4498

G1 X21.650 Y130.635 E1775.5607

G1 X153.350 Y130.635 E1873.0921

G1 X153.350 Y132.135 E1874.2029

G1 X21.650 Y132.135 E1971.7344

G1 X21.650 Y133.635 E1972.8452

G1 X153.350 Y133.635 E2070.3766

G1 X153.350 Y135.135 E2071.4875

G1 X21.650 Y135.135 E2169.0189

G1 X21.650 Y136.635 E2170.1297

G1 X153.350 Y136.635 E2267.6611

G1 X153.350 Y138.135 E2268.7720

G1 X21.650 Y138.135 E2366.3034

G1 X21.650 Y139.635 E2367.4142

G1 X153.350 Y139.635 E2464.9457

G1 X153.350 Y141.135 E2466.0565

G1 X21.650 Y141.135 E2563.5879

G1 X21.650 Y142.635 E2564.6988

G1 X153.350 Y142.635 E2662.2302

G1 X153.350 Y144.135 E2663.3410

G1 X21.650 Y144.135 E2760.8724

G1 X21.650 Y145.635 E2761.9833

G1 X153.350 Y145.635 E2859.5147

G1 X153.350 Y147.135 E2860.6255

G1 X21.650 Y147.135 E2958.1570

G1 X21.650 Y148.635 E2959.2678

G1 X153.350 Y148.635 E3056.7992

G1 X153.350 Y150.135 E3057.9101

G1 X21.650 Y150.135 E3155.4415

G1 X21.650 Y151.635 E3156.5523

G1 X153.350 Y151.635 E3254.0837

G1 X153.350 Y153.135 E3255.1946

G1 X21.650 Y153.135 E3352.7260

G1 X21.650 Y154.635 E3353.8368

G1 X153.350 Y154.635 E3451.3683

G1 X153.350 Y156.135 E3452.4791

G1 X21.650 Y156.135 E3550.0105

G1 X21.650 Y157.635 E3551.1214

G1 X153.350 Y157.635 E3648.6528

G92 E0

G1 E-1.0000 F2400

; layer 2, Z = 1.6

M106 S255

G4 P500

M106 S127

; infill

G1 X153.350 Y157.635 F800

G1 Z1.600 F800

G1 E0.0000 F2400

G92 E0

G1 X21.650 Y157.635 E97.5314 F300

G1 X21.650 Y156.135 E98.6423

G1 X153.350 Y156.135 E196.1737

G1 X153.350 Y154.635 E197.2845

G1 X21.650 Y154.635 E294.8159

G1 X21.650 Y153.135 E295.9268

G1 X153.350 Y153.135 E393.4582

G1 X153.350 Y151.635 E394.5690

G1 X21.650 Y151.635 E492.1005

G1 X21.650 Y150.135 E493.2113

G1 X153.350 Y150.135 E590.7427

G1 X153.350 Y148.635 E591.8536

G1 X21.650 Y148.635 E689.3850

G1 X21.650 Y147.135 E690.4958

G1 X153.350 Y147.135 E788.0272

G1 X153.350 Y145.635 E789.1381

G1 X21.650 Y145.635 E886.6695

G1 X21.650 Y144.135 E887.7803

G1 X153.350 Y144.135 E985.3118

G1 X153.350 Y142.635 E986.4226

G1 X21.650 Y142.635 E1083.9540

G1 X21.650 Y141.135 E1085.0649

G1 X153.350 Y141.135 E1182.5963

G1 X153.350 Y139.635 E1183.7071

G1 X21.650 Y139.635 E1281.2385

G1 X21.650 Y138.135 E1282.3494

G1 X153.350 Y138.135 E1379.8808

G1 X153.350 Y136.635 E1380.9916

G1 X21.650 Y136.635 E1478.5231

G1 X21.650 Y135.135 E1479.6339

G1 X153.350 Y135.135 E1577.1653

G1 X153.350 Y133.635 E1578.2762

G1 X21.650 Y133.635 E1675.8076

G1 X21.650 Y132.135 E1676.9184

G1 X153.350 Y132.135 E1774.4498

G1 X153.350 Y130.635 E1775.5607

G1 X21.650 Y130.635 E1873.0921

G1 X21.650 Y129.135 E1874.2029

G1 X153.350 Y129.135 E1971.7344

G1 X153.350 Y127.635 E1972.8452

G1 X21.650 Y127.635 E2070.3766

G1 X21.650 Y126.135 E2071.4875

G1 X153.350 Y126.135 E2169.0189

G1 X153.350 Y124.635 E2170.1297

G1 X21.650 Y124.635 E2267.6611

G1 X21.650 Y123.135 E2268.7720

G1 X153.350 Y123.135 E2366.3034

G1 X153.350 Y121.635 E2367.4142

G1 X21.650 Y121.635 E2464.9457

G1 X21.650 Y120.135 E2466.0565

G1 X153.350 Y120.135 E2563.5879

G1 X153.350 Y118.635 E2564.6988

G1 X21.650 Y118.635 E2662.2302

G1 X21.650 Y117.135 E2663.3410

G1 X153.350 Y117.135 E2760.8724

G1 X153.350 Y115.635 E2761.9833

G1 X21.650 Y115.635 E2859.5147

G1 X21.650 Y114.135 E2860.6255

G1 X153.350 Y114.135 E2958.1570

G1 X153.350 Y112.635 E2959.2678

G1 X21.650 Y112.635 E3056.7992

G1 X21.650 Y111.135 E3057.9101

G1 X153.350 Y111.135 E3155.4415

G1 X153.350 Y109.635 E3156.5523

G1 X21.650 Y109.635 E3254.0837

G1 X21.650 Y108.135 E3255.1946

G1 X153.350 Y108.135 E3352.7260

G1 X153.350 Y106.635 E3353.8368

G1 X21.650 Y106.635 E3451.3683

G1 X21.650 Y105.135 E3452.4791

G1 X153.350 Y105.135 E3550.0105

G1 X153.350 Y103.635 E3551.1214

G1 X21.650 Y103.635 E3648.6528

G92 E0

G1 E-1.0000 F2400

; layer end

G91 ; relative mode

G1 Z40 ; lift 10mm

G90 ; absolute mode

G28 X0 ; home X axis

M84 ; disable motors

; Build Summary

; Build time: 0 hours 32 minutes

; Filament length: 7297.3 mm (7.30 m)

; Plastic volume: 11233.33 mm^3 (11.23 cc)

; Plastic weight: 14.04 g (0.03 lb)

; Material cost: 0.65

G-Code for tensile and impact test samples

; G-Code generated by Simplify3D(R) Version 3.1.1

; Jun 25, 2024 at 9:26:03 AM

; Settings Summary

; processName,Process1

; applyToModels,150403_D256_45x5x1.5(2)(2)(2)

; profileName,Christian - PLA correct (modified)

; profileVersion,2017-06-27 14:09:50

; baseProfile,MakerGear M2 Dual (modified)

; printMaterial,PLA

; printQuality,Medium

; printExtruders,Right Extruder Only

; extruderName,Right Extruder

; extruderToolheadNumber,1

; extruderDiameter,1.5

; extruderAutoWidth,0

; extruderWidth,1.5

; extrusionMultiplier,0.95

; extruderUseRetract,1

; extruderRetractionDistance,1

; extruderExtraRestartDistance,0

; extruderRetractionZLift,0

; extruderRetractionSpeed,2400

; extruderUseCoasting,0

; extruderCoastingDistance,0.2

; extruderUseWipe,0

; extruderWipeDistance,5

; primaryExtruder,0

; layerHeight,0.8

; topSolidLayers,0

; bottomSolidLayers,0

; perimeterOutlines,0

; printPerimetersInsideOut,1

; startPointOption,2

; startPointOriginX,0

; startPointOriginY,0

; startPointOriginZ,300

; sequentialIslands,0

; spiralVaseMode,0

; firstLayerHeightPercentage,100

; firstLayerWidthPercentage,100

; firstLayerUnderspeed,1

; useRaft,0

; raftExtruder,0

; raftLayers,3

; raftOffset,3

; raftSeparationDistance,0.14

; raftInfill,85

; disableRaftBaseLayers,0

; useSkirt,0

; skirtExtruder,0

; skirtLayers,1

; skirtOutlines,2

; skirtOffset,5

; usePrimePillar,0

; primePillarExtruder,999

; primePillarWidth,12

; primePillarLocation,7

; primePillarSpeedMultiplier,1

; useOozeShield,0

; oozeShieldExtruder,999

; oozeShieldOffset,2

; oozeShieldOutlines,1

; oozeShieldSidewallShape,1

; oozeShieldSidewallAngle,30

; oozeShieldSpeedMultiplier,1

; infillExtruder,0

; internalInfillPattern,Rectilinear

; externalInfillPattern,Rectilinear

; infillPercentage,100

; outlineOverlapPercentage,40

; infillExtrusionWidthPercentage,100

; minInfillLength,0.1

; infillLayerInterval,1

; infillAngles,0

; overlapInfillAngles,0

; generateSupport,0

; supportExtruder,0

; supportInfillPercentage,30

; supportExtraInflation,0

; denseSupportLayers,0

; denseSupportInfillPercentage,70

; supportLayerInterval,1

; supportHorizontalPartOffset,0.3

; supportUpperSeparationLayers,1

; supportLowerSeparationLayers,1

; supportType,0

; supportGridSpacing,4

; maxOverhangAngle,45

; supportAngles,0

; temperatureName,Right Extruder,Left Extruder,Heated Bed

; temperatureNumber,1,0,2

; temperatureSetpointCount,1,1,1

; temperatureSetpointLayers,1,1,1

; temperatureSetpointTemperatures,195,0,60

; temperatureStabilizeAtStartup,1,0,1

; temperatureHeatedBed,0,0,1

; temperatureRelayBetweenLayers,0,0,0

; temperatureRelayBetweenLoops,0,0,0

; fanLayers,1,2

; fanSpeeds,0,50

; blipFanToFullPower,1

; adjustSpeedForCooling,1

; minSpeedLayerTime,15

; minCoolingSpeedSlowdown,20

; increaseFanForCooling,0

; minFanLayerTime,45

; maxCoolingFanSpeed,100

; increaseFanForBridging,0

; bridgingFanSpeed,100

; use5D,1

; relativeEdistances,0

; allowEaxisZeroing,1

; independentExtruderAxes,0

; includeM10123,0

; stickySupport,1

; applyToolheadOffsets,0

; gcodeXoffset,0

; gcodeYoffset,0

; gcodeZoffset,0

; overrideMachineDefinition,1

; machineTypeOverride,0

; strokeXoverride,175

; strokeYoverride,250

; strokeZoverride,200

; originOffsetXoverride,0

; originOffsetYoverride,0

; originOffsetZoverride,0

; homeXdirOverride,-1

; homeYdirOverride,-1

; homeZdirOverride,-1

; flipXoverride,1

; flipYoverride,-1

; flipZoverride,1

; toolheadOffsets,0,0|-31.1,0|0,0|0,0|0,0|0,0

; overrideFirmwareConfiguration,1

; firmwareTypeOverride,RepRap (Marlin/Repetier/Sprinter)

; GPXconfigOverride,r2

; baudRateOverride,115200

; overridePrinterModels,1

; printerModelsOverride,MakerGear_M2Dual.stl

; startingGcode,M108 S255 ; Turn on M2 fans,T1 ; Switch to right extruder offsets for homing,G28 ; Home all axes,T0 ; Switch to left extruder,G1 X0 Y50 Z0.3 F9600 ; Move forward to avoid binder clips,,

; layerChangeGcode,

; retractionGcode,

; toolChangeGcode,

; endingGcode,G91 ; relative mode,G1 Z40 ; lift 10mm,G90 ; absolute mode,G28 X0 ; home X axis,M84 ; disable motors

; exportFileFormat,gcode

; celebration,0

; celebrationSong,Random Song

; postProcessing,

; defaultSpeed,300

; outlineUnderspeed,1

; solidInfillUnderspeed,1

; supportUnderspeed,1

; rapidXYspeed,800

; rapidZspeed,800

; minBridgingArea,50

; bridgingExtraInflation,0

; bridgingExtrusionMultiplier,1

; bridgingSpeedMultiplier,1

; filamentDiameter,1.4

; filamentPricePerKg,46

; filamentDensity,1.25

; useMinPrintHeight,0

; minPrintHeight,0

; useMaxPrintHeight,0

; maxPrintHeight,0

; useDiaphragm,0

; diaphragmLayerInterval,20

; robustSlicing,1

; mergeAllIntoSolid,0

; onlyRetractWhenCrossingOutline,1

; retractBetweenLayers,1

; useRetractionMinTravel,0

; retractionMinTravel,3

```
;   retractWhileWiping,0
;   onlyWipeOutlines,1
;   avoidCrossingOutline,0
;   maxMovementDetourFactor,3
;   toolChangeRetractionDistance,12
;   toolChangeExtraRestartDistance,-0.5
;   toolChangeRetractionSpeed,600
;   allowThinWallGapFill,1
;   thinWallAllowedOverlapPercentage,10
;   horizontalSizeCompensation,0
G90
M82
M106 S0
M140 S60
M190 S60
M104 S195 T1
M104 S0 T0
M109 S195 T1
M108 S255 ; Turn on M2 fans
T1 ; Switch to right extruder offsets for homing
G28 ; Home all axes
T0 ; Switch to left extruder
G1 X0 Y50 Z0.3 F9600 ; Move forward to avoid binder clips
G92 E0
G1 E-1.0000 F2400
G1 Z0.800 F800
; layer 1, Z = 0.8
T1
```

; tool H0.800 W1.500

; infill

G1 X39.150 Y108.135 F800

G1 E0.0000 F720

G92 E0

G1 X135.849 Y108.135 E71.6112 F300

G1 X135.849 Y109.635 E72.7220

G1 X39.150 Y109.635 E144.3332

G1 X39.150 Y111.135 E145.4440

G1 X135.849 Y111.135 E217.0552

G1 X135.849 Y112.635 E218.1660

G1 X39.150 Y112.635 E289.7772

G1 X39.150 Y114.135 E290.8880

G1 X135.849 Y114.135 E362.4992

G1 X135.849 Y115.635 E363.6101

G1 X39.150 Y115.635 E435.2212

G1 X39.150 Y117.135 E436.3321

G1 X135.849 Y117.135 E507.9432

G1 X135.849 Y118.635 E509.0541

G1 X39.150 Y118.635 E580.6653

G1 X39.150 Y120.135 E581.7761

G1 X135.849 Y120.135 E653.3873

G1 X135.849 Y121.635 E654.4981

G1 X39.150 Y121.635 E726.1093

G1 X39.150 Y123.135 E727.2201

G1 X135.849 Y123.135 E798.8313

G1 X135.849 Y124.635 E799.9421

G1 X39.150 Y124.635 E871.5533

G1 X39.150 Y126.135 E872.6641

G1 X135.849 Y126.135 E944.2753

G1 X135.849 Y127.635 E945.3862

G1 X39.150 Y127.635 E1016.9973

G1 X39.150 Y129.135 E1018.1082

G1 X135.849 Y129.135 E1089.7193

G1 X135.849 Y130.635 E1090.8302

G1 X39.150 Y130.635 E1162.4414

G1 X39.150 Y132.135 E1163.5522

G1 X135.849 Y132.135 E1235.1634

G1 X135.849 Y133.635 E1236.2742

G1 X39.150 Y133.635 E1307.8854

G1 X39.150 Y135.135 E1308.9962

G1 X135.849 Y135.135 E1380.6074

G1 X135.849 Y136.635 E1381.7182

G1 X39.150 Y136.635 E1453.3294

G1 X39.150 Y138.135 E1454.4402

G1 X135.849 Y138.135 E1526.0514

G1 X135.849 Y139.635 E1527.1622

G1 X39.150 Y139.635 E1598.7734

G1 X39.150 Y141.135 E1599.8843

G1 X135.849 Y141.135 E1671.4954

G1 X135.849 Y142.635 E1672.6063

G1 X39.150 Y142.635 E1744.2174

G1 X39.150 Y144.135 E1745.3283

G1 X135.849 Y144.135 E1816.9395

G1 X135.849 Y145.635 E1818.0503

G1 X39.150 Y145.635 E1889.6615

G1 X39.150 Y147.135 E1890.7723

G1 X135.849 Y147.135 E1962.3835

G1 X135.849 Y148.635 E1963.4943

G1 X39.150 Y148.635 E2035.1055

G1 X39.150 Y150.135 E2036.2163

G1 X135.849 Y150.135 E2107.8275

G1 X135.849 Y151.635 E2108.9383

G1 X39.150 Y151.635 E2180.5495

G1 X39.150 Y153.135 E2181.6604

G1 X135.849 Y153.135 E2253.2715

G92 E0

G1 E-1.0000 F2400

; layer 2, Z = 1.6

M106 S255

G4 P500

M106 S127

; infill

G1 X135.849 Y153.135 F800

G1 Z1.600 F800

G1 E0.0000 F2400

G92 E0

G1 X39.150 Y153.135 E71.6112 F300

G1 X39.150 Y151.635 E72.7220

G1 X135.849 Y151.635 E144.3332

G1 X135.849 Y150.135 E145.4440

G1 X39.150 Y150.135 E217.0552

G1 X39.150 Y148.635 E218.1660

G1 X135.849 Y148.635 E289.7772

G1 X135.849 Y147.135 E290.8880

G1 X39.150 Y147.135 E362.4992

G1 X39.150 Y145.635 E363.6101

G1 X135.849 Y145.635 E435.2212

G1 X135.849 Y144.135 E436.3321

G1 X39.150 Y144.135 E507.9432

G1 X39.150 Y142.635 E509.0541

G1 X135.849 Y142.635 E580.6653

G1 X135.849 Y141.135 E581.7761

G1 X39.150 Y141.135 E653.3873

G1 X39.150 Y139.635 E654.4981

G1 X135.849 Y139.635 E726.1093

G1 X135.849 Y138.135 E727.2201

G1 X39.150 Y138.135 E798.8313

G1 X39.150 Y136.635 E799.9421

G1 X135.849 Y136.635 E871.5533

G1 X135.849 Y135.135 E872.6641

G1 X39.150 Y135.135 E944.2753

G1 X39.150 Y133.635 E945.3862

G1 X135.849 Y133.635 E1016.9973

G1 X135.849 Y132.135 E1018.1082

G1 X39.150 Y132.135 E1089.7193

G1 X39.150 Y130.635 E1090.8302

G1 X135.849 Y130.635 E1162.4414

G1 X135.849 Y129.135 E1163.5522

G1 X39.150 Y129.135 E1235.1634

G1 X39.150 Y127.635 E1236.2742

G1 X135.849 Y127.635 E1307.8854

G1 X135.849 Y126.135 E1308.9962

G1 X39.150 Y126.135 E1380.6074

G1 X39.150 Y124.635 E1381.7182

G1 X135.849 Y124.635 E1453.3294

G1 X135.849 Y123.135 E1454.4402

G1 X39.150 Y123.135 E1526.0514

G1 X39.150 Y121.635 E1527.1622

G1 X135.849 Y121.635 E1598.7734

G1 X135.849 Y120.135 E1599.8843

G1 X39.150 Y120.135 E1671.4954

G1 X39.150 Y118.635 E1672.6063

G1 X135.849 Y118.635 E1744.2174

G1 X135.849 Y117.135 E1745.3283

G1 X39.150 Y117.135 E1816.9395

G1 X39.150 Y115.635 E1818.0503

G1 X135.849 Y115.635 E1889.6615

G1 X135.849 Y114.135 E1890.7723

G1 X39.150 Y114.135 E1962.3835

G1 X39.150 Y112.635 E1963.4943

G1 X135.849 Y112.635 E2035.1055

G1 X135.849 Y111.135 E2036.2163

G1 X39.150 Y111.135 E2107.8275

G1 X39.150 Y109.635 E2108.9383

G1 X135.849 Y109.635 E2180.5495

G1 X135.849 Y108.135 E2181.6604

G1 X39.150 Y108.135 E2253.2715

G92 E0

G1 E-1.0000 F2400

```
; layer 3, Z = 2.4
; infill
G1 X39.150 Y108.135 F800
G1 Z2.400 F800
G1 E0.0000 F2400
G92 E0
G1 X135.849 Y108.135 E71.6112 F300
G1 X135.849 Y109.635 E72.7220
G1 X39.150 Y109.635 E144.3332
G1 X39.150 Y111.135 E145.4440
G1 X135.849 Y111.135 E217.0552
G1 X135.849 Y112.635 E218.1660
G1 X39.150 Y112.635 E289.7772
G1 X39.150 Y114.135 E290.8880
G1 X135.849 Y114.135 E362.4992
G1 X135.849 Y115.635 E363.6101
G1 X39.150 Y115.635 E435.2212
G1 X39.150 Y117.135 E436.3321
G1 X135.849 Y117.135 E507.9432
G1 X135.849 Y118.635 E509.0541
G1 X39.150 Y118.635 E580.6653
G1 X39.150 Y120.135 E581.7761
G1 X135.849 Y120.135 E653.3873
G1 X135.849 Y121.635 E654.4981
G1 X39.150 Y121.635 E726.1093
G1 X39.150 Y123.135 E727.2201
G1 X135.849 Y123.135 E798.8313
G1 X135.849 Y124.635 E799.9421
```

G1 X39.150 Y124.635 E871.5533

G1 X39.150 Y126.135 E872.6641

G1 X135.849 Y126.135 E944.2753

G1 X135.849 Y127.635 E945.3862

G1 X39.150 Y127.635 E1016.9973

G1 X39.150 Y129.135 E1018.1082

G1 X135.849 Y129.135 E1089.7193

G1 X135.849 Y130.635 E1090.8302

G1 X39.150 Y130.635 E1162.4414

G1 X39.150 Y132.135 E1163.5522

G1 X135.849 Y132.135 E1235.1634

G1 X135.849 Y133.635 E1236.2742

G1 X39.150 Y133.635 E1307.8854

G1 X39.150 Y135.135 E1308.9962

G1 X135.849 Y135.135 E1380.6074

G1 X135.849 Y136.635 E1381.7182

G1 X39.150 Y136.635 E1453.3294

G1 X39.150 Y138.135 E1454.4402

G1 X135.849 Y138.135 E1526.0514

G1 X135.849 Y139.635 E1527.1622

G1 X39.150 Y139.635 E1598.7734

G1 X39.150 Y141.135 E1599.8843

G1 X135.849 Y141.135 E1671.4954

G1 X135.849 Y142.635 E1672.6063

G1 X39.150 Y142.635 E1744.2174

G1 X39.150 Y144.135 E1745.3283

G1 X135.849 Y144.135 E1816.9395

G1 X135.849 Y145.635 E1818.0503

G1 X39.150 Y145.635 E1889.6615

G1 X39.150 Y147.135 E1890.7723

G1 X135.849 Y147.135 E1962.3835

G1 X135.849 Y148.635 E1963.4943

G1 X39.150 Y148.635 E2035.1055

G1 X39.150 Y150.135 E2036.2163

G1 X135.849 Y150.135 E2107.8275

G1 X135.849 Y151.635 E2108.9383

G1 X39.150 Y151.635 E2180.5495

G1 X39.150 Y153.135 E2181.6604

G1 X135.849 Y153.135 E2253.2715

G92 E0

G1 E-1.0000 F2400

; layer 4, Z = 3.2

; infill

G1 X135.849 Y153.135 F800

G1 Z3.200 F800

G1 E0.0000 F2400

G92 E0

G1 X39.150 Y153.135 E71.6112 F300

G1 X39.150 Y151.635 E72.7220

G1 X135.849 Y151.635 E144.3332

G1 X135.849 Y150.135 E145.4440

G1 X39.150 Y150.135 E217.0552

G1 X39.150 Y148.635 E218.1660

G1 X135.849 Y148.635 E289.7772

G1 X135.849 Y147.135 E290.8880

G1 X39.150 Y147.135 E362.4992

G1 X39.150 Y145.635 E363.6101

G1 X135.849 Y145.635 E435.2212

G1 X135.849 Y144.135 E436.3321

G1 X39.150 Y144.135 E507.9432

G1 X39.150 Y142.635 E509.0541

G1 X135.849 Y142.635 E580.6653

G1 X135.849 Y141.135 E581.7761

G1 X39.150 Y141.135 E653.3873

G1 X39.150 Y139.635 E654.4981

G1 X135.849 Y139.635 E726.1093

G1 X135.849 Y138.135 E727.2201

G1 X39.150 Y138.135 E798.8313

G1 X39.150 Y136.635 E799.9421

G1 X135.849 Y136.635 E871.5533

G1 X135.849 Y135.135 E872.6641

G1 X39.150 Y135.135 E944.2753

G1 X39.150 Y133.635 E945.3862

G1 X135.849 Y133.635 E1016.9973

G1 X135.849 Y132.135 E1018.1082

G1 X39.150 Y132.135 E1089.7193

G1 X39.150 Y130.635 E1090.8302

G1 X135.849 Y130.635 E1162.4414

G1 X135.849 Y129.135 E1163.5522

G1 X39.150 Y129.135 E1235.1634

G1 X39.150 Y127.635 E1236.2742

G1 X135.849 Y127.635 E1307.8854

G1 X135.849 Y126.135 E1308.9962

G1 X39.150 Y126.135 E1380.6074

G1 X39.150 Y124.635 E1381.7182

G1 X135.849 Y124.635 E1453.3294

G1 X135.849 Y123.135 E1454.4402

G1 X39.150 Y123.135 E1526.0514

G1 X39.150 Y121.635 E1527.1622

G1 X135.849 Y121.635 E1598.7734

G1 X135.849 Y120.135 E1599.8843

G1 X39.150 Y120.135 E1671.4954

G1 X39.150 Y118.635 E1672.6063

G1 X135.849 Y118.635 E1744.2174

G1 X135.849 Y117.135 E1745.3283

G1 X39.150 Y117.135 E1816.9395

G1 X39.150 Y115.635 E1818.0503

G1 X135.849 Y115.635 E1889.6615

G1 X135.849 Y114.135 E1890.7723

G1 X39.150 Y114.135 E1962.3835

G1 X39.150 Y112.635 E1963.4943

G1 X135.849 Y112.635 E2035.1055

G1 X135.849 Y111.135 E2036.2163

G1 X39.150 Y111.135 E2107.8275

G1 X39.150 Y109.635 E2108.9383

G1 X135.849 Y109.635 E2180.5495

G1 X135.849 Y108.135 E2181.6604

G1 X39.150 Y108.135 E2253.2715

G92 E0

G1 E-1.0000 F2400

; layer end

G91 ; relative mode

G1 Z40 ; lift 10mm

G90 ; absolute mode

G28 X0 ; home X axis

M84 ; disable motors

; Build Summary

; Build time: 0 hours 40 minutes

; Filament length: 9013.1 mm (9.01 m)

; Plastic volume: 13874.57 mm^3 (13.87 cc)

; Plastic weight: 17.34 g (0.04 lb)

; Material cost: 0.80